UNIVERSITAT DE BARCELONA

Aging impacts epidermal and dermal cell interaction

Paloma Solá Castrillo

Aging impacts epidermal and dermal cell interaction

Doctoral Thesis
Paloma Solá Castrillo
2023

Aging impacts epidermal and dermal cell interaction

Paloma Solá Castrillo

Universitat de Barcelona

Facultad de Biología

Programa de doctorado en Biomedicina

Febrero de 2023

UNIVERSITAT DE BARCELONA

Aging impacts epidermal and dermal cell interaction

Memoria presentada para optar al grado de doctor por la Universitat de Barcelona

Facultad de Biología
Programa de doctorado en Biomedicina
IRB Barcelona

Paloma Solá Castrillo

Directores:
Guiomar Solanas Fuster Salvador Aznar Benitah

Tutor: Antonio Zorzano Olarte

Febrero 2023

“Me gusta el arco tenso y la flecha ligera.
Poner la locura como meta.
Y alcanzar lo imposible a través
de posibles muy pequeños”

A mis padres y abuelos,
que me construyeron el camino

Acknowledgements

For me, this PhD has been about the journey. From all the accomplishments obtained during these years, the one I am the proudest of is all the friendships, laughter, and experiences lived with the people I am lucky enough to have in my life. This thesis is only a small representation of all of these things, and includes the help of many people that made it a reality.

Primero, me gustaría agradecerle a **Salva** darme la oportunidad de estar en el lab, a pesar de que le haya tratado de usted tantas veces. También, por toda la confianza y libertad depositada en mí desde el principio.

Guio, es imposible que pueda agradecerte suficientemente lo muchísimo que me has ayudado personal y profesionalmente. Si no fuese por ti, no estaría ni cerca de donde estoy ahora mismo. No me refiero a los proyectos, porque eso es obvio. Has estado siempre ahí, en momentos en los que lo he necesitado mucho, y también en los que solamente necesitaba saber que estabas. Todo lo que sé es gracias a ti y, aunque hayamos tenido momentos en los que hayamos tenido que ir a la terraza de arriba del todo, ha habido otros en los que nos han mandado callar desde otros laboratorios por reírnos demasiado alto, que han hecho que todo merezca la pena. Quiero que sepas que nos lleve donde nos lleve el futuro, siempre voy a llevar conmigo los infartos que me das cuando me voy a equivocar en algo, los chillidos de cada vez que sale algo, y el poder leer tu pensamiento cuando te miro en el momento perfecto. Volvería a repetir toda esta experiencia, solo si supiese que volverías a estar tú en ella. S.L. forever!

Gracias a **Júlia** (o Julia, que es como prefieres que te llamen) por ser una compi de lab perfecta desde el primer día. Gracias por siempre estar dispuesta a todo, desde genotipar un millón de ratones, hasta ir a por desayuno, patatas, o una cerveza; y siempre con una sonrisa. Gracias por las miles de horas buenas que hemos pasado juntas, incluyendo momentos en los que los trajes del animalario deciden darte ventilación, o en los que hablamos idiomas muy diferentes. También, por las no tan buenas (no hace ni falta que mencione el TEWL aquí). Gracias por estar siempre disponible, por escucharme y por confiar en mí de vuelta. Quiero que sepas que pase lo

que pase, no te vas a librar de mí. Y, sobre todo, quiero darte las gracias por ponerte tan roja siempre.

Para ti **Andrés**, salir en los agradecimientos de tesis ya es un hobby. Es tradición ya que cualquier persona que cruza camino contigo, acaba dedicándote un apartado importante (y merecido) en sus agradecimientos. Sin tus ganas de ayudar, tu conocimiento que hace palidecer a Siri y Google juntos, y tremenda empatía, ni este trabajo ni yo seríamos lo que somos hoy. Estoy segurísima de que todo el mundo que te conoce está de acuerdo en que Andrés no hay más que uno (y menos mal, que si hubiese más nos quedaríamos sin chocolate).

I want to thank you **Tom** for always finding a way to brighten my day and for making me laugh (at you, mostly ☺), and for bringing tuppers that make my food look a little less sad. A **Mónica**, por la alegría y risas que traes al lab a diario, que son capaces de alegrar el día a cualquiera. Por todos tus consejos, y por ser mi salvadora cada vez que me atacan las cucarachas. A **Clàudia**, más que gracias, pedirle perdón por haber tenido que sentarse a mi lado. Te agradezco no haberme clavado un cuchillo cuando hayas tenido ganas, y por sonreírme y reírte a cambio. A **Josefina**, gracias por irradiar tanta felicidad, calma y simpatía. Tener a alguien como tu en el día a día es una suerte increíble. A **Blanca**, por tu gran compañerismo desde el primer día, por tu constante buen humor y por tus consejos. To the rest of the **SAB lab members**, thank you for making working in the lab so much fun, and for putting up with my jokes.

También, quería agradecer a aquellos SAB lab members que, aunque ya no estén en el lab, me han acompañado durante el camino. Gracias a **Uxue**, por ser mi compañera de PhD durante todos estos años. Porque, aunque haya habido momentos difíciles, siempre hayamos acabado apoyándonos y esperando el apocalipsis juntas. Por todos aquellos vermuts y cervezas que nos hemos tomado, y por los que nos tomaremos. To **Patrick**, for always being there to support me. Thank you for your unlimited friendship, no matter how much time we spend without managing to meet. For all the helados we have had, for all those cakes you have baked, and for those you still have to bake (hopefully becoming a doctor will be enough to bully you into baking

one). To **Michi**, for sharing our first day in the lab. Thank you for being a Minion with me, and for all these years of long-distance friendship. If I listen carefully, I can hear you laugh all the way from Basel. A **Miguel**, gracias por estar siempre dispuesto a perder conmigo al pádel. También, gracias a **Diana** por tantos momentos dentro y fuera del lab, y por todas las rosquillas. Además, quería resaltar que mi experiencia en el IRB habría sido desastrosa si no hubiese sido por **Andrea**. Gracias por apoyarme tanto durante estos años. Gracias por saber siempre qué decir para hacerme sentir mejor, y por hacerme oír risas donde solo hay gaviotas. También, gracias a **Inés** por hacer que unirse al Student Council mereciese la pena. Thank you, **Karen** and **Nikos**, for being constant providers of amazing food, and for always having time for me even when I do not have time for myself. A **David**, por tu amistad desde el primer día.

Marta y **Rebeca**, dicen que una casa es como un refugio, y tengo la suerte de saber que el mío es perfecto. A Rebeca, gracias por enseñarme que la generosidad y el buen corazón no tienen límites, y a Marta por tu empatía y comprensión constantes, en momentos buenos y menos buenos. Gracias a **Lucía**, por también formar parte de ese refugio, aunque ahora sea desde un poco más lejos. Por todos esos momentos en los que nos hemos apoyado entre nosotras.

Una enorme parte de los buenos momentos que he tenido durante estos años viene de la mano de un grupo con una fuente inagotable de nombres y de personas increíbles. De ellos, quería agradecer primero a las churreras, **Almu**, **Elena M**, **Elena F**, y **Laura**, por ser mi escapatoria entre semana. Gracias por ayudarme a encontrar tiempo donde no lo hay, y por darme siempre un poco de sanidad entre tanta locura. A **Barri**, por no acordarte de que nos conocimos en la playa, y por tu paciencia y apoyo constantes. Gracias por estar siempre dispuesto a escucharme, y por hacerme reír pase lo que pase. Por todas las brasas que me has dado, y por todas las que quedan. También, a mis antiguos soportes en IRB, **Marcos** y **Ernest**, gracias por aguantarme por partida doble, dentro y fuera del lab. También a **Clara**, **Rodri**, **María**, **Luis**, **Javi**, y **Marc**, y a **Enrique** y **Jacobo** aunque estén más lejos. Gracias a todos por ser mi familia en Barcelona. A **Mauri**, gracias por

mudarte a Barcelona, y por reconocer que soy la mejor profesora que has tenido.

To all the **Wickström** lab members, and especially to Kate and Sara. **Sara**, thank you for welcoming me into your lab, giving me one of the best experiences of my PhD. **Kate**, thank you for all the memories and chocolates, and for being a perfect and beautiful racoon.

A Marta, Pati y Paloma, por apoyarme desde Madrid. **Marta**, gracias por tantas visitas, y por compartir siempre todas mis alegrías y momentos difíciles como si fuesen tuyos. A **Pati**, por siempre conseguir sacarme una sonrisa, y por ser el ejemplo perfecto de que con esfuerzo y determinación nada es imposible. También, por la mejor portada de tesis del mundo. A **Paloma**, gracias por ser siempre un apoyo absoluto, y por estar dispuesta a dejarlo todo para ayudar. No sé qué haría sin vosotras.

Por último, y más importante, gracias a mi familia. Gracias a **Pepe** y **Friqui**, por ser ejemplos constantes de superación, siempre con una sonrisa. A **Marilo** y **María**, por sus inacabables palabras de ánimo. A **Bego** y **Álvaro**, por formar una parte tan importante de la familia y de mi vida. Por vuestra paciencia, y por apoyarme. A **Alejandro**, por ir siempre por delante, abriendo el camino. Por ser la persona con la que comparto sentido del humor, y a la que cada día descubro que me parezco más. A **Lucía**, por ser mi mejor amiga. Porque nunca me sentiré sola gracias a ti. Por ayudarme a confiar en mí misma. Gracias por estar a mi lado incondicionalmente. Para mis padres, no existen palabras. **Mamá**, gracias por ser la persona a la que aspiro llegar a ser algún día. Por toda tu fortaleza, cariño, empatía, y amor. **Papá**, gracias por enseñarme a ser como soy y como debo ser. Por hacerme saber que pase lo que pase, y aunque ni siquiera sepa que lo necesito, vas a estar ahí. Sin vosotros, nada habría sido posible. Porque todas las metas a las que consigo llegar, son por y para vosotros. Para terminar, gracias a mis abuelos, **Asun**, **Lola**, **Curro** y **Marcelino**. Gracias por ser parte de mi vida. Siempre os llevaré conmigo.

Table of contents

Abstract

Aging can be defined as a decline or loss of adaptation during the increase of age, caused by a progressive deterioration of functions and integrity. This occurs in tissues such as the skin, which presents deep structural and functional changes during aging. However, the precise alterations occurring in each skin compartment, as well as their origin and characteristics are still not completely understood.

We show that there is a predominant increase in IL-17-expressing lymphoid cells in the aged dermis. These excessive IL-17 levels are key in the development of a chronic inflammatory context, as well as in the development of age-associated traits in the skin. Surprisingly, neutralizing IL-17 activity *in vivo* significantly delayed the appearance of age-related skin characteristics, such as the increase in cornified layer thickness, inefficient wound healing, deteriorated barrier regeneration, and delayed hair follicle cycling. Besides, we also describe a functional interaction between YAP, a downstream effector of the Hippo pathway crucial for mechanotransduction processes, and BMAL1, the main transcription factor of the circadian clock machinery. Here, we show that there is an increase in YAP activity in aged epidermal cells, which correlates with a stiffness increase in their niche. Also, we describe that YAP and BMAL1 bind to adjacent genomic locations on the same genes. In aged epidermal cells, these genes mainly present pro-inflammatory functions and a rhythmic pattern of expression.

Our results demonstrate that chronic inflammation in aged skin can be ameliorated by targeting IL-17 signaling. Also, our data indicates that mechanical changes in the aged skin impact the rhythmicity of genes in the epidermis, and generates a link between these two pathways. Altogether, our findings provide new insights into different aspects of skin aging, which could contribute in the search for new strategies for anti-aging therapies.

Resumen

El envejecimiento se define como un declive o pérdida de la capacidad de adaptación a cambios a lo largo del tiempo, causando un deterioro progresivo de integridad y funciones. Esto sucede en tejidos como la piel, que presenta cambios estructurales y funcionales profundos al envejecer. Sin embargo, aún se desconocen gran parte de las alteraciones específicas que ocurren en cada capa de la piel, al igual que su origen y características.

Hemos descrito un incremento en el número de células linfoides que expresan IL-17 en la dermis envejecida. Este incremento es clave en el desarrollo de la inflamación crónica y en el deterioro de las funciones de la piel al envejecer. Sorprendentemente, la neutralización de la actividad de IL-17 *in vivo* retrasó significativamente la aparición de propiedades típicas de la piel envejecida, como el incremento en grosor de la capa cornificada, el deterioro en el proceso de curación de heridas y de la regeneración de la barrera, al igual que el retraso en la entrada en fase de crecimiento del folículo piloso. Aparte, describimos una hasta ahora desconocida interacción entre YAP, un efector de la cascada de señalización Hippo e importante para procesos de mecanotransducción, y BMAL1, un factor de transcripción crítico de la maquinaria del reloj circadiano. Además, mostramos un incremento en la actividad de YAP en células envejecidas de la epidermis, que correlaciona con un aumento en la rigidez de su nicho. También observamos que YAP y BMAL1 se unen a las mismas regiones en el genoma. Esto incluye la unión a genes con funciones pro-inflamatorias y comportamiento circadiano específicamente en células envejecidas de la epidermis.

Nuestros resultados demuestran que la inflamación crónica que existe en la piel envejecida se puede disminuir bloqueando de la actividad de IL-17. También, nuestros datos indican que los cambios mecánicos que ocurren en la piel al envejecer tienen un impacto sobre la expresión de

forma oscilatoria de los genes en la epidermis. Con esto, hemos descrito un vínculo entre los procesos de mecanotransducción y el reloj circadiano. Finalmente, nuestros hallazgos proporcionan nuevas ideas y perspectivas a distintos aspectos del proceso de envejecimiento en la piel, que podrían contribuir en la búsqueda de nuevas estrategias para terapias anti-envejecimiento.

Abbreviations

Actomyosin complex= Actin-myosin complex

AFM= Atomic force microscopy

APC= Antigen presenting cell

APM= Arrector pili muscle

ATAC-seq= Assay for Transposase-Accessible Chromatin using sequencing

BM= Basement membrane

BMAL1ep cKO= *Bmal1* epidermal conditional knock-out

BMP= Bone morphogenetic protein

BP= Biological process

C/EPB= CCAAT/enhancer-binding protein

Ca^{2+}= Calcium

ChIP-seq= Chromatin immunoprecipitation followed by sequencing

COL17A1= Collagen XVII α-1 chain

dDC= Dermal dendritic cell

DEG= Differentially expressed gene

Doxy= Doxycycline

DP= Dermal papilla

E-box= Enhancer box

EAE= Experimental autoimmune encephalomyelitis

EC= Endothelial cells

ECM= Extracellular matrix

EGFR= Epidermal growth factor receptor

EMA= European Medicines Agency

EpSC= Epidermal stem cells

ERK= Extracellular signal-regulated kinase

Evpl= Envoplakin

FACS= Florescence-activated cell sorting

FC= Fold change

FISH= fluorescent *in situ* hybridization

$\gamma\delta$ T= $\gamma\delta$ T cells

GO= Gene ontology

GTPase= Hydrolase enzymes that bind to guanosine triphosphate

HE= Hematoxylin and eosin

HF= Hair follicle

HFSC= Hair follicle stem cell

HIF1α= Hypoxia-inducible factor 1-α

HSC= Hematopoietic stem cell

IF= Immunofluorescence

IFE= Interfollicular epidermis

Ifn-γ= Interferon-γ

IKK= IkB kinase

IL-17A/F= IL17A and IL17F

Il= Interleukin

ILC= Innate lymphoid cell

IRS= Inner root sheath

iSALT= Inducible skin-associated lymphoid tissue

iYAP= inducible YAP

JNK= JUN N-terminal kinase

JTK= Jonckheere-Terpstra-Kendall

K14= Keratin 14

KO= Knock-out

MAPK= Mitogen-activated protein kinase

MHC= Major histocompatibility complex

NF-κB= Nuclear factor-κB

NKT= Natural killer T cells

ORS= Outer root sheath

PAMPS= Pathogen-associated molecular patterns

PBMC= Peripheral blood mononuclear cell

PNS= Peripheral nervous system

Pol II= RNA polymerase II

PRRs= Pattern recognition receptors

QC= Quality control

qPCR= Quantitative polymerase chain reaction

ROCK= Rho-associated protein kinase

RORγt= retinoic acid-related orphan receptor γt

ROS= Reactive oxygen species

rtTA= Reverse tetracycline-controlled transactivator

RSPO3= R-Spondin 3

S127= Serine 127

SAASP= Skin aging-associated secreted proteins

SASP= Senescence-associated secretory phenotype

SC= Stem cell

SCN= Suprachiasmatic nucleus

scRNA-seq= Single-cell RNA-sequencing

SEFIR= Similar expression to fibroblast growth factor genes and IL-17R

T cyt= T cytotoxic cells

T regs= T regulatory cells

TAZ= Transcriptional co-activator with PDZ-binding motif

TEAD= Transcriptional enhanced associate domain

TEWL= Trans-epidermal water loss

TF= Transcription factor

TGFβ= Transforming growth factor-β

Th= T helper cells

Tnf= Tumour necrosis factor

TRAF= TNF-receptor associated factor

TRM= Tissue-resident memory cells

UMAP= Uniform Manifold Approximation and Projection

UV=Ultraviolet light

WH= Wound healing

WT= Wild-type

YAP= Yes-associated protein

ZT= *Zeitgeber*, time giver

Introduction

1. The skin

The skin is the largest organ in the body, and it consists of different sections and structured compartments. There are several anatomical and functional differences between murine and human skin, and this work will focus on murine skin unless stated otherwise.

In the murine skin, there are three main layers named the epidermis, the dermis and the hypodermis. The epidermis is the outermost layer, and it forms an impermeable cover that protects against external insults and prevents evaporation from bodily fluids[1,2]. The dermis is beneath the epidermis, separated by the basement membrane (BM), and provides a network of interactions between a variety of cell types including fibroblasts, immune, endothelial, muscle and neuronal cells. This structure is connected by an organized mesh of extracellular matrix (ECM), which also supports the epidermis. The hypodermis or subcutaneous layer is mainly composed of adipose tissue[3,4].

1.1. Epidermis

The epidermis is a multi-layered stratified epithelium, and its functions include the formation of a protective barrier against the external environment, thermoregulation and lubrication. It is composed of several specialized structures, such as the interfollicular epidermis (IFE), hair follicles (HFs), sweat glands, sebaceous glands and the arrector pili muscle (APM) (**Figure I1.1**).

These structures are home to a variety of cell types, where the most predominant cell types are the keratinocytes or epidermal cells, which will be further addressed throughout this work. There are also γδ T cells, Merkel cells, melanocytes and a small population of Langerhans cells [1,2]. First, γδ T cells are a subtype of T cells that will be further explained later on (see 1.2.2. Dermal cell types). Merkel cells are epithelial

mechanosensory cells that communicate with sensory neurons in the skin[5]. Melanocytes are derived from the neural crest and localize primarily in hair follicles (HFs), although some can be found scattered in the epidermis to pigment hair and skin. They produce melanin pigments to protect the skin from ultraviolet light (UV)[6]. Langerhans cells are a population of cells that share similarities with both dendritic cells and macrophages, and they act as epidermal immune sentinels[7].

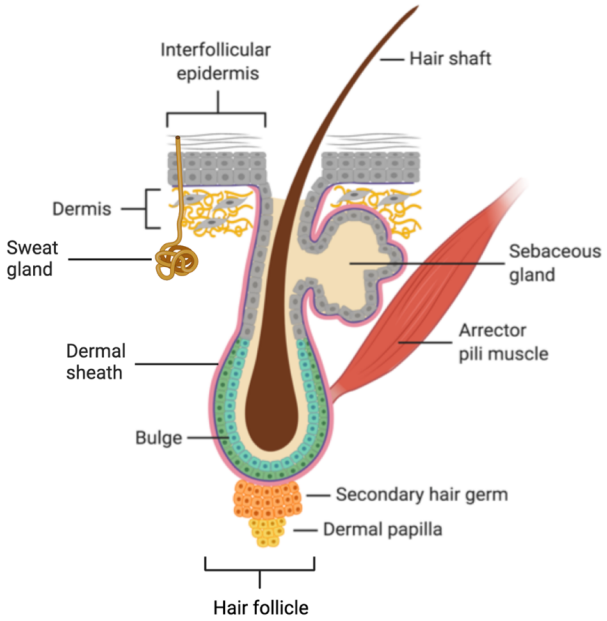

Figure I1.1. The epidermis. Schematic of the structure of the epidermis and the hair follicle, including sweat glands, sebaceous glands and the arrector pili muscle. The IFE confers protection against dehydration and external aggressions. HFs are found scattered throughout the epidermis and flank the IFE, and they include several compartments such as the bulge, dermal papilla and secondary hair germ. Figure adapted[8] and created with Biorender.

1.1.1. Interfollicular epidermis (IFE)

The IFE is the main structure of the epidermis, and is the region of the stratified epidermis flanking hair follicles. It is formed of four layers; basal layer, spinous or suprabasal layer, granular layer and the stratum

corneum or cornified layer (**Figure I1.2**). These layers are formed mainly of keratinocytes at different stages of differentiation[4].

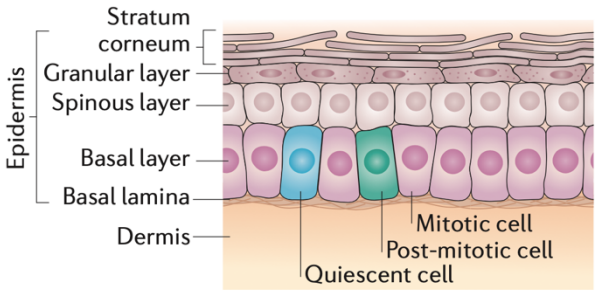

Figure I1.2. The interfollicular epidermis (IFE). The layers of the IFE include the basal layer, spinous layer, granular layer and stratum corneum. Epidermal stem cells (epSCs) are located in the basal layer, and they can divide to give rise to either mitotic or progenitor cells or post-mitotic or committed cells. These cells are in direct contact with the basal lamina, which constitutes a portion of the basement membrane that separates epidermis from dermis. Figure obtained from publication[1].

- **Epidermal Stem Cells (epSCs)**

Epithelial tissue homeostasis is maintained by epidermal stem cells (epSCs), which are present in the basal layer of the IFE and are unipotent progenitors. Unipotent progenitors are defined by their self-renewal capacity and their ability to differentiate towards the cell lineages of their tissue of origin[9].

The epidermis has a high turnover rate due to the continuous shedding of its outermost layer, and these epSCs maintain a constant number of renewing cells. They divide in a stochastic manner, as they can undergo either an asymmetric or symmetric division. In the asymmetric division, one daughter cell remains a SC and continues its self-renewal, and the other becomes committed towards terminal differentiation. Symmetrical cell division gives rise to two daughter cells with the same fate, which can be either the generation of two SCs (symmetric self-renewal) or two differentiated cells (symmetric differentiation) (**Figure I1.2**)[1,10].

When progenitor cells start terminally differentiating, they initially migrate towards the upper suprabasal layer. At the same time, they stop proliferating and detach from the BM as they move outwards in a columnar fashion. This is accompanied by remodeling of intracellular proteins and intercellular junctions, lipids that become secreted and cells losing their nucleus as they migrate through the different layers. This leads to a total cell differentiation and formation of the cornified layer as they reach the uppermost layer of the skin. This outermost cornified layer is composed of highly cross-linked and keratin-enriched cells named corneocytes that form a barrier and confer impermeability, stability and protection[2,3].

1.1.2. Hair follicles (HF)

HFs are mini-organs generated during embryogenesis as an appendage of the epidermis, and they give rise to hair shafts. HFs are composed of a permanent portion, which is formed (from top to bottom) by the junctional zone, the infundibulum, the isthmus and the bulge[1]. The sebaceous gland, the dermal sheath (DS) and the arrector pili muscle (APM) are also included as part of the HF (**Figure I1.1**). The sebaceous gland produces sebum, an antiseptic oily substance that helps with hair and skin surface lubrication. The DS is composed by a smooth muscle that lines the HF and is separated from the IFE by a thin basal lamina produced by the epithelium and two layers of collagen fibers likely secreted by the DS. The APM is also a smooth muscle formed by adjacent fibroblasts attached to the bulge responsible for piloerection[2,3,11].

- **Hair follicle stem cells (HFSCs)**

There are several pools of HFSCs in the HFs. The main one primarily resides in the bulge, which is the hair follicle region that limits the bottom

of the permanent portion of the HF, and comprises bulge epSCs (**Figure I1.1**). These HFSCs have major roles in hair follicle regeneration during anagen or hair growth[12]. However, there is also a pool of HFSCs which are crucial for hair growth situated in the secondary hair germ, which is an epithelial population present below the bulge and in direct contact with the dermal papilla (DP)[13]. This DP is a specialized mesenchymal compartment formed by fibroblasts at the base of HFs that communicates with neighboring epithelial cells and provide signals for HF generation[14]. There are other pools of HFSCs and progenitors at the HF, located at the infundibulum, isthmus and sebaceous glands[1,3,15]. All these HFSCs contribute to different hair growth stages and regions of the HFs, and the most relevant to this work will be further addressed in following sections[1].

- **Hair follicle cycle**

HFs undergo cyclic transformations from phases of growth (anagen), to regression or degeneration (catagen) and relative quiescence (telogen) (**Figure I1.3**). During these cycles, HFs go through morphological and molecular changes as HFSCs activate and proliferate, allowing the subsequent generation of a new hair shaft[1]. Of note, hair cycling is synchronized uniformly in the mouse during the first postnatal cycle. After this, hair cycles become asynchronous between individual follicles[2].

The hair growth stages are influenced by a number of growth factors, cytokines, hormones, *etc*, from which Wnt and bone morphogenetic protein (BMP) signaling are key in specification and activation of cells in the HFs in adult and during development[16]. More specifically, BMP signaling acts as a negative regulator of the hair cycle, whereas WNT signaling provides activating signals[17].

The hair growth phase is named **anagen**, and is divided into six sub phases, from I to VI. Anagen entry occurs when there are sufficient inhibitory signals for BMP as well as activation of WNT, which occurs

when the WNT effector β-catenin stabilizes in the nucleus[1,16,18]. These signals lead to the activation and proliferation of HFSCs, primarily those present in the secondary hair germ (anagen I). This could be due to these cells being the first responders to the generation of a new cycle, or due to the migration of bulge cells to the hair germ before the onset of hair growth[15,19]. Then, lower bulge epSC also become activated, and both these HFSC populations proliferate, change their shape and cause a rapid elongation of the HF, extending into the dermis and progressively surrounding the DP (this process starts with anagen II and ends with anagen III once the DP is completely invaginated)[18]. The HFSCs in the leading front that invaginate into the dermis are named matrix cells, which are highly proliferative and only survive during anagen[15,19,20]. This highlights the relevance of HFSCs localization in the niche, as it dictates their role in hair growth[21,22]. At this point, the sustained contact between matrix and DP cells leads to matrix cell differentiation, producing the inner root sheath (IRS), which is formed of seven different layers that will generate the hair shaft[15,20,23].

In addition, the continuous proliferation and differentiation of matrix cells around the DP leads to an upwards expansion of a column of differentiated cells (anagen III- anagen IV). This expansion continues until reaching the canal (anagen V) from which the new hair shaft exits from the epidermis, and causes a displacement of progenitor cells present in the developing HF (anagen VI). The displaced cells will then form the outer root sheath (ORS), which surrounds the growing hair follicle and is formed by a pool of heterogeneous epithelial cells[20,22,23].

Catagen is the transition phase between anagen and telogen. During this phase, there is massive apoptosis of cells in the lower portion of the HFs and in the ORS, causing epithelial HF regression. The cells from the ORS that remain after apoptosis migrate back and take part in forming the new secondary hair germ for future cycles[15,24]. Finally, **telogen** is a stage of relative quiescence, in which there is an apparent inactivity at the cellular

level. At this stage, there are inhibitory BMP signals coming from the DP, as well as from dermal fibroblasts and adipocytes that avoid HF growth activation[24].

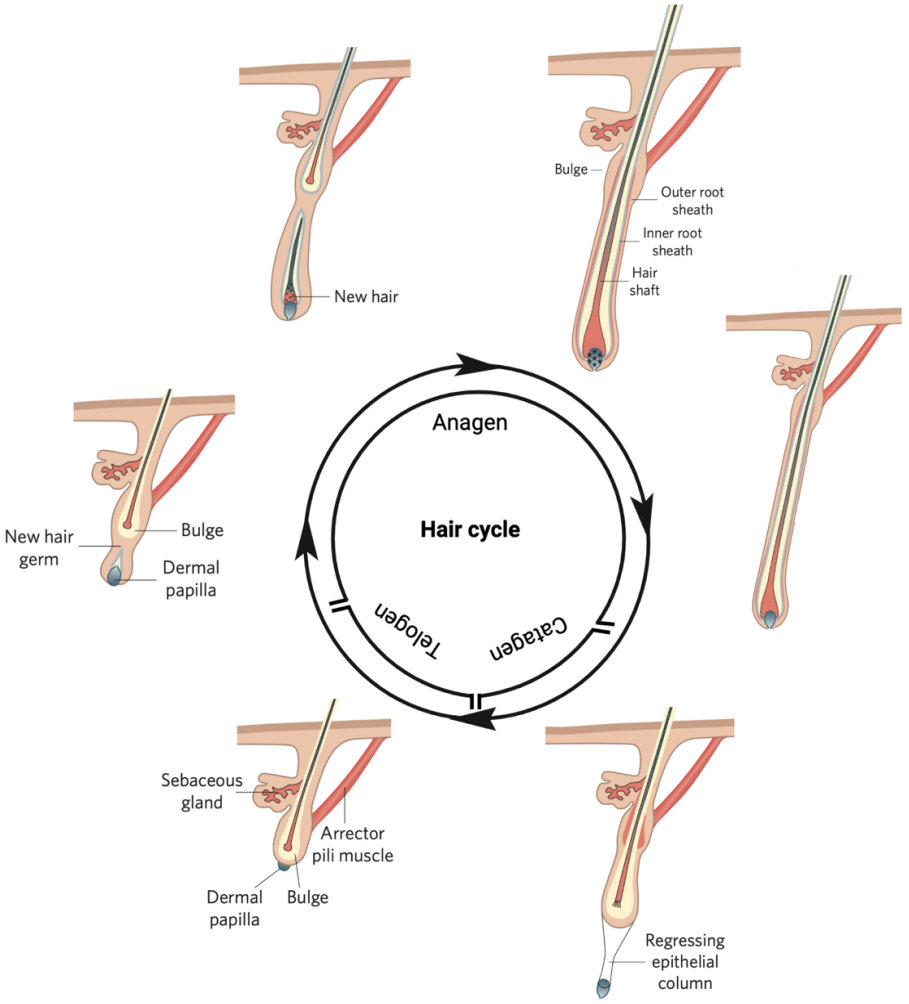

Figure I1.3. The hair follicle cycle. Summary of the hair follicle cycle, which includes phases of growth (anagen), degeneration (catagen) and relative quiescence (telogen). During anagen, there are several subphases of growth that include the activation of HFSCs, which proliferate and elongate the HF, extending into the dermis. Then, the interaction formed in this phase between DP and highly proliferating matrix cells leads to matrix cell differentiation, forming the hair shaft, IRS and ORS. Catagen includes apoptosis of cells in the lower portion of the HF, which leads to epithelial HF cell regression. Telogen is a stage of relative quiescence, with an apparent inactivity. Figure adapted from publication[23], modified with Biorender.

- **Other hair follicle stem cell (HFSC) functions**

HFSC functions are mainly related to HF generation, but they have also been described to have other specific roles. In stressful situations, HFSCs can differentiate and have functions different from those they have under homeostatic conditions[10]. Primarily, bulge epSCs have been shown to be very plastic, as they can give rise to all epithelial cell types in the HF[12]. In addition, bulge epSCs are crucial in wound repair. They have been shown to respond rapidly after injury, as they exit the bulge, migrate to the sites of injury towards the center of the wound, and proliferate, acquiring an epidermal phenotype. Nonetheless, this function is relevant only for acute injury, as these are eliminated from epidermal sites after a short time[25,26].

1.2. Dermis

The dermis is located beneath the epidermis, and these two layers are linked by a structure named basement membrane (BM). This BM is enriched in type IV collagen and laminin produced by epidermal keratinocytes and dermal fibroblasts[27].

The dermis is a mesenchymal tissue that includes a wide variety of cell types and compartments, such as fibroblasts, blood vessels (including endothelial cells, smooth muscle cells, and pericytes), lymphatic vessels, neural cells, sensory receptors, and immune cells (**Figure I1.4**). There are also epidermal structures that are invaginated into the dermis such as hair follicles (HFs), sweat glands, sebaceous glands and the arrector pili muscle (APM) (**Figure I1.1**)[27-29]. All these cell types reside in the rich ECM mesh, mainly type I and III collagens, proteoglycans and elastin that serve as a structural scaffold.

1.2.1. Dermal layers

The dermis can be divided into two layers: papillary and reticular. The upper papillary layer is distinguishable from the lower reticular dermis by the higher fibroblast density and by thinner and poorly oriented collagen fibers (primarily collagen I and III) that give support to the basement membrane. Opposite to this, the reticular dermis includes a high abundance, dense and directionally oriented fibrillar collagen with higher amount of collagen III[29-31].

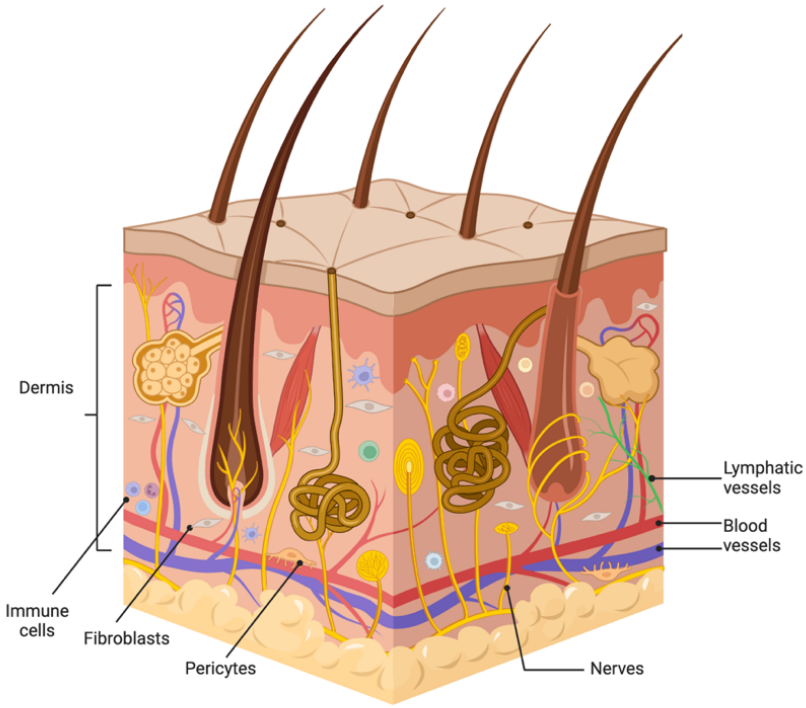

Figure I1.4. The dermis. The dermis is located beneath the epidermal layer. It is composed of several components including invaginations of structures from the epidermis such as hair follicles (see **Figure I1.1**). The main dermal cell types include fibroblasts, endothelial cells (as part of blood and lymphatic vessels), neural cells (primarily Schwann cells), and pericytes. Figure created with Biorender.

- **The extracellular matrix (ECM)**

The ECM is a highly flexible and dynamic scaffold that undergoes continuous remodeling and restructuring. It is contained in the interstitial space of the dermis, gives physical support and interacts tightly with the variety of dermal cell types and structures. It provides mechanical stability to the skin and helps it to adapt to its environment, as it senses the continuous changing conditions occurring and facilitates cell communication through its tight network[31-33].

The ECM is composed of collagens, elastic fibers, glycoproteins, proteoglycans, glycosaminoglycans and several matricellular and matrix-associated proteins. Collagens are the main components of the ECM and are primarily secreted by fibroblasts, although basal keratinocytes have also been shown to express certain collagens[34]. Collagen types I, III and V are the main collagen types in the interstitial dermal matrix. They provide tensile strength and their specific distribution varies depending on the dermal layer (see 1.2.1. Dermal layers). Elastic fibers are mostly formed by elastin and microfibrils (mainly fibrillin-1 and -2), where microfibrils wrap around elastin. Elastin then covalently binds to collagen and other components to provide the ECM with tissue elasticity and resilience to stretching[31,33]. Fibronectin is the main glycoprotein forming the ECM, followed by laminin, which forms the BM. Their functions include collagen fiber stabilization, to provide either flexibility or rigidity, as well as to act as ligands providing anchor points to the ECM for cell surface receptors. Then, proteoglycans in the ECM are heavily glycosylated and accompanied by glycosaminoglycans side chains. These proteoglycans/glycosaminoglycans polysaccharides are in charge of regulating hydration and ion homeostasis, as they take in water molecules and store ions. Finally, matricellular and matrix-associated proteins (such as tenascins) are composed by regulatory proteins with binding sites for matrix molecules and cell surface receptors, and have regulatory roles[31,33].

The ECM is linked to the cellular cytoskeleton and to cells in the niche through integrins, which are a family of heterodimeric transmembrane receptors comprising of $\alpha\beta$ subunits that combine to form a variety of heterodimers. Integrins signal through the cell membrane in a bi-directional manner (transporting information inside and outside of the cell), and can regulate processes like cell adhesion, migration, proliferation, differentiation and apoptosis. In addition, coupling of integrins to the cytoskeleton can generate traction forces as well as cell shape and mechanics (see 5.1. Mechanical forces in the skin)[32,35].

1.2.2. Dermal cell types

The most common cellular cell types of the dermis are fibroblasts, immune cells, blood and lymph vessels, pericytes and nerves (**Figure I1.4**). All these cell types create a complex network of cells that interact to help support the skin[30].

- **Fibroblasts**

Dermal fibroblasts are an essential component of the skin. They are the most abundant cell type in the dermis, and are crucial for regulating skin physiology[36]. Fibroblasts continuously deposit and remodel their surrounding ECM, and they can modulate the mechanical properties of their environment. They are also capable of regulating immune responses in the skin by expression of a diversity of cytokines, and can respond to inflammatory stimuli[22,36]. Moreover, fibroblasts are crucial to respond upon tissue damage. When sensing damage, fibroblasts can quickly activate and migrate towards the injury site, and can either differentiate into contractile myofibroblasts and/or increase ECM deposition and remodeling to deal with the injury[36-40]. However, even if having a role in wound repair is a common feature across fibroblasts,

there are differences in the specific step and resulting tissue they contribute to[38,41-43].

In addition, the differences in ECM composition in the dermal layers mentioned above (see 1.2.1. Dermal layers) reflect fibroblast heterogeneity. Fibroblasts can be defined as either papillary or reticular, depending on where they reside, and present specific functions based on their localization[28]. Upper papillary fibroblasts are described as important for hair growth and piloerection, as they include fibroblasts in the DP as well as those associated to the APM (epidermal specialized structures, see 1.1. Epidermis). Fibroblasts residing in the reticular dermis are responsible for producing the densely packed and thick collagen bundles that form the ECM and provides the skin with its mechanical strength[30,42].

Nonetheless, this fibroblast distinction is mostly evident in neonatal mouse skin and fades as organisms mature[28]. Actually, sequencing studies in adult skin reveal that transcriptional profiles mostly overlap across fibroblasts in different skin layers[44]. This leads to hypothesize that the different characteristics and functions of the dermal layers are a result of a combination of cell types and fibroblast types working together[30]. Advances in the field are allowing for a better understanding of the diversity of these cells, although there is still much to be known about the similarities and differences they present.

- **Immune compartment**

The skin forms the first line of immunological defense against external insults and infections. The dermis contains a diversity of cells of hematopoietic origin, including populations of myeloid and lymphoid lineages[28].

a. Myeloid cells

Skin-resident myeloid cells contribute to skin homeostasis by secreting growth factors, phagocytosing debris and apoptotic cells, and by supporting vascular integrity. In inflammatory conditions, they are one of the first responders, secreting pro-inflammatory factors that activate surrounding cells. With this, they act as a link between innate and adaptive immune response[45].

Dermal dendritic cells (dDCs) are professional antigen-presenting cells that act during adaptive immune responses. They are responsible of maintaining homeostasis between host and skin-resident commensal bacteria[46]. There are two types of dDCs, DC1 and DC2. DC1s are associated with Th1 responses, while DC2s are the most abundant subtype in murine skin, and their activity is related to Th2 and Th17 responses[45].

Macrophages inspect the tissue and are one of the first cell types detecting and responding to external antigens. There are macrophages that can support tissue repair by aiding in granulation tissue formation (based on newly formed ECM, blood vessels, macrophages and fibroblasts that cover the wound), and by accelerating re-epithelialization in case of wounding[47]. They are plastic, and can be categorized based on their functions as pro-inflammatory (M1) or anti-inflammatory and pro-repair (M2). This distinction was widely accepted for years, but lately it has been shown that macrophages can express markers from both subtypes simultaneously and this nomenclature is being abandoned[48].

Monocytes traffic through the skin and support DCs and macrophages in their functions. They carry out surveillance through the dermis and transport antigens to draining lymph nodes. They are also recruited during inflammation, and can either differentiate to macrophages or dDCs, or carry out their functions without differentiating[49]. Besides, monocytes are plastic and mobilize in large numbers to inflamed sites to

provide inflammatory resolving activities, dually acting as pro-inflammatory and/or regulatory[50].

Mast cells are mainly located in the upper dermal section. They travel to the skin from the bone marrow and mature locally when receiving specific signals[51]. This population is regulated by the skin microbiome, and germ-free conditions lead to a fewer amount of mast cells. They have granules that contain predominantly histamine, and are related with allergic reactions[45].

There are **other myeloid cells** present in the dermis in small numbers, such as neutrophils and eosinophils, which survey the dermis for pathogens[52].

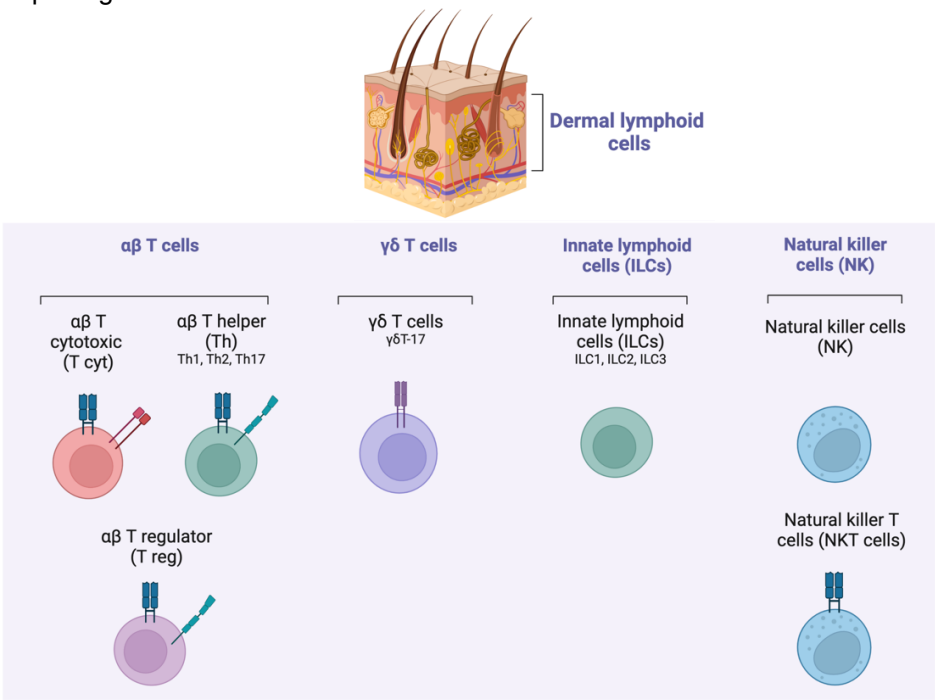

Figure I1.5. Lymphoid dermal cell subsets. The dermis includes several lymphoid cell types, and the most relevant ones to this work are summarized here. These are αβ T cells, which are mainly formed by subtypes of T cytotoxic cells (T cyt), T helper cells (Th), which include several subsets, and T regulatory cells (T reg). Also, γδT cells, which includes γδT17 cells, innate lymphoid cells (ILCs), and natural killer (NK) cells, including a subset of NK T cells (NKT cells). Figure created with Biorender.

b. Lymphoid cells

The skin is home to several types of lymphoid cells, which are crucial for both steady state and inflammatory responses. These consist of αβ T cells, which are mainly formed by subtypes of T cytotoxic cells (T cyt), T helper cells (Th) and T regulatory cells (T regs); γδ T cells, which include a subgroup of γδ T17 cells; innate lymphoid cells (ILCs); and natural killer (NK) cells, including a subset of NK T cells (NKT cells) (**Figure I1.5**).

αβT cells express the conventional αβ TCR as well as CD3+ in their membrane. They include the **T cytotoxic cells** (T cyt), which are also known as T effector cells and are characterized by expression of CD8+ in their membrane, and have potent cytolytic functions. They also include **T helper cells** (Th), which are characterized by expression of CD4+ in their membrane. Their main functions are to recruit and activate other immune and non-immune cells, and can also have cytolytic functions. These activated αβ T cells (T cyt and Th) are crucial following injury and infection, but are also kept once the tissue has healed. This includes long-lived circulating memory T cells, effector-memory T cells (which circulate peripheral tissues), and tissue-resident memory cells (TRM)[53]. These TRM are crucial reacting to secondary challenges, as they are much faster responding to known insults than the non-resident memory T cells. Most TRM cells belong to the T cyt subset[54].

There are several subsets of skin Th cells, namely Th1, Th2 and Th17. Th1 cells are characterized by a high production of Interferon-γ (IFN-γ) and differentiation towards this subtype is controlled by interleukin (IL) -12 and IL-18. Their functions are crucial for clearing intracellular pathogens. Th2 differentiation is triggered by IL-4, and these cells organize host defense against pathogens and help B cells to produce antibodies by secreting IL-4, IL-13 and IL-25. These subtypes are mostly considered to be mutually exclusive, as IFN-γ and IL-4 antagonize each other[55,56].

Th17 are known to produce IL-17, IL-21, IL-22, and IL-23, and are responsible for the clearance of pathogens that are not correctly cleared by Th1 or Th2. They have also been described as potent inducers of inflammation, and are associated with the pathogenesis of many autoimmune diseases such as psoriasis[55]. These cells usually require specific cytokines, such as transforming growth factor-β (TGF-β) combined with IL-6 or IL-21, and expression of the transcription factor (TF) retinoic acid-related orphan receptor (RORγt) for their differentiation. These cytokines (particularly TGF-β and IL-6) synergize to induce RORγt expression by activating the TF STAT3, which is crucial for Th17 development[57,58]. After differentiation, IL-23 is implicated in Th17 stabilization and expansion[57].

T regulatory cells (T regs) form a specialized immunosuppressive lineage of CD3+ CD4+ lymphocytes, defined by the expression of the TF FOXP3. Their most well-known function is immunomodulatory, but they can also take part in homeostatic tissue maintenance and repair after injury[53]. In inflammatory conditions, their numbers increase around stem cell niches, where they secrete several factors that promote stem cell renewal, tissue repair, and dampening of inflammation[59,60].

γδ T cells, the dominant T cell population in murine skin, are innate cells acting as sentinels, and providing early immune responses. They are characterized by expression of CD3 and CD4 and the non-conventional γδ TCR, as well as of the nuclear retinoid orphan receptor RORγt[53]. Their role is crucial in processes like wound healing, skin inflammation and protection against external microbial infections[45]. A large fraction of these cells can acquire their effector function during thymus development, which leads to a quick functional response and cytokine secretion after stimulation[61].

γδ T cells can become polarized towards different cytokine production, and the most relevant to this work is IL-17, which leads to **γδ T17 cells**.

These cells are the major IL-17 producers in settings like homeostasis, infection, autoimmunity and cancer[62]. In this case, they are defined as having an 'innate-like' activation because stimulation with IL-1β and IL-23 is sufficient to activate their cytokine secretion even in absence of TCR stimulation. This excessive and rapid secretion of IL-17 underlines the key role of γδ T17 cells in settings such as psoriatic disease, as they have been shown to be crucial in cytokine secretion related to disease progression. Thus, these cells have dual roles in homeostasis versus inflammatory contexts, which are topics being currently investigated[61,63,64].

Innate lymphoid cells (ILCs) produce similar cytokines to Th cells and coordinate immunity and inflammation, and do not express the major surface molecules that recognize other immune cells. They can be divided into three subsets, ILC1 to ILC3. ILC1 cells include NK cells, produce cytokines such as tumor necrosis factor (TNF) and IFN-γ and aid in anti-viral and anti-parasite immune responses. Group 2 ILCs (ILC2) produce cytokines such as IL-4 and IL-13 and they contribute to tissue repair and parasite elimination. Group 3 ILCs (ILC3) can produce IL-22 and IL-17, and express the RORγt receptor. Their functions include fighting against extracellular microbes. They have also been associated to the pathogenesis of psoriasis, as they accumulate in the skin of these patients and promote inflammation[47,65].

Natural killer (NK) cells are innate lymphoid cells important for early immune responses against infections, and their main role is to produce cytotoxicity by cytokine secretion[66]. They have also been described to be relevant for autoimmune disease progression[66]. From these cells, there is a subset of **NK T cells,** which are unconventional innate-like cells that express αβ TCR receptor and have a crucial role in antimicrobial immune responses. They represent a very small fraction of cells in the dermis, and can have both immunosuppressive and immuno-stimulatory functions depending on the specific stimuli[67].

- **Vascular and lymphatic vessels**

There are two major types of vasculature: lymphatic and blood vessels, both crucial for skin homeostasis. Lymphatic and vascular vessels include an inner layer of specialized endothelial cells (ECs) that form the lumen of the vessel tube. ECs are heterogeneous, as they differ in their properties depending on the location (i.e. in the skin there is microvasculature), and on the type of vessel[68,69]. Angiogenesis and lymphagiogenesis are defined as the growth of vessels from existing ones, and are known to be indispensable for processes such as wound healing and the hair growth cycle[70-72].

The **lymphatic** vasculature is involved in intestinal fat absorption and immune surveillance, as well as draining excess tissue fluid back into the blood circulation. The **blood** vasculature is essential for trafficking, delivery and exchange of gases, hormones, metabolic waste and immune cells and factors. There are three types of blood vessels, arteries, veins and capillaries. Arteries specialize on controlling vascular tone and veins are the primary site of leukocyte trafficking from the blood into the tissue (especially at post-capillary sites). Capillaries are the main areas of oxygen exchange between arteries and veins, as arteries contain oxygenated blood and veins carry blood with lower oxygen levels. In the case of the dermis, the vascular system is composed of microvasculature, which translates these vessel types into arterioles, venules and capillaries. These vessels maintain their corresponding functions, but are smaller in size[68,73].

The role of blood vessels during immune processes has been addressed throughout the past[73-75]. More specifically, venule ECs have been shown to be extremely relevant during inflammatory processes due to their close contact with circulating lymphocytes at post-capillary areas. At these sites, venule ECs present a higher permeability than adjacent ECs, which is why these areas are named as 'perivascular extravasation units'[76].

Resting ECs do not interact with leukocytes, but when activated they express adhesion molecules that mediate leukocyte attachment such as P-selectin and E-selectin[74]. This expression leads to adhesion and rolling of leukocytes through the endothelium specifically at perivascular extravasation units, where the leukocytes can extravasate into the tissue and migrate towards the affected area[73].

Additionally, it has been shown that T cells, DCs and macrophages can form transient clusters around the perivascular extravasation units termed iSALT (inducible skin-associated lymphoid tissue), which provide sites for antigen presentation in the skin. This structure has been described in various immunogenic contexts and aids in extravasation as well as in antigen presentation processes[52,77,78].

Antigen presenting is a primary adaptive immune response that occurs when foreign antigens are presented to T cells by professional antigen presenting cells (APCs, like DCs and macrophages), and in some cases by non-professional antigen presenting cells. ECs have been shown to act as non-professional APCs, as they can express in their surface molecules belonging to major histocompatibility complexes (MHC) I (expressed on almost all nucleated cells) and II (expressed only in professional and non-professional APCs)[52,79,80]. Although the expression of MHCII has been linked to chronic and autoimmune inflammatory diseases, this is still under study[80-84].

- **Pericytes**

Pericytes are located around blood vessels (termed as perivascular cells), specifically within the basement membrane of arterial, venous and lymphatic vessels. They interact with endothelial cells to regulate blood flow by vessel constriction, and they can also maintain vessel wall integrity, permeability and control angiogenesis[29].

- **Schwann cells**

Schwann cells are neural crest-derived glial cells present in the peripheral nervous system (PNS). Accordingly, they are also present in the dermis, accompanying dermal nerves. These cells can differentiate towards myelinating or non-myelinating Schwann cells, although the majority of the cells present in the dermis are unmyelinated. Their functions include repair, axon regeneration after injury to the PNS, cutaneous wound healing and initiation of pain sensation[85-87]. When responding to injury, they dedifferentiate towards a precursor-like state, undergo epithelial-to-mesenchymal-like transformation and migrate towards the site of damage. In addition, they also secrete inflammatory mediators and growth factors, proliferate and remodel the extracellular niche to promote regeneration[87,88].

Schwann cells have also been described as relevant in skin diseases such as psoriasis, as these patients have been shown to present significant degeneration of superficial nerves accompanied by Schwann cell proliferation, activation and degeneration, pointing towards the crucial role of these cells in tissue regeneration[85,89].

1.3. Hypodermis

The hypodermis is formed by a thick layer of white adipocytes, composed of a mixture of pre-adipocytes and mature adipocytes, and blood vessels. This layer is responsible for responding to changes in systemic nutrient availability, and to local signals from HFs[30,90].

2. IL-17 signaling

The IL-17 cytokine family is composed of six members (IL-17A to IL-17F) that mediate their functions through the IL-17 receptors (IL-17RA to IL-17RE). The most well-studied family members are IL-17A and IL-17F, which are very closely related in structure and function and can act as either homodimers or heterodimers[91,92]. They mainly bind to IL-17RA and IL-17RC receptors, although IL-17RD has also been described to be bound by IL-17A[93].

2.1. IL-17 downstream effectors

IL-17A and IL17F (IL17A/F) signaling starts after binding to their receptors, which leads to ACT1 protein recruitment and activation. ACT1 interacts with IL-17 receptors through a cytoplasmic domain named SEFIR (similar expression to fibroblast growth factor genes and IL-17R), which is present in both ACT1 and IL-17 receptors. Then, ACT1 activates several signaling pathways through TNF-receptor associated factor (TRAF) proteins. The most well-known factor is TRAF6, and its activation triggers potent inflammatory pathways, which are the CCAAT/enhancer-binding TF protein (types C/EPBβ and C/EPBδ), mitogen-activated protein kinase (MAPK) (leading to AP-1 TF activation) and canonical nuclear factor-κB (NF-κB) signaling pathways[92,94] (**Figure I2.1**). C/EPBβ and C/EPBδ TFs, as well as MAPK and AP-1 signaling pathway activation, are triggered by extracellular signal-regulated kinase (ERK1/2), JUN N-terminal kinase (JNK) and p38 in a TRAF6-dependent manner[92] (**Figure I2.1**).

Nonetheless, even if these are all important inflammatory pathways, the canonical NF-κB pathway is the best described target of IL-17 signaling as well as the most relevant for this work. Canonical NF-κB activation occurs through IκB kinase (IKK) activation and IκBα degradation, and is known to occur when this pathway is activated by TRAF6[94,95]. This in turn

leads to NF-κB TFs p50 and p65 (p50/p65; p65 also known as RELA) activation, which are the most common heterodimers in the NF-κB signaling pathway. In basal conditions, p50/p65 are sequestered in the cytoplasm by proteins from IκB family (mainly IκBα), but when there is canonical NF-κB activation, IκBα is degraded and p50/p65 are liberated[92,96]. Then, these heterodimers can translocate into the nucleus and bind to the DNA to activate the expression of inflammation-related genes (**Figure I2.1**). All of this contributes to the generation of a pro-inflammatory context by IL-17 signaling.

2.2. IL-17 in the skin

IL-17A/F are mostly produced by Th17, γδ T17, ILC3, NKs, NKT and mast cells in the skin. In addition, the target cell types for IL-17 signaling, which express IL-17RA and IL-17RC include fibroblasts, macrophages, and keratinocytes[94].

IL-17A/F functions in the skin are mainly related to microbial clearance, as they are one of the first responders when a pathogen enters through the epidermal barrier. In this scenario, innate immune cells recognize pathogen-associated molecular patterns (PAMPS) expressed by the entering pathogens using their pattern recognition receptors (PRRs), and become activated. There are many PRR families, where the most well-known are the Toll-like receptors (TLRs), which recognize PAMPs such as lipids, lipoproteins, proteins, and nucleic acids in external pathogens[97]. These activated immune cells present antigens and further activate T cells and other immune cells, which in turn secrete a variety of pro-inflammatory cytokines including IL-17A/F. This leads to an increased immune recruitment, including macrophages and neutrophils, which clear out the pathogen[98]. Nonetheless, IL-17A/F can also have other functions, as they have also been described as crucial for epithelial wound healing in coordination with hypoxia-inducible factor 1-α (HIF1α)[99], as well as a

major pathogenic cytokine in multiple autoimmune and inflammatory diseases[92,98,100].

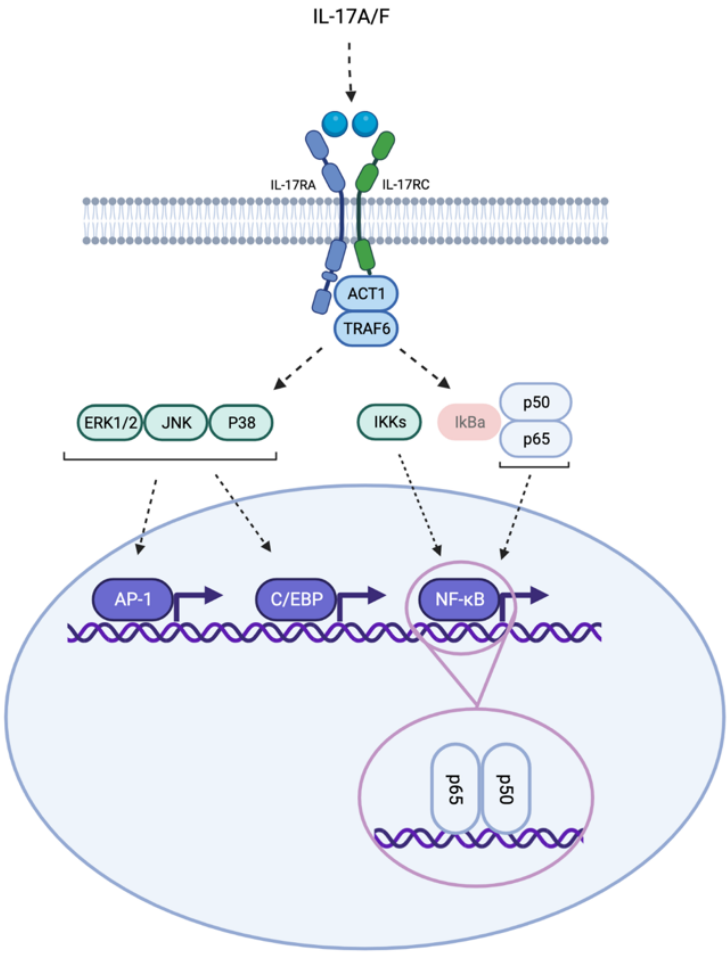

Figure I2.1. IL-17A/F downstream signaling pathway. Summary of IL-17A/F signaling pathway, in which they can signal through IL-17RA and IL-17RC receptors as homo or heterodimers. This leads to triggering of ACT1 and TRAF6, which then activate pro-inflammatory pathways including the canonical nuclear factor-κB (NF-κB), CCAAT/enhancer-binding protein (C/EPB) family, and the AP-1 TF. During NFκB activation, there is IKK stimulation and IkBα degradation. This leads to p50/p65 complex liberation and translocation into the nucleus, leading to the expression of inflammatory genes. For C/EPB and AP-1 signaling, there is an activation of ERK1/2, JNK and p38 in a TRAF6-dependent manner, all of which leads to both signaling pathways being triggered. Figure created with Biorender.

This variety of functions and downstream effectors means IL-17 signaling must be tightly regulated, as defective IL-17 production allows the expansion of external pathogens, and excessive IL-17 production causes damaging immune responses. These damaging inflammatory responses include the progression of autoimmune diseases, as there are several that have been directly related to excessive IL-17 production[98,101]. This is the case of psoriasis, which is an autoimmune chronic inflammatory disease of the skin. Psoriasis is characterized by a deep modification and hyperproliferation of the epidermis, and causes an alteration in keratinocyte differentiation accompanied by the presence of inflammatory infiltration and neo-angiogenesis in the skin[102]. IL-17A/F are pinpointed as key factors that lead to psoriasis initiation, and have been successfully used as targets for disease treatment. Blockade of IL-17A/F using neutralizing antibodies has led to greater skin clearance when compared to other methods targeting other steps of the disease[91,102-104].

3. Skin aging

Aging can be defined as a decline or loss of adaptation during the pass of time, caused by a general and progressive deterioration that affects most living organisms[105,106]. Aging is caused by a combination of factors, and some years ago there were several cellular and molecular hallmarks of aging. They were proposed to contribute and determine the aging process and phenotype, and have been recently updated[106-108].

The skin shows deep structural and functional changes during aging, including dermal and epidermal thinning, loss of dermal elasticity and wrinkling, increased frailty, impaired wound healing, and compromised barrier function and immune response[109-111]. Some of these are specific to each skin layer, and will be addressed in the following text divided in epidermal and dermal age-related characteristics.

3.1. Epidermal aging

Aging causes a deterioration of the epidermis, including characteristics such as a thinner IFE, a thicker cornified layer, a flattening of the dermal-epidermal junction and thickening of the BM, a sustained pro-inflammatory context as well as overall changes in epidermal polarity and architecture[110,112-114]. As for epSCs, they lose the expression of the hemidesmosome component collagen XVII α-1 chain (COL17A1) during aging[111]. The hemidesmosome is a protein complex (including mainly integrins α6 and β4) that connects epidermal cells to the ECM, and is crucial for homeostasis[115]. Thus, aging leads to an overall proteolysis of COL17A1 in epSCs, leading to hemidesmosome fragility and promoting skin aging[111]. Nonetheless, the number of epSCs is thought to be retained throughout the aging process[110,116].

The appendages present in the epidermis also present age-associated changes. HFs show a reduced size, density and regeneration potential, sweat glands are smaller and scarcer, and sebaceous glands become hypertrophic[110,111,113]. All these changes affect the epidermal regenerative potential and barrier function, and are further aggravated by changes in their daily oscillations (see 4.3. Aging of the circadian clock). The most relevant epidermal age-associated changes related to this work will be further described in the following sections.

3.1.1. Defective barrier function

The physical skin barrier is mostly formed by the cornified layer, which increases its thickness during aging and decreases the content of structural proteins crucial for barrier integrity (including filaggrin and loricrin). This, combined with other deteriorating characteristics, leads to an alteration of the permeability of the skin[117].

Skin permeability is commonly measured using trans-epidermal water loss (TEWL), which measures water vapor evaporation from the skin immediately on its surface.

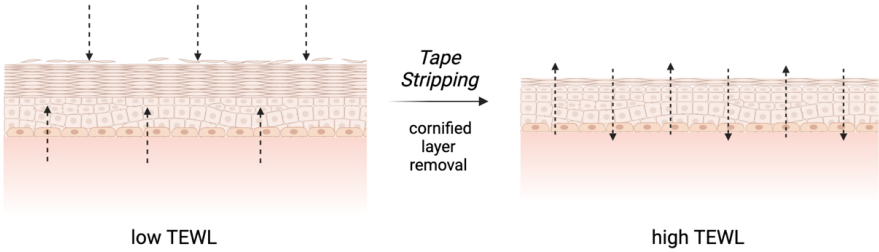

Figure I3.1. Trans-epidermal water loss (TEWL) as a measure of water evaporation in the skin. Schematic representation of TEWL levels before and after cornified layer disruption by means of tape stripping. There is a low TEWL value when there is an intact cornified layer and an impermeable skin barrier. The TEWL evaporation value is increased when the cornified layer is removed by tape stripping, affecting the impermeability of the skin. Figure created with Biorender.

Basal TEWL values have shown no clear differences during aging, but significant differences have been observed after challenge, such as acute barrier disruption[117-120]. Cornified layer disruption is commonly achieved by tape stripping, which is a well-established model of skin injury. This procedure mechanically removes the cornified layer using adhesive tape, leaving the adjacent basal layer and dermis relatively uninjured. This damage affects the permeability of the skin, as decreased cornified layer thickness leads to increased water evaporation and, concordantly, higher TEWL values[121-123] (**Figure I3.1**).

Tape stripping also forces a re-epithelialization and regeneration response in the epidermis, activating keratinocyte proliferation and differentiation to restore barrier function. The speed of cornified layer recovery is delayed during aging, which is reflected by higher TEWL values along time[118,120]. Thus, TEWL values after tape stripping have been used as surrogate measures of decreased barrier function during aging.

3.1.2. Wound healing impairment

Wound healing impairment has been included in the epidermal aging section, although it also involves dermal aging. When the skin is injured, the SCs and niche cells must respond rapidly to deal with the damage and restore the affected barrier. This process is termed wound healing (WH), and is divided into three phases: inflammation, tissue formation and tissue remodeling[124,125]. Inflammation takes place immediately after the wound is formed and includes the generation of a scab and recruitment of immune cells. These cells, primarily leukocytes, secrete pro-inflammatory cytokines promoting angiogenesis, migration and proliferation of surrounding keratinocytes and fibroblasts. Then, tissue regeneration includes the formation of granulation tissue, which consists of newly formed ECM, blood vessels, macrophages and fibroblasts that cover the wound. At this stage, epidermal cells activate and migrate towards the granulation tissue to re-epithelialize the wound[3,126] (**Figure I3.2**).

During the last phase of tissue remodeling, epidermal cells and fibroblasts deposit newly formed ECM proteins to provide support to the repaired tissue. There must also be a complete maturation of the newly obtained epidermal cells, which includes the complete loss of nucleus of the epidermal upper layers (orthokeratosis)[126-128] (**Figure I3.2**).

During aging, there is a delay in the speed and efficiency of wound healing. This is caused by an ineffective immune infiltration, angiogenesis, ECM production and epithelialization, as well as a loss of communication between epidermal and immune cells[129-132]. There is also an incomplete maturation of epidermal cells, as the nucleus is retained in the upper cornified layer of the epidermis (parakeratosis), as well as a defective formation of granulation tissue[133]. This all leads to an inefficient barrier regeneration post-injury during aging.

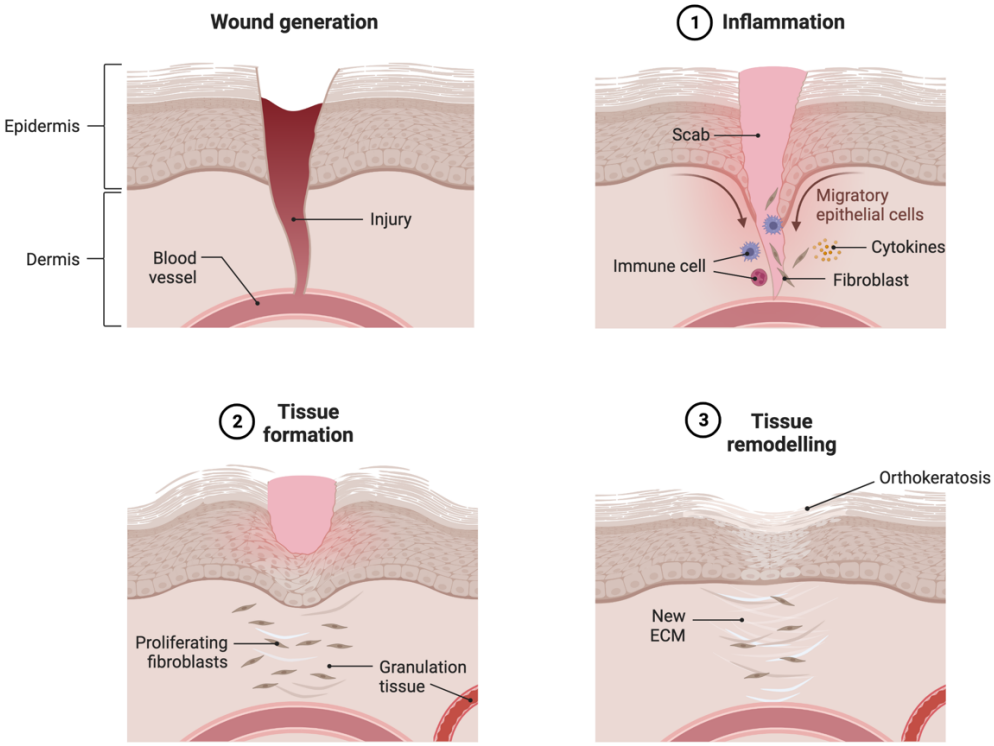

Figure I3.2. Steps in the wound healing process. WH starts with injury generation, and the first step into healing is inflammation. There is scab formation, immune cell recruitment, pro-inflammatory cytokine secretion, and migration of keratinocytes and fibroblasts at this stage. The next step is tissue formation, which includes the generation of granulation tissue, including new blood vessels, and recruitment of macrophages and fibroblasts that aid in the healing process. In the last stage there is tissue remodeling with newly generated ECM deposited, and complete maturation of keratinocytes or orthokeratosis (loss of the nucleus of cells in the upper epidermal layers). Figure created with Biorender.

3.1.3. Hair follicle degeneration

Skin aging is accompanied by changes in HFs and HFSCs, which include hair loss and greying at the macroscopic level. At the cellular level, aged HFs present a reduction in hair cycling characterized by a difficulty to enter the growth phase (anagen), leading to a decreased hair density and to HF miniaturization[134,135]. This is driven by the prolonged DNA damage that occurs during aging, which leads to proteolysis of COL17A1. This

hemidesmosome component is critical for HFSC maintenance, and its loss causes HFSC to leave their niche when activated in the hair cycle. Then, HFSC commit towards the epidermal lineage and are gradually eliminated from the skin after terminally differentiating, which in turn causes gradual HF miniaturization and progressive loss[134].

At the same time, aged HFSCs can maintain their lineage identity while presenting ECM structural alterations that affect the bulge niche. This is accompanied by a decreased stem cell proliferative capacity, which has been shown to occur due to HFSCs escaping to the dermis. This phenomenon is regulated by FOXC2 and NFATC1, which become less expressed during aging and, thus, favor the escape[113,136,137].

At the epigenetic level, there is a reduction of chromatin accessibility in genes related to self-renewal and differentiation in aged HFSC. This occurs specifically in promoters of bivalent genes related to lineage specification that fail to activate efficiently, and is caused by age-associated increased mechanical stress in the skin[113].

Nonetheless, studies have shown that the aging phenotype of HFs can be partially rescued when transplanted into a young environment[113,138]. This leads to the hypothesis that HF aging is controlled and affected by both intrinsic stem cell characteristics and extrinsic environmental factors.

3.2. Dermal aging

During aging, there is a decrease of cell density in the dermis and an increase in subcutaneous fat. These changes affect the variety of residing cell types, where fibroblasts and immune cell type are among the most age-affected dermal components (detailed in the following sections). There are also architectural changes that occur primarily due to ECM changes in composition and structure.

3.2.1. Fibroblast aging

Fibroblast aging has been widely studied in the past years, and there are several traits of fibroblast aging, many of which are tissue specific, that have been described to better understand their aging process[139]. In the case of the skin, the main characteristics of aged fibroblasts are the reduction of ECM components production, the acquisition of adipogenic traits, a decrease in their efficacy to aid in wound healing, as well as the increase of pro-inflammatory factors that contribute to an increased inflammatory state[131,140-142].

More specifically, this increase in inflammatory characteristics has been related to senescence, a cell state or program that limits cell proliferation[143]. Fibroblasts have been shown to secrete, under specific scenarios, a profile of inflammatory factors and cytokines that have been termed as a senescence-associated secretory phenotype (SASP)[139,144]. This has been associated to aging progression because there is an increase in expression of SASP factors during aging, although there are studies that show that this mainly occurs in a geriatric and frail stage[145,146]. In the skin, senescence has been associated to an increase of a specific signature of secreted proteins (referred to as SAASP - skin aging-associated secreted proteins)[143,147-149]. However, there is no consensus as to what can be specifically described as senescence and SASP factors, and many studies have been terming aged fibroblasts as pro-inflammatory in order to better define them[131,140-142].

3.2.2. Extracellular matrix aging

The aging ECM presents a progressive degeneration, which is thought to be one of the main causes of skin aging. These changes include a reduction in the amount of total ECM (primarily of collagen) and an increase in its degradation, accompanied by a structural remodeling of its components. Collagen fibers show a high rate of age-related changes,

as they become fragmented and lose their organized distribution during aging. Moreover, aged fibroblasts are not capable of replenishing the damaged fibers efficiently, contributing to the ECM degeneration[150-152].

In addition, there are other ECM components that are affected during aging such as elastin, which accumulates in a crosslinked, fragmented and non-fibrillar organization, as well as an overall reduction of integrin expression[90,153]. This all leads to wrinkling as well as loss of elasticity and an increase of stiffness in aged skin[113,154,155].

3.2.3. Immune compartment aging

Deterioration of immune cell function and composition, as well as changes in pro-inflammatory cytokine signaling occur in aged skin. This is accompanied by a chronic and systemic low-grade inflammation, which has been termed as “inflammaging”. There is an overall increase of inflammatory cytokines in serum levels during aging (such as IL-6. IL-8, TNF-α), secreted in excess primarily by defective immune cells[156,157].

Hematopoietic stem cells (HSCs) have been shown to be biased in their cell divisions during aging. These cells divide preferentially in a symmetric manner during aging, whereas adult HSCs divide primarily asymmetrically[158]. This is driven by the expression of *Cdc42*, a small Rho protein of the family of hydrolase enzymes that bind to guanosine triphosphate (GTPase), which regulates actin and tubulin organization, cell-cell and cell-ECM adhesion, and cell polarity[159]. The expression of *Cdc42* is increased during aging, which in addition to specific epigenetic alterations, affects the polarity of cells and leads to the symmetric HSC divisions[159]. These age-associated symmetric divisions lead to daughter cells with decreased regenerative potential[158].

As for cell type specific age-related changes, myeloid cells in barrier tissues have been shown to increase in frequency during aging[160]. This occurs because there is an increase in HSC differentiation potential

towards the myeloid lineage, resulting in an overall increase in cell number. Moreover, their integrity and functions are affected during aging[158,161]. Also, the appearance of a new population of "frail monocytes" has been described in human peripheral blood. These monocytes express inflammatory markers, and downregulate genes important for their homeostatic functions such as activation and MHCII molecule expression[162]. Lymphoid cell aging has shown that the overall number of T cell subsets produced in the thymus and exported to other organs is reduced, particularly affecting the total number of naïve cells in tissues[163]. On the contrary, the number of NK cells increases with age, although these cells present a deterioration in their cytotoxic activity[163].

For this work, we will focus mainly in T cell aging. The aging of T cells is known to play a major role in tissue decline, and has been related to the development of autoimmune, autoinflammatory and infectious diseases[156]. These aged cells have also been shown to infiltrate aged niches which are usually void of T cells to promote inflammation[164]. Moreover, it has also been shown that defects in autophagy and mitochondrial bioenergetics can lead to an increase in Th-17 cytokine production driven by Th cells in the blood of aged individuals[165].

Aged T cells in the skin present an impaired T cell effector function, an increased number of resident Tregs, as well as the already mentioned reduced ratio of naïve T cells[163]. T cells have a crucial role in aggravating the inflammatory profile of the aged skin, although there is still much to be understood. This dampened cell type-specific immunity that emerges progressively contributes to aggravate the decay in overall skin functions during aging[166].

4. The circadian clock

Most organisms contain self-sustained circadian clocks that allow their anticipation to the rotation of the earth, generating 24-hour rhythm changes. These circadian clocks are molecular oscillators that permit maintaining periods close to 24 hours, which is reflected in mammalian behaviors such as sleep/wake cycle, body temperature fluctuations and circulating hormone levels[167,168].

Circadian clocks have to be periodically synchronized in order to adjust to time, and the main environmental entrainment factor or *Zeitgeber* (ZT, time giver) is the photoperiod or light cycle. There are other factors that can entrain these clocks to a specific time or phase, such as temperature, feeding, metabolic cycles, and neural or humoral changes. Nonetheless, it has been shown that circadian clocks can remember time in absence of external cues[169-172].

This entraining information is detected by the neurons of the hypothalamic suprachiasmatic nucleus (SCN). The SCN converts the information received and transmits it to other regions and peripheral organs, all of which outlines it as a master regulator of circadian clocks[170]. Then, this information is translated into a 24-hour rhythmic gene expression by the circadian clocks present in peripheral tissues. This rhythmicity presents specific characteristics, which are commonly summarized into parameters to better define the oscillatory expression pattern of genes (**Figure I4.1**)[173]. First, the oscillatory expression of genes is characterized by a specific amplitude, which is the difference between the maximum and a minimum of an oscillation. Then, the period length is the time span difference between two identical phase points (two maximum or two minimum points), which determines the duration of one cycle[173,174]. Finally, the phase reflects the timing of a reference point in the cycle within the 24 hours, for example the peak relative to the

beginning of the 24-hour cycle[173,174]. Thus, these parameters allow defining the circadian behavior of genes.

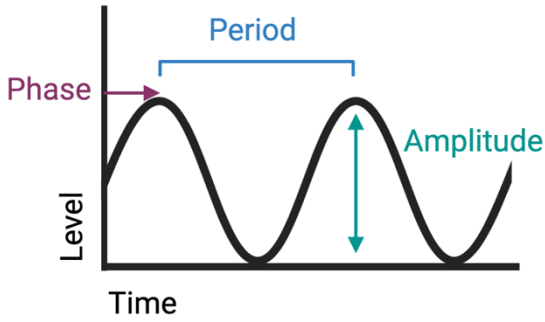

Figure I4.1. Parameters of circadian rhythmicity. A circadian rhythm oscillatory curve is depicted in which some parameters are specified. The amplitude of this curve is the difference between the maximum and the minimum of the oscillation. The period is the time span difference between two identical phase points. The phase refers to a specific timing of a reference point in the cycle, in this case the peak in relation to the beginning of the cycle. Figure created with Biorender.

4.1. The molecular circadian clock

The molecular mechanism that controls circadian clocks in mammals is formed by a cell-autonomous transcriptional and translational autoregulatory feedback loop. There is a core loop of clock proteins that include the transcriptional activators and their inhibitors. On the positive limb of the loop, we find the activators CLOCK and its paralog NPAS2 (encoded by *Clock* and *Npas2*), and BMAL1 (or ARNTL; codified by *Arntl*). The repressors of the core clock are period proteins, mainly PER1 and PER2 (encoded by *Per1* and *Per2*), and chryptochrome proteins CRY1 and CRY2 (codified by *Cry1* and *Cry2*)[175,176].

CLOCK and BMAL1 proteins form a complex (CLOCK:BMAL1) that binds to promoter regions that contain enhancer boxes (E-boxes) present in target rhythmic genes during daytime. These regulated genes include those encoding for the negative limb components of the core loop; PER1, PER2, CRY1 and CRY2[177,178]. These negative limb proteins interact and dimerize with each other (as well as with other clock components),

accumulate during the day and translocate into the nucleus at night, once they have reached high enough protein levels. In the nucleus, they interact with CLOCK:BMAL1 to inhibit their transcription. In this process, PER and CRY also inhibit the transcription of their own genes, leading to a decrease in *Per* and *Cry* mRNA levels. Later, PER and CRY protein levels decrease, as these proteins have a short half-life, and are degraded in an ubiquitin-dependent manner. Then, once PER and CRY levels are lower, due to the repression of their gene expression as well as their protein degradation, CLOCK:BMAL1 start another cycle of transcription at the beginning of the day[167,179,180] (**Figure I4.2**).

Besides from being in charge of their own regulation, circadian clocks control the expression of a vast number of genes and proteins, which are known as the clock output. In this regard, the CLOCK:BMAL1 complex activates the transcription of genes that codify for proteins in a tissue-dependent manner[167,170,181]. This means that the clock-controlled genes are unique among different tissues, and codify for proteins with functions specific for each tissue. Thus, clock output genes and proteins include those whose expression is controlled by the circadian clock in a tissue-dependent manner[167]. An example of this is the skin, as the specific clock output has been studied and is relevant for this work, and will be further explained.

4.2. The circadian clock in the skin

Skin cells contain circadian clocks, and among those epidermal clocks are the ones that have been studied more extensively and will be the main focus of this thesis.

Epidermal cells require rhythmic daily oscillations to maintain homeostasis, which are controlled by circadian clocks. In epSCs, these clock-controlled functions include differentiation, metabolic processes and proliferation[182,183]. As for the circadian control of proliferation, basal

epidermal cells proliferate preferentially at night in an antiphasic timing to where reactive oxygen species (ROS) peak and there is higher UV exposure. In addition, many genes involved in DNA damage repair are rhythmically expressed in the epidermis, with their peak of expression occurring at times where UV light exposure is low[112,172,184]. This segregation in time protects epidermal cells from potential ROS or UV-induced DNA damage, and allows for DNA repair to occur at times where it will be more efficient[185,186].

Disruption of the clock can lead to the development of diseases such as cancer (melanoma and non-melanoma), atopic dermatitis, psoriasis, and premature aging[172,187-189]. This points to a possible relationship between circadian clocks and skin aging, which will be further addressed.

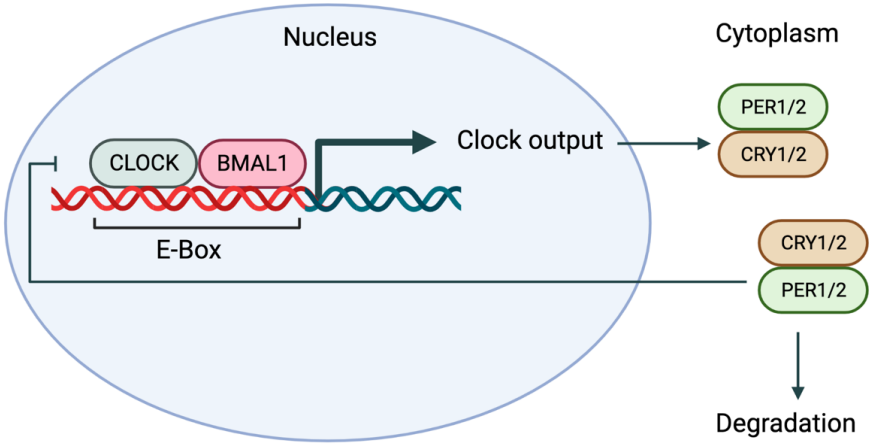

Figure I4.2. The molecular core clock machinery. Summary of the core clock feedback loop, in which BMAL1 and CLOCK bind to E-boxes and activate the transcription of clock-controlled genes during the day. These genes include those codifying for PER1, PER2, CRY1 and CRY2, which are the negative and inhibitory components of the loop. These proteins accumulate in the cytoplasm throughout the day and enter the nucleus at night once they reach a certain threshold, inhibiting their own transcription. When their levels decrease by proteasome-mediated degradation, the loop starts another cycle. Figure created with Biorender.

4.3. Aging of the circadian clock

Aging impacts the systemic regulation carried out by circadian clocks. These changes affect the SCN output, which reduces its capacity to respond to entrainment signals in peripheral organs, leading to an overall lack of adaptation to changing environmental cues[169,184].

Besides from the central clock deterioration, there are studies describing little to no change in the core clock rhythmicity in aged peripheral tissues, meaning that the core clock machinery activity is maintained robust during aging[112,169,190]. Surprisingly, even if the machinery is expressed correctly, there are age-related changes in the clock-controlled genes. Aged circadian clocks express a different set of genes in a circadian and tissue-specific manner, in a process termed circadian reprogramming[112,190].

In the skin, age-related changes in circadian clocks have been studied for epSCs, where the core clock gene amplitude of oscillation and phase of expression are maintained robustly throughout the aging process. However, epSCs present a reprogrammed circadian clock output, as only a few genes related to basic processes (such as circadian rhythm regulation and cell division) remain rhythmic during aging at the transcriptional level. These aged cells lose the circadian regulation of epidermal homeostatic processes, including keratinocyte differentiation, wound healing, and epidermis development. Interestingly, there is a new set of genes that become rhythmic exclusively in aged epSCs related to inflammation, ROS and DNA damage response[112] (**Figure I4.3**). Nonetheless, even though the specific age-associated changes in the epidermal clock output in the skin have been studied, the mechanisms by which aged epSCs reprogram their circadian output are still to be elucidated.

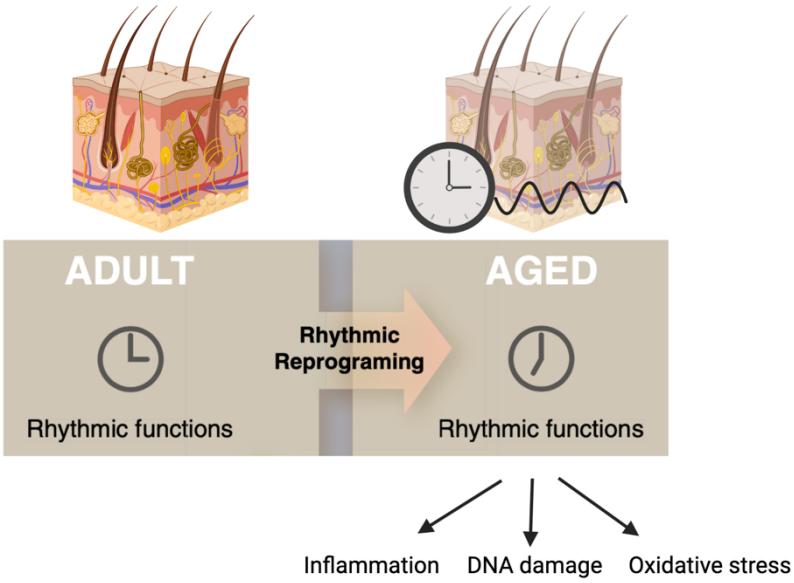

Figure I4.3. Circadian reprogramming of aged epSCs. EpSCs reprogram their daily functions during aging, changing the genes controlled by the circadian clock. Aged epSC lose the circadian regulation of genes related to epidermal homeostatic processes, and there are new genes that become rhythmic during aging related to inflammatory processes, reactive oxygen species (ROS) and DNA damage response. Figure adapted from publication[112], modified with Biorender.

5. Mechanical forces

Tissues and cells generate and are subject to mechanical forces that induce changes at different levels, such as regulating their fate, modulating homeostasis and maintaining tissue structure. These forces carry information that is translated into biochemical or mechanochemical signals. This mechanochemical information is then transported through various intracellular, nuclear, and nucleus-associated complexes, and this process is named mechanotransduction[191]. Mechanical forces include shear flow stress, tension, compression, substrate stiffness and hydrostatic pressure (**Figure I5.1)**. Shear flow stress is caused by a fluid pushing one part of a cell into one direction and the rest in the opposite direction (usually by cell adhesion to other cells or ECM). While tension

is the force of pulling and stretching of cells, compression concerns only pushing of the cells. Stiffness is determined by the rigidity of the substrate on which the cells lay, and hydrostatic pressure is generated by a fluid pressuring into the cell surface[191,192] (**Figure I5.1**).

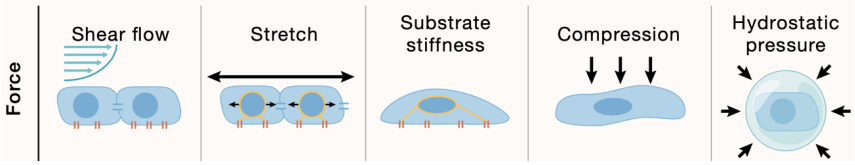

Figure I5.1. Types of mechanical forces. Representation of different types of mechanical forces in the cell. Shear flow is caused by a fluid pushing cells towards a specific direction. Stretching is the force of pulling and extending of cells, stiffness is based on the specific substrate rigidity, compression is pushing and pressing of cells, and hydrostatic pressure is caused by a fluid oppressing the cell surface. Figure obtained from publication[193].

Mechanical sensing or mechanosensing of stimuli can occur at the plasma membrane and in the nucleus. At the plasma membrane, mechanosensing takes place primarily through transmembrane receptor complexes, including cadherin- and integrin-based cell-cell and cell-matrix adhesions, respectively. Cadherin-mediated cell-cell junctions join intercellular adhesions to the cytoskeleton, coordinating cell behavior throughout the tissue. Integrin-mediated cell-matrix adhesions link the actin-myosin (actomyosin) complex of the cytoskeleton to the ECM, allowing cell contractility[194,195]. These mechanical signals are transmitted directly into the cells and to the nucleus through the actomyosin cytoskeleton by the use of adhesion complexes, which allows the cell to adapt to these external changes[195,196]. An example of this adaptation is nuclear deformation. Nuclear deformation can prevent damage to the cell, as nuclear softening has been shown to protect against stretch-induced damage[197].

There are many tissue specific differences in mechanical inputs and outputs, as well as in the type of stimuli. The skin is subject to constant

mechanical forces that cause a variety of changes in the tissue, which will be addressed in the following section.

5.1. Mechanical forces in the skin

Skin cells are exposed to different kinds of mechanical inputs, as they are in direct contact with the external environment. These inputs can alter skin homeostasis and in order to avoid this, cells must respond to these insults, as well as adapt its shape and size to maintain its barrier functions[31].

5.1.1. Epidermal forces

Epidermal cells bear a great amount of tensile strength and are joined to each other by cell-cell adhesions. In addition, basal cells are also bound to the BM by cell-matrix adhesions. These adhesions determine the mechanical properties of epidermal cells, and generate a network of components including actin, microtubules and keratins. From this network, keratins are in charge of supporting the greatest amount of mechanical load and therefore are crucial for epidermal architecture maintenance[31,198].

Mechanical inputs sensed by cells in the epidermal basal layer have been described to regulate cell fate, proliferation, and migration[199]. In this regard, epidermal differentiation and delamination towards the upper skin layers has been shown to be promoted by the mechanical state of the IFE. EpSC are crowded in the basal layer, and this causes them to adopt specific shapes and adhesion properties. When these cells proliferate, their properties shift and there is an increase in cell-cell adhesion, in cell compression and a change of cell shape. All this causes a decrease in cell-substrate contact area, as well as in cortical tension[200]. Cortical tension is based on a sustained contraction of the cortical cytoskeleton,

which is mainly generated by the actomyosin complex immediately beneath the plasma membrane[201]. As a result, epSC differentiation and upper delamination are triggered in order to restore basal cell density[200]. In addition, epSCs can be primed towards proliferation when subject to mechanical stretching. Stretching alters the crowded state of the IFE, and this causes a shift in the mechanical properties of epSCs. As a result, there is a subset of epSCs that is primed towards self-renewal, allowing the expansion of basal cells, while another epSCs subset stays committed to differentiation. This subgroup specification contributes to tissue expansion while maintaining epidermal homeostasis, as it generates a balance that keeps cell density regulated[202].

5.1.2. Extracellular matrix (ECM) forces

The dermal ECM sustains a great amount of force and provides a structural scaffold for the skin (see 1.2.1. Dermal layers). Mechanical stress in the dermis is mainly dissipated through the ECM, thanks to its composition including collagen and elastin fibrils. ECM is the major contributor to tissue stiffness, and an increase in its rigidity has been associated with multiple pathologies[198].

In addition, the BM is an ECM structure that separates dermis from epidermis, and provides skin integrity protecting from mechanical challenges. As previously mentioned (see 1.2. Dermis) the BM is composed of mainly collagen IV and laminins, and also includes perlecan (proteoglycan), and nidogen (glycoprotein). It is the stiffest structure in contact with epidermal cells, and its composition varies depending on its location, whether it is in contact with the IFE or HFs[31].

Besides, the BM also has functions regarding epidermal cell fate determination and function, by signaling through mechanosensing pathways regulated by integrin and cadherin complexes[194,203]. These

mechanosensing pathways include the YAP/TAZ pathway, which is crucial for skin and more specifically epidermal homeostasis[204].

5.2. YAP/TAZ signaling pathway

The yes-associated protein (YAP or YAP1) and the transcriptional co-activator with PDZ-binding motif (TAZ or WWTR1) are downstream effectors of the Hippo kinase cascade. The Hippo pathway is crucial for organ growth and regeneration, and is the main regulator of YAP and TAZ activity[205].

YAP and TAZ (YAP/TAZ) are paralogs and their most well-known role is as transcriptional coactivators. YAP/TAZ become inhibited when phosphorylated by active Hippo pathway kinases (specifically by LATS1 and 2 kinases)[205,206]. This means that YAP/TAZ are inhibited when the Hippo pathway is active[207]. Phosphorylated YAP/TAZ are then exported from the nucleus and degraded in the cytoplasm or sequestered at cellular junction sites. However, when there are no active kinases, de-phosphorylated YAP/TAZ translocate and accumulate in the nucleus to carry out their activity. Once in the nucleus, they do not bind directly to the DNA, as they do not contain DNA-binding domains. They interact and form a complex with a family of TFs named transcriptional enhanced associate domain (TEAD), binding mainly to gene enhancers, although they can also bind to promoters. There, they interact with chromatin-remodeling factors and modulate RNA polymerase II (Pol II) activity to activate or repress the expression of target genes. These target genes are related to organ size, cell cycle, cell migration and cell fate determination as well as other functions (**Figure I5.2**)[205,206,208-211].

The activity of YAP/TAZ can be regulated by several upstream mechanisms, such as changes in mechanical stiffness in the ECM. In the classical Hippo pathway, these mechanical changes are detected by integrins in the cell surface and travel through the actin cytoskeleton inside the cell.

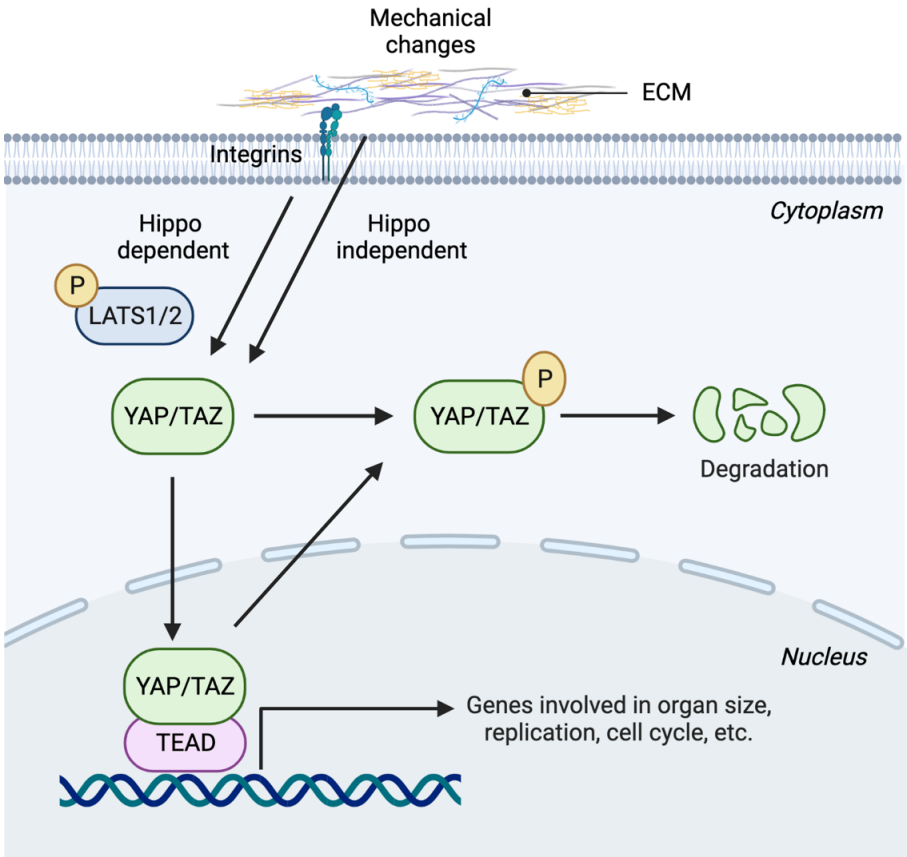

Figure I5.2. YAP/TAZ signaling pathway. Summary of YAP/TAZ activity inside the cell. Mechanical changes in the ECM can lead to YAP/TAZ activation through Hippo-dependent and -independent pathways. Hippo-dependent activation requires integrin sensing of the mechanical forces, and goes through a series of steps that lead to YAP/TAZ de-phosphorylation in the cytoplasm and translocation into the nucleus. When YAP/TAZ become phosphorylated by LATS1/2 kinases, they are exported from the nucleus and can get degraded. Hippo-independent YAP/TAZ activation can occur after stimulus such as changes in mechanical forces, and do not require LATS1/2 kinases. In both pathways, YAP/TAZ bind to TEAD sites in the DNA and activate the transcription of genes related to cell cycle, organ size determination, etc. Figure created with Biorender.

However, these mechanical forces can lead to YAP/TAZ activation by means independent of LATS kinase or Hippo activity (**Figure I5.2**)[209,212]. This Hippo-independent mechanism may be dependent on the Rho family of small GTPase, particularly the Rho-associated protein kinase (ROCK), and the integrity of the actomyosin cytoskeleton[202,213]. Regardless of the specific activation pathway followed, mechanical stress and stiffness in the ECM triggers YAP/TAZ nuclear translocation, whereas ECM softening causes YAP/TAZ nuclear export[31,206,214,215]. Thus, changes in ECM mechanical forces are detected by the cell surface and then translated into cytoskeleton changes, where an increase in stiffness leads to YAP/TAZ activation through different pathways.

5.2.1. YAP/TAZ in the skin

The skin requires the Hippo signaling pathway, and YAP/TAZ expression particularly, to regulate functions associated to development, homeostasis and regeneration[204]. Nonetheless, the specific functions carried out by YAP/TAZ vary depending on the skin layer.

In dermal fibroblasts, their expression aids in sensing the mechanical environment, promoting ECM remodeling and mechanical changes, as well as helping in the wound healing process[204,216]. In the epidermis YAP/TAZ expression mostly controls cell and tissue growth, differentiation, stem cell clonal expansion and HF morphogenesis[199,217-220]. Their nuclear localization (i.e. their active form) is mostly found in the epSCs that reside in the basal layer, as integrins in the cell surface are in contact with the BM and corresponding ECM, and, therefore, sense mechanical changes. As a result, epSCs start losing nuclear YAP/TAZ expression as they differentiate towards the upper layers. During this process, contact between integrins in the cells and the ECM, as well as their ability to sense mechanical changes, is lost[216]. This goes in line with other studies that have shown a decrease in YAP/TAZ expression levels

in accordance with a decrease in the proliferative capacity of epSCs during maturation[218].

However, even if YAP/TAZ expression is crucial for skin maintenance, increased YAP/TAZ levels have also been associated to skin cancer initiation[220]. High nuclear YAP expression has been reported in invasive and metastatic skin cells, as well as in cancer cell clonal expansion. This shows that there are major differences in YAP/TAZ functionality depending on their expression levels[219,221].

5.3. Mechanical forces in the aged skin

Aged skin undergoes changes in architecture and composition that have already been addressed (see 3. Skin aging), and changes in tissue mechanics are described as key in aging progression[154]. The causes leading to these age-associated mechanical changes are still under study, and are thought to be produced either by ECM deterioration or alteration in the functionality of mechanotransduction pathways. Regarding the age-related mechanotransduction pathway alteration, only the YAP/TAZ pathway will be addressed in this work.

5.3.1. Extracellular matrix deterioration

As previously mentioned (see 3.2.2. Extracellular matrix aging), aged skin presents structural characteristics such as a thickening and stiffening of the BM, as well as loss of overall elasticity, epSC integrin expression, and decreased collagen production in the ECM. This all leads to an increased stiffness in the aged skin[110,113,222]. Then, these BM and ECM stiffness changes are sensed by epSCs in the basal layer, which, in turn, adapt to said changes (see 5.2.1. YAP/TAZ in the skin). Thus, the stiffening of the skin causes epSCs to respond to mechanical forces that are progressively developed during aging. As a result, epSCs undergo

changes in shape and adhesion during aging, all of which can lead to a decrease in stemness of epSCs and generalized age-associated deterioration[110,155].

5.3.2. YAP/TAZ in the aged skin

Mechanotransduction pathways also become altered during aging. This includes YAP/TAZ, as their levels have been shown to vary during aging across several tissues. A decline in YAP/TAZ expression has also been described in stromal cells as responsible for an increase in cGAS_STING signaling, leading to the development of age-associated senescent cells in several tissues[223]. However, an increase in YAP/TAZ expression during aging has also been described. Exposure of mammary epithelial multipotent progenitors from adult women to stiff age-like substrates led to an increase in YAP/TAZ expression, as well as a YAP-dependent differentiation bias[224]. This leads to hypothesize that the role of YAP/TAZ during aging is still poorly understood, and that there might be tissue-specific functions that still need to be addressed.

5.4. Mechanical forces and the circadian clock in the skin

The skin and its functions are tightly controlled by circadian clocks (see 4.2. The circadian clock in the skin). This includes regulation of ECM components, as collagens, proteases and elastic fibers are regulated by circadian rhythms[225].

This regulation can occur bidirectionally, as it has been shown that changes in the mechanical properties and stiffness of the mammary epithelial microenvironment can result in changes in its circadian clock activity[226]. These studies show that rigid or stiff microenvironments, such as the ones existing in the mammary gland during aging, lead to a deterioration in the circadian robustness of tissues. This deterioration is

reflected by a dampening in the amplitude, as well as shifts in the period and phase of clock output genes[226]. However, *in vitro* studies show that fibroblasts synchronized in their oscillations can maintain robust circadian clock activity when in contact with stiff substrates. Moreover, aged epSCs have also been described to maintain their circadian integrity *in vivo* during aging[112,227], even if this tissue has also been shown to have increased stiffness upon aging[110,113]. Moreover, there are studies that show that different cell types show preferences for matrices with different rigidities in order to maintain efficient daily oscillations[228]. Thus, there is no consensus as to how changes in stiffness and circadian clocks affect each other. This all highlights how circadian clocks and the mechanical environment regulate each other, although the exact mechanisms and output of this regulation is unknown.

5.4.1. YAP/TAZ and the circadian clock in the skin

YAP/TAZ have also been linked to the circadian clock and to BMAL1 in specific scenarios. In the intestine, loss of BMAL1 expression in tissue-resident SCs has been shown to potentiate tumor initiation. The absence of BMAL1 leads to an increase in YAP expression and in self-renewal of these SCs. This, coupled with the circadian clock disruption caused by the lack of BMAL1, leads to tumor generation in this context[229].

Moreover, YAP/TAZ become active preferentially in stiff substrates (see 5.2. YAP/TAZ signaling pathway), and this activation can also affect the activity of the circadian clock[230]. This is why the response of YAP/TAZ to mechanical stimuli could have an effect on the circadian clock regulation, especially in contexts of a continuous increased stiffness microenvironment such as aging. However, this field has not been explored in depth and the connection between circadian clocks and YAP/TAZ still needs to be elucidated.

Objectives

Chapter 1. Local IL-17 orchestrates skin aging

The skin presents distinct cell-type changes during aging, accompanied by an increase in age-related inflammation. This rise in chronic inflammation has been explored in the past, and is known as “inflamm-aging”[156]. Nonetheless, the specific gene expression variations happening in the entire skin compartment during aging, as well as the particular pro-inflammatory signals that occur are not well understood, which is what led to the development of our objectives:

1. Describe the gene expression changes undergone by distinct dermal cell types during aging at the single cell level

2. Determine if there is an increase in pro-inflammatory cues in the aged dermis, as well as their specific nature and secreting cell types

3. Understand if the increase of the pro-inflammatory signals described in aged cells can be targeted, to ameliorate the progression of aging traits in the skin

4. Study the communication of inflammatory signals between the dermal and epidermal compartments during aging

5. Analyze the downstream effectors of the pro-inflammatory cues described

Chapter 2. Age-associated mechanical changes impact on rhythmic epidermal homeostasis

The aged skin undergoes architectural and structural changes[110]. Also, aged epSCs rewire their oscillatory functions to adapt to stress[112]. However, the consequences of these physical changes are not completely known, as well as the causes leading to the age-associated rhythmic rewiring. To better understand these processes, and to address if they are connected, our objectives have been:

1. Identify the physical and mechanical changes undergone by the aged skin, specifically in the epSC niche

2. Decipher which mechanotransduction pathway relevant to epidermal cells could be responding to the age-associated mechanical variations defined

3. Assess if there is a communication between the mechanotransduction pathway activated during aging, and the circadian clock machinery. Also, understand which are the specific factors involved in each pathway

4. Characterize the relationship between the specific mechanotransduction and core clock factors found, as well as their role in the described age-associated skin changes

Results

Chapter 1.
Local IL-17 orchestrates skin aging

1. Dermal cells present cell type-specific changes during aging

In order to have a complete picture of how the skin ages, we initially characterized how dermal cells age. The dermis is home to a wide variety of cell types, and many age-associated traits in the skin are highly influenced by cells in this compartment[139,156,231]. Thus, we carried out single-cell RNA-sequencing (scRNA-seq) of the dermal cell populations of adult (17 to 25 weeks old) and aged (80 to 90 weeks old) mice back skin (**Figure R1.1**). With this, our aim was to detect the age-associated transcriptomic changes in each individual cell type in the dermis.

We isolated dermal cells using fluorescence-activated cell sorting (FACS), with which we sorted first for CD45+ immune cells, and then for CD45-/EpCAM- non-immune cells for subsequent sequencing (**Figure R1.2.**). The sorting strategy was separated for both immune and non-immune compartments in order to enrich for less abundant cells, as the proportion of immune cells in the dermis is lower when compared to non-immune cells (i.e. fibroblasts)[36]. While sorting for non-immune cells, we included the epidermal marker EpCAM as a negative selection to exclude possible contaminant epidermal cells.

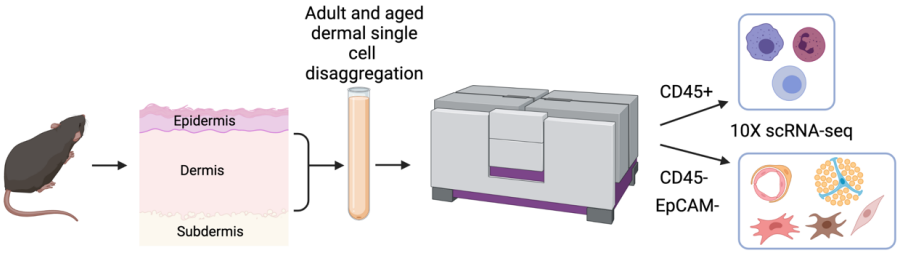

Figure R1.1. Workflow of dermal cell isolation. Schematic of the steps followed for dermal single cell isolation and sorting of CD45+ immune, and CD45-EpCAM- non-immune cells separately for 10X scRNA-seq. For the CD45+ cells, $n = 7$ mice for the adult group, and $n = 4$ mice for the aged group, with three technical replicates; for the CD45–/EpCAM– cells, $n = 2$ mice for the control group, and $n = 2$ mice for the aged group, with two technical replicates. Figure created with Biorender.

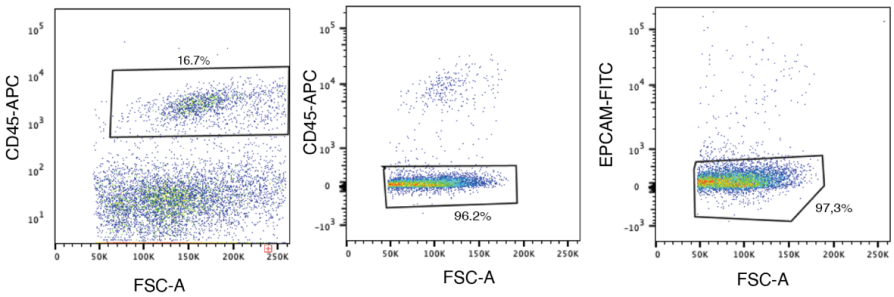

Figure R1.2. Flow cytometry plots for scRNA-seq sorting. Representation of the sorting strategy of CD45+ and CD45-/EpCAM- cells for 10X scRNA-seq.

Then, these cells were applied the 10X Genomics platform (version 3) to characterize 11,940 cells for the CD45+ compartment and 5,213 for the CD45–/EpCAM– cells. After batch correction of all replicates (for CD45+ cells, n=3 replicates per condition, for CD45-/EpCAM- cells, n=2 replicates per condition), good sample mixing verification (LISI value)[232] (**Figure R1.3a**) and validation of the representation of each replicate in all populations (**Figure R1.3b**), we clustered together all the cell types obtained by generating a shared nearest neighbor graph using the Louvain algorithm[233]. Then, we visualized the clusters using Uniform Manifold Approximation and Projection (UMAP) (**Figure R1.4**).

In this visualization we could see all dermal cells clustered together, including cells from both adult and aged conditions and from CD45+ and CD45-/EpCAM- lineages. Then, we performed differential gene expression analysis between clusters, to obtain markers defining each population and to annotate them to their corresponding cell-type.

The annotation of CD45+ immune clusters showed distinct cluster populations corresponding to lymphoid and myeloid clusters, where lymphoid cells included CD4+ Th, CD8+ T cyt, T regs, γδT, ILCs, NK, and proliferating T cells (**Figure R1.4**). Myeloid clusters were composed of three macrophage clusters, three monocyte clusters, one dendritic and one proliferating myeloid cluster (**Figure R1.4**).

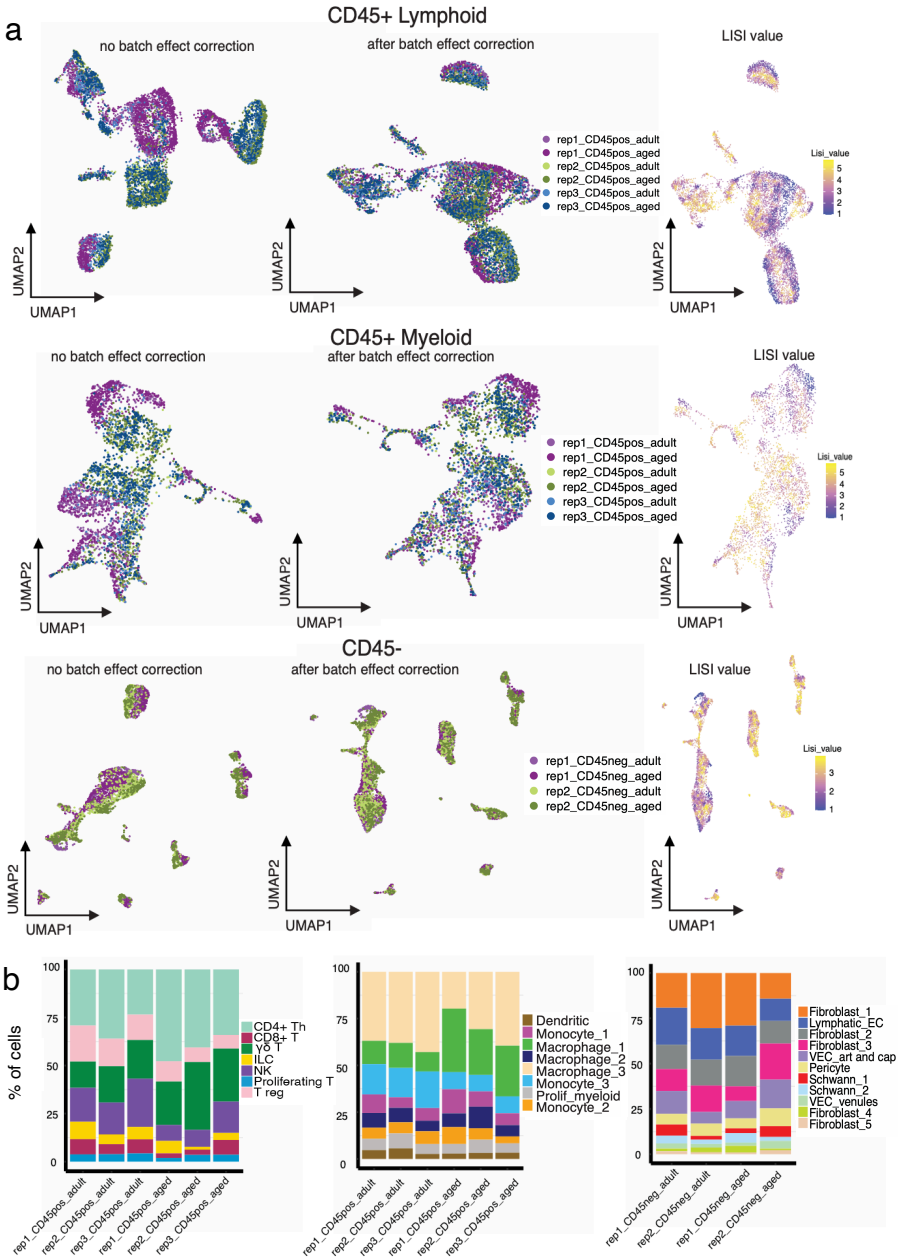

Figure R1.3. Plots depicting batch effect correction, good sample mixing and replicate contribution across conditions. **a**, UMAP representation of CD45+ lymphoid (upper panel), CD45+ myeloid (middle panel) and CD45-/EpCAM- (lower panel) cells. These plots show the before and after batch correction, then the good sample mixing values (calculated with LISI, far right panels)[232]. **b**, Bar plots showing the percentage of each cell type per replicate, showing in the left CD45+ lymphoid, in the middle CD45+ myeloid and in the right CD45-/EpCAM- cells.

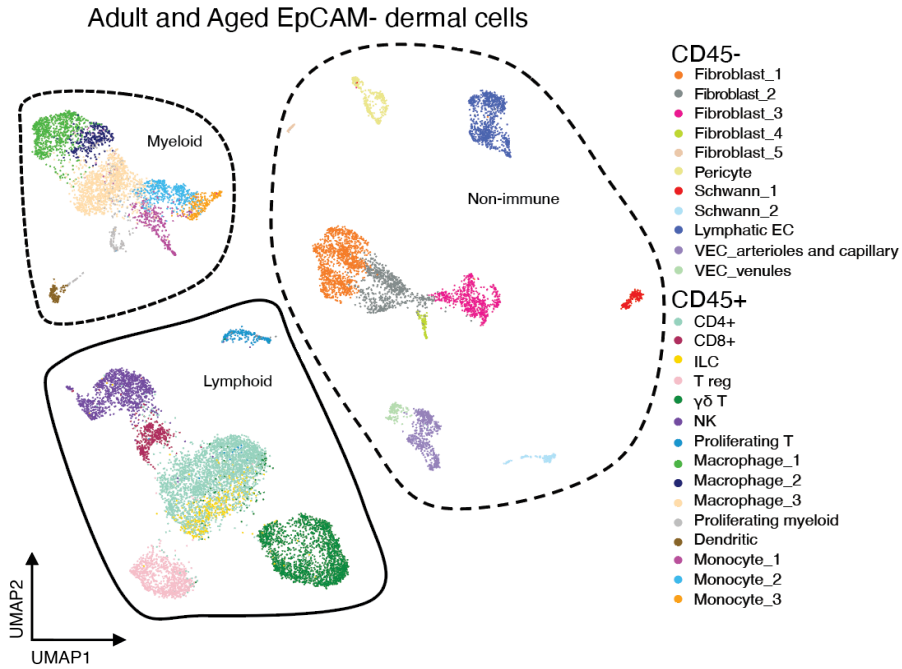

Figure R1.4. UMAP representation of all adult and aged dermal cell types clustered together. This UMAP shows all adult and aged CD45+ lymphoid (circled with a continuous line), CD45+ myeloid (short-dashed line) and CD45-/EpCAM- (long-dashed line) cells clustered together.

Annotating CD45-/EpCAM- non-immune cells into clusters allowed us to describe five fibroblast clusters, three endothelial cell clusters, two Schwann cell clusters and one pericyte cluster (**Figure R1.4)**. After this, we plotted all the annotated cell-types with some of their main defining markers, to validate that the annotation was representing those cell-types correctly (**Figure R1.5**). To start getting insights as to how these cells age, we plotted the Jaccard index comparing adult and aged clusters, to analyze the similarity at the transcriptional level between each cluster as they age. For this, we looked at the top 100 expressed genes per cluster, and compared how this expression had changed with age in each case (**Figure R1.6**). This index showed that cell types are affected by aging in different ranges, as there were some showing mild differences in gene expression while aging (i.e. Monocyte_3 and Lymphatic ECs), and other showing stronger differences in expression (i.e. ILCs and γδ T cells).

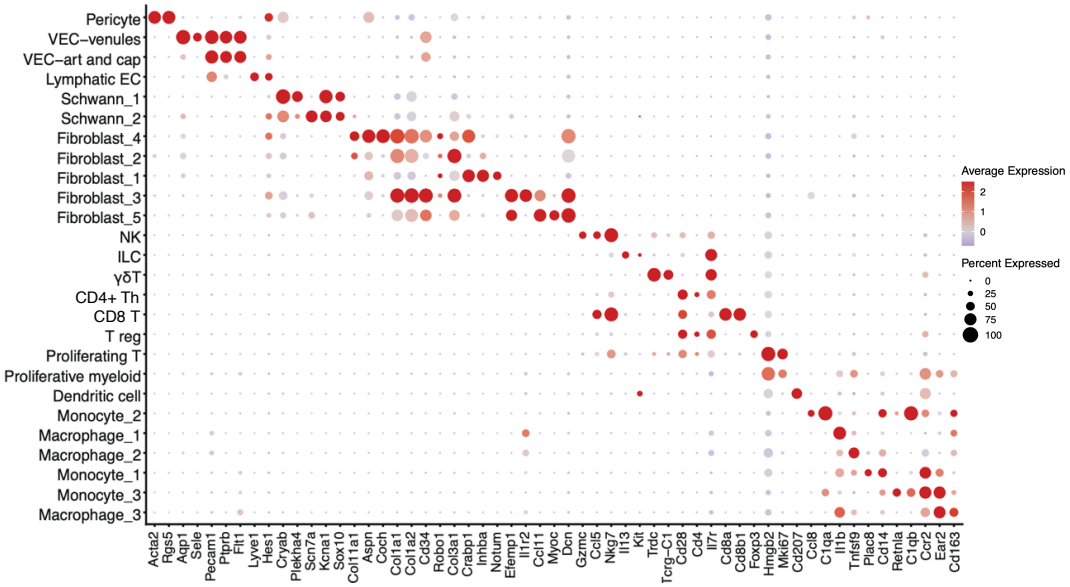

Figure R1.5. Dot plot representation of all cell types obtained and their main markers. This dot plot shows all adult and aged CD45+ lymphoid, CD45+ myeloid and CD45-/EpCAM- cell types plotted against some of their main defining markers.

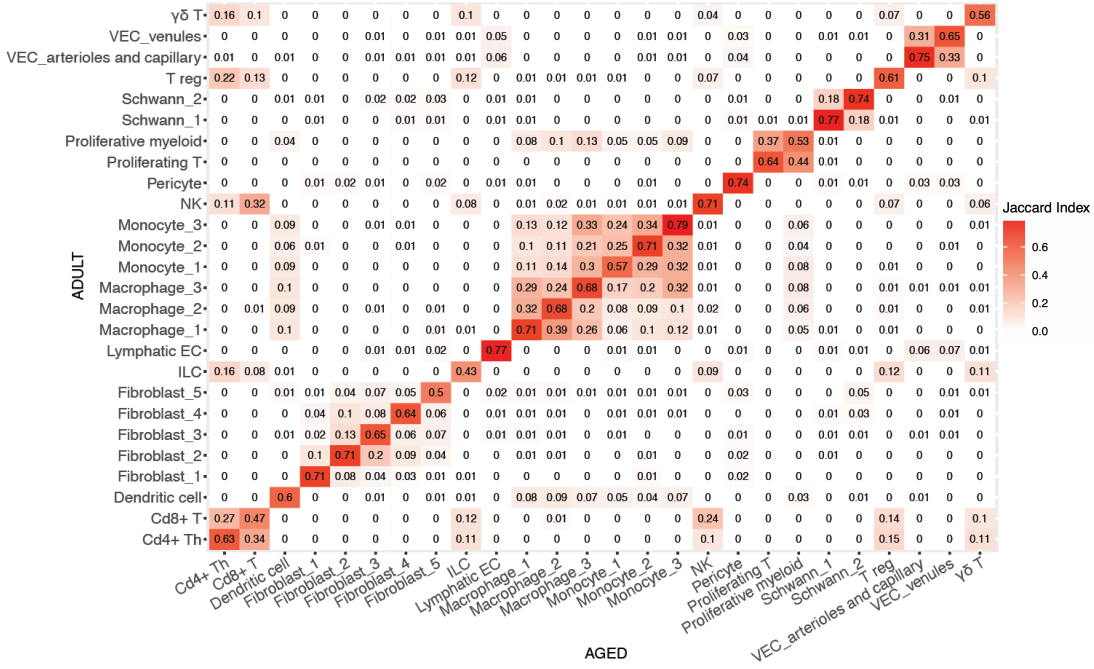

Figure R1.6. Jaccard index of the top 100 markers in adult and aged clusters. This index compares the top 100 expressed markers per cluster in adult and aged cells, showing the similarity between clusters in both ages.

2. Dermal non-immune cells present a pro-inflammatory and deteriorated transcriptional profile during aging

Non-immune dermal cells are the most abundant lineage in the dermis[4,36]. We first plotted some of the most relevant markers for each cell type, as well as for subpopulations of some of the cell types (i.e., dermal papilla fibroblasts). This was done in a UMAP projection including only non-immune cells, to gain clarity as to how the division of clusters had been done based on their specific marker expression (**Figure R2.1**). Then, we checked if any cell type or cluster was changing in proportion during aging using a differential variability analysis for composition data (*sccomp*)[234], and we observed that there were no significant changes in proportion in any non-immune cell type between adult and aged conditions (**Figure R2.2**).

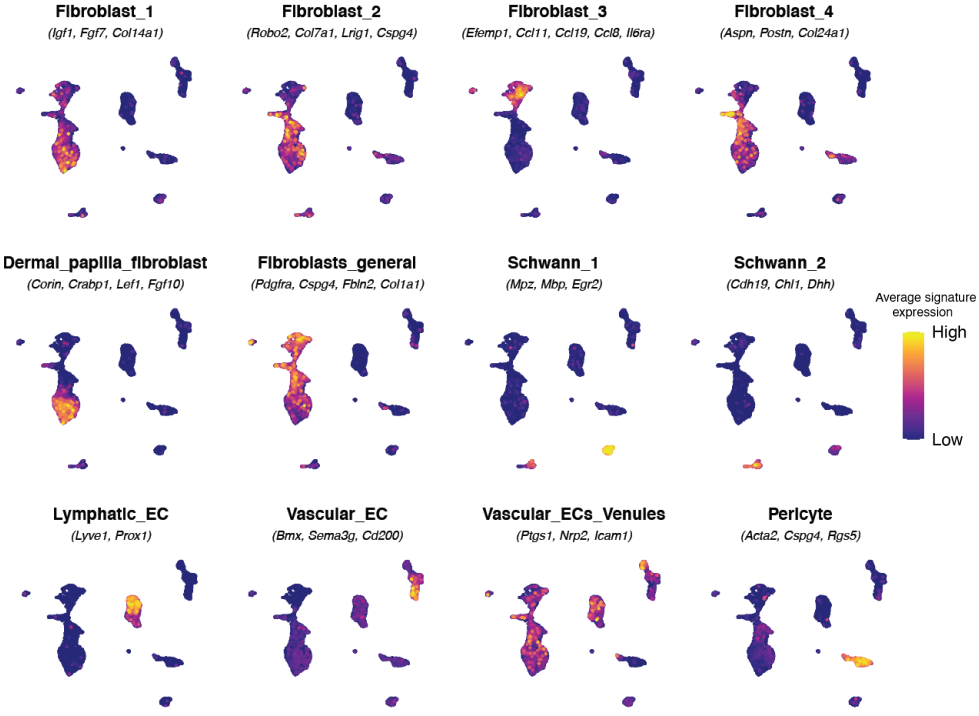

Figure R2.1. UMAP showing cell-type specific gene expression markers. Division of cell types and of cell-type subpopulations into clusters based on the expression profile of specific signature genes.

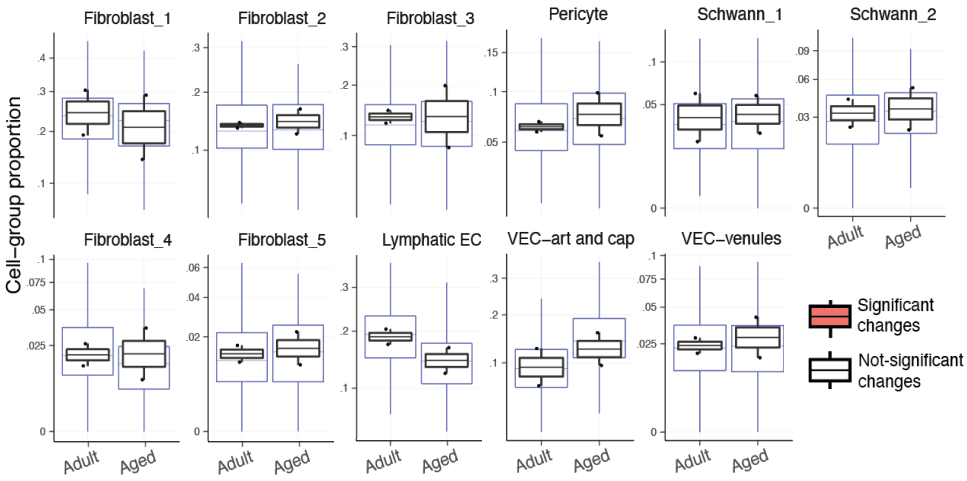

Figure R2.2. Analysis of cell proportion changes between adult and aged non-immune clusters. Analysis of cell proportion differences carried out with *sscomp*[234]. Orange colored boxes show significant changes in cell proportion.

Our next step was to look at cell-type specific age-related changes, and we analyzed those changes in cell types that presented more than one cluster (Schwann cells, ECs and fibroblasts).

2.1. Schwann cells

In our analysis, we identified two distinct Schwann cell populations (**Figure R1.4, R1.5, R2.1**). One of these clusters expressed genes related to myelinating and differentiated cells (Schwann_1), based on the expression of *Mpz* and *Mbp* markers, which are crucial for myelination[235]. Then, the other Schwann cell cluster (Schwann_2) presented a precursor-like state based on its expressed markers, that include *Cdh19*, *Chl1*, *Dhh*[236] (**Figure R2.1**). During aging, we observed a mild downregulation of genes relevant for cell differentiation and migration (such as *Pllp* and *Nf1*)[237] in the Schwann_1 cluster, which was reflected in gene ontology (GO) analysis (**Figure R2.3**). These are key functions of dermal Schwann cells[85,87], and this downregulation shows that aged Schwann cells are less fit for carrying out their regenerative functions in

the skin. Nonetheless, this was exclusive for cells in the Schwann_1 cluster, as Schwann_2 cells did not present any relevant change during aging when looking at their differences in gene expression and GO analysis between conditions.

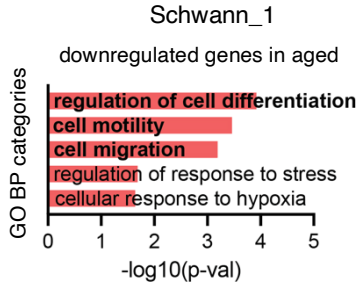

Figure R2.3. Schwann cells downregulate during aging genes crucial for their functions. Selected GO categories belonging to biological process (BP) enriched in the downregulated genes in aged Schwann_1 cells show that there is a decrease in the expression of genes crucial for their regenerative functions during aging. The x axis represents $-(\log_{10})$ of the adjusted *P*-value for each depicted GO category.

2.2. Endothelial cells

Endothelial cells are divided into two main groups: lymphatic ECs and vascular ECs. Lymphatic ECs are known to express *Lyve1*[238], and vascular EC markers differ depending on the subtype of vessel, which in the dermal microvasculature are arterioles, capillaries or venules[68]. In this case, arteriole and capillary ECs were clustered together, whereas venule ECs constituted a separate cluster (**Figure R2.1**).

Venule ECs showed the highest transcriptional changes of all ECs during aging (**Figure R1.6**). These cells upregulated the expression of pro-inflammatory genes during aging, which was shown by an overrepresentation of inflammation-related terms in GO analysis of the aged upregulated genes (**Figure R2.4a**). As venule ECs have been shown to play an important role in immunity, and can act as APCs[74,239], we further investigated the pro-inflammatory state of these aged ECs. For this, we analyzed the expression of MHCII complex in adult and aged

ECs. This was done including all EC subtypes because of the complexity of the tissue digestion process. Separating EC subtypes would require further prolonging the digestion protocol by adding extra intracellular markers, which would greatly affect the viability of our cells of study. As a result, these assays might be diluting the conclusions drawn about MHCII expression only in venule ECs. First, we checked for gene expression changes by quantitative polymerase chain reaction (qPCR) of sorted adult and aged ECs, analyzing the expression of MHCII complex genes *Cd74* and *H2Aa*[240].

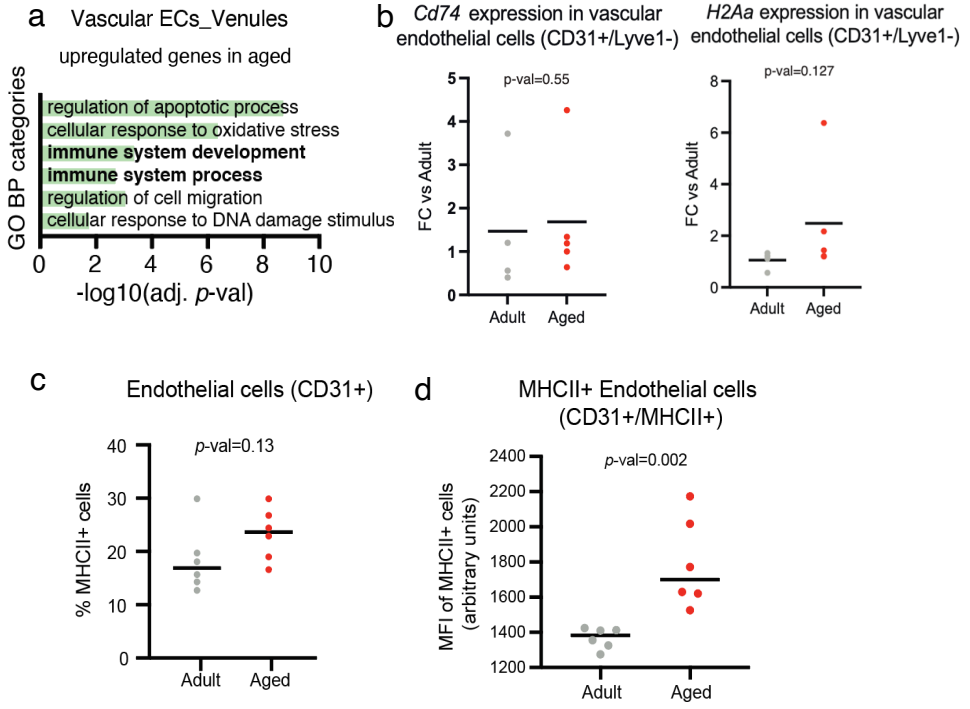

Figure R2.4. Aged endothelial cells upregulate pro-inflammatory genes during aging. **a**, Selected GO categories belonging to BP show that venule ECs upregulate genes related to pro-inflammatory functions during aging. The x axis represents $-(\log_{10})$ of the adjusted *P*-value for each depicted GO category. **b**, Aged ECs show a mild increase in the expression of MHCII complex genes *Cd74* and *H2Aa*. Data shown as fold change (FC) in aged compared to adult. **c**, ECs show a trend towards an increase in MHCII proteins in their surface during aging. **d**, ECs expressing MHCII proteins in their surface increase their expression during aging.

In both cases, we detected an increase in their gene expression levels in aged ECs, although this increase was not significant (**Figure R2.4b)**.

Then, we analyzed by FACS if there was an MHCII upregulation by checking for the expression of the complex proteins I-A/I-E. Results showed that the overall number of ECs expressing MHCII in their surface was elevated during aging when compared to adult, although this was not significant (**Figure R2.4c)**. Interestingly, the levels of MHCII expression in the surface of MHCII-expressing cells was significantly increased during aging, meaning that cells that were already expressing MHCII in adults increase their overall MHCII expression during aging (**Figure R2.4d**). This leads to hypothesize that there is a specific subset of cells that express MHCII in their surface and that have APC functions, which goes in line with what is already described for venule ECs in post-capillary regions[73]. Also, it highlights that aged ECs, particularly venule ECs, present a shift towards a pro-inflammatory profile during aging.

2.3. Fibroblasts

Fibroblasts are the most abundant cell type in the dermis[41], and as mentioned above, we obtained five fibroblast clusters in our analysis (**Figure R1.4**). Their gene expression allowed us to annotate each of these clusters to different fibroblast subtypes. For example, Fibroblast_1 cells expressed markers of reticular fibroblasts, Fibroblast_2 cluster cells resembled papillary fibroblasts, and Fibroblast_3 included pro-inflammatory cells[22,41,142,241] (**Figure R2.1)**. We were also able to find specific markers of DP cells in the Fibroblast_1 cluster, which highlights that these specialized fibroblasts were contained in this cluster[242]. Importantly, even if fibroblast subpopulations were defined by differences in their cluster markers, there were well-known fibroblast markers, such as ECM proteins (including collagens), commonly expressed in all fibroblast clusters[36,41] (shown as Fibroblasts_general) (**Figure R2.1)**.

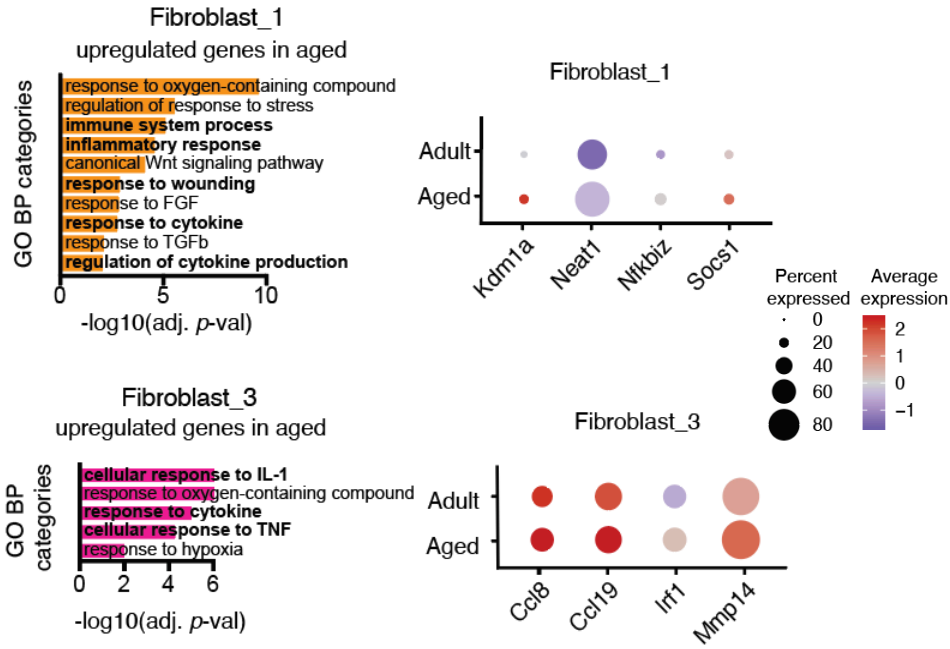

Figure R2.5. Fibroblast_1 and Fibroblast_3 clusters show an inflammatory profile during aging. Fibroblast clusters _1 and _3 upregulate genes related to pro-inflammatory functions, observed in the selected GO categories belonging to BP as well as in individual gene expression. The x axis represents –(log_{10}) of the adjusted *P*-value for each depicted GO category.

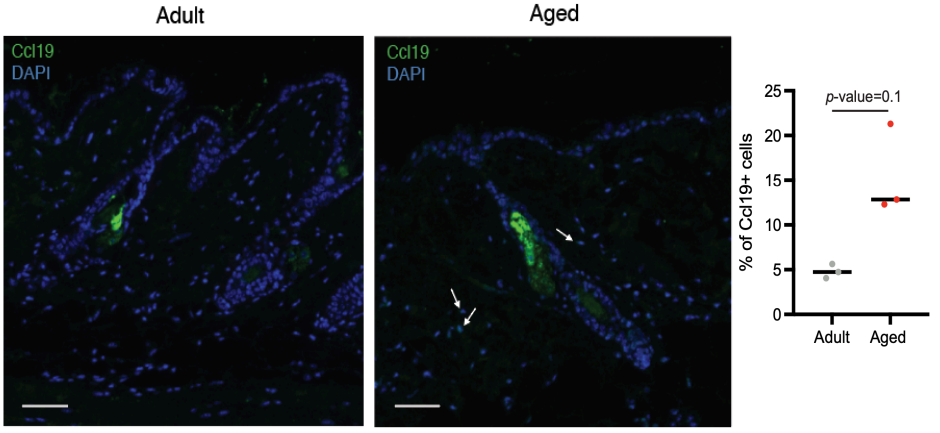

Figure R2.6. CCL19 protein is upregulated in the aged dermis. Immunostaining of CCL19 in adult and aged back skin, including a quantification of the percentage of positive cells. Bar= 50μm.

Clusters Fibroblast_1 and Fibroblast_3 showed the most predominant transcriptional changes during aging, characterized by a general increase in pro-inflammatory gene expression. This was observed by GO analysis of the upregulated genes during aging, but also when looking at individual gene expression (**Figure R2.5**), and was also validated for CCL19 expression at the protein level by immunostaining (**Figure R2.6)**. CCL19 has been linked to a subset of fibroblasts in autoimmune and chronic inflammatory diseases[243], and its upregulation during aging evidences how aged dermal cells switch towards a pro-inflammatory state.

Senescence has been described as one of the major contributors to the aging process[106,244]. We wondered if this switch in fibroblast gene expression could be due to an increased accumulation of senescent cells in the skin, and we checked for markers that have been linked to cell cycle arrest and senescence; such as *Cdkn2a* (*p16*) and *Cdkn1a* (*p21*)[245] (**Figure R2.7a**).

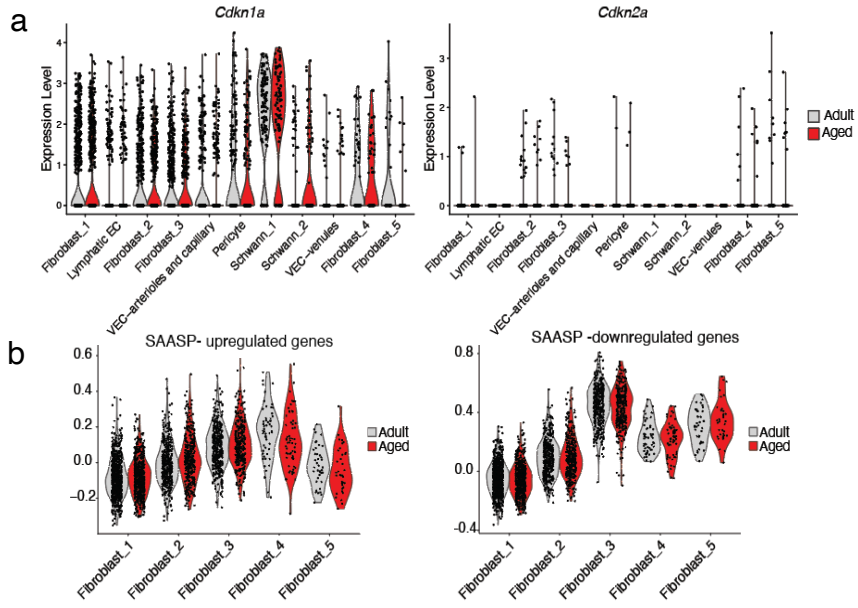

Figure R2.7. There is no upregulation of senescence markers in the aged dermis in our model. **a**, Expression of genes *Cdkn2a* (*p16*) and *Cdkn1a* (*p21*) across all non-immune populations in adult and aged. **b**, Expression of genes upregulated and downregulated in SAASP[149] in all our fibroblast clusters in adult and aged conditions.

We did not detect an upregulation of either of these genes across our non-immune clusters, which led us to broaden our analysis by checking for the expression of the skin-specific SAASP signature[149] (**Figure R2.7b**). Again, there was no upregulation of senescence-associated genes, or downregulation of those that become decreased in this senescence scenario[149]. With this, we corroborated that accumulation of senescent cells in our datasets is not a major cause for the transcriptomic changes we observe, discarding this process as a driver of aging in our experimental setup.

3. Aged lymphoid cells increase IL-17-related inflammation in the skin

In order to understand the nature of the pro-inflammatory signature described for non-immune cells, we shifted our attention towards the immune cell compartment. Immune cells are responsible for creating a pro-inflammatory scenario in contexts such as aging[156], and we wondered if this could be occurring in this case. To address this, we first clustered all immune cells together in a UMAP representation (**Figure R3.1**), and analyzed the myeloid and lymphoid compartments separately.

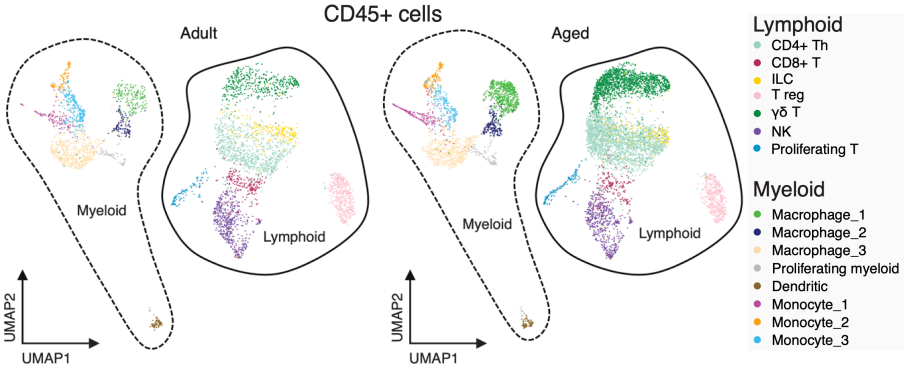

Figure R3.1. UMAP representation of all CD45+ cells. UMAP of adult cells shown in the left panel, and aged cells in the right panel. Lymphoid cells are circled with a continuous line, and myeloid are circled in a dashed line.

3.1. Dermal myeloid cells

Myeloid cells in the skin are first line in responding to external insults, and can carry out either pro- or anti-inflammatory responses to these stimuli[47]. In our analysis, we detected eight myeloid cell clusters, including three macrophage clusters (Macrophage_1 to _3), three monocyte clusters (Monocyte_1 to _3), one dendritic cell cluster (DCs), and one of proliferating myeloid cell cluster (Proliferating myeloid) (**Figure R3.1**).

Looking into the gene expression profiles per cluster, Macrophage_1 and Monocyte_1 clusters were characterized by the expression of pro-inflammatory genes, such as *Il1b* and *Tnfaip3*, as well as MHCII complex genes like *H2Ab1, H2-Eb1, H2-Aa* and *Cd74*. For Monocyte_1 cells, there was expression of inflammatory genes including *Ccr2, Cxcl2, Fcgr4, Cxcr4*. With this, we defined these two cell clusters as pro-inflammatory. Then, Macrophage_2 cluster cells expressed markers of regulatory macrophages, such as *Il4I1, Cd200r1* and *Lgals1*[47]. As for the rest of the myeloid clusters, DCs presented a gene expression typical of APCs, which corresponds to their known functions in the skin[46], and the cluster Proliferating_myeloid included a combination of myeloid cells expressing proliferation markers.

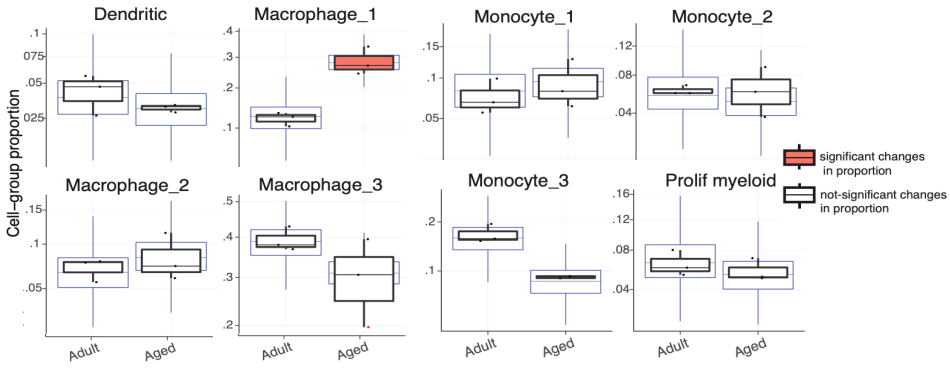

Figure R3.2. Analysis of cell proportion changes between adult and aged myeloid cells. Analysis with *sscomp* tool[234] to detect changes in cell proportion during aging. Orange colored boxes show significant changes in cell proportion, and outliers are marked as red triangles outside of the box plots.

Then, to study the age-associated changes in these cells, we checked for differences in cell proportion during aging using the previously mentioned *sccomp* tool[234]. With this, we detected a significant increase in Macrophage_1 cells during aging, as well as a decrease in aged Monocyte_3 cells (**Figure R3.2**). However, even if there were differences in proportion, this was not accompanied by major changes in the transcriptome of these cells. Nonetheless, when looking at other clusters, we detected an increase in the pro-inflammatory gene expression profile of some of them. There was an upregulation of *Il1b* in Monocyte_2, Macrophage_2 and DC clusters (**Figure R3.3**)**,** and expression of the protein IL-1β is crucial for the initiation of an immune response in myeloid cells[124]. Of note, Monocyte_1 and _2 clusters showed the highest rate of gene expression changes in myeloid cells during aging, and GO analysis in these clusters showed an overrepresentation of pro-inflammatory functions in aged cells (**Figure R3.4**). These results indicate that specific myeloid cell subsets increase their number during aging, while other groups increase their inflammatory characteristics. Overall, this supports the idea of an exacerbated inflammatory state in aged skin.

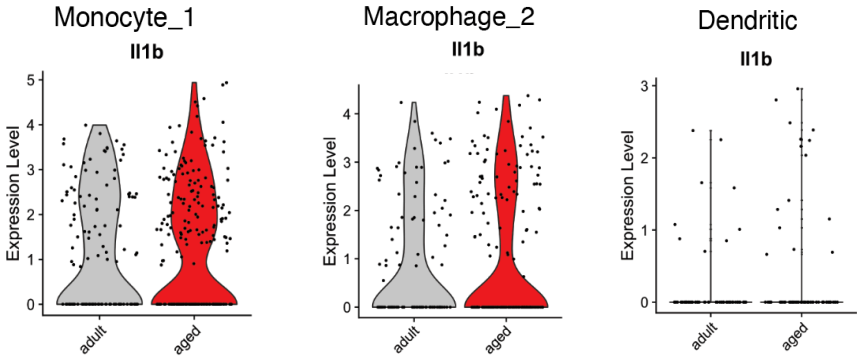

Figure R3.3. Upregulation of *Il1b* in aged myeloid cell subsets. Violin plot showing the expression levels of *Il1b* in Monocyte_1 (left panel), Macrophage_2 (center panel), and Dendritic (right panel) cells in adult and aged conditions.

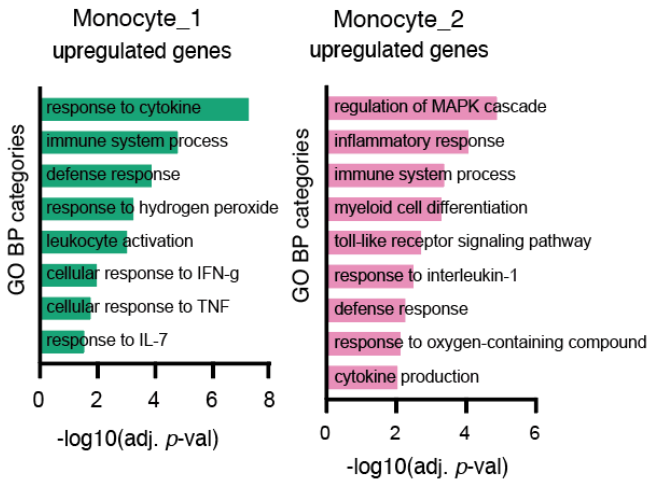

Figure R3.4. GO analysis of the upregulated genes in aged myeloid cell subsets show an increase in inflammatory functions. Selected GO categories belonging to BP analysis in Monocyte_1 and _2 clusters. The x axis represents –($\log_{10}$) of the adjusted *P*-value for each depicted GO category.

3.2. Dermal lymphoid cells

As for lymphoid cell clusters, we obtained CD4+ Th, Tregs, CD8+ Tcyt, γδ T, proliferating T cells, ILCs and NK cells (**Figure R3.1**). These cells are crucial in homeostatic conditions, as well as during inflammatory responses and in wound healing[47,53]. Surprisingly, we detected a significant increase in cell proportion of CD4+ Th and γδ T cells during aging[234] (**Figure R3.5**). We corroborated the increase of CD4+ Th cells at the protein level by immunofluorescence (IF) of CD4 in the dermis, which validated our *in-silico* analysis and further shows that there is a higher recruitment of these cells during aging (**Figure R3.6**).

Moreover, in order to understand the overall age-associated changes in lymphoid cells, we developed a deep learning model to measure the deviance of each immune cell type during aging compared to their adult counterparts (**Figure R3.7a**). With this, we can detect how different the cells in the aged clusters are in comparison to the cells of the same cluster in adult. To do this, we assumed that the most age-affected cells would present the biggest transcriptomic changes when compared to the

adults, and would therefore be more distant in the multidimensional gene expression space. We then used our adult lymphoid 10X scRNA-seq data as a reference for each cell type in our model, and compared it to the cells in aged lymphoid clusters. As a result, we found that CD4+ Th, γδ T and ILCs were showing the highest deviance score of all lymphoid cell subsets during aging (**Figure R3.7a**). This was also reproduced when looking at the percentage of cells affected by aging, including all immune cells. This tool detects the proportion of cells that change transcriptionally during aging, per cell type. Here, only the cell types with a higher percentage of changes are depicted (**Figure R3.7b**). This means that CD4+ Th, γδ T and ILCs accumulate the biggest rate of changes during aging when compared to the rest of the cells in the immune compartment.

The high rate of age-associated changes in CD4+ Th, γδ T and ILCs prompted us to analyze deeper the specific changes they undergo. As they are the cells changing the most during aging, it is likely that their alterations could affect other cell types as well as whole skin aging.

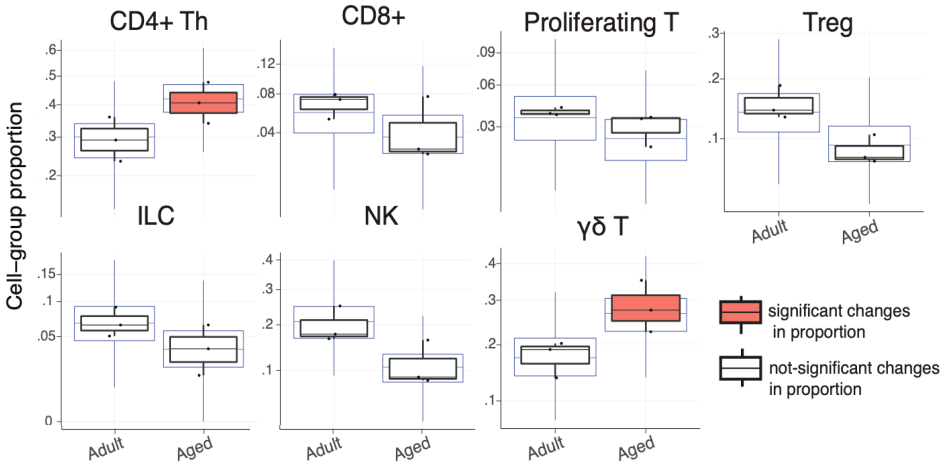

Figure R3.5. Analysis of cell proportion changes between adult and aged lymphoid cells. Analysis with *sscomp* tool[234] to detect changes in cell proportion during aging. Orange colored boxes show significant changes, and outliers are marked as red triangles outside of the box plots.

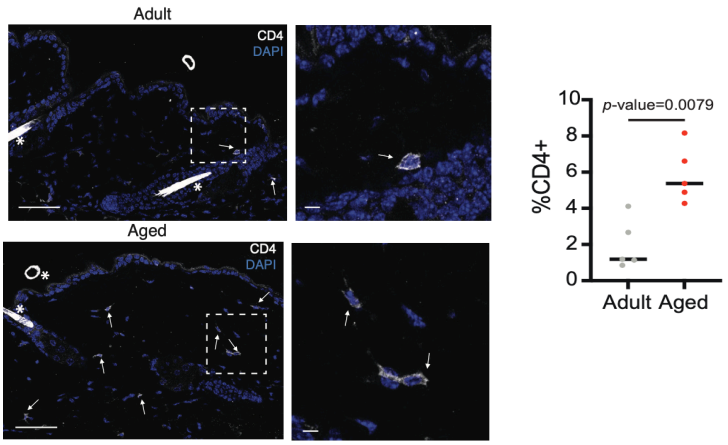

Figure R3.6. Immunofluorescence of CD4 cells show an increase in proportion in murine aged dermis. Representative images of CD4 IF in adult (top panel), aged (middle panel) murine back skin, and the quantification of positive cells (right panel). White arrows point at positive cells. Quantification reflects the percentage of CD4 positive cells. Bar= 50μm. Insets bar = 10μm. * = unspecific hair shaft autofluorescence. Only for visualization purposes, brightness and contrast were adjusted on these images

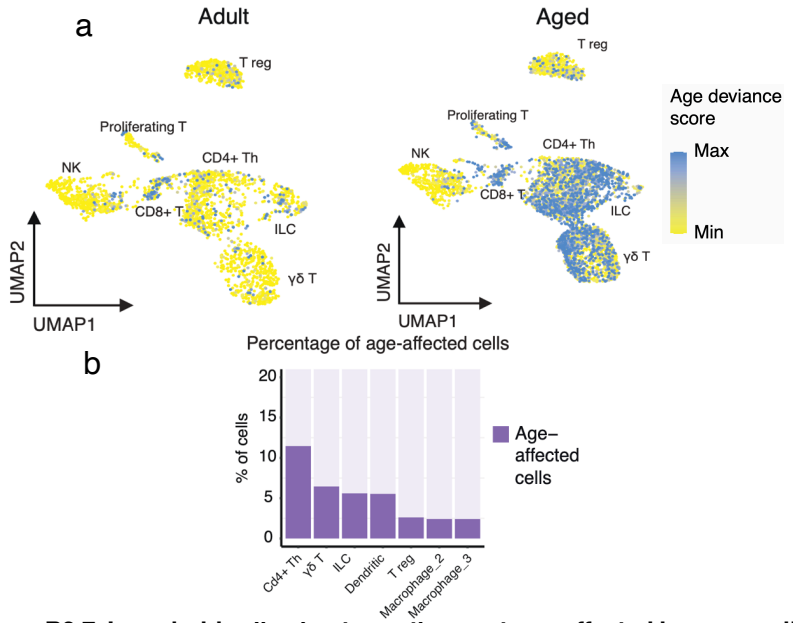

Figure R3.7. Lymphoid cell subsets are the most age-affected immune cells. **a**, UMAP showing the age deviance score of adult (left panel) and aged (middle panel) lymphoid cells. Blue dots show cells with the highest rate of changes. **b**, Bar plot representing the percentage of cells affected by aging per immune cell type. For clarity reasons, only the cell types with a higher percentage of changes are shown.

This is why we primarily focused on these cell types, and further analyzed their gene expression changes during aging. GO analysis of the upregulated genes during aging in all three cell types showed an increase in inflammatory functions in aged cells when compared to adults (**Figure R3.8**).

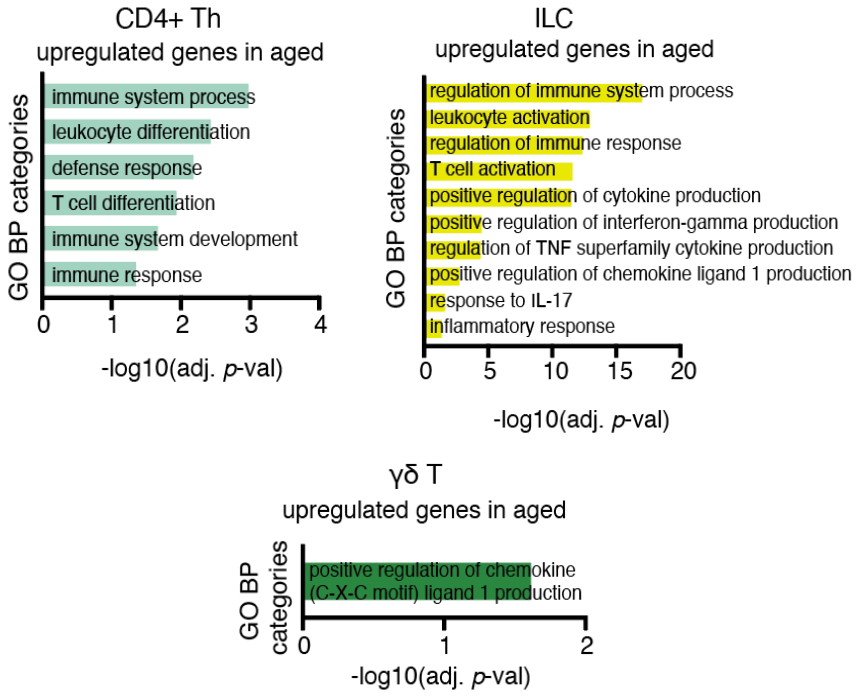

Figure R3.8. GO analysis of the upregulated genes in aged CD4+ Th, ILCs and γδ T show pro-inflammatory traits. Selected GO categories belonging to BP analysis of aged CD4+ Th (left panel), ILCs (right panel), and γδ T (bottom panel).. The x axis represents $-(\log_{10})$ of the adjusted *P*-value for each depicted GO category.

3.2.1. Dermal lymphoid cell subsets upregulate IL-17 during aging

Interestingly, when looking at the specific pro-inflammatory gene expression, we detected the cytokine interleukin 17 (IL-17) family members *Il17a* and *Il17f* among the most upregulated genes in these cell types (**Figure R3.9a**). These cytokines are the most well-known IL-17 family members, and bind to the IL-17RA and IL-17RC receptors to

trigger their signaling cascade[94]. Once activated, this pathway is important for fighting against external pathogens in the skin[100]. Interestingly, IL-17A and IL-17F (IL-17A/F) have also been strongly related to the progression of autoimmune and inflammatory diseases such as psoriasis[98,102]. We then plotted the expression of *Il17a* and *Il17f* (*Il17a/f*) in individual cells. With this, we observed that the upregulation of these cytokines was reflected in an increase in the number of IL-17-expressing cells, more than an overall increase in their expression levels (**Figure R3.9b**). We were able to validate these results by IF, as we detected an increased proportion of IL-17A-expressing cells in the aged dermis (**Figure R3.9c**). After this, we checked if there were other cell types in the skin that increased *Il17a/f* during aging (**Figure R3.10**). This showed that *Il17a/f* expression increase was restricted to the analyzed aged lymphoid cell types, and that the expression of their receptors (*Il17ra*, *Il17rc*) remained mostly unaltered during aging across dermal cell types (**Figure R3.10**). All this suggests that there could be an internal polarization towards an *Il17a/f*-expressing phenotype of these lymphoid cell subsets, independently to other cell types.

Additionally, we analyzed *IL17A*/*F* expression in adult and aged human dermis by fluorescent *in situ* hybridization (FISH) to determine if this upregulation was maintained through different species. Remarkably, we observed a trend towards an increase in *IL17A*/*F* expression in the aged human dermis, as there was a higher percentage of cells expressing these cytokines in the aged condition (**Figure R3.11**). Besides, we questioned if the levels of IL-17A/F in the aged human dermis were comparable to those described for psoriasis patients. Excessive IL-17 has been described as key in the development of this disease, which then leads to the appearance of disease-associated lesions, as well as epidermal hyperproliferation, alterations in their differentiation programs and exacerbated inflammation[246].

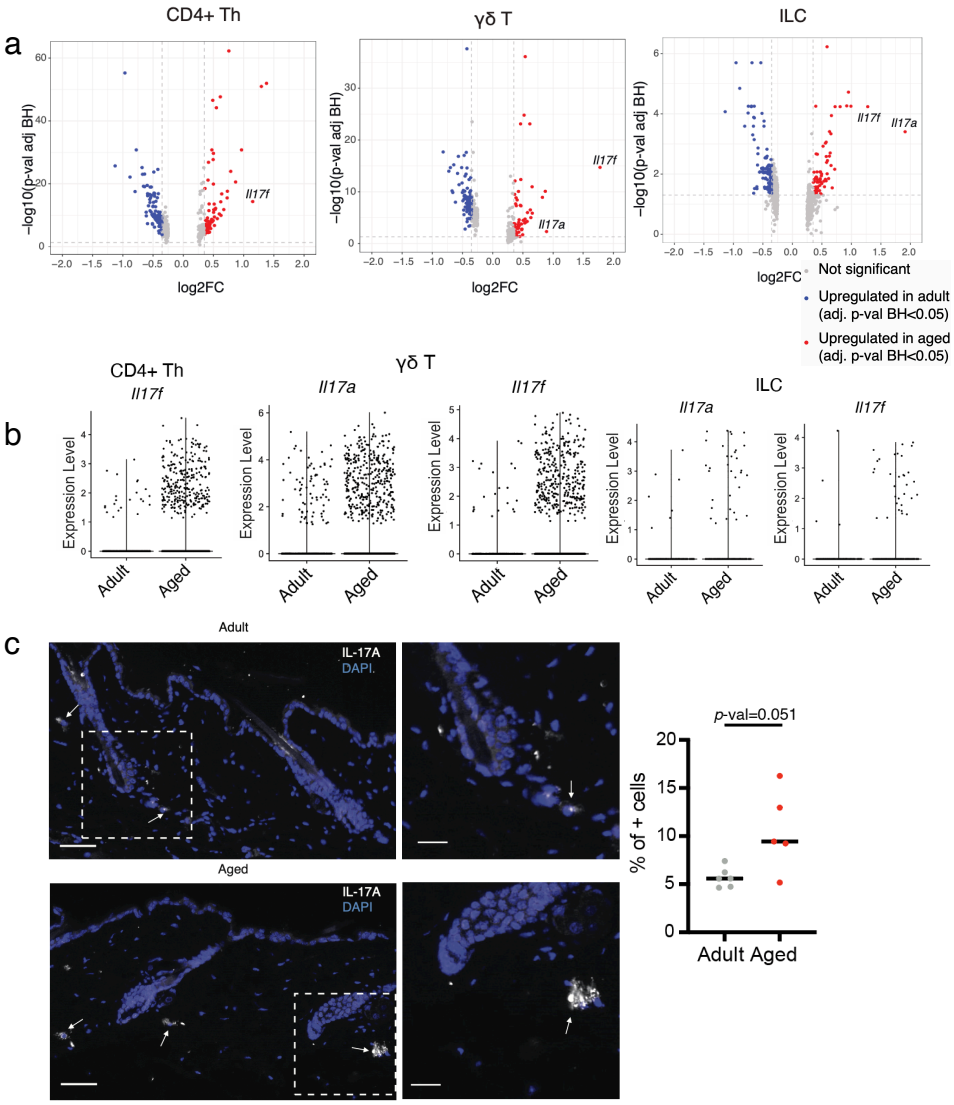

Figure R3.9. Aged CD4+ Th, γδ T and ILCs show an upregulation of *Il17a* and *IL17f* expression levels. **a**, Volcano plots depicting the differentially expressed genes between adult and aged CD4+ Th (left panel), γδ T (middle panel) and ILCs (right panel). Upregulated genes during aging are shown in red, and downregulated during aging are in blue. *Il17a* and *Il17f* are highlighted when found as differentially expressed in a statistically significant manner between ages. **b**, Violin plots showing the expression levels of *Il17a* and *Il17f* in CD4+ Th (left panel), γδ T (middle panel) and ILCs (right panel). **c**, Immunofluorescence of IL-17A in adult (upper panel) and aged (lower panel) mouse back skin. Insets with higher magnification are included. Quantification (right panel) is shown as a percentage of dermal positive cells. Bar= 50μm, insets= 20μm. Only for visualization purposes, brightness and contrast were adjusted on these images.

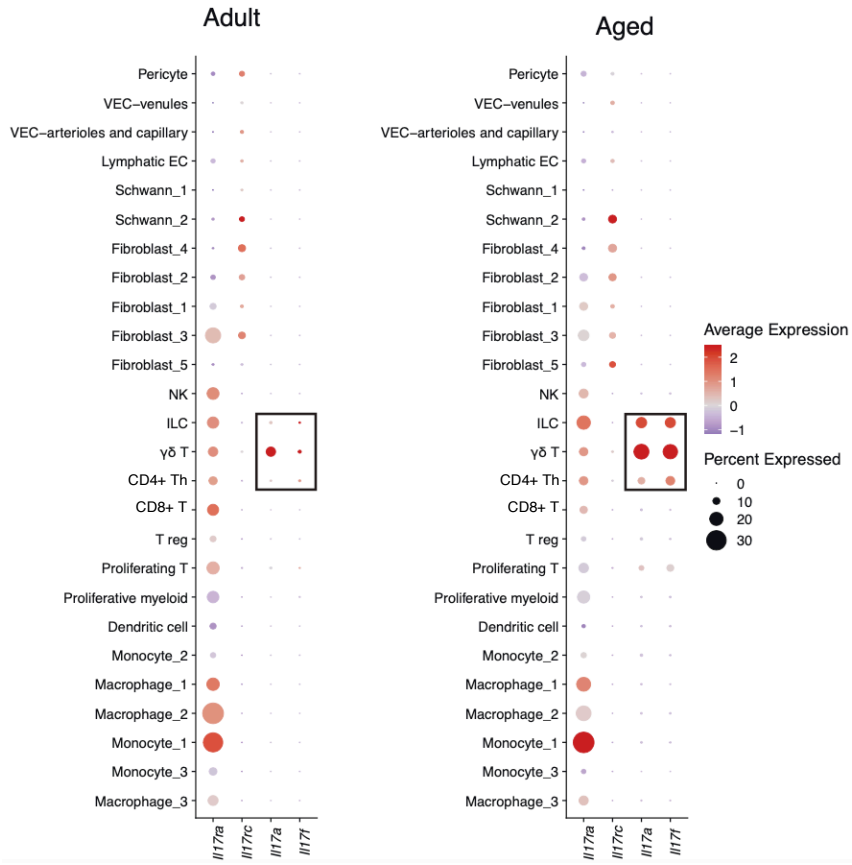

Figure R3.10. Dot plot depicting the percentage of expressing *Il17ra*, *Il17rc*, *Il17a*, *Il17f* cells in dermal adult and aged cells, as well as their average expression. Expression of the IL-17 receptors *Il17ra* and *Il17rc*, as well as of *Il17a* and *Il17f* across dermal cell types in adult and aged conditions. Black boxes enclose the lymphoid cell subsets that show the highest differential expression of *Il17a* and *Il17f* during aging.

These characteristics, as well as the visual phenotypic comparison of aged *vs.* psoriatic skin (**Figure R3.12a**), already highlights the differences between healthy aging and psoriatic disease. Nonetheless, we compared the levels of skin *IL17F* in healthy adult and aged human skin to those of psoriatic patients that were not currently undergoing treatment or were in remission phases of the disease by FISH (**Figure R3.12b**). The patient samples used, therefore, present high grade of variability in the phase of the disease, with irregular increased epidermal thickening levels, and low

grade of immune cell infiltration. Quantifying the number of dermal cells with *IL17F* expression in psoriatic skin showed no significant difference compared to healthy adult or aged skin (**Figure R3.12b,c**). Regardless of the lack of statistical significance, there was a trend towards an increase in *IL17F* expression in human aged dermis and in psoriatic skin, compared to adult human skin. This suggests that our findings could also be relevant in the aging process of other species, as they could potentially be applied to humans.

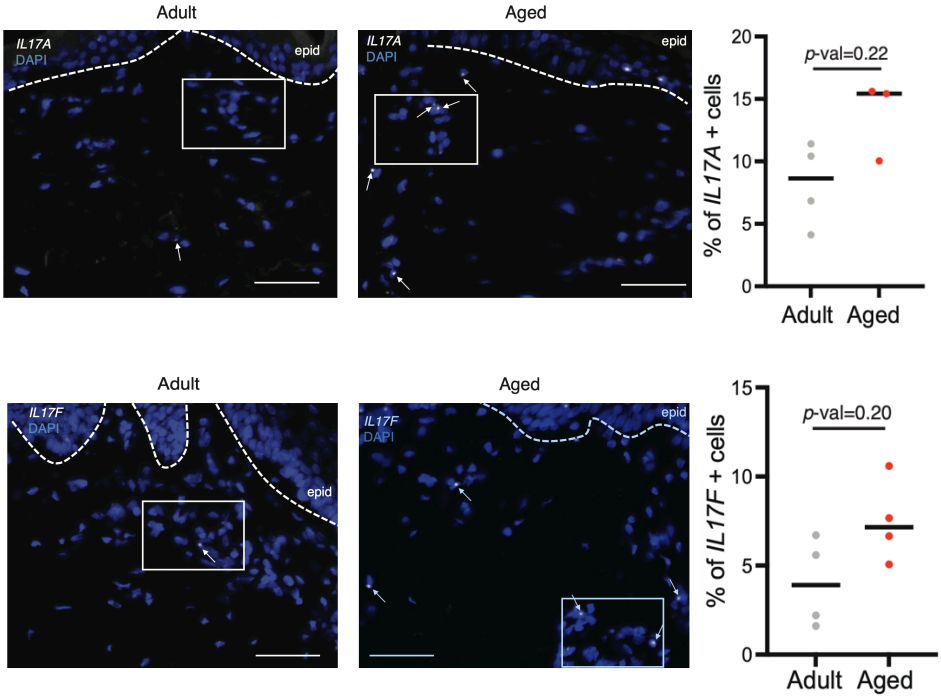

Figure R3.11. Fluorescent *in situ* hybridization (FISH) of *IL17A* and *IL17F* in adult and aged human skin. FISH of *IL17A* (top panel) and its quantification (top right panel), as well as of *IL17F* (bottom panel) and its quantification (bottom right panel) show a mild increase in *IL17A/F* expression during aging in human skin. Quantification shows percentage of positive cells. Bar= 50μm. Brightness and contrast were adjusted only for visualization purposes.

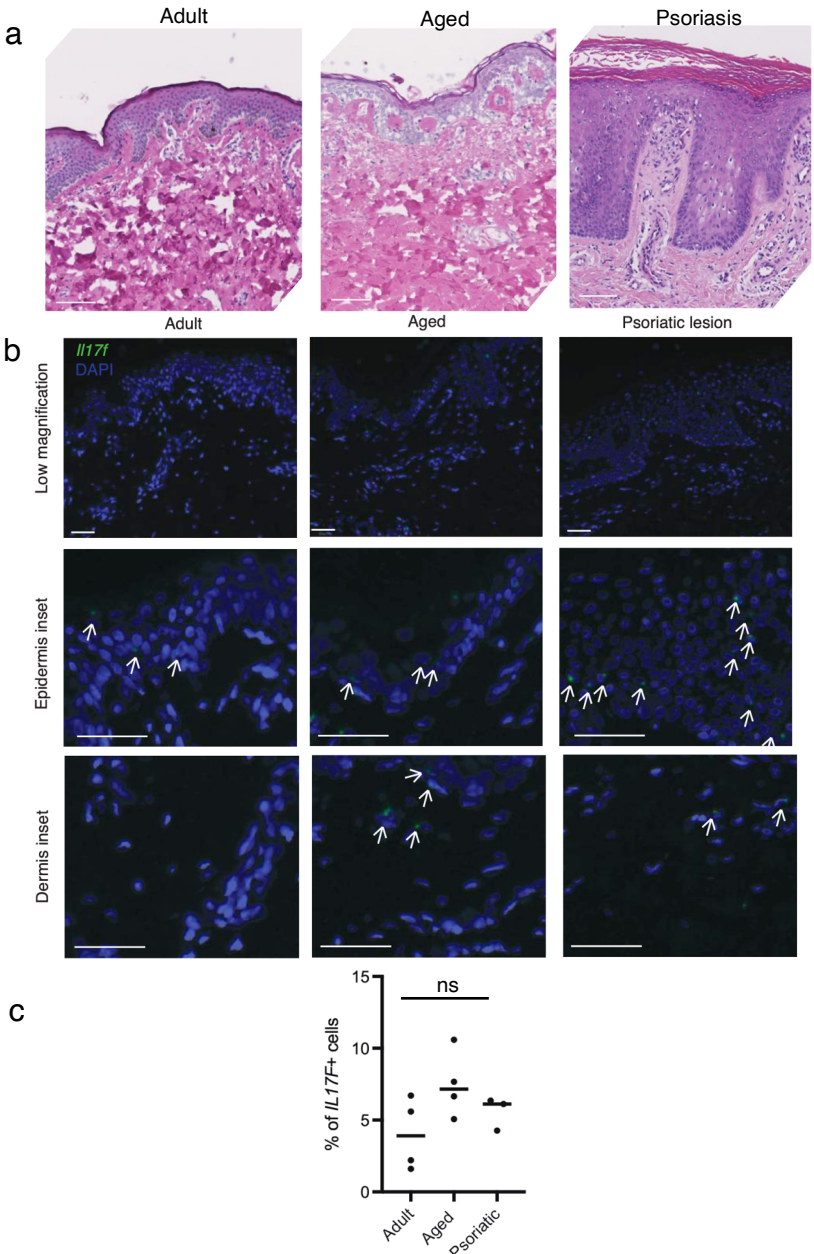

Figure R3.12. Human psoriatic skin *IL17F* levels differ greatly from adult and aged skin levels. a, Hematoxylin and eosin (HE) staining of adult (left panel), aged (middle panel) and psoriatic (right panel). Bar= 100μm. **b**, FISH of *IL17F* in human adult, aged and remitting psoriatic skin lesions. FISH of *IL17F* in a low magnification as an overview (top panels), epidermal insets (middle panels) and dermis insets (bottom panels). White arrows point to positive cells. Bar= 50μm. **c**, Quantification shows percentage of *IL17F* positive cells per condition.

Focusing back on our murine 10X scRNA-seq data, and in order to further characterize the nature of this IL-17 upregulation, we zoomed into the IL-17-expressing lymphoid cell clusters. This was done to analyze different cell states and to identify potential subsets that could be in charge of the IL-17-upregulation. Of note, ILCs did not have enough cells to carry out a subclustering analysis, and was characterized as one unique cluster (**Figure R3.1**). These cells are known to be crucial in inflammatory responses, and secrete cytokines similar to those produced by CD4+ Th cells[47,65]. Our analysis showed that ILCs expressed higher levels of markers associated to ILC3 subtype in aged skin, including *Il17a*, *Il17f*, *Tmem176a* and *Tmem176b* (**Figure R3.9a**,**b**; **Figure R3.13**). ILC3 subtype has been strongly associated to psoriasis and other autoimmune and chronic inflammatory diseases[65], and this age-associated increase suggests that aged ILCs resemble those of chronic inflammatory contexts.

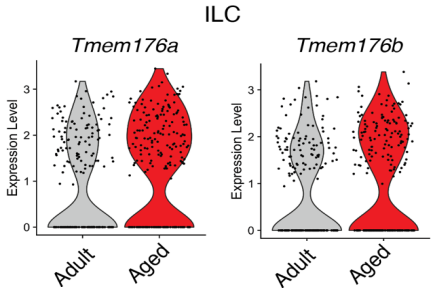

Figure R3.13. ILCs upregulate genes associated to the ILC3 subtype during aging. Violin plots showing the expression values of *Tmem176a* and *Tmem176b* in adult and aged ILCs, which are characteristic of ILC3.

CD4+ Th cell subclustering revealed three subclusters (**Figure R3.14a**). Their differential gene expression allowed assigning them to specific CD4+ Th subpopulations. CD4+ Th_c cluster expressed markers defined as exclusive of Th1 cells (like *Ifng*[247]), and CD4+ Th_b cells showed markers characteristic of Th17 cells, such as *Il17f*, *Rora*, *Tmem176a/b*, *Ccr6* and *JunB* as well as others[248,249] (**Figure R3.14b**).

Nevertheless, CD4+ Th_a was not assigned to any specific Th subtype, as it did not express any marker exclusive to a specific CD4+ Th subpopulation. It is likely that this subcluster was composed of a mixture of cell states that cannot be further separated, leading to the expression of non-defining markers (**Figure R3.14b**).

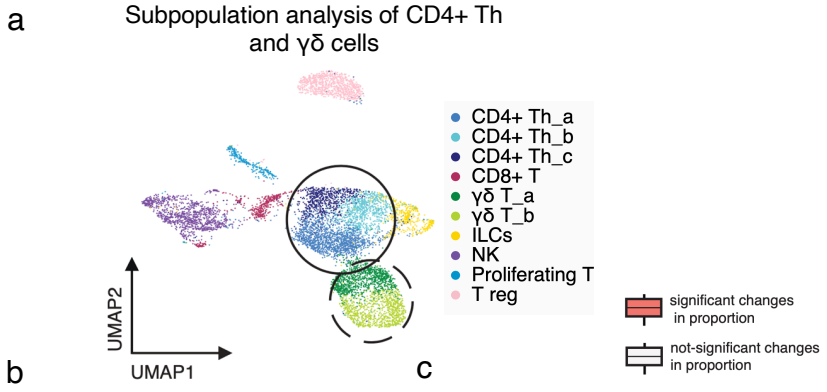

Cluster	Cell subtype	Marker genes
CD4+ Th_a	not determined	
CD4+ Th_b	Th17	*Il17f, Tmem176a/b, Ccr6, JunB, Ltb4r1, Odc1, Rora*
CD4+ Th_c	Th1	*Ifng, Tbx21, Irf1, Cxcr3*

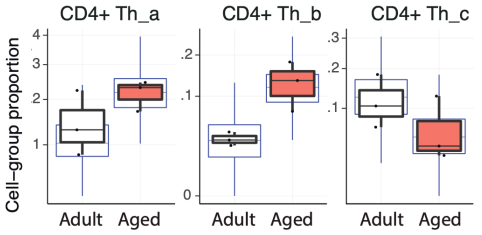

Cluster	Cell subtype	Marker genes
γδT_a	not determined	
γδT_b	γδ17	*JunB, Il17a, Odc1, Klf4, Rora, Icos, Jak1*

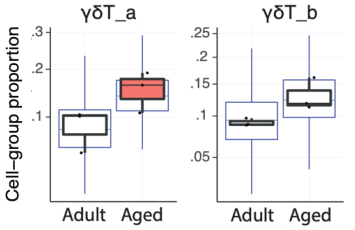

Figure R3.14. Subclustering analysis of CD4+ Th and γδ T cells detects specific cell subpopulations. a, UMAP representation showing the newly detected subclusters. Three new clusters of CD4+ Th were found (CD4+Th_a, _b and _c), shown in blue and circled by a continuous line. Two new clusters of γδ T were found (γδ T_a, and _b), in green and circled by a dashed line. **b**, Table with cluster names, the cell subtype detected, and the marker genes defining each subtype. CD4+ Th subclusters in the top panel, γδ T cells in the bottom panel**. c**, Box plots showing the changes in proportion of CD4+ Th subclusters (top panel) and γδ T cells (bottom panel) between adult and aged performed with *sscomp*[234].

Also, the subpopulation of Th17 cells (CD4+ Th_b) significantly increased in proportion during aging, whereas Th1 cells (CD4+ Th_c) was decreased (**Figure R3.14c**). Thus, these results show that there is a specific and significant increase of Th17 cell subsets during aging.

Subclustering of γδ T cells gave rise to two subpopulations (**Figure R3.14a**). Again, we found a subcluster, Cluster γδT_a, that was not assigned to any specific γδ T cell subset, likely due to a mix of different subpopulations (**Figure R3.14b**). Then, cluster γδT_b gene expression was compatible with γδ T17 cells, as they expressed defining genes including *Il17a*, *Rora*, *JunB* and *Jak1*[248,249] (**Figure R3.14b**). In this case, cell proportion analysis showed that both cell subtypes become more abundant in aged skin, although only the increase in number of γδ T17 cells was significant (**Figure R3.14c**). These results reinforce the possibility of an existing skew of dermal lymphoid cell subsets towards a Th17 phenotype during aging.

3.2.2. Age-associated IL-17 upregulation is likely to be caused by an internal skew

We sought to unravel what the main cause of the increase in IL-17A/F expression in the aged dermis could be. It is known that IL-17 signaling is key when fighting against external pathogens[98]. Thus, the breaching of pathogens through the epidermis and into the dermis due to age-associated defective skin integrity could be responsible for the increase in IL-17A/F expression. To test if immune cells were responding against external antigens, we analyzed the expression of PRRs throughout all our immune cell populations in adult and aged cells. If there had been a pathogen breach through the skin, an increase of PRR expression would be observed, as PRR upregulation after pathogen-induced activation has been previously reported[250,251]. The specific PRR upregulated would depend on the nature of the pathogen, but we focused on the expression

of TLRs, as they are the most well-known and studied PRRs, and recognize a wide variety of antigens[97]. We did not observe an increase in expression of any TLR in our aged dermal immune cell populations, pointing against the possibility of a major pathogen entry through aged skin (**Figure R3.15**). These results shed light into thinking that the increase of IL-17 is caused by an internal skew.

Moreover, we interrogated the expression of IL-17 in the small intestine. This was done to understand if the skew towards IL-17-producing lymphoid cells was also observed in another organ, as this would point towards a systemic effect of our observations. We focused our analysis on the intestine because of its similarities with the skin; it is an epithelial barrier tissue, and has similar number of γδ T cell subsets, which is higher than in other organs[252]. Also, we specifically analyzed the small intestine because it comprises around 80% of the intestine. Anatomically, the small intestine is composed of small projections called villi that increase the intestinal surface area for maximal nutrient absorption[253] (**Figure R3.16a**). Even though the main role of these villi is to absorb nutrients, they are also in tight contact with immune cells[253]. Intestinal villi are composed of an external epithelium that is in direct contact with the absorbed nutrients, and is supported by an interior lamina propria (**Figure R3.16a**). This lamina propria is home to a variety of immune cells, which respond whenever detecting external pathogens, and communicates with further intestinal layers[253]. We did not observe a significant increase in the percentage of cells that expressed either *Il17a* or *Il17f* by FISH in the aged small intestine lamina propria (**Figure R3.16b,c**). Nonetheless, we detected a trend towards an increased *Il17a* expression in the aged counterparts (**Figure R3.16c**). These results indicate that there is no apparent external pathogen affecting the intestine and upregulating *Il17a/f* as a response, and adds up to the skin results to show that neither of the aged barrier organs studied are seemingly exposed to external pathogens. Moreover, all these results lead towards thinking that this

skew towards IL-17 production is most likely caused by internal signals and may be skin specific.

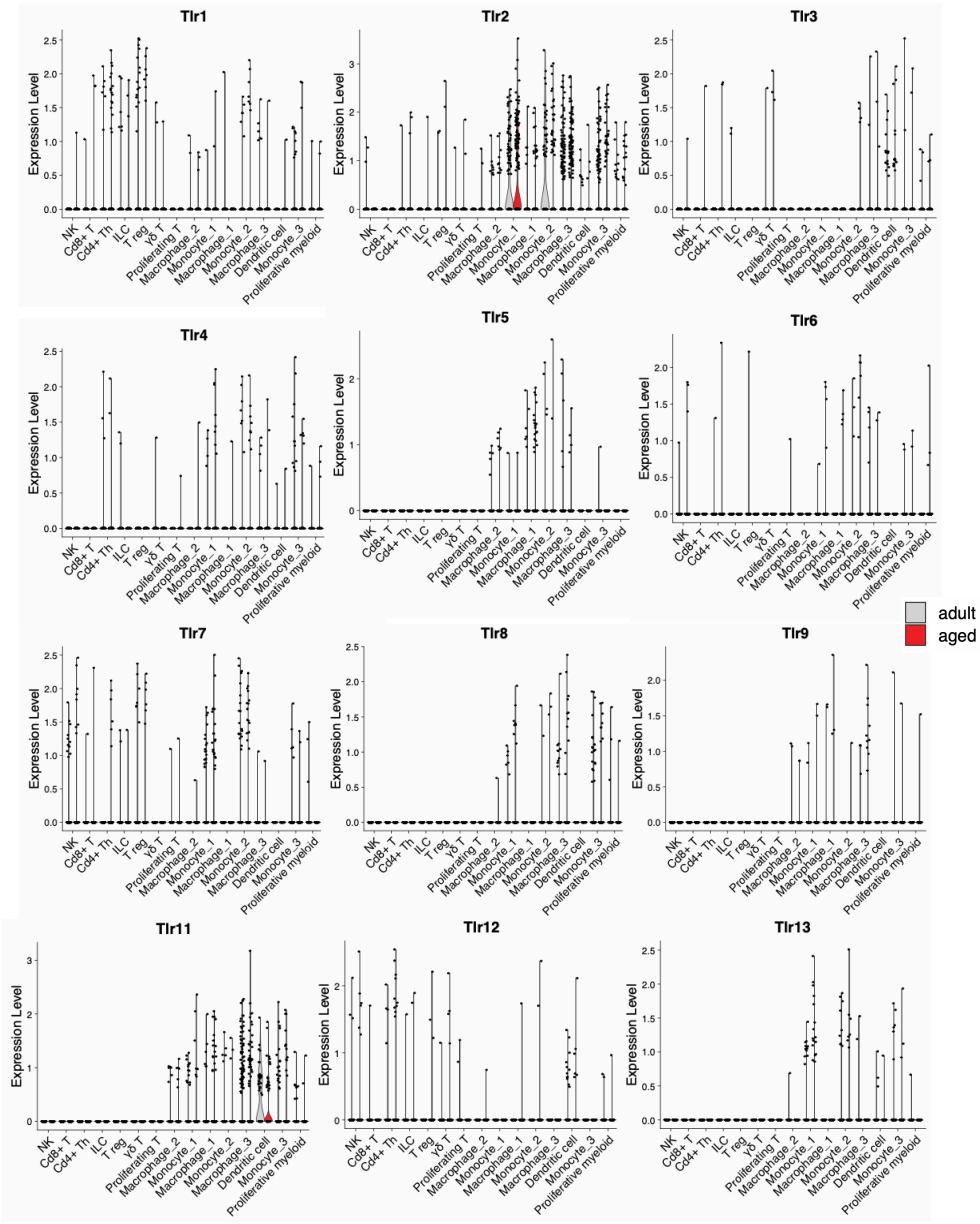

Figure R3.15. TLR expression is not increased in aged immune cells. Violin plots showing the gene expression of the TLR family of PRRs, showing that there is no increase in any family member in aged dermal immune cells. In each case, the first column per cell type depicts gene expression levels in adult cells (colored in grey), and the second column shows levels in aged cells (in red).

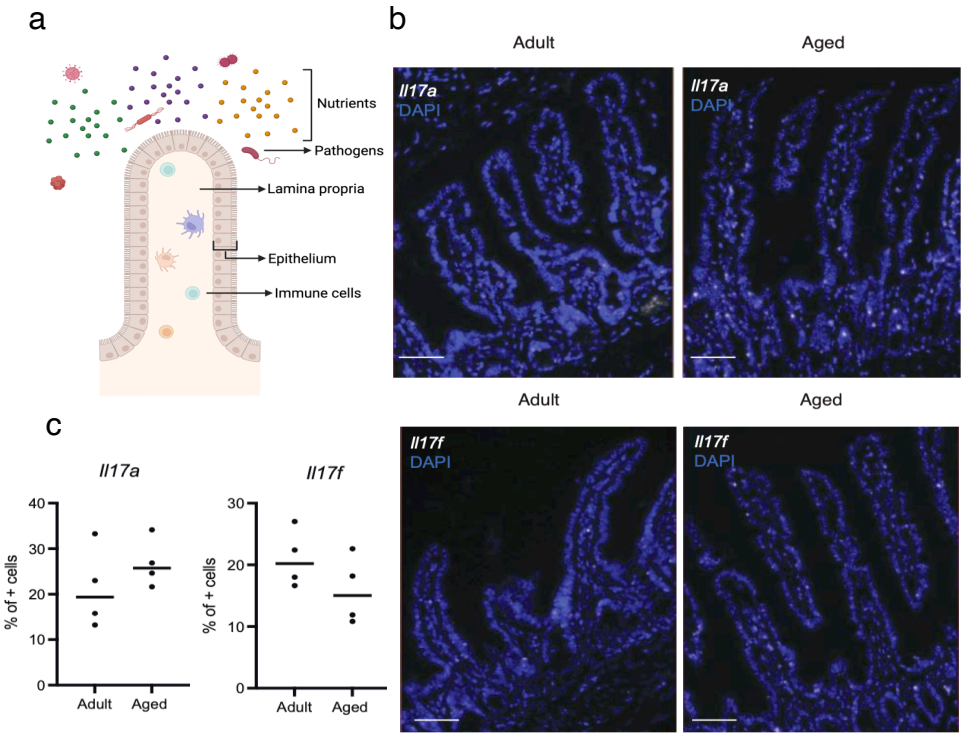

Figure R3.16. IL-17 is not significantly upregulated in the lamina propria of the aged small intestine. a, Schematic summary of the structure of intestinal villi, created with Biorender. **b**, FISH of *Il17a* (top panel) and *Il17f* (bottom panel) in adult and aged mouse small intestine. **c**, Quantification showing percentage of positive cells in the lamina propria. Bar= 50μm

4. IL-17A/F blockade ameliorates the age-associated inflammatory context of dermal cells

We hypothesized that the increase in IL17-A/F could be a main contributor to the pro-inflammatory context present in aged skin. To test this, we blocked the function of IL-17A/F with the use of neutralizing antibodies. This strategy has been used previously in the treatment of autoimmune and chronic inflammatory diseases such as psoriasis, and IL-17 blockade has shown a decrease in the appearance of disease-associated lesions[103].

In this case, we decreased IL-17 function by systemically injecting blocking antibodies against IL-17A and IL-17F three times per week and for a total of three months, in aging mice (73 weeks old) until they aged (85 weeks old) (**Figure R4.1**). The control group was injected an isotype control IgG in mice following the same conditions. Then, our approach was based on analyzing the dermal cells transcriptionally by 10X scRNA-seq, following the previously described workflow (**Figure R1.1**). In this case, we obtained a total of 16,975 CD45+ and 33,262 CD45–/EpCAM– cells, which were analyzed with the same bioinformatics pipeline as the adult and aged cells. We checked for batch effect, verified good sample mixing as well as cell type representation in all replicates[234]. For both CD45+ and CD45-/Epcam-, n=4 replicates per condition (**Figure R4.2a,b**). Here, visual assessment showed that there was no batch effect adjustment needed. After this, we clustered all the CD45+ and CD45-/EpCAM- cells together as we had done for adult and aged cells. We then plotted them using a UMAP representation, and were able to detect the same cell types as with the adult and aged analysis (**Figure R4.3**).

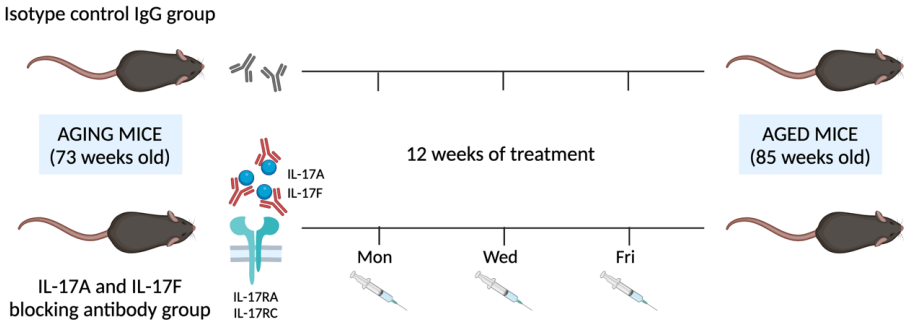

Figure R4.1. Diagram depicting the IL-17 blocking strategy followed. Strategy of the IL-17 blocking treatment in aging mice, with blocking injections carried out three times per week and for 12 weeks. Control mice were injected with an IgG control antibody during the treatment. Figure created with Biorender.

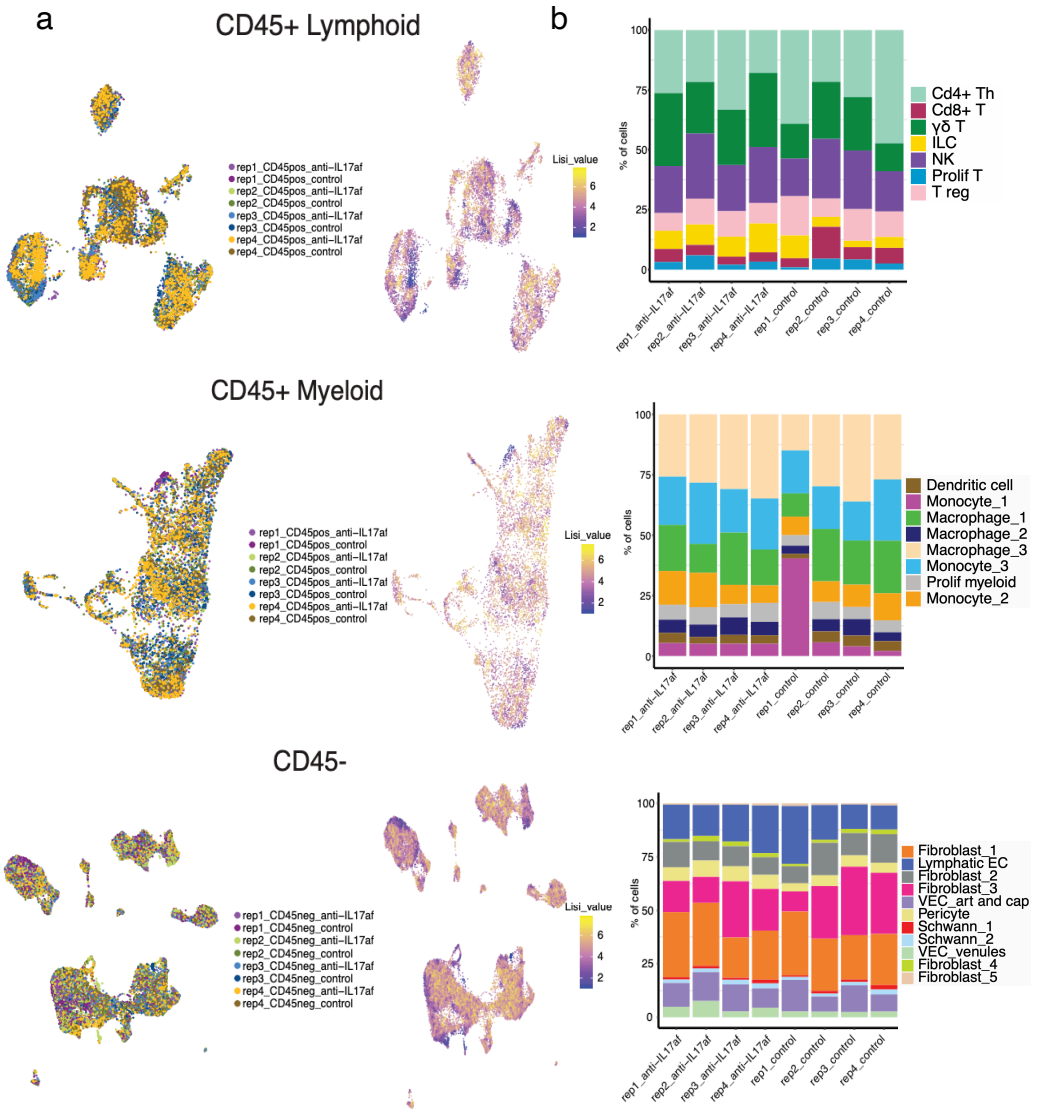

Figure R4.2. Plots depicting batch effect correction, good sample mixing replicate contribution across conditions. **a**, UMAP representation of CD45+ lymphoid (upper panel), CD45+ myeloid (middle panel) and CD45-/EpCAM- (lower panel) cells without batch correction. Then, the good sample mixing values (calculated with LISI) are shown in the right panels. **b**, Bar plots showing the percentage of each cell type per replicate, showing at the top the CD45+ lymphoid, in the middle CD45+ myeloid and in the bottom CD45-/EpCAM- cells.

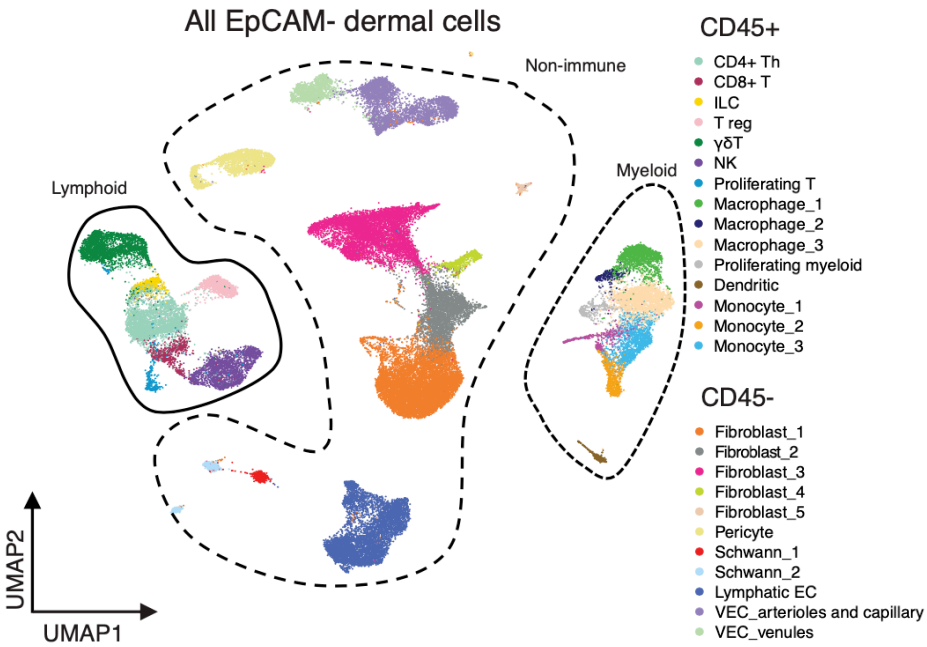

Figure R4.3. UMAP representation of all aged/anti-IL-17A/F blocked and aged/control IgG dermal cell types clustered together. This UMAP shows all cells from IL-17 blocked and control mice, with CD45+ lymphoid (circled with a continuous line), CD45+ myeloid (short-dashed line) and CD45-/EpCAM- (long-dashed line) cells clustered together.

4.1. Schwann cells

We analyzed the Schwann cell clusters in order to understand if they were responding to the IL-17 blockade. In this case, Schwann_1 cells were not undergoing major significant changes as a consequence of IL-17A/F blockade, whereas Schwann_2 cells presented a higher responsiveness to the treatment. Although Schwann_2 cells did not present many differentially expressed genes (DEG) during aging, blocking IL-17A/F function led to an upregulation of genes involved in their precursor-like homeostatic functions. By GO analysis of the upregulated genes post IL-17A/F blocking, we observed an overrepresentation of terms such as differentiation, migration, and ECM organization compared to the aged/control IgG cells (**Figure R4.4**). This suggests that Schwann cell subpopulations are heterogeneous, and do

not respond to stimuli (in this scenario, aging and IL-17A/F blockade) in an equivalent manner.

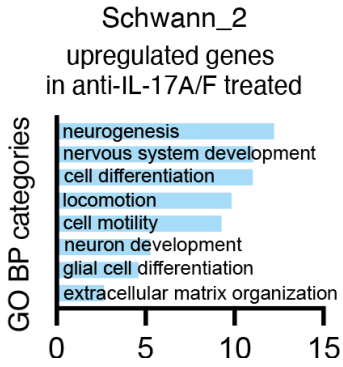

Figure R4.4. Schwann cells upregulate genes crucial for their functions after IL-17A/F blocking treatment. Selected GO categories belonging to biological process (BP) of the upregulated genes in aged Schwann_2 cells show that there is a increase in the expression of genes crucial for their progenitor functions post IL-17A/F blockade. The x axis represents $-(\log_{10})$ of the adjusted *P*-value for each depicted GO category.

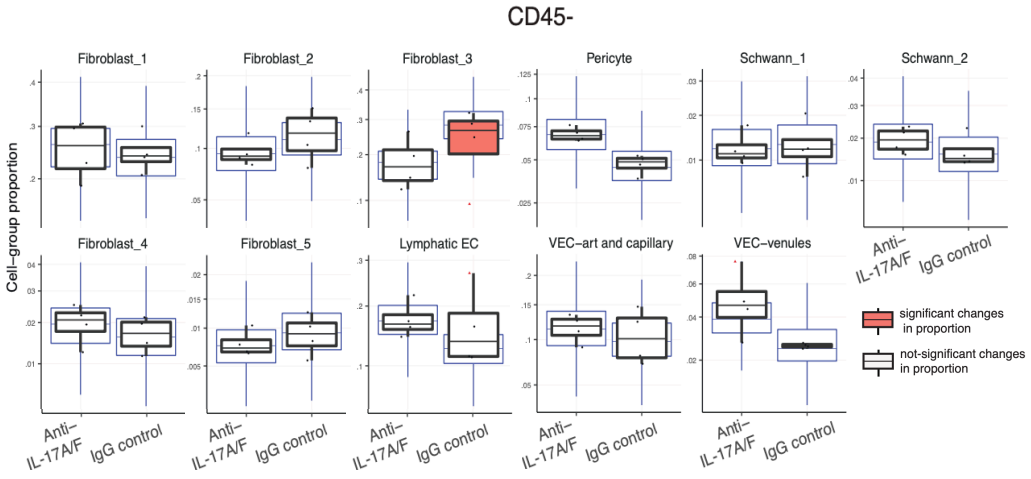

Figure R4.5. Analysis of cell proportion changes in non-immune cells between aged/anti-IL-17A/F treated and aged/control IgG cells. Analysis with *sscomp* tool[234] to detect changes in cell proportion following IL-17A/F blockade. Orange colored boxes show significant changes in cell proportion, and outliers are marked as red triangles outside of the box plots.

In addition, cell proportion analysis showed that neither of these cell clusters were affected in numbers regardless of the IL-17A/F blocking treatment (**Figure R4.5**). Hence, only specific Schwann cell subpopulations respond to the IL-17A/F treatment by altering their gene expression towards an increment of their homeostatic functions, without altering their cell proportion.

4.2. Endothelial cells

Venule ECs responded to the IL-17A/F blocking treatment by decreasing inflammatory functions that had previously been upregulated during aging (**Figure R2.4a**). This was detected by GO analysis of the downregulated genes following the blocking treatment (**Figure R4.6a**). There was also a downregulation of the MHCII complex gene *Cd74* (**Figure R4.6b**), which was upregulated in aged venule ECs (**Figure R2.4b**). Moreover, *Sele* expression defines EC activation and promotes lymphocyte rolling and extravasation[74], and is also downregulated after IL-17A/F blockade (**Figure R4.6b**).

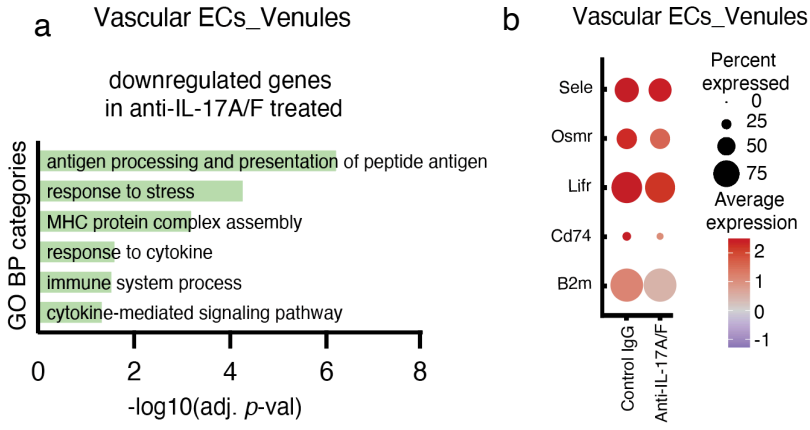

Figure R4.6. Venule ECs downregulate inflammatory functions post IL-17A/F blockade. **a**, Selected GO categories belonging to BP analysis of the downregulated genes after blocking IL-17A/F functions show a decrease in pro-inflammatory functions in venule ECs. **b**, Dot plot of selected genes that contribute to the GO categories shown in (**a**). The x axis represents $-(\log_{10})$ of the adjusted *P*-value for each depicted GO category.

The proportion of venule ECs is not significantly reduced in aged/control IgG mice when compared to aged/IL-17A/F blocked mice (**Figure R4.5**). This shows that this decrease in inflammatory categories post IL-17A/F blocking treatment is not accompanied by a reduction in cell number. Nonetheless, these changes show that ECs decrease their pro-inflammatory state upon IL-17A/F neutralization.

4.3. Fibroblasts

Fibroblast analysis following IL-17A/F neutralization showed a significant decrease in abundance of Fibroblast_3 cells (**Figure R4.5**), which were previously defined as pro-inflammatory fibroblasts. Thus, this shows that these pro-inflammatory cells are reduced in aged skin after IL-17A/F blocking.

In adult and aged conditions, we obtained 5 fibroblast clusters (**Figure R1.4**). In this case, we also observed these same fibroblast populations (**Figure R4.3**). Nevertheless, fibroblasts are major players during skin aging and are also responders to IL-17 signaling, so we decided to study more in depth the specific fibroblast subpopulations that could be responsive to the neutralization of IL-17A/F. For this purpose, we performed a subclustering analysis specifically of the fibroblast populations, obtaining a total of 11 fibroblast clusters. The previous Fibroblast_1 cluster was now divided into three subclusters (Fibroblast_1_0 to _1_2), Fibroblast_2 into two (Fibroblast_2_0 to _2_1), Fibroblast_3 into four (Fibroblast_3_0 to _3_3), and Fibroblast_4 and Fibroblast_5 clusters stayed with one cluster (**Figure R4.7**). Here, we could detect that the fibroblast subpopulations Fibroblast_1_2 and Fibroblast_3_3 were the main responders to the *in vivo* treatment, as they showed the highest number of DEGs between conditions.

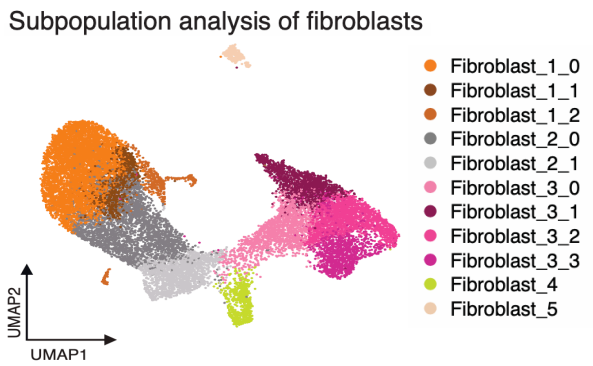

Figure R4.7. UMAP representation of fibroblast subclustering analysis. Fibroblast subpopulations obtained for the aged/control IgG and aged/anti-IL-17A/F treated dermal cells. In total, CD45–/EpCAM– cells included $n = 5$ mice for the aged/control IgG group, and $n = 5$ mice for the aged/IL-17A/F blocked group, with four technical replicates.

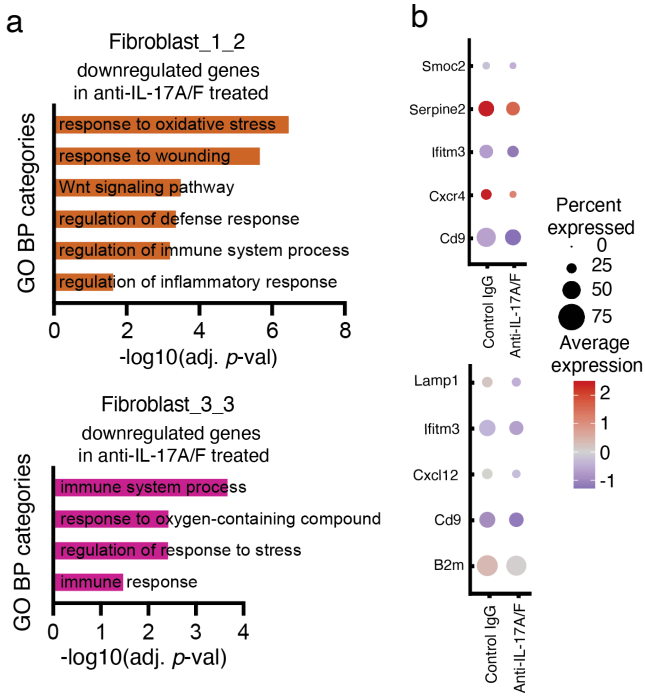

Figure R4.8. Fibroblast subpopulations react to the IL-17A/F blocking treatment by ameliorating their inflammatory traits. **a**, Plot of selected GO categories belonging to BP analysis of the downregulated genes upon blocking IL-17A/F functions in Fibroblast_1_2 (top panel) and Fibroblast_3_3 (bottom panel) subclusters. The x axis represents $-(\log_{10})$ of the adjusted *P*-value for each depicted GO category. **b**, Dot plot of selected genes contributing to GO categories shown in (**a**) for Fibroblast_1_2 (top panel) and Fibroblast_3_3 (bottom panel).

This was reflected in the GO analysis of the downregulated genes upon IL-17A/F treatment (**Figure R4.8a**), as there was a decrease in representation of the pro-inflammatory functions which were previously upregulated during aging in their corresponding clusters (**Figure R2.5**). This was also maintained when looking at the individual gene expression of genes with inflammatory functions, as their expression levels were decreased after blocking IL-17A/F functions (**Figure R4.8b**). These results confirm that fibroblasts are also responsive to the excessive age-related IL-17A/F signaling.

4.4. Immune cells

Myeloid cells are known to respond to IL-17 signaling, and can further aggravate the pro-inflammatory context by secreting pro-inflammatory cytokines[254]. In line with the non-immune results, IL-17A/F blockade resulted on a downregulation of pro-inflammatory functions in specific myeloid populations. This was seen by looking at GO of the downregulated genes in cells from the IL-17A/F blocked condition in Monocyte_1 cluster, which were previously described as pro-inflammatory cells (**Figure R4.9a**). Also, there was a decrease in *Il1b* expression in clusters that were upregulating its expression during aging; Monocyte_1, Macrophage_2 and DC clusters (**Figure R4.9b**). Of note, there was no significant change in cell proportions following IL-17A/F inhibition, which shows that these gene expression changes were not corresponded with changes in cell number (**Figure R4.10**).

Moreover, lymphoid cells did not respond transcriptionally or in cell proportion to the anti-IL-17A/F treatment (**Figure R4.10**), which is why they are not further described after the blocking treatment.

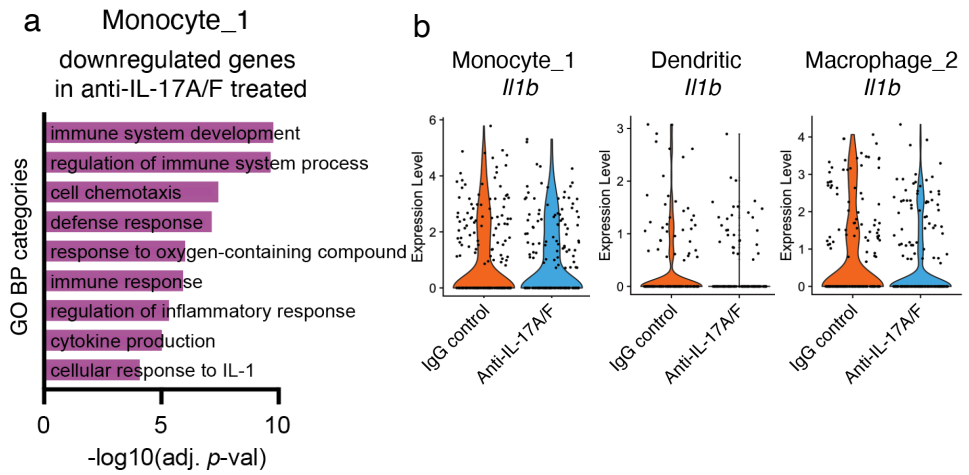

Figure R4.9. Only specific myeloid cell populations downregulate inflammatory functions post IL-17A/F blockade. **a**, Plot of selected GO categories belonging to BP analysis of the downregulated genes after blocking IL-17A/F functions in Monocyte_1 cluster. The x axis represents –($\log_{10}$) of the adjusted *P*-value for each depicted GO category. **b**, Violin plots of *Il1b* expression in aged/control IgG and aged/anti-IL-17A/F treated cells in Monocyte_1, Dendritic and Macrophage_2 clusters.

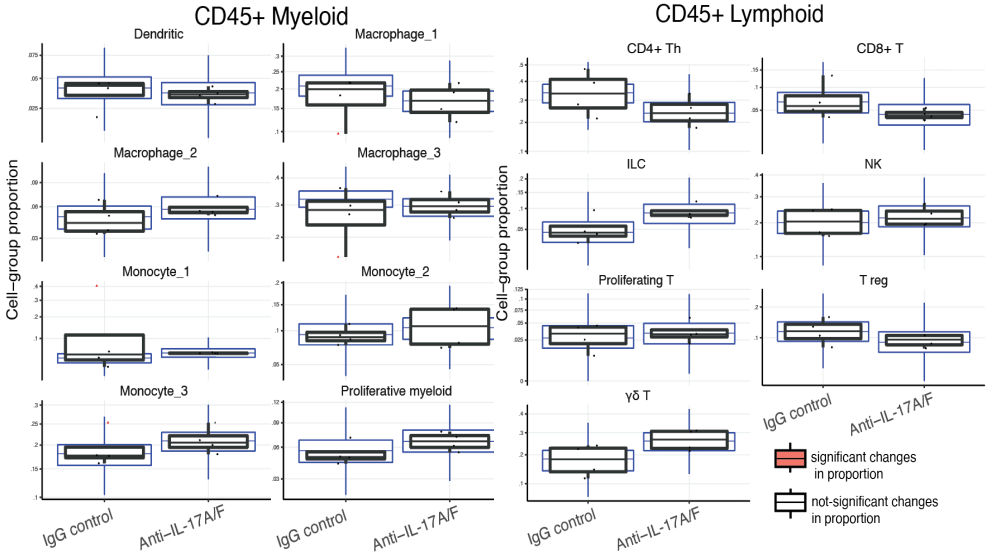

Figure R4.10. Analysis of cell proportion changes in immune cells between aged/anti-IL-17A/F treated and aged/control IgG cells. Analysis with *sscomp* tool[234] to detect changes in cell proportion post IL-17A/F blockade. Orange colored boxes show significant changes in cell proportion, and outliers are marked as red triangles outside of the box plots.

5. Keratinocytes are sensitive to excessive dermal IL-17A/F signaling during aging

Keratinocytes are known to be major responders of exacerbated IL-17 signaling in chronic inflammatory diseases of the skin[102,246]. This is why we interrogated if keratinocytes were reacting to the IL-17A/F blockade during aging. Aged keratinocytes have been shown to increase their pro-inflammatory functions, and we wondered if this changed after IL-17A/F blocking treatment[112,114,136].

Bulk RNA-seq analysis of adult and aged keratinocytes confirmed that epidermal cells upregulate pro-inflammatory functions during aging. This was seen by GO analysis of the age-upregulated genes. We observed an increased representation of pro-inflammatory functions, as well as of categories related to ROS, which is a well-known aged epidermal trait[112] (**Figure R5.1**).

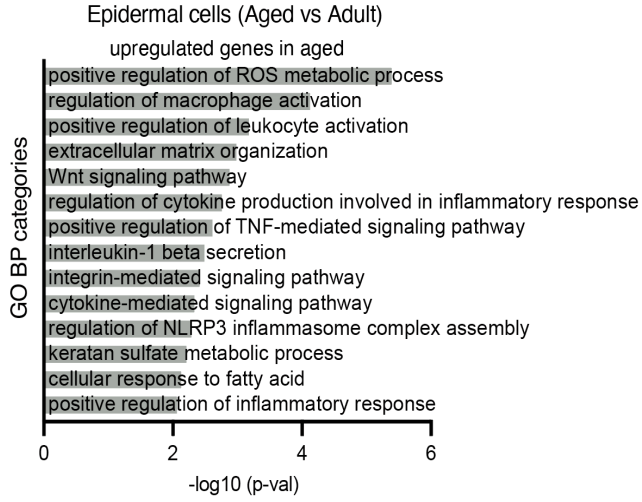

Figure R5.1. RNA-seq of aged epidermal cells show an increase in inflammatory and age-associated functions. Selected GO categories belonging to BP analysis of the age-upregulated genes in epidermal cells. N=4 mice per condition. The x axis represents $-(\log_{10})$ of the adjusted *P*-value for each depicted GO category.

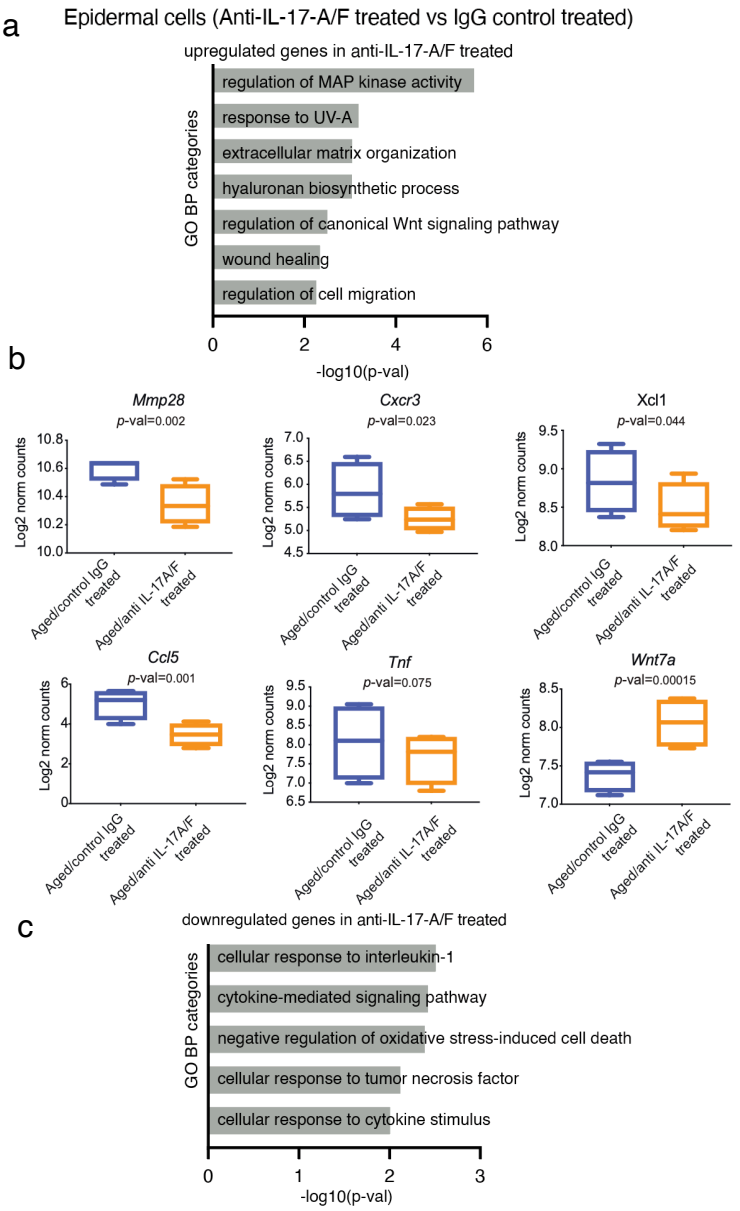

Figure R5.2. Epidermal cells decrease their inflammatory and age-associated functions after blocking IL-17A/F. **a**, Selected GO categories belonging to BP analysis of the upregulated genes in IL-17A/F blocked epidermal cells. The x axis represents $-(\log_{10})$ of the adjusted *P*-value for each depicted GO category. **b,** Box plots showing expression levels of selected genes from the DEGs in epidermal cells upon treatment. **c**, Selected GO categories belonging to BP analysis of the downregulated genes in IL-17A/F blocked epidermal cells. The x axis represents $-(\log_{10})$ of the adjusted *P*-value for each depicted GO category.

Then, bulk RNA-seq of aged keratinocytes upon IL-17A/F blocking treatment, compared to aged/control IgG cells, showed a decrease in the expression of inflammatory genes. GO analysis of the downregulated genes in keratinocytes from the IL-17A/F blocking condition included an underrepresentation of functions related to cytokine signaling and oxidative stress (**Figure R5.2a**). Importantly, this downregulation was also seen when looking at individual genes, as following IL-17A/F treatment there was a reduction in the expression of genes with pro-inflammatory functions such as *Mmp28*, *Cxcr3*, *Xcl1, Ccl5*, and *Tnf* (**Figure R5.2b**).

Moreover, GO analysis of the upregulated genes after IL-17A/F blockade showed an increased representation of epidermal functions that become deteriorated during aging (**Figure R5.2c**). This included the upregulation of genes related to ECM organization, Wnt signaling pathway as well as wound healing, and was also seen when looking at the expression level of genes crucial for these functions such as *Wnt7a*[255] (**Figure R5.2b**). These results lead to conclude that epidermal cells are responding to IL-17A/F signaling during aging, increasing their pro-inflammatory functions and contributing to their deterioration.

6. The development of age-related skin traits is delayed after IL-17A/F neutralization

After describing the transcriptional changes occurring in aged skin cell types as a consequence of IL-17A/F signaling blockade, we wondered if these changes had an impact in overall skin integrity. For this, we measured several parameters that are known to be deteriorated in aged skin following the IL-17A/F blocking treatment.

6.1. Cornified layer thickness

The cornified layer is the most exterior layer of the skin, composed of highly cross-linked and keratin-enriched cells, and confers impermeability, stability and protection[2,3].

The increased cornified layer thickness in aged skin is a well-known age-associated trait[110,112], and we have detected an increase of around double the size in aged/control IgG treated mice compared to adult mice (**Figure R6.1a,b**). Surprisingly, blocking IL-17A/F function in aging mice led to a decreased cornified layer thickness of these mice when compared to aged/control IgG mice (**Figure R6.1a,b**).

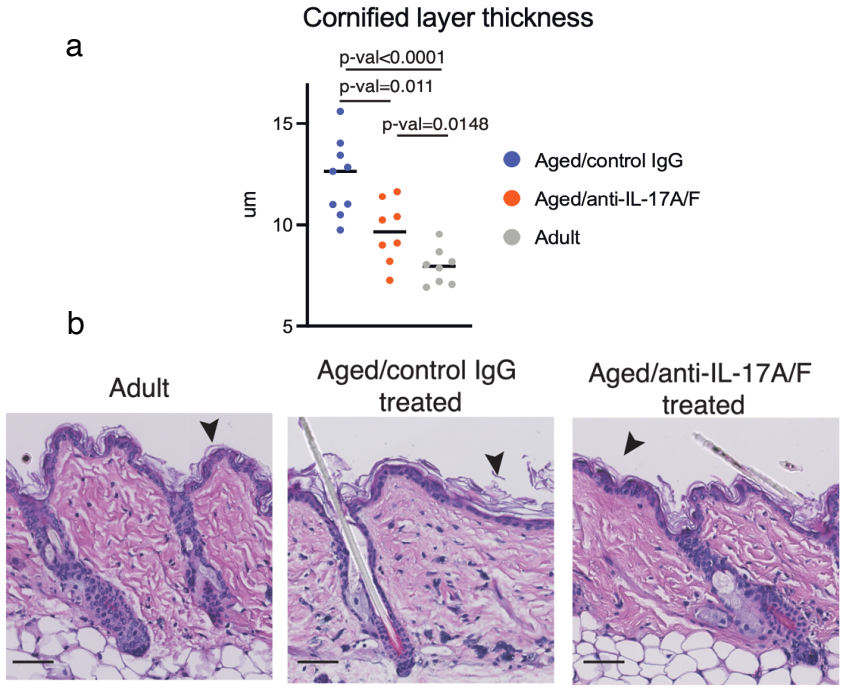

Figure R6.1. The cornified layer thickness of aged/anti-IL-17A/F mice is decreased compared to aged/control IgG mice. **a**, Quantification plot of the cornified thickness measurements in aged/control IgG, aged/anti-IL-17A/F antibody treated and adult mice. Each dot represents the average of 10 measures per mouse ($n = 8$ mice) performed in HE stainings of skin sections shown in (**b**). The line depicts the median of these individual values per age and condition. *P*-values were calculated by Mann Whitney *U* test. **b**, Representative images of the HE stainings used to quantify the cornified layer thickness in (**a**). Black arrowheads point to the cornified layer measured. Bar= 50µm.

6.2. Hair follicle cycling

During aging there is a decrease in hair density, and HF miniaturization[113,134]. Moreover, HF cycling is impaired during aging, and is characterized by a delay in anagen entry, which is the hair growth phase. Our results corroborated this by showing a delay in anagen stage entry after hair plucking in aged/control IgG mice when compared to adult mice 8 days post epilation (**Figure R6.2a,b**). Then, the anagen stages in which the HFs were at were measured, indicating how much the HF growth had advanced[16]. Interestingly, aged/anti-IL-17A/F treated mice were in a very similar anagen stage to adult mice, showing a faster hair regrowth than the aged/control IgG mice (**Figure R6.2a,b,c**).

Of note, blocking IL-17A/F did not induce spontaneous anagen entry in non-plucked mice (**Figure R6.2d**). This points towards showing that HFSCs of aged/anti-IL-17A/F blocked mice are more fit to be reactivated when the hair shaft is removed than those of aged/control IgG treated. Moreover, when analyzing in depth the specific changes that HFs from aged/anti-IL-17 treated mice had undergone, we detected a mild increase in *Rspo3* expression levels in the DP by FISH (**Figure R6.3a**). R-Spondin 3 (RSPO3) is a Wnt agonist, and its expression in DP cells is crucial for these cells to carry out their essential functions in hair growth[41,256,257]. We then checked for *Rspo3* expression in Fibroblast_1_0 and 1_2 subclusters, as they included DP cells. Here, we found that the increase in *Rspo3* levels was maintained when looking at the 10X scRNA-seq data (**Figure R6.3b**).

Thus, this increase in *Rspo3* levels in the DP of aged/anti-IL-17A/F treated mice contributes to show that there is a slowing down of the deterioration of HF function after neutralizing excessive IL-17A/F signaling.

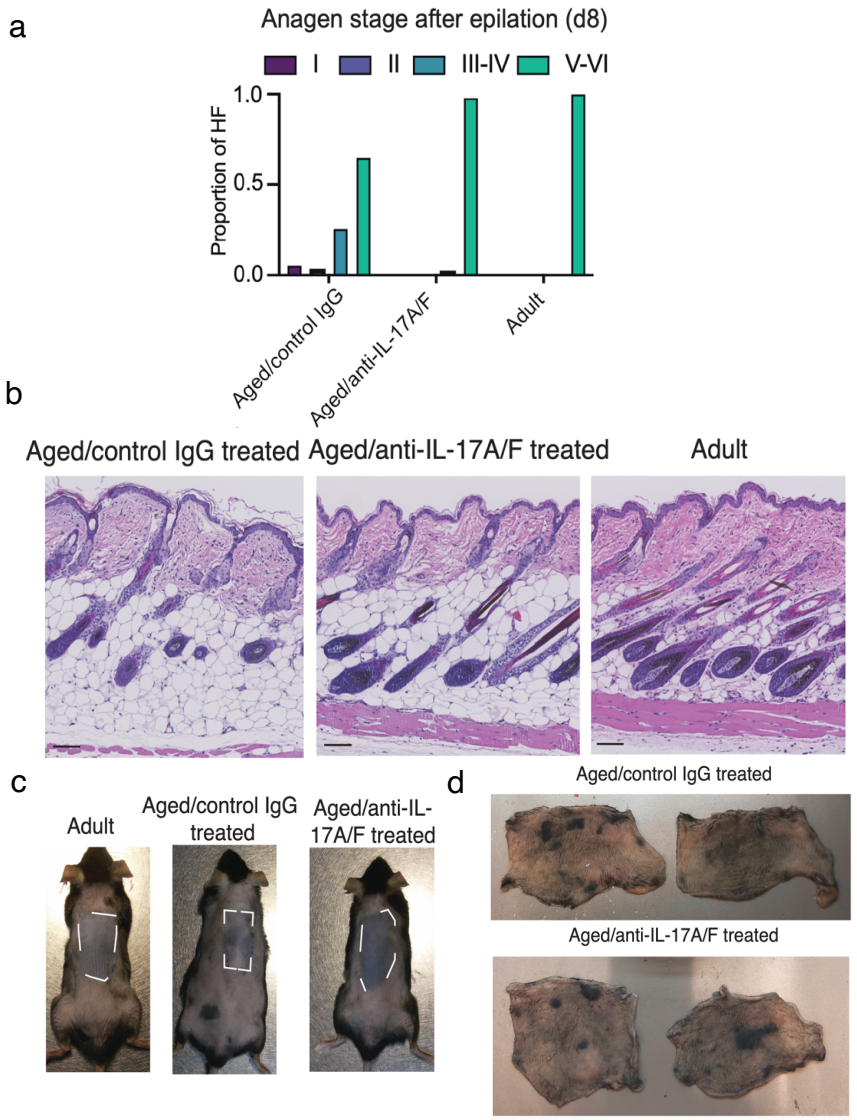

Figure R6.2. Aged/anti-IL-17A/F mice enter anagen faster than aged/control IgG mice. **a**, Quantification plot of the anagen stages (I to V-VI) in aged/control IgG, aged/anti-IL-17A/F antibody treated and adult mice 8 days after epilation. N=6 mice per condition. **b**, Representative images of the HE stainings 8 days post epilation used to quantify (**a**). Bar= 100μm. **c**, Images of shaved mouse back skins showing epilated areas (areas inside of the white dashed lines) 8 days post epilation. Adult mice are shown in the left panel, aged/control IgG in the middle panel and aged/anti-IL-17A/F in the right panel. Black patches denote anagen. **d**, Images of back skins of aged/control IgG (top image) and aged/anti-IL-17A/F (bottom image) non-epilated mice. Black patches denote anagen.

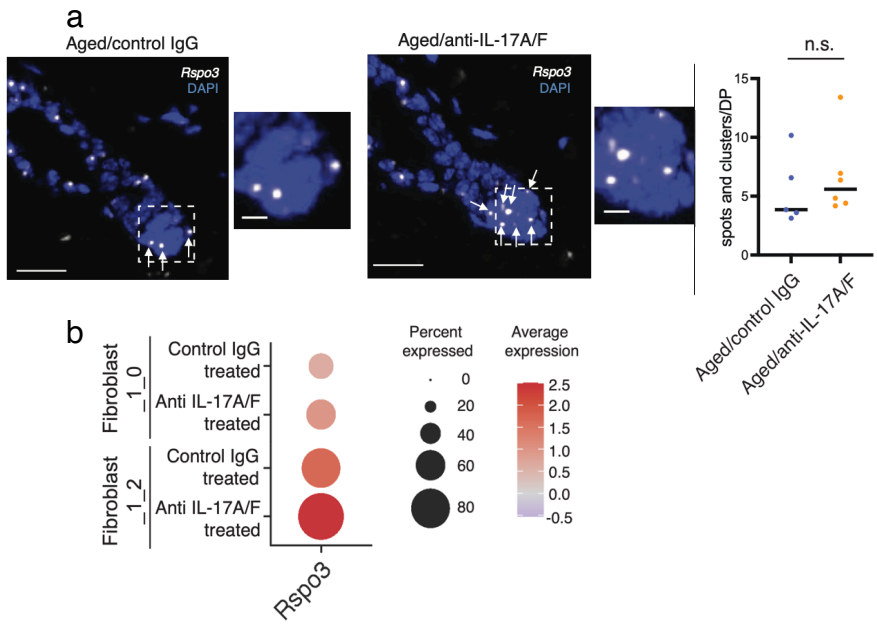

Figure R6.3. *Rspo3* expression is increased in aged/anti-IL-17A/F dermal papilla compared to aged/control IgG mice. **a**, Representative images of FISH (left and middle panels) of *Rspo3* in aged/control IgG and aged/anti-IL-17A/F mouse back skin. The quantification plot (right panel) shows the number of *Rspo3* spots and clusters detected per DP. Bar= 50μm. Insets show magnifications, bar= 20μm. Only for visualization purposes, brightness and contrast were adjusted on these images. **b**, Dot plot of the average expression and percent expressed of *Rspo3* gene expression in subclusters Fibroblast_1_0 and _1_2, which is where DP are clustered, in aged/control IgG and aged/anti-IL-17A/F conditions.

6.3. Trans-epidermal water loss recovery

The permeability of the skin is affected during aging, which is mainly caused by deterioration of the cornified layer[117]. The skin permeability is commonly measured using TEWL values, which quantifies water evaporation through the skin surface[118,119]. During aging, there are no clear differences in basal TEWL values, as the skin barrier can still keep its impermeable functions in a homeostatic range. However, these age-related differences in evaporation are clear after a barrier disruption, using techniques such as tape stripping[118-120]. This is a technique that causes an acute barrier disruption to the skin by mechanically removing the cornified later[122,123]. Removing the cornified layer leads to increased

water evaporation through the skin and, as a result, higher TEWL values. In order to restore the barrier, epidermal cells need to proliferate and differentiate[122,123]. In homeostatic conditions the recovery of basal TEWL values after tape stripping is achieved in a few hours, but this recovery is impaired during aging[118,120]. This is because aged epidermal cells take longer to proliferate and differentiate to recover the barrier than adult cells.

Thus, we have measured the TEWL values over time of aged/control IgG, aged/anti-IL-17A/F and adult mice after tape stripping to measure how fast they were restoring their impermeable barrier upon disruption. With this, we have seen that the TEWL values during the first 24 hours following tape stripping showed a significant delay in recovery in aged/control IgG mice compared to adults (**Figure R6.4a,b**).

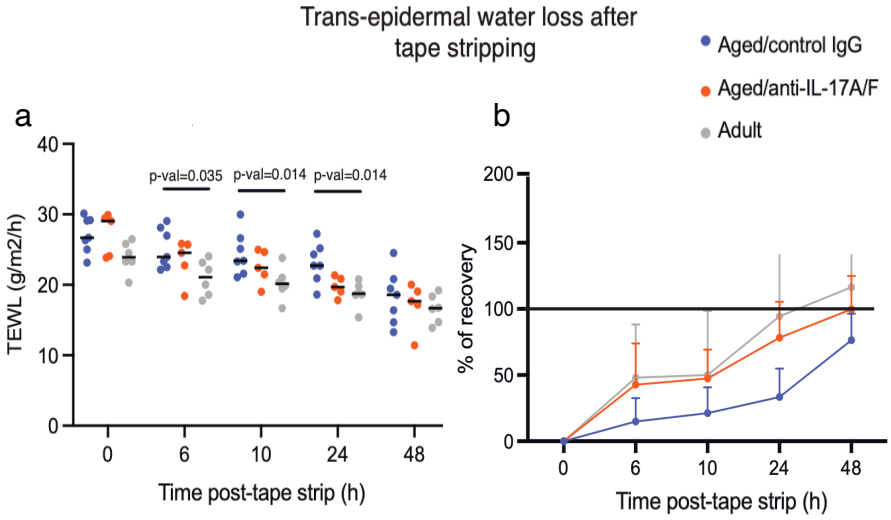

Figure R6.4. Barrier permeability regeneration occurs faster post IL-17A/F inhibition than in aged controls. **a**, Plot depicting TEWL values (g/m²/h) after tape stripping (0, 6, 10, 24, 48 hours upon tape stripping) in aged/control IgG, aged/anti-IL-17A/F and adult back skin. *P*-values were calculated by Mann Whitney *U* test, n=5 to 7 mice per condition. **b**, Plot showing the percentage of recovery compared to the initial value of TEWL values after tape stripping in the same conditions than (**a**).

This was detected when looking at total TEWL values, as aged/control IgG mice have increased evaporation values compared to the other conditions (**Figure R6.4a**), and in the percentage of recovery in comparison to the initial values as well (**Figure R6.4b**).

Surprisingly, this delayed recovery was not significant any more when comparing aged/anti-IL-17A/F mice to adult mice (**Figure R6.4a,b**). Aged/anti-IL-17A/F treated mice present more similar TEWL values and recovery to adults over time. This shows that aged/anti-IL-17A/F mice recover their barrier integrity faster than aged/control IgG mice, and resemble more the state of adults.

6.4. Wound healing efficiency

WH requires SCs and niche cells to respond rapidly to deal with the damage generated and restore the skin layer. Therefore, it requires a coordinated action from epidermal and dermal cells[124]. During aging, there is an impairment of the efficiency of WH, which leads to an overall decrease in speed of recovery[129-132]. We wondered if the neutralizing injections against IL-17A/F had impacted the efficiency of WH in aging mice. To test this, we carried out 5mm wounds on each flank of adult, aged/control IgG and aged/anti-IL-17A/F back skin. Of note, antibody injections were stopped one week prior to the wound generation in light of studies showing the relevance of IL-17 in the WH process, to differentiate the function of the cytokine specifically in WH to that in skin aging[99].

First, we looked at speed of wound closure and did not find differences between conditions, which goes in line with studies showing that macroscopic changes may not properly indicate WH efficiency[131] (**Figure R6.5a**). Then, we focused on analyzing epidermal maturation status 10 days post-wound generation. Epidermal cells must completely mature to obtain efficient WH, by migrating to the upper layers while losing their

nucleus, which is a state named othokeratosis[126]. We were able to observe orthokeratotic epidermis in the wounded areas of the adult epithelium (**Figure R6.5b,c**). However, in aberrant WH scenarios, epithelial cells are not able to completely mature before reaching the upper layers, and as a result retain their nucleus. This is named parakeratosis, and is known to occur in contexts such as chronic wounds and aging[133]. In line with this, we observed a high proportion of parakeratotic epidermis in wounded areas of aged/control IgG mice, showing an incorrect barrier recovery (**Figure R6.5b,c**). Interestingly, when analyzing epidermal maturation status of aged/anti-IL-17A/F treated mice, we observed an intermediate state between adult and aged/control IgG wounds. In this case, there was less parakeratosis observed than in the aged control mice wounds, but the orthokeratosis levels where in many cases not as advanced as in adult mice wounds (**Figure R6.5b,c**).

Moreover, we also interrogated the dermal maturation state in all conditions 10 days after wounding. Correct WH requires the maturation of granulation tissue towards fibrotic tissue. The granulation tissue includes newly formed ECM, blood vessels, fibroblasts, macrophages and other immune cells that cover the wound[124,126-128]. In adult wounds, we observed a more mature granulation tissue in the affected areas (**Figure R6.5b,d**), as opposed to the immature tissue detected in the aged/control IgG condition. Surprisingly, granulation tissue in aged/anti-IL-17A/F treated wounds presented a similar maturation state to that of adults, presenting a similar efficiency between these conditions (**Figure R6.5b,d**). Hence, the increase in WH efficiency in mice after IL-17A/F blockage occurs at both epidermal and dermal level.

Therefore, we have found that excessive IL-17A/F signaling in aged skin is key in the development of age-associated parameters, and that its prolonged neutralization during aging ameliorates the development of these traits.

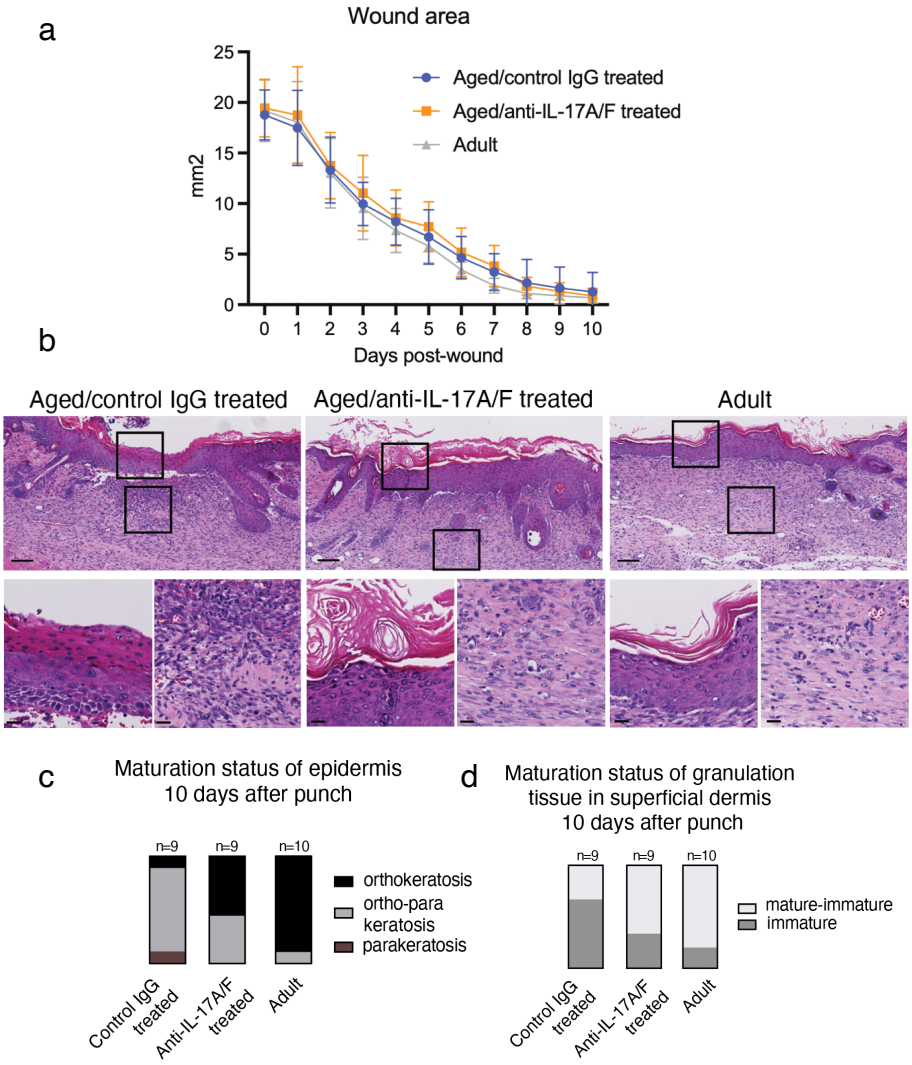

Figure R6.5. Wound healing efficiency is increased in aged/anti-IL-17A/F treated mice compared to aged controls. **a**, Plot depicting wound area measurements (mm^2) from start to 10 days post-wounding in aged/control IgG, aged/anti-IL-17A/F and adult back skin. Measurements include average of both wounds per mice. **b**, Representative HE stainings of wounds 10 days post wounding (top panels) in aged/control IgG (left panel), aged/anti-IL-17A/F (middle panel) and adults (right panel). Bar= 100μm. Insets of each image (lower panels) show details of dermis and epidermis in each case. Bar= 20μm. **c**, Plot showing the maturation status of epidermal cells, by quantification of presence (parakeratosis) or absence (orthokeratosis) of nuclei in the cornified layer 10 days after wounding. **d**, Plot showing the maturation status of the dermal granulation tissue 10 days post wound generation in all conditions.

7. IL-17A/F activity relies on downstream epidermal NF-κB signaling

IL-17A/F are mostly produced by immune cell subsets in the skin, and keratinocytes are one of the main target cell types[94]. IL-17A/F signaling triggers potent inflammatory pathways, and the most well-known is the canonical NF-κB pathway, which is crucial for epidermal homeostasis[94]. Therefore, we wondered if the canonical NF-κB pathway could be responsible for the activation of the pro-inflammatory context generated in an IL-17A/F-dependent manner. For this, we carried out chromatin immunoprecipitation followed by sequencing (ChIP-seq) of p65 (or RELA) in epidermal cells of aged/control IgG, aged/anti-IL-17A/F and adult mice. We obtained a total of 4169 peaks in aged/control IgG, 6014 in aged/anti-IL-17A/F–treated and 8525 in adult epidermal cells, coming from 4 biological replicates per condition (**Figure R7.1a**). We annotated those peaks to their closest gene, we filtered out those that were not associated to a protein-coding gene and analyzed the biological function of the remaining genes bound by p65 by GO term analysis.

In order for the canonical NF-κB pathway to be active, p65 must be bound to the DNA, activating the transcription of inflammation-related genes[92]. Thus, if p65 and NF-κB signaling were relevant for IL-17A/F activity, there would be an increase in genes with inflammatory functions in conditions with increased IL-17A/F. Reassuringly, genes bound by p65 in aged/control IgG epidermal cells showed an increase in inflammatory functions compared to those bound in adults, which coincides with the age-related increase in IL-17A/F signaling. This was detected looking at the degree of significance of GO categories between conditions, as inflammatory processes were more significant in aged/control IgG conditions compared to adults (**Figure R7.1b,c**). In addition, there was less binding of p65 in regulatory areas of genes such as *Il9* and *Crlf2* in adult compared to aged/control IgG epidermal cells, which are genes

known to be relevant in pro-inflammatory contexts[258,259] (**Figure R7.1b,c**). The reduced presence of p65 in regulatory areas of pro-inflammatory genes in adult cells contributes to show that NF-κB signaling controls the activity of pro-inflammatory genes in contexts with an increased IL-17 expression. Moreover, IL-17A/F blockade reduced the binding of p65 to genes with pro-inflammatory functions in aged epidermal cells. This is reflected by less significant inflammation-related GO categories, as well as by a decreased of binding to regulatory areas of inflammatory genes, which reflects what was seen for adult cells (**Figure R7.1b,c**). However, this effect was only seen partially, as there were other genes with inflammatory functions still bound by p65 following IL-17A/F blocking treatment (**Figure R7.1d**). This could be due to the existence of other NF-κB regulators, or to the hampering of IL-17A/F being short-term and not generating sufficient blockade of its functions.

Interestingly, we found that p65 binding to regulatory areas of genes with functions crucial for homeostatic functions was lost during aging (**Figure R7.2a**). This agrees with studies that state that NF-κB pathway activity is aberrant during aging, contributing to epidermal deterioration[260,261]. This was the case of Envoplakin (Evpl) and Keratin 14 (Krt14), which are essential for skin maintenance[262,263], and lost p65 binding during aging (**Figure R7.2b**). In contrast, p65 binding was maintained in aged/anti-IL-17A/F blocked cells, even if this effect was only seen for a specific subset of genes. There were other genes important for epidermal maturation, such as *Dll1*[264], which did not retain p65 binding subsequent to IL-17A/F blocking treatment (**Figure R7.2c**).

Overall, these results show that p65 binding and NF-κB activity are strongly influenced and regulated by IL-17A/F, and that it accounts for part of the pro-inflammatory and less homeostatic context seen in aged skin.

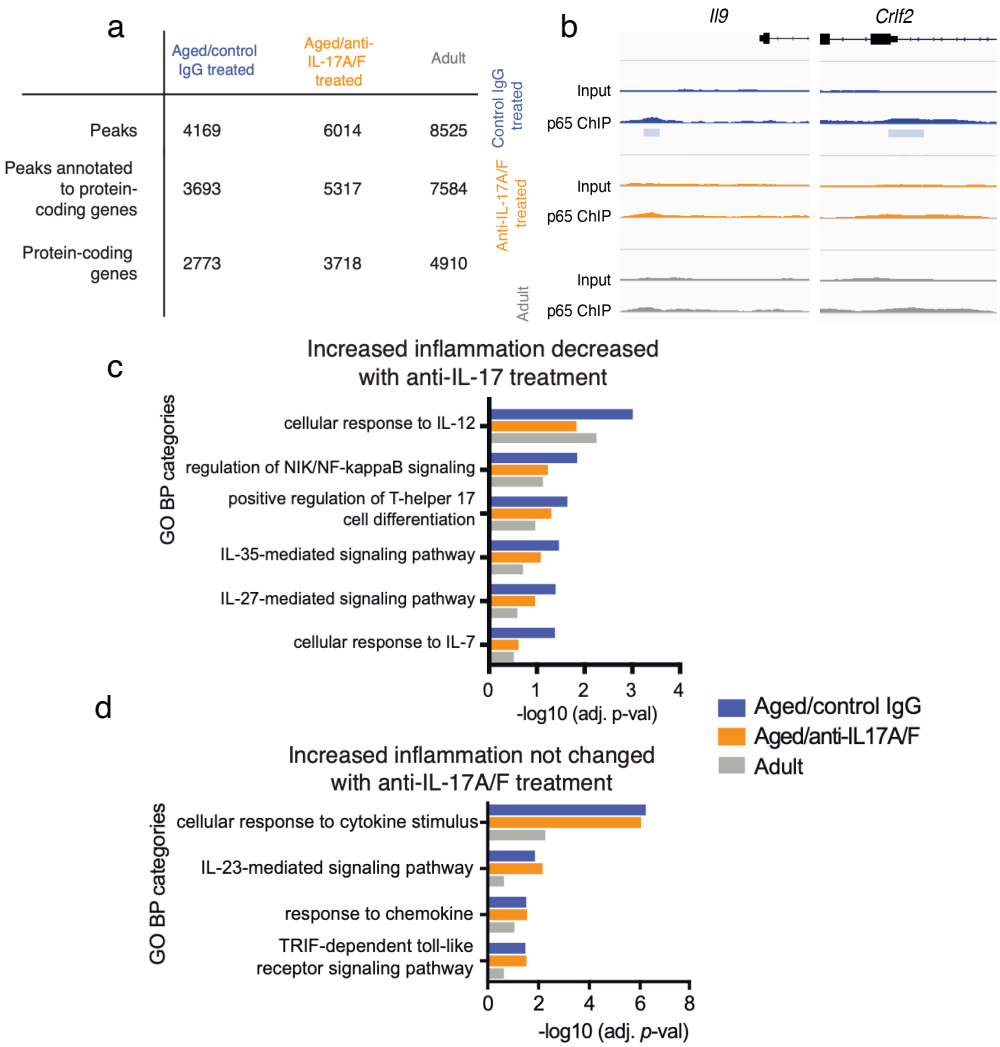

Figure R7.1. NF-κB pathway activates inflammatory functions downstream of IL-17A/F. **a**, Table summarizing the number of peaks, the peaks annotated to protein-coding genes and the number of protein-coding genes obtained in the p65 ChIP-seq. These results were obtained from pooling the reads obtained from 4 biological replicates analyzed separately per condition, which were aged/control IgG, aged/anti-IL-17A/F and adults. **b**, Snapshot of p65 binding to regulatory areas of genes with inflammation-related functions found in (**c**). **c**, Plot showing GO selected categories of BP analysis depicting pro-inflammatory functions being less significant in aged/anti-IL-17A/F and adult cells in comparison to aged/control IgG epidermal cells. The x axis represents $-(\log_{10})$ of the adjusted *P*-value for each depicted GO category. **d**, Plot depicting GO selected categories belonging to BP analysis showing pro-inflammatory functions that were not changed post IL-17A/F blockade compared to aged/control IgG cells. The x axis represents $-(\log_{10})$ of the adjusted *P*-value for each GO category.

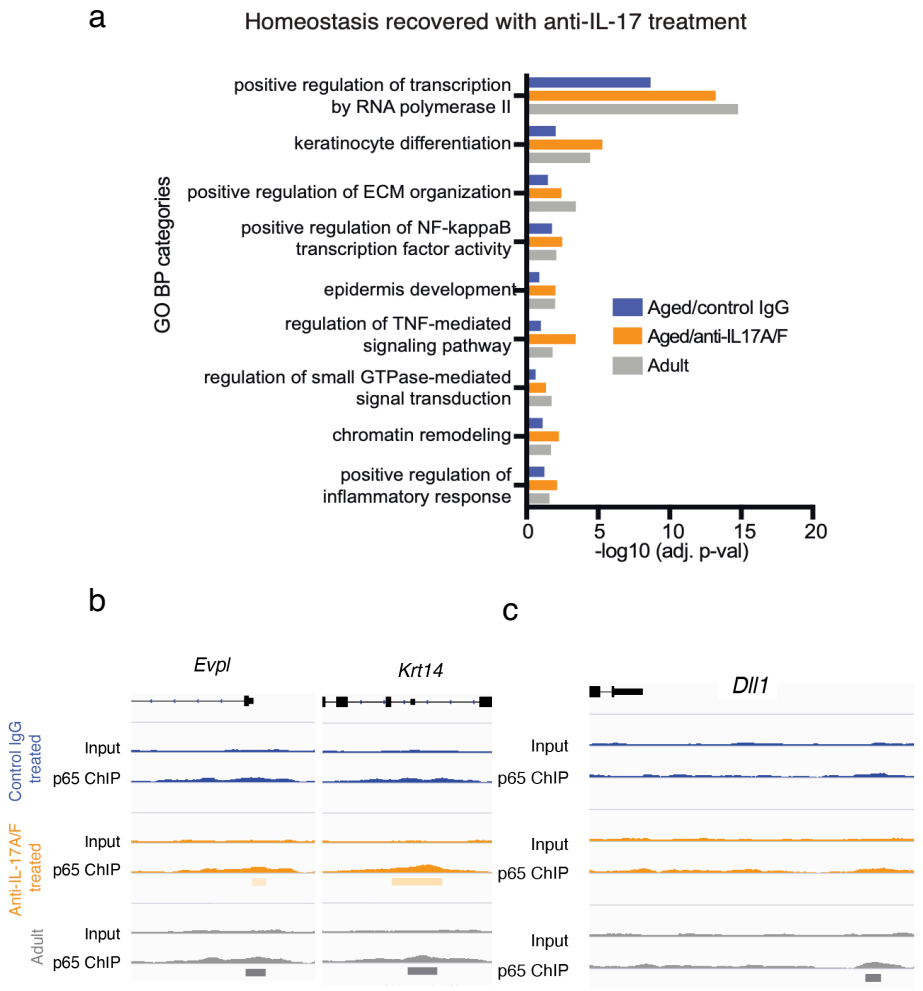

Figure R7.2. IL-17A/F inhibition retains p65 binding to epidermal homeostatic genes during aging. a, Plot showing GO selected categories belonging to BP analysis depicting homeostatic functions that lose significance in aged/control IgG epidermal cells, and retain it in aged/anti-IL-17A/F and adult cells. The x axis represents $-(\log_{10})$ of the adjusted *P*-value for each GO category. **b**, Snapshots of genes with epidermal homeostatic functions bound by p65 in aged/anti-IL.17A/F and adults, obtained from GO analysis in (**a**). **c**, Snapshot of p65 binding to a regulatory area of *Dll1* gene in adults exclusively.

Chapter 2. Age-associated mechanical changes impact on rhythmic epidermal homeostasis

1. The mechanical properties of the epidermal niche are altered during aging

The skin undergoes changes in structure and architecture during aging, which affect its overall functions. In the dermis, these changes include a decrease in cell density and ECM, a loss of collagen secretion by fibroblasts, a decrease in elasticity, as well as the appearance of a pro-inflammatory context[109,110]. This is accompanied by an increased stiffness in the aged ECM and dermis[110].

EpSCs in the basal layer reside in direct contact with the BM. These cells are known to communicate with and be influenced by the BM, as well as by other residing structures and cell types in the dermis[28,31]. We wondered if the age-associated changes in the ECM and in dermal stiffness could be extrapolated to the BM, especially to areas in contact with epSCs. This includes primarily the IFE, which is the region of stratified epidermis flanking HFs that englobes epidermal cells and epSCs[1]. If the BM region surrounding the IFE was becoming stiffer during aging, it is likely that there would be alterations in the communication between epSCs and their niche. To determine this, we measured the Young modulus existing in the BM adjacent to the IFE of adult and aged murine back skin. The Young modulus measures the ability of a material to withstand changes when it is under tension or compression, known as elasticity. Atomic force microscopy (AFM) measures showed that there was an increased stiffness in the aged BM of areas in contact with the IFE compared to those in adults (**Figure R8.1**).

In addition, we analyzed if the density of epidermal cells was altered during aging. To do this, we counted the number of cells per μm across IFE regions of adult and aged murine back skin, and detected a lower number of cells in aged. This shows that aged epidermal cells have to cover a larger area, leading to their stretching (**Figure R8.2a,b**). This is probably influencing the mechanical properties of these cells, as stretching is known to affect cell adhesion to other cells and to the

BM[191,192]. To sum up, there is a shift in the mechanical properties of the skin during aging, including an increase in overall stiffness in the epSC niche, as well as a stretching of epidermal cells.

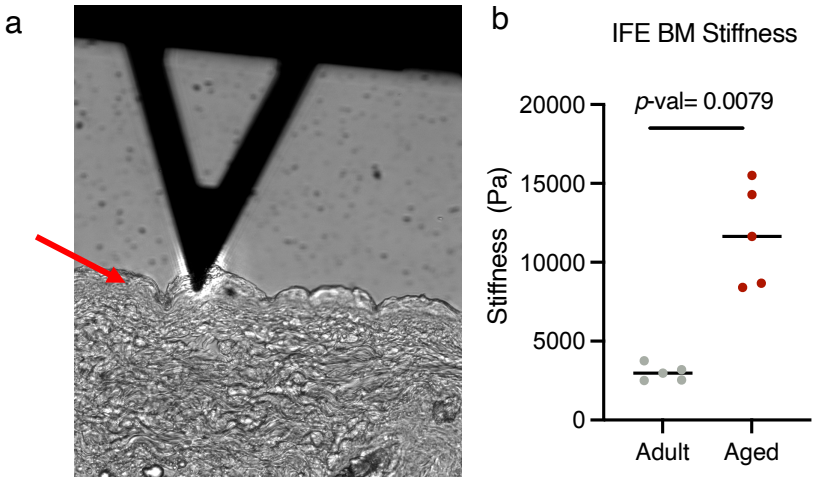

Figure R8.1. There is an increased stiffness in the aged BM of murine back skin. a, Representative image depicting the measured BM areas, subjacent to the IFE. Red arrow points to the measured regions. **b**, Quantification of AFM measurements of BM stiffness in areas below the IFE show an increased stiffness in aged compared to adults. Young's Modulus (Poisson's ratio of 0.5) was obtained, and shown in Pascals (Pa). N=5 mice per condition, with 5 regions analyzed per mouse. *P*-values were obtained of the average of all values per mice.

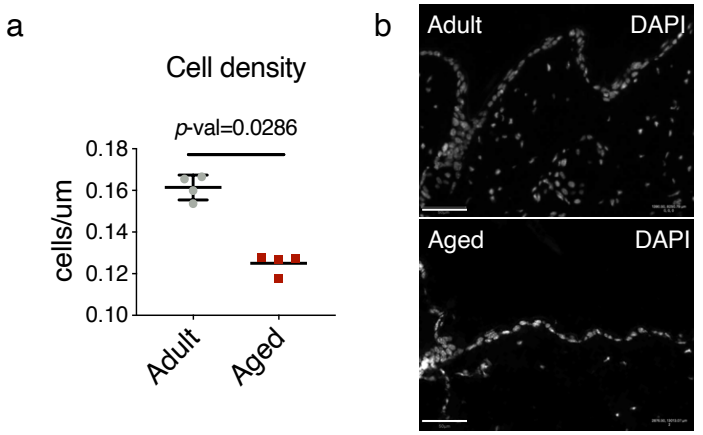

Figure R8.2. Aged epidermal cells present a lower overall density in the IFE compared to adults. a, Quantification of cell density by counting cell number per μm. N=4 animals/group. **b**, Representative image of epidermal areas used for analysis. Bar= 50μm.

Next, we sought to understand which mechanotransduction pathway could be responding to these age-associated physical alterations. Mechanotransduction pathways activate after detecting mechanical stimuli, which allows them to carry out their functions[191]. YAP/TAZ, downstream effectors of the Hippo pathway, have been described as crucial for skin homeostasis[204]. They become activated when sensing mechanical changes. More specifically, active YAP/TAZ translocate into the nucleus upon dephosphorylation to act as transcriptional coactivators. In the epidermis, they are mostly expressed by epSCs, and regulate cell growth and differentiation[204]. We investigated if the age-related changes in stiffness detected in the IFE could be activating YAP/TAZ in aged epidermal cells of the basal layer.

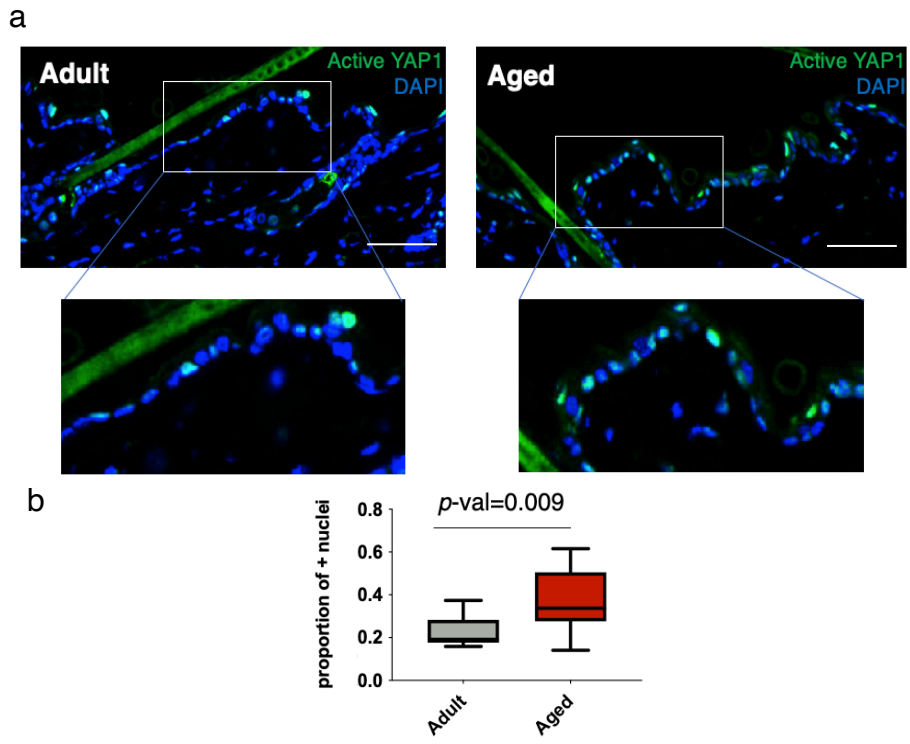

Figure R8.3. YAP activity is increased in aged epidermal cells. a, Representative image of YAP immunofluorescence in the epidermis. Insets of each image are shown below. **b**, Quantifications show proportion of YAP positive nuclei. N= 10 adult, 12 aged mice. Bar= 50μm.

For this, we carried out IF of YAP in the back skin of adult and aged epidermal cells, focusing our analysis on the IFE, with an antibody that only recognizes the active dephosphorylated nuclear form of YAP. We detected a significant increase in the staining for active YAP in the aged epidermis (**Figure R8.3a,b**). Hence, the increased stiffness and stretching correlates with an increased presence of active YAP in aged epidermal cells of the IFE.

2. YAP is recruited to regulatory regions of inflammatory genes in aged epidermal cells

In order to further understand the age-related changes in YAP function, we analyzed YAP genomic location by ChIP-seq in adult and aged epidermal cells. From these results, we annotated the regions enriched for YAP binding (ChIP peaks) to the closest gene. For further analysis, we only focused on binding sites annotated to protein-coding genes, to analyze their possible function in epidermal cells. Additionally, as binding to the DNA does not necessarily correlate with transcriptional activity[265], we also performed Assay for Transposase-Accessible Chromatin using sequencing (ATAC-seq)[266]. This technique detects DNA accessibility by using a hyperactive transposase that inserts sequencing adapters into chromatin accessible areas. As a result, if a region of the chromatin is accessible, the hyperactive transposase will insert an adapter that will be sequenced, allowing the detection of the specific area[266].

Our approach was based on overlapping the peaks of both datasets (ChIP-seq and ATAC-seq). This gave us the information of those YAP peaks that were in open chromatin areas. With this, we increased the possibility that the YAP-bound genes detected were actually being transcribed.

Analysis of the YAP-bound genes showed that the adult group had a very low number of exclusively bound genes that did not seem to have any

common relevant function (**Figure R9.1a**). Interestingly, there was a new subset of genes bound by YAP in open chromatin areas exclusively in the aged group (2783 genes) (**Figure R9.1a**). GO analysis of these genes showed that they had a variety of functions, ranging from homeostatic (such as epithelial migration and ECM organization) to inflammatory pathways (STAT and cytokine signaling pathway) (**Figure R9.1c**).

We then examined the genes bound by YAP in open chromatin areas of adult and aged cells, by comparing the GO categories obtained for each condition separately (**Figure R9.1a**). To do this, we conducted GO analysis of all the genes bound by YAP in adult (11 genes exclusively bound in adult, and 1692 genes in common with aged cells together), and in aged (2783 genes exclusive for aged, and 1692 in common added up) independently. Then, we compared the significance of the categories obtained by looking at their *P*-values. Examining these GO categories led us to find that in both conditions, there was representation of functions related to epidermal homeostasis and development, including categories such as TGFβ and epidermal growth factor receptor (EGFR) signaling pathways, and binding to developmental genes like *Bmpr2* and *Tcf7l2* (**Figure R9.1b,d**). Hence, the binding of YAP to genes with functions regarding epidermal maintenance is conserved regardless of the age of the cells.

Interestingly, this strategy allowed us to detect an overall increased expression of inflammatory-related genes bound by YAP in aged cells (**Figure R9.1e**). This was reflected by a higher significance (lower *P*-value) of these inflammatory categories in the aged group, with new peaks appearing in genes such as *Tbk1*, whose protein product regulates NF-κB signaling (**Figure R9.1f**). This means that even if YAP binds to many common targets between adult and aged cells, there is a new pool of genes bound only during aging that contributes to the pro-inflammatory functions of the aged epidermis.

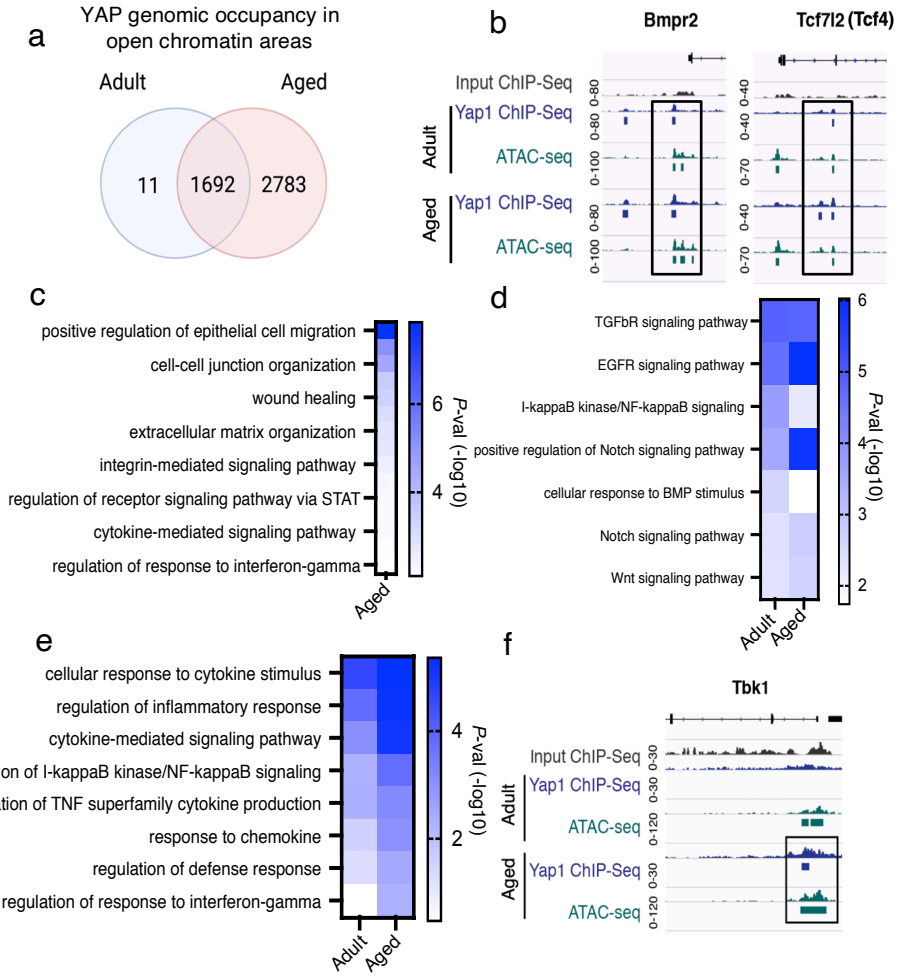

Figure R9.1. YAP binds to inflammation-related genes preferentially in aged cells. **a**, Number of protein-coding genes annotated to YAP ChIP-seq peaks in open chromatin areas, in adult (11 genes) and aged (2783 genes) epidermal cells, and in both conditions (1692 genes). For YAP ChIP-seq, n=3 replicates/age, and for ATAC-seq, n= 4 replicates/age. **b**, Snapshot of YAP binding (ChIP-seq), and of open chromatin regions (ATAC-seq) of *Bmpr2* and *Tcf7l2* (*Tcf4*) genes, important for categories selected in (**d**). Peaks considered for the analysis are marked inside the black box. **c**, **d**, **e**, Selected GO categories belonging to BP of the genes bound by YAP in open chromatin areas (**c**) exclusively in aged epidermal cells, (**d**), (**e**) including all the genes bound in adult and all the genes bound in aged separately. In all the GO categories shown, the y axis represents $-(\log_{10})$ of the adjusted *P*-value for each depicted GO category, and for adult and aged conditions separately (**d**,**e**). **f**, Snapshot of YAP binding (ChIP-seq), and of open chromatin regions (ATAC-seq) of *Tbk1* gene, important for (**e**). Relevant peaks are marked inside the black box.

The genes bound exclusively during aging did not reflect by themselves this predominant increase in inflammation by GO analysis (**Figure R9.1d**), but the sum of all the aged-bound genes clearly indicated an increase in GO pro-inflammation processes (**Figure R9.1e,f**). Thus, even if YAP maintains its functions during aging, there is a higher number of inflammatory-related genes more frequently bound in the aged epidermis.

3. YAP genomic occupancy reflects a relationship with the circadian clock

Further analyzing YAP genomic occupancy revealed that there was YAP binding to open chromatin regions and in regulatory areas of core clock genes (**Figure R10.1**). This occurred in adult and aged epidermal cells, although there was preferential binding during aging.

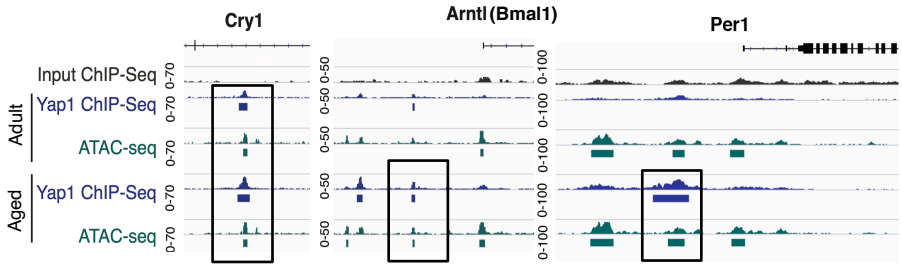

Figure R10.1. YAP binds to open chromatin in regulatory areas of core circadian clock genes. YAP ChIP-seq and ATAC-seq data show binding to open chromatin regions in regulatory areas of *Cry*, *Arntl* and *Per1* genes, which are core clock genes. Binding to *Cry* occurs in adult and aged cells, whereas in *Arntl* and *Per1*, significant binding in open chromatin areas is exclusive of aged cells. Relevant peaks are marked inside the black box.

The connection between YAP/TAZ signaling and the circadian clock has been briefly described in some studies. YAP/TAZ can influence the activity of the circadian clock in scenarios such as in the aged mammary gland niche, which presents an increased stiffness[230], and the circadian

clock has also been related to YAP/TAZ activity in intestinal tumor initiation[229]. In this case, loss of expression of the TF BMAL1 in intestinal SCs has been shown to cause an increase in YAP levels, which results in an increment in SC proliferation and tumor generation. Nonetheless, the specific interactions that exist between them and the main players of this communication are yet to be elucidated.

3.1. Epidermal cells reprogram their oscillatory transcriptome during aging

To further understand the connection between YAP/TAZ and the circadian clock, we first analyzed the circadian transcriptome of adult and aged epidermal cells. We performed bulk RNA sequencing of these cells at specific times of the day in order to detect the oscillatory genes in each condition. The samples were obtained at different *Zeitgeber* (environmental entrainment factor) times; ZT0, 4, 8, 12, 16, 20 after turning on the lights. This means that samples were obtained 0, 4, 8, 12, 16 and 20 hours after turning on the lights, as light is the entrainment factor in this case.

We then used the Jonckheere-Terpstra-Kendall (JTK) algorithm, which detects rhythmic genes in genomic datasets[267], analyzing the expression values of each gene along the day. We employed a periodicity of 24 hours and a threshold of adjusted *P*-value of 0.05, and obtained 2388 rhythmic genes exclusively in adult, 1146 genes exclusively in aged, and 1207 genes as rhythmic in both conditions (**Figure R10.2a**).

We then validated the oscillatory behavior of these genes by plotting their expression levels in heatmaps, in a total period of 24 hours (**Figure R10.2b**). These heatmaps corroborated that adult and aged exclusive circadian genes were only rhythmic in their respective condition, as these genes showed oscillatory patterns of expression only in their corresponding group. Then, circadian genes in adult and aged conditions showed a rhythmic pattern of expression in both of them.

Our next step was to explore the functions of these oscillatory genes in each case, for which we performed GO analysis. Focusing on the *P*-value significance of the categories, adult circadian genes showed overrepresentation of functions related to epidermal homeostasis (**Figure R10.2c**). Also, they rhythmically expressed genes with DNA damage repair functions in common with aged cells (**Figure R10.2c**).

Genes that were circadian in aged epidermal cells showed overrepresentation of functions related to inflammatory processes, along with DNA damage repair. Although some of these latter categories were in common with adult cells, they showed stronger *P*-values in the aged rhythmic genes (**Figure R10.2c**). Thus, genes relevant for epidermal homeostatic processes lost their rhythmic expression during aging, and a new subset of genes with inflammatory and DNA repair functions were becoming oscillatory in aged cells.

These results agree with previous studies showing that aged epSCs reprogram their daily oscillatory functions during aging towards inflammatory processes, as well as other functions[112]. Of note, our results are focused on all epidermal cells, whereas this past study only analyzed the transcriptome of epSCs. This difference of the cell subtype analyzed explains the subtle differences that exist between both datasets. As a result, we have corroborated that adult epidermal cells stop regulating epidermal homeostatic processes during aging, and rewire their circadian functions towards an age-related pro-inflammatory context.

3.2. BMAL1 binds to pro-inflammatory genes preferentially during aging

Next, we sought to unravel the specific core clock factor that could be interacting with YAP. We focused on BMAL1, as it is one of the main core clock TFs. Studies have shown that BMAL1 is unique, as it is the only non-redundant core clock factor that leads to circadian clock disruption when absent[169,172].

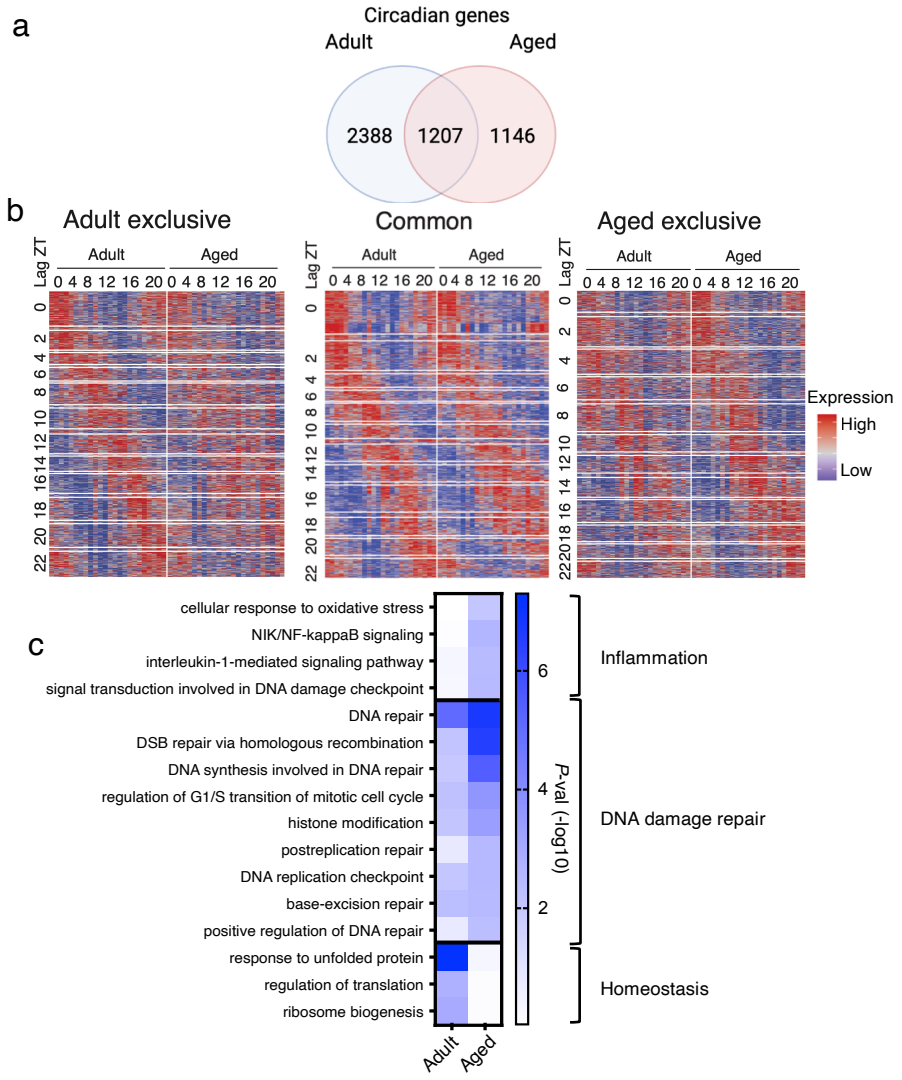

Figure R10.2. Epidermal cells rewire their rhythmic functions during aging. **a**, Number of circadian genes in adult and aged epidermal cells exclusively, as well as common between conditions. Oscillatory genes have been obtained with the JTK-CYCLE algorithm[267], with a threshold of adj *P*-val <0.05. N=4 biological replicates. **b**, Heatmap depicting the oscillatory expression of genes in each condition in a period of 24 hours. The x axis shows the ZT times of expression in adult (left columns) and aged (right columns) groups, and the y axis shows the lag ZT values of expression of the corresponding oscillatory genes per condition. **c**, Selected GO categories (BP) of the circadian genes in each group. The left column depicts the *P*-val for adult cells, and the right column shows that for aged cells. The categories have been grouped based on their overall function. The y axis represents $-(\log_{10})$ of the adjusted *P*-value.

First, we centered our efforts in unraveling if BMAL1 is a key player in this age-associated rewiring of circadian functions. For this, we carried out BMAL1 ChIP-seq in adult and aged cells, and overlapped the protein-coding genes obtained with open chromatin area information (ATAC-seq). In this case, we obtained 103 genes that were bound by BMAL1 in open chromatin areas exclusively in adult cells, 936 genes exclusively in aged cells and 2422 genes in common to adult and aged epidermal cells (**Figure R10.3a**).

Genes bound exclusively in adult cells were short in number and did not seem to present functional relevance. We then performed GO analysis of all the genes bound by BMAL1 in adult (joining the 103 genes exclusive for adult, and the 2422 genes in common with aged cells), and in aged (936 genes exclusive for aged, and 2422 in common added up). Comparison of the categories obtained showed that BMAL1 was binding to genes relevant for epidermal developmental pathways such as TGFβ, Wnt and Notch signaling pathways in both adult and aged cells (**Figure R10.3b**). Also, BMAL1 was bound to genes with homeostatic functions in both conditions, including GO categories like keratinocyte proliferation and differentiation, and regulation of cell-matrix adhesion (**Figure R10.3c**). Even though all these functions were conserved in both ages, there was a higher predominance of binding to genes with these roles in adult cells, shown by a lower *P*-value in most of the GO categories shown (**Figure R10.3b,c**).

Importantly, this approach also revealed that BMAL1 was binding to genes mainly with pro-inflammatory functions, and also to some relevant for response to ROS, as shown by GO analysis (**Figure R10.3d**). These categories were in some cases also relevant for adult cells, although there was a higher number of categories related to inflammatory functions in the aged group. Thus, the genes bound by BMAL1 in open chromatin areas of aged cells have an increased representation of pro-inflammatory roles. Concomitantly, there is a decreased binding to genes

with functionality associated to homeostasis and basic cellular processes. These results shed light into showing that BMAL1 is crucial for the age-related circadian rewiring, as the changes it shows in DNA occupancy during aging recapitulate most of the age-associated rewiring.

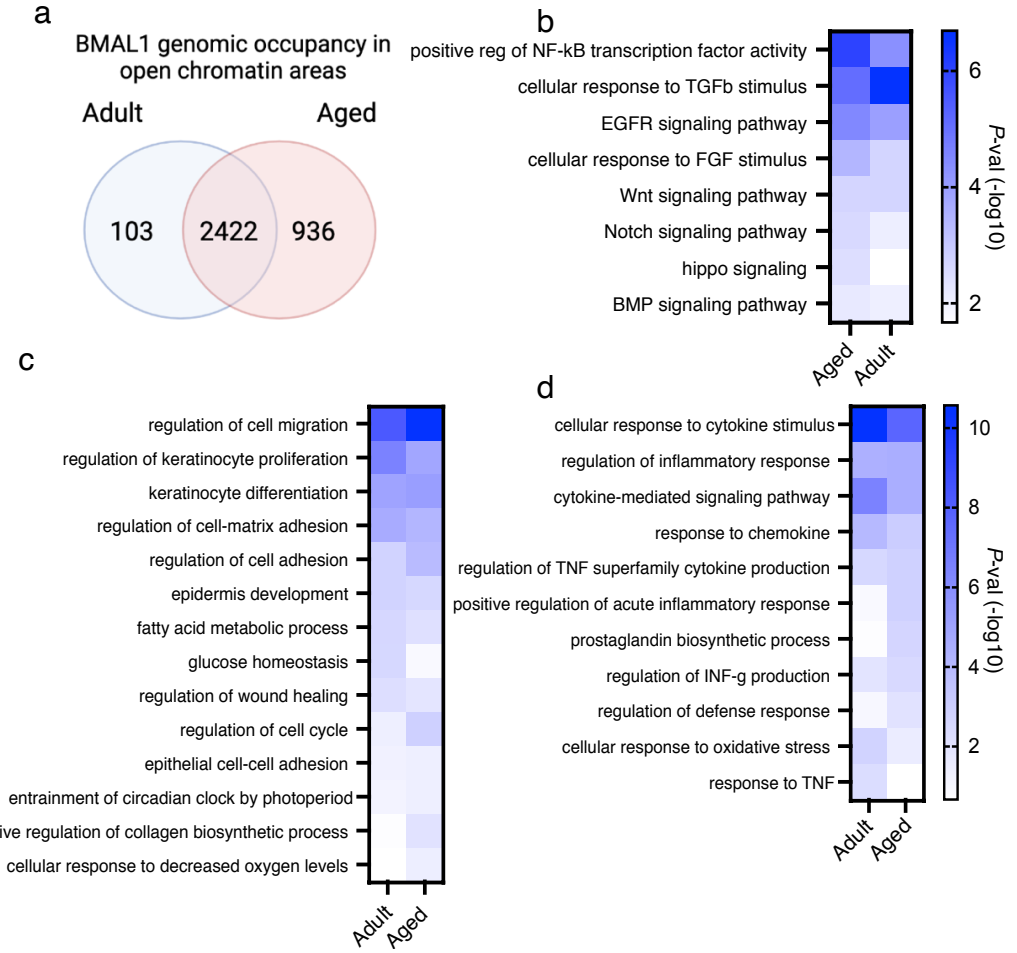

Figure R10.3. BMAL1 binds to genes related to homeostasis and basic cellular processes in adult and aged cells, and to pro-inflammatory genes preferentially during aging. a, Number of protein-coding genes annotated to BMAL1 ChIP-seq peaks in open chromatin areas, in adult (103 genes) and aged (936 genes) epidermal cells, and in both conditions (2422 genes). N=4 replicates/age for BMAL1 ChIP-seq. **b**,**c** Selected GO categories belonging to BP of the BMAL1-bound genes in all adult and all aged cells separately, with functions related to (**b**) developmental pathways essential for the epidermis, (**c**) epidermal homeostasis, (**d**) pro-inflammatory processes. In all GO analysis, the y axis represents $-(\log_{10})$ of the adjusted *P*-value.

3.3. YAP and BMAL1 present a high overlap in genomic occupancy

3.3.1. YAP and BMAL1 bind to inflammatory circadian genes in aged epidermal cells

After describing the role of BMAL1 in the age-associated rewiring, we wondered if it could serve as a link for the functional interaction between the circadian clock and YAP/TAZ. This is why we overlapped the data from YAP and BMAL1 genomic occupancy in open chromatin areas with the information of the circadian genes. This overlap was done to understand to what extent the genes involved in the age-associated rewiring correspond to the genes bound by BMAL1 and YAP.

In this case we only focused on aged epidermal cells, as it is the condition in which we detected new subsets of genes being newly bound by BMAL1 and YAP. Here, we obtained 2574 genes that were bound by YAP and BMAL1 in open chromatin areas, and that were not circadian (comparison 1), 1756 genes that were circadian in aged but not bound by YAP and BMAL1 (comparison 3), and 597 genes that were bound by YAP and BMAL1 in open chromatin areas, and that were circadian (comparison 2) (**Figure R10.4a**).

Moreover, GO analysis showed that DNA damage repair functions were mostly represented in the pool of circadian genes in aged not bound by YAP and BMAL1 (comparison 3) (**Figure R10.4b**). This reveals that this DNA damage-related subset of circadian genes is not controlled by BMAL1 and YAP directly, and that other factors could be responsible for their activation in a circadian manner.

Then, GO analysis of the genes bound by YAP and BMAL1 in open chromatin areas, but that are not circadian (comparison 1), showed enrichment in categories related to epidermal homeostasis (**Figure R10.4c**).

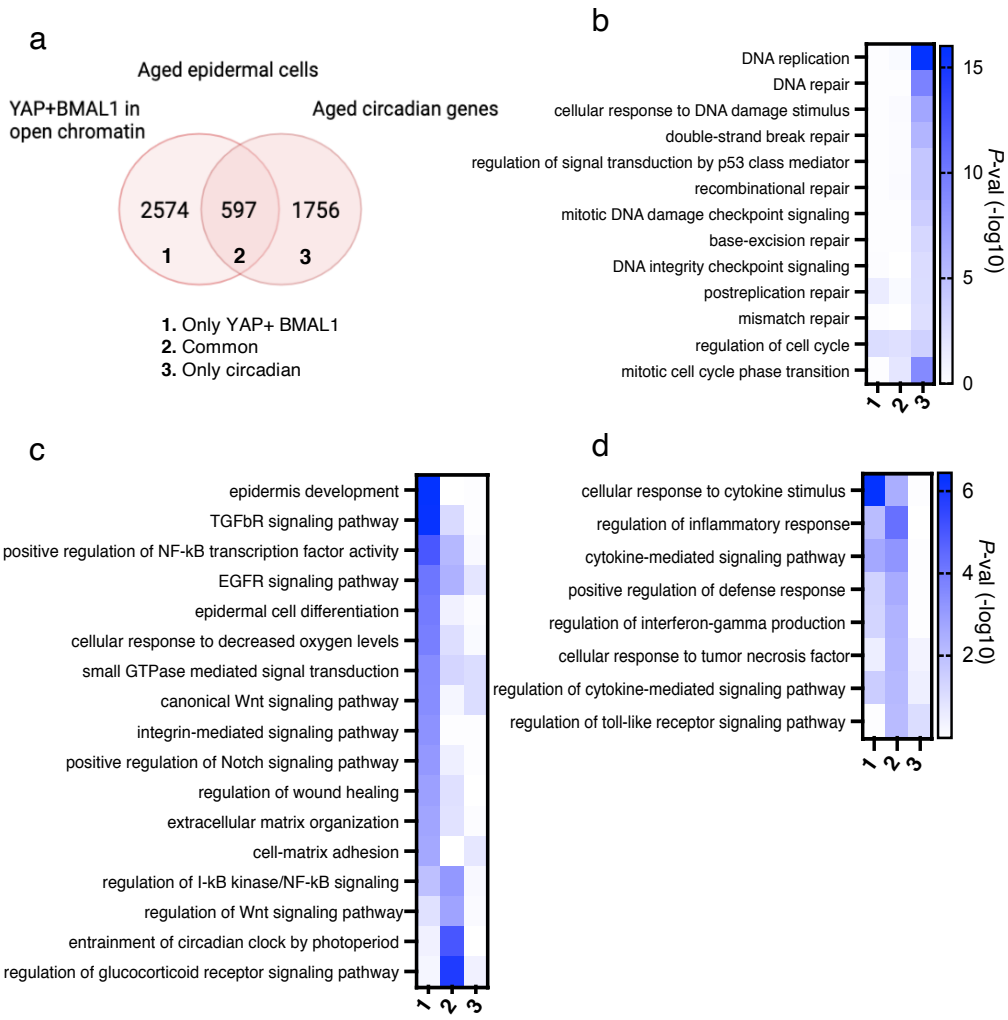

Figure R10.4. YAP and BMAL1 bind to circadian genes with inflammatory functions during aging. a, Number of protein-coding genes bound by YAP and BMAL1 in open chromatin areas in aged epidermal cells, in overlap with the aged rhythmic genes. Comparison number 1 includes those genes bound by YAP and BMAL1 in open chromatin regions, but not circadian. Comparison 2 englobes genes bound by YAP and BMAL in open chromatin, and circadian, and comparison 3 reflects non-bound circadian genes. **b**, **c**, **d**, Selected GO categories belonging to BP of the (**b**) DNA damage categories, (**c**) epidermal homeostatic categories, (**d**) inflammation-related categories. In all GO analysis, the y axis represents $-(\log_{10})$ of the adjusted *P*-value.

This suggests that YAP and BMAL1 still remain bound to genes with homeostatic-related functions during aging, although these genes stop oscillating transcriptionally. Finally, GO analysis of the common genes, which are those genes bound by YAP and BMAL1 in open chromatin areas, and that are circadian (comparison 3), revealed functions related to inflammatory processes (**Figure R10.4d**). These include regulation of inflammatory response, cytokine signaling pathway and interferon-γ production. Nonetheless, there is a fraction of inflammatory genes that are bound by YAP and BMAL1, but that are not circadian, seen by *P*-value significance in some pro-inflammatory GO categories (**Figure R10.4d**).

To sum up these results, YAP and BMAL1 are bound to many inflammatory genes that are circadian in the aged epidermis. This highlights their potential role in the age-related circadian rewiring, which would include helping regulate genes in a circadian and a mechano-dependent manner.

3.3.2. YAP and BMAL1 bind to adjacent sites in the DNA

Additionally, we wanted to unravel the specific interaction occurring between YAP and BMAL1. Genomic occupancy data showed that they were both binding to overlapping sites in the genome, which also corresponded to regions with open chromatin (**Figure R10.5a**). This occurred in both adult and aged conditions, stating that this interaction happens regardless of age.

We then conducted a statistical analysis with RegioneR[268], to assess the significance of the overlap between YAP and BMAL1 genomic occupation. Interestingly, we found that the genomic regions bound by YAP and BMAL1 overlapped in a significant manner in adult and aged cells, when comparing all peaks obtained for both TFs (**Figure R10.5b**). This was also seen when measuring *in silico* the distance between the binding sites in regions with overlapping peaks for YAP (binding to TEAD

in the DNA, in this case sites for TEAD3 binding) and BMAL1 (binding to Ahr::Arnt boxes) (**Figure R10.5c**). Here, we analyzed the distribution of distances between both TFs in overlapping peaks. There was a high density of YAP and BMAL1 binding in overlapping areas, with almost no base pair distance between the binding sites described for each, further showing the tight connection in their genomic binding. This further proves that YAP and BMAL1 coordinate in their binding to the genome, underscoring the existence of a functional relationship between both.

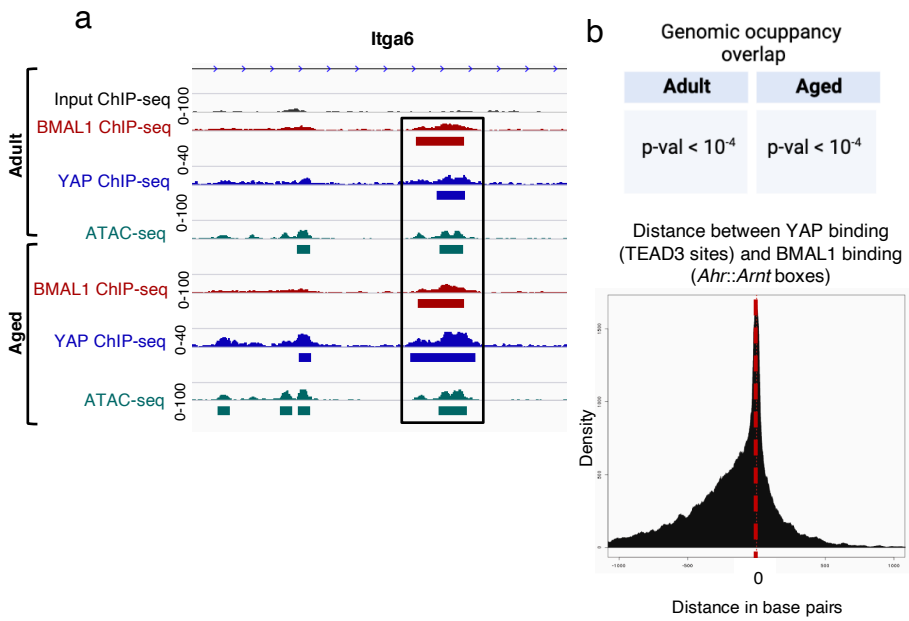

Figure R10.5. YAP and BMAL1 bind to highly overlapping regions of the genome. a, Representative snapshot showing binding of YAP and BMAL1 binding to the same sites in the genome in adult and aged cells, and in open chromatin areas. In this case, the *Itga6* gene. BMAL1 binding data is shown in red, YAP in blue and ATAC in green. Overlapping peaks are marked inside the black box. **b**, *P*-value of the overlap of YAP and BMAL1 binding sites in adult and aged cells, including all peaks from both. Obtained with RegioneR[268]. **c**, Computational analysis of the distance between YAP and BMAL1 binding sites in regions with overlapping peaks. YAP binds to TEAD sites, in this case we chose to analyze the distance between TEAD3 sites, and Ahr::Arnt sites. Obtained with RegioneR[268].

4. There is an age-related functional association between YAP and BMAL1

Next, we wanted to explore the molecular basis of YAP and BMAL1 functional interaction. To address this, we followed two different approaches using genetically modified mouse models in which the expression of BMAL1 and YAP can be altered.

4.1. YAP requires BMAL1 to bind to essential epidermal genes in adults

To explore these scenarios, we first made use of an animal model in which BMAL1 was conditionally KO in the epidermis (BMAL1ep cKO)[187]. This transgenic mouse line presents *loxP* sites surrounding exon 8 of the *Arntl* gene, and expression of Cre recombinase results in truncation and loss of the functional BMAL1 protein. At the same time, the Cre recombinase is expressed under the control of the K14 promoter (K14Cre/*Arntl*$^{LoxP/LoxP}$). Thus, the Cre recombinase is only expressed in epithelial cells. Focusing in the skin, these cells include basal layer epSCs, leading to BMAL1 KO in the epidermis of these mice. These BMAL1ep cKO mice have been shown to present traits of epidermal premature aging at an adult age, including an inefficient epSC self-renewal, and an increased cornified layer thickness[187].

We conducted YAP ChIP-seq analysis in adult BMAL1ep cKO mice, compared to wild-type (WT) control mice (expressing the Cre recombinase but not the *Arntl* floxed alleles), to see if YAP binding was altered in absence of BMAL1. This would suggest that BMAL1 has an effect on YAP activity. Results showed that YAP requires BMAL1 to carry out many of its functions, as there were almost no genes exclusively bound by YAP in absence of BMAL1, and they did not appear to have relevant functions (**Figure R11.1a**). There was a big pool of genes that remained expressed in absence of BMAL1 (2541 genes), although more

than half of genes bound by YAP lost its binding in this scenario (3160 genes) (**Figure R11.1a**). We then examined the GO categories obtained for all genes in the WT condition (3160 exclusive in WT joined with 2541 common genes), in contrast to those in the BMAL1ep cKO group (16 exclusive added to 2541 common genes). This revealed that there was expression of genes relevant for developmental pathways, epidermal homeostasis, and crucial for YAP to carry out its mechanotransduction activity in both groups (**Figure R11.1b,c,d**). Nevertheless, all these processes were more significant in presence of BMAL1, as seen by their *P*-value, highlighting the relevance of BMAL1 expression for YAP to carry out its epidermal functions (**Figure R11.1b,c,d**).This suggests that even though not all of YAP activity is directly dependent on BMAL1, its expression is crucial for YAP to carry out its functions in the epidermis.

4.2. Active YAP overexpression drives BMAL1 binding to inflammatory genes

After describing the relevance of BMAL1 for YAP binding to its targets, we wondered if YAP also had an effect in BMAL1 genomic occupancy. In this case, we used a genetically engineered mouse model that expresses a constitutively active mutant human YAP form (iYAP) in an inducible manner[269]. In this mouse line, the human mutant *YAP* transgene is inserted in the collagen 1a1 locus, expressed in a wide variety of tissues that include the skin. This *YAP* transgene contains a mutation in the phosphorylatable Serine 127 (S127), which is mutated to Alanine. Phosphorylation of a serine residue is known to cause YAP cytoplasmic sequestration and degradation, and this S127 mutation impedes its phosphorylation. This increases the nuclear localization and transcriptional activity of the YAP protein generated. As a result, these mice present an increase of active YAP in a variety of tissues such as the skin[210,269].

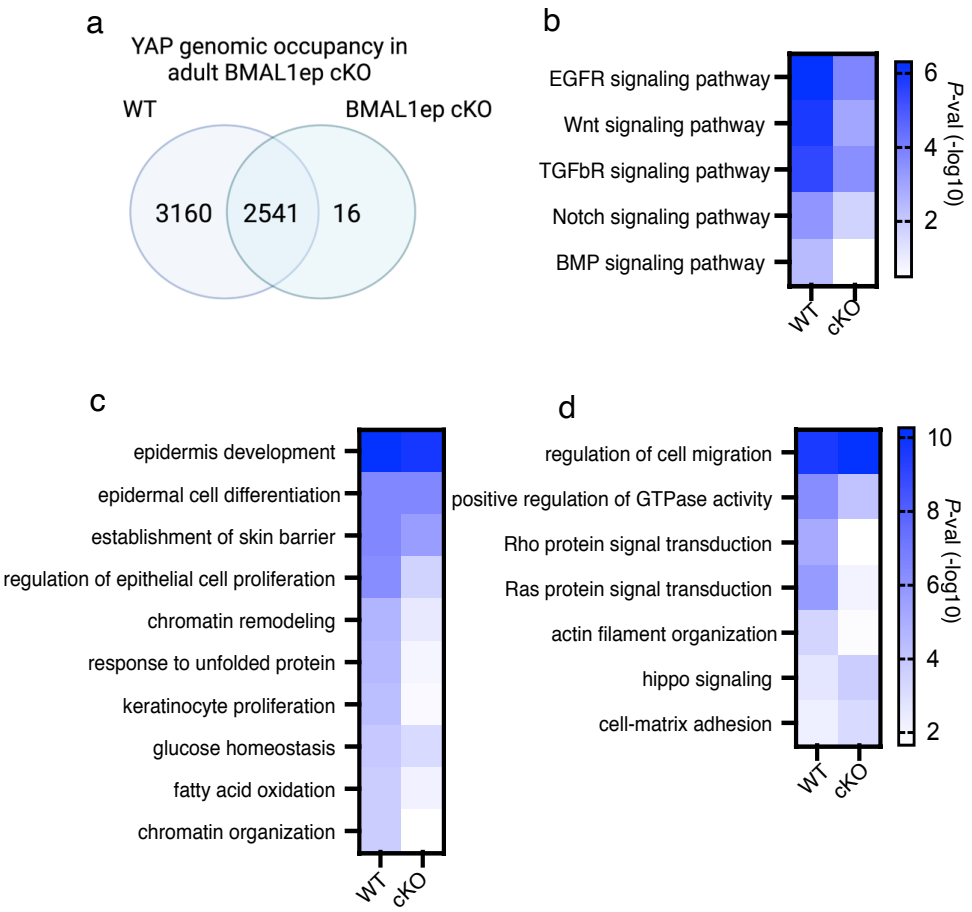

Figure R11.1. YAP requires BMAL1 to bind to essential genes in the adult epidermis. a, Number of protein-coding genes annotated to YAP ChIP-seq peaks in WT adult mice (15 weeks old), and in BMAL1ep cKO adult (15 weeks old) mice. N=3 reps/group for YAP ChIP-seq. **b**, **c**, **d**, Selected GO categories belonging to BP of all the genes bound by YAP in adult mice expressing BMAL1 (WT), and in adult BMAL1ep cKOs analyzed separately. Categories shown in (**b**) reflect developmental pathways, in (**c**) epidermal homeostasis, and in (**d**) are important for YAP mechanotransduction activity. In all GO analysis, the y axis represents $-(\log_{10})$ of the adjusted *P*-value.

The expression of the *YAP* transgene is controlled by the inducible gene expression TetO-model (Tet-On-YAP). In this system, the expression of the reverse tetracycline-controlled transactivator (rtTA) is required. This is a fusion protein that recognizes target tetO sequences present in the

transgene inserted, only in presence of an inducer like doxycycline (doxy). Of note, the *rtta* gene is inserted in the ROSA26 locus of these mice. Consequently, transcription of mutant YAP in these mice is stimulated by rtTA only in the presence of doxy, leading to an active YAP overexpression[210,269].

First, we validated the efficacy of the model by inducing expression of the transgene with doxy for 36 hours. This specific time of induction was chosen because excessive YAP expression for long periods of time lead to hyperproliferation and increased epidermal thickness, creating a non-homeostatic and detrimental scenario in the skin[204,221]. Therefore, we induced YAP overexpression for a reduced period of time to avoid creating a non-homeostatic context. This loss of epidermal stability would be far from what is seen during aging, which is the condition we want to extrapolate our results to. We detected an induction of YAP expression in skin cells after 36 hours by IF of YAP, and there were no structural changes seen in the skin (**Figure R11.2a**). In this case, total YAP was analyzed due to the inability of the antibody against active YAP to detect the mutant human protein expressed by the transgenic mouse model. With this, we visually corroborated that the short induction time was sufficient to induce overexpression of YAP without affecting epidermal and skin integrity.

Next, we carried out BMAL1 ChIP-seq in adult iYAP mice after 36 hours of YAP overexpression, compared to control WT mice (presenting the rtTA but not the *YAP* transgene) treated with doxy. Preliminary results show that BMAL1 is directed to different targets when YAP increases its expression, as there was a loss of a pool of BMAL1-bound genes when YAP is activated (1962 genes), another number of genes that were kept between conditions (3746 genes), and a gain of a newly subset of bound genes only after induction (398 genes) (**Figure R11.2b**). GO analysis of the genes bound by BMAL1 showed that when YAP is overexpressed, BMAL1 is directed towards genes with pro-inflammatory functions in this

scenario (**Figure R11.2c**). This indicates that BMAL1 binding is controlled by YAP expression to some extent, as its activation leads to a shift in many BMAL1-bound genes, especially towards those with pro-inflammatory functions. Of note, there is a high number of genes that do not lose BMAL1 binding when there is YAP activity, which implies that YAP is not the only factor regulating BMAL1.

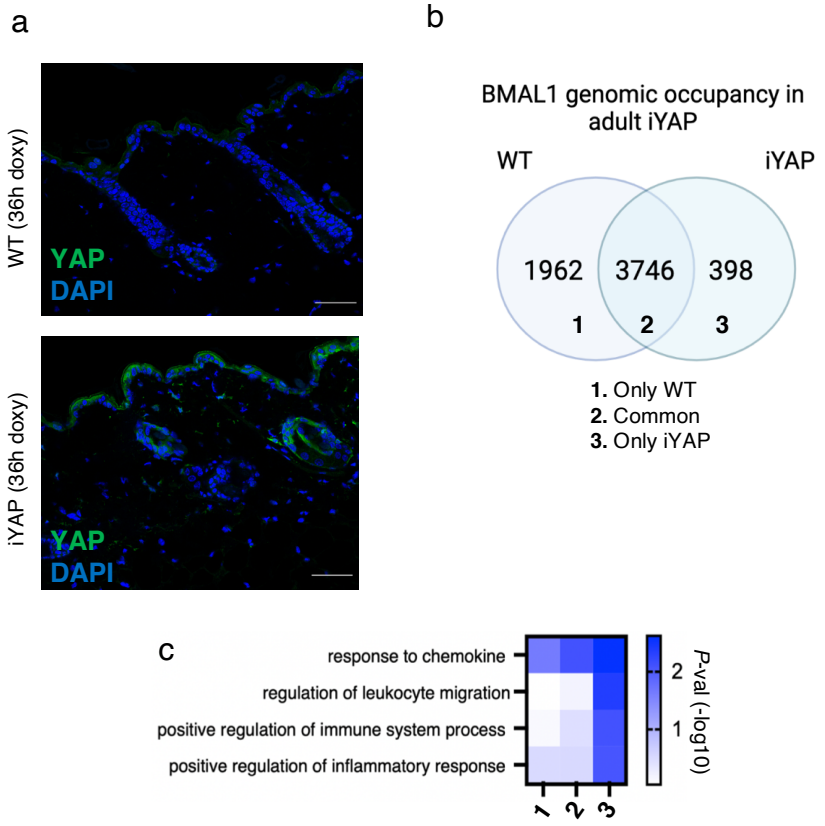

Figure R11.2. BMAL1 relocates to genes related to pro-inflammatory functions when YAP is hyperactivated. a, Representative image of YAP IF in WT and iYAP mice, after 36 hours of doxycycline induction. Bar= 50μm. **b**, Number of protein-coding genes bound by BMAL1 in adult WT mice (comparison 1) (15-19 weeks old), in adult mice after YAP overexpression (comparison 3), and in common between both (comparison 2). N=2 replicates per group. **c**, Selected GO categories belonging to BP of the genes bound by BMAL1 in mice after iYAP induction (condition 3). The y axis represents $-(\log_{10})$ of the adjusted *P*-value.

In conclusion, there is a tight communication between YAP and BMAL1, as they both affect one another in their genomic binding to the DNA, and therefore, in their functionality. This gains relevance during aging, as overall changes in skin properties lead to alterations that affect both YAP/TAZ signaling pathway and circadian clock function. Consequently, our results are the first to describe the association existing between the YAP/TAZ mechanotransduction pathway and the circadian clock, primarily BMAL1, during aging.

Discussion

Chapter 1. Local IL-17 orchestrates skin aging

1. Increased IL-17A/F levels in aged skin

During aging, there is an overall increase in chronic and systemic pro-inflammatory functions. This has been termed as “inflamm-aging”, and is considered one of the hallmarks of aging[108,156]. At present, it is unknown if this chronic inflammation is a driver of aging, or a consequence of the age-associated overall tissue deterioration. Also, even though there are studies describing specific signals contributing to this “inflamm-aging”, such as the secretion of inflammatory cytokines and senescent-related factors, dampening of adaptive immune responses, infiltration of T cells into neural niches, epidermal JAK-STAT signaling imbalance, *etc.*, there are many inter-organ differences that require further description[114,130,131,157,164,270].

The immune compartment of the aged skin is affected in a different manner depending on the lineage of origin. There is an increase in myeloid cell proportion, as well as a deterioration in their functions[160,161]. Lymphoid cells show a reduced ratio of naïve cells, and dysfunctional CD4+ Th and CD8+ T cells[156]. Moreover, specific inflammatory functions become regulated in a circadian manner in aged skin, which highlights the relevance of these functions during aging[112]. Nonetheless, there is still much to be understood about the cues that contribute to the existing age-associated chronic inflammation.

Here, we describe exacerbated IL-17A/F expression as a driver of skin aging. IL-17A/F signaling has already been related to autoimmune and chronic inflammatory contexts systemically. In particular, it has been characterized in dermatological, cardiovascular, liver, intestinal and respiratory diseases, among others[271-273]. Focusing on the skin specifically, excessive IL-17A/F signaling has been linked to diseases such as psoriasis, hidradenitis suppurativa, alopecia areata, pemphigus vulgaris and pityriasis rubra[91]. However, to our knowledge, our study is first in describing the role of this cytokine in aging progression.

Previous studies have associated the impaired autophagy that exists during aging to the development of a Th17-related "inflamm-aging", showing increased IL-17-producing cells in peripheral blood mononuclear cells (PBMCs) of aged humans[165]. In this study, the authors show that IL-17 cytokine secretome in aged cells highly correlated to the one existing in Th17 cells in type 2 diabetes, which is a chronic condition defined partly by an increase in inflammation. Thus, it gives insights into the possible relationship between IL-17 production in chronic inflammatory diseases and aging. Importantly, the reasons leading to the IL-17 increase are not addressed in this work.

Of note, this study also stated there was no increase in Th17 frequency with age, and describes this increase in IL-17 production as a consequence of impaired age-associated autophagy and not as a driver of the aging process. An explanation for these conclusions could be that this work focuses on analyzing the changes in cell proportion and metformin response, which is a drug for type 2 diabetes that improves chronic inflammation, by FACS sorting of only CD4+ Th cells. As a result, it is possible that variations in expression of cell surface markers (like CD4) might have driven the loss of relevant cell subpopulations. Following this line, there are age-related changes in other cell types that are overlooked by analyzing only CD4+ Th, such as cell inter-communication and coordination. This restricts the expansion of the observations made, as it is a description of changes of one cell type subpopulation. Besides, as metformin is a drug that improves chronic inflammation, it is not surprising to observe that its use can lead to a decrease in IL-17 production.

In addition, another study also described an increased expression of IL-17A, as well as in Th17 cell number, in PBMCs of aged humans compared to adults[274]. There was a strong tendency of aged naïve CD4+ Th polarization towards a Th17 phenotype, as well as higher expression of the TF RORγt in these cells, which is crucial for Th17 cell polarization.

Surprisingly, this IL-17 increase was no longer maintained in a geriatric and frail state. The authors discuss that variations between Th17 and Treg cell numbers at different ages are the cause of these differences. With this, they conclude that Tregs are increased in frail individuals as a way of counteracting the increased Th17-related cytokine secretion during aging, leading to a decreased geriatric Th17 proportion. Nevertheless, the authors do not dig into the functional relevance of the increased IL-17-related inflammation during aging, but focus on the changes in cell proportion between Th17 and Tregs in a geriatric stage. Conversely, our study directly highlights the relevance of IL-17A/F in skin aging, and describes a significantly increased proportion of IL-17-secreting CD4+ Th, γδT cells and ILCs during aging. We show that IL-17A/F is not only a passenger in the "inflamm-aging" phenomenon, but that it is key in its development during aging.

Psoriasis is a chronic inflammatory disease of the skin characterized by the profound modification of the epidermis, which hyperproliferates and presents an altered differentiation of epSCs, as well as by the presence of inflammatory infiltrates in the skin[102]. As a result, there is a disrupted skin barrier, as well as downregulation of molecules crucial for epidermal homeostasis and integrity[102]. Also, these patients have also shown a deteriorated skin permeability by presenting increased TEWL values[275]. This disease has been described as IL-17A driven, and more recently also IL-17F, which pinpoints the critical role of these cytokines in the development of psoriatic inflammation[276].

Given the similarities found between characteristics existing in psoriatic and aged skin, such as epidermal permeability deterioration, and an increased inflammatory context driven partly by an increased IL-17A/F production, we wondered if the levels of IL-17A/F could also be comparable in both situations. Nonetheless, we were not able to compare both scenarios, as the variability between the psoriatic samples we obtained was too high, and we were not able to detect significantly

increased IL-17A/F levels in the dermal compartment compared to healthy adults. This could be due to the specific disease stage in which the patients were at when the samples were obtained, as the critical role of IL-17A/F in psoriasis is mostly concentrated in the initial stages of the disease, which is when the excessive inflammatory context is originated[276]. Also, the lack of an increase in IL-17A/F in psoriatic patients could be due to the previous treatments they had undergone, which is likely to be influencing the secretory profile of inflammatory cells.

Regardless of the inability to detect increased IL-17A/F levels in the dermis of our analyzed samples, there are clear differences between psoriasis and aging that limit the comparisons that can be done between them. First, psoriasis is characterized by an exacerbated outburst of inflammatory signals, which causes a disruption in skin homeostasis and the development of highly aberrant characteristics[102]. On the contrary, aging is known as a decline in overall functions and integrity, but does not include the loss of basic homeostatic processes or overall integrity in the skin[106,112]. Hence, psoriatic skin presents a much more abnormal and chaotic scenario than aged skin.

Also, WH occurs faster and more efficiently in psoriatic patients when compared to adult individuals, as well as in imiquimod-treated animal models compared to non-treated[277,278]. Imiquimod is a synthetic compound that can be added topically to skin, inducing psoriatic-like skin lesions, and has been used as a model to study psoriatic traits and inflammation[279]. This more effective WH contrasts with what happens in aged skin, as one of its main defining features is a less efficient and defective WH[129,130,132]. In addition, imiquimod treatment during telogen in adult mice induced HFSCs to enter anagen prematurely, and some psoriatic patients have been described to present an increased density of hair in specific contexts[279,280]. This is not a recurrent phenotype in psoriasis, as patients have also shown hair loss[281,282]. This suggests that hair growth in psoriatic patients may depend on the concordance

between a specific disease stage and hair cycle phase. This disagrees with what is observed during aging, as it is widely accepted that HF aging is characterized by HF miniaturization and overall decrease in density[134]. All this underscores that, even though there are some similarities between psoriatic and aged skin, there are insuperable differences in their IL-17 driven inflammation and phenotypic characteristics that do not allow comparing both scenarios.

2. Source of exacerbated IL-17A/F levels

IL-17A/F functions are mainly related to protection against pathogens. They are secreted by immune cells when an external antigen is detected, leading to further cytokine secretion and immune cell recruitment, all of which aids in pathogen clearance[100]. Our results point against the possibility of the increase in IL-17A/F during aging being caused by pathogen entry through the epidermal barrier, as there were no signs of an immune response reaction against external antigens. This suggests that this increase in IL-17A/F secreting cells could be caused by an internal skew.

There are studies that show that immune cells can be skewed towards a specific subtype during aging. First, aged HSCs have been shown to differentiate preferentially towards a myeloid lineage, due to differences in cell polarity[158,159]. Then, focusing on lymphoid cell polarization, a study showed that *in vitro* aged CD4+ T cells can be polarized towards Th17 more efficiently than adult cells, which is reflected in an increased cell activation and Th17-related cytokine secretion in the aged counterparts[283]. Another study supported these findings showing that aged splenocytes, which are immune cells present in the spleen, present an increased proportion of IL-17-producing CD4+ Th cells compared to adults[284]. This was seen for both naïve and memory cell populations, and was accompanied by an increase in RORγt expression in these aged cells. Also, when splenocytes from adult and aged conditions were

cultured under Th17 polarizing conditions, aging mice were able to produce a higher number of IL-17-producing cells than adults[284]. Moreover, a similar trend has been described for γδT cells, as it has been shown that upon aging, γδT cells in the peripheral lymph nodes are biased towards the γδT17 lineage[285]. These results reveal that age-related lymphoid cell polarization towards an IL-17 producing phenotype can occur during aging in specific cell subsets and tissues in a pathogen-independent manner. Hence, our results showing an internal skew towards IL-17 producing CD4+ Th, γδT cells and ILCs in aged skin go in line with previous studies, and reveals for the first time the relevance of this age-related IL-17 polarization increase.

Nonetheless, the specific signals leading to this IL-17 polarization are still not well understood. IL-1 signaling has been described as key in Th17 differentiation, and *Il1β* production has been shown to be increased during aging by our study as well as by others[286-288]. In absence of IL-1 signaling (in knock-out [KO] models of IL-1 receptor, IL-1R1), CD4+ Th cells are unable to differentiate towards Th17 cells *in vivo*, pinpointing the relevance of IL-1 signaling in the early phase of Th17 cell differentiation[286]. Thus, it is likely that the increase in *Il1β* production and increased IL-1 signaling in aged skin is supporting the skew towards IL-17 production in CD4+ Th, γδT cells and ILCs. Future studies in which IL-1 signaling is dampened in a skin aging context should be conducted, in order to detect if it affects IL-17 production by aged lymphoid cells and overall skin aging.

Furthermore, it is still unknown if this increased IL-17 production occurs exclusively in the skin or in a systemic manner. We observed a trend towards an increase in *Il17a* levels, but not of *Il17f* increase in the aged small intestine. These differences between *Il17a* and *Il17f* levels could be surfacing the individual roles that IL-17A and IL-17F may have under specific microbial infections[100]. Their roles have also been described as non-equivalent in an autoimmune context, as IL-17A KO mice show an

improved recovery for the disease experimental autoimmune encephalomyelitis (EAE), whilst IL-17F KO mice do not[289]. These differences could explain why *Il17f* is not upregulated in the aged small intestine, but *Il17a* is, as they could have different functions in this organ. Of note, in our studies the levels of *Il17a* increase were not detected as significant in the aged small intestine by FISH, which in combination with the lack of increased *Il17f*, point towards thinking that the age associated increase of IL-17 signaling perhaps happens mainly in the skin. This would be in contraposition with previous studies mentioned in this section that explain an increased polarization towards IL-17-producing cells in aged spleen cells and peripheral lymph nodes, as well as in PBMCs as described in the previous section[165,274,284,285]. Our conclusions may have been caused by our type of analysis, as we only conducted FISH for *Il17a/f* in the small intestine, while *Il17a/f* levels in murine skin were detected by scRNA-seq and IL-17A at the protein level by IHC. The differences in the methods used do not allow for direct comparison of the levels of IL-17A/F between organs. Therefore, future work should further analyze IL-17A/F expression levels in the aged small intestine by other methods, as well as broadening the analysis by studying other aged tissues and organs. This would give insights into unraveling if IL-17A/F is as relevant in aging of other organs as it is for the skin.

3. IL-17A/F blockage ameliorates age-associated traits in aged skin

IL-17A/F inhibition is used for the treatment of autoimmune and chronic inflammatory diseases. In psoriasis, the use of neutralizing antibodies against IL-17A/F has shown an increased efficacy in reducing disease-associated symptoms compared to other existing treatments[103]. This is why its use has already been approved by the European Medicines Agency (EMA) for psoriatic patients with moderate to severe forms of the disease. Three studies involving 1,480 patients in total showed that 84%

to 93% of patients using this targeted therapy presented a clear o almost clear skin after 16 weeks of treatment, which shows the efficacy of IL-17A/F blockade therapies in this chronic inflammatory disease[290,291].

Hidradenitis suppurativa is a chronic inflammatory disease characterized by the presence of inflammatory nodules, with lesions commonly appearing in the groin, inframammary folds and axillae[292]. Studies found an increase in IL-17 gene expression levels of 30-fold in lesional tissue compared to normal skin, whereas another study described an increase of 115-fold for IL-1β and of 149-fold for IL-17A in diseased skin compared to healthy counterparts[292,293]. Therapies targeting IL-17A/F in these patients are in phase 3 of clinical trials, and the results are promising because there are clinically meaningful improvements across all disease outcome measures taken, compared to other treatments[294].

In alopecia areata, patients suffer from loss of the immune privilege of the HFs. It is an autoimmune chronic inflammatory disease that targets the HFs, and leads to an overall hair loss[295]. Increased IL-17 levels have been detected in the blood and skin of these patients, and there is a significant correlation between serum concentrations of IL-17 and the severity of the disease[295,296]. Nevertheless, these IL-17 serum levels do not correlate with the total duration of the disease, and the specific role of this cytokine in disease appearance and progression is still not well understood[296]. This is why there are not as many clinical trials testing the efficacy of IL-17A/F blockade in this disease. On one hand, existing treatments for alopecia areata are indirect potent inhibitors of the IL-17 signaling pathway, and have shown promising results[295]. This suggests that IL-17A/F blockade could be beneficial for these patients. On the other hand, there are clinical cases in which psoriatic patients develop alopecia areata post IL-17A/F blockade treatment[297,298]. This highlights that the function of IL-17A/F in this disease is dual, and that its specific role in this context must be further studied before IL-17A/F blockade is used as a therapy for these patients.

Patients with bullous pemphigoid suffer from subepidermal blisters, which occurs in an autoimmune and chronic inflammatory manner and preferentially in the elderly population. In this disease, exacerbated IL-17 has been detected in the peripheral blood of patients, as well as in the skin[299]. Clinical trials blocking IL-17A/F are already being developed in order to test the efficacy of this cytokine blockade in patients, although the results are still under study[300]. Nonetheless, pre-clinical data shows promising results as IL-17A inhibition reduced disease induction in mice[299].

However, even if the use of IL-17A/F neutralizing antibodies has shown efficacy in many autoimmune and chronic inflammatory diseases, their use is still not common in the clinic. This is due to side effects that are developed in some patients. It has been reported that a drawback of using IL-17A/F neutralizing antibodies is the development of infections, particularly in epithelial tissues[103]. For example, IL-17A/F blocking strategies are not allowed for patients with a significant ongoing infection, such as active tuberculosis[103]. This is not entirely surprising because IL-17A/F are crucial for fighting against external pathogens, and their blockade causes the loss of their instrumental role as drivers of anti-microbial immunity. Thus, by ameliorating the chronic inflammation existing in these patients, the immune efficacy against pathogens is also decreased. Work in this area should focus on fine tuning the tight balance of hampering excessive IL-17A/F signaling, which is detrimental in autoimmune diseases and in aging, with complete blockade of their functions, which are crucial for organismal homeostasis. This would allow IL-17A/F signaling neutralization to exist as a *bona fide* therapy against autoimmune and chronic inflammatory diseases, as well as in anti-aging therapies.

4. IL-17A/F acts through NF-κB to carry out its inflammatory function

The canonical NF-κB pathway is a well-known target of IL-17A/F signaling[94]. IL-17A/F signaling activation causes IκB protein degradation in the cytoplasm, which allows p50/p65 translocation into the nucleus and the activation of pro-inflammatory genes[94]. Interestingly, not all IκB family proteins act as negative regulators of the NF-κB pathway activity, and one of the most studied members is IκBζ. This protein becomes activated and translocates into the nucleus when detecting inflammatory stimulus (including IL-17A/F signaling) and interacts with p50/p65 TFs. Then, it acts as a transcriptional coactivator and supports pro-inflammatory gene transcription[301].

The role of NF-κB in autoimmune diseases is starting to be elucidated, and the IκBζ protein has been described as key in diseases such as psoriasis[302,303]. IκBζ is known to be a main player in the differentiation of CD4+ Th cells towards Th17, and its levels (as well as of the gene that encodes it, *NFKBIZ*) have been shown to be increased in psoriatic patients. Studies have shown that IL-17A/F activate psoriasis-associated genes and proteins through IκBζ, emphasizing the critical role of the NF-κB pathway in IL-17A/F signaling in chronic inflammatory diseases[301-303]. Our data goes in line with these results, as we are pinpointing the canonical NF-κB pathway as one of the main downstream effectors of IL-17 signaling during aging. We have shown that many pro-inflammatory genes that are upregulated during aging are directly bound by p65 in an IL-17-dependent manner. As p65 and IκBζ are known to interact in order to activate the transcription of pro-inflammatory genes in psoriatic disease, future work should unravel if this interaction is also occurring during aging. Altogether, IL-17A/F signaling through of the canonical NF-κB pathway activation is revealed as crucial in the upregulation of pro-

inflammatory genes during aging, mirroring what has been described for psoriasis.

Nonetheless, this NF-κB-mediated signaling does not explain the upregulation of all inflammation-related genes during aging. There are some inflammatory genes that still remained bound by p65 after IL-17A/F blockade. This suggests that IL-17A/F may not be the only factor activating p65/NF-κB activity, or that blocking IL-17A/F for three months in aging mice may not be enough to affect all NF-κB-dependent genes. For this reason, studies in which IL-17A/F and NF-κB activity can be separated from each other (perhaps by using genetically modified model organisms) should be conducted, in order to further understand the regulatory relationship between both pathways.

Summarizing, all this underlines the critical role of increased IL-17A/F levels in skin aging, and suggests that its neutralization could be beneficial for anti-aging skin therapies.

Chapter 2. Age-associated mechanical changes impact on rhythmic epidermal homeostasis

1. The epidermal niche stiffens during aging

The aged skin presents deep structural and functional changes, including a progressive degeneration of the ECM. This is caused by collagen fragmentation and disorganization of its distribution, and crosslinking of elastin, accompanied by a reduction of integrin expression. All of this leads to a loss of elasticity and increased stiffness in the aged skin[110,154]. These changes directly affect the BM, which is formed by a connected network of ECM[31]. As a result, there are age-related changes in the BM, including an increase in thickening and stiffness[113].

It is known that changes in stiffness affect the functionality of cells. In the skin epidermis, mechanical changes have been shown to alter IFE keratinocyte behavior. *In vitro*, these cells alter their migration and proliferation as a response to a rigidity increase in their niche[31,304-306]. Regarding migration, keratinocytes cultured *in vitro* on stiff substrates showed faster closure in scratch assays[305]. Also, keratinocyte culture in a range of matrices with increasing stiffness led to stimulation of their proliferation[306]. This goes in line with what has been described for HFSCs. In organoid culture systems that mimic the stiffness of adult and aged BMs, the stiffness present during aging is sufficient to cause age-related alterations in these cells[113]. Thus, these studies highlight that the mechanical properties of the epidermal cell niche directly affect their characteristics, although all this work has been done exclusively in an *in vitro* setting. As for *in vivo* studies, niche stiffening has also been described as crucial in regulating epidermal functions during aging. A recent study has described that stiffening of the aged BM around the HF bulge impacts HFSC behavior[113]. This causes aged HFSCs to present decreased activation and differentiation, as well as loss of overall self-renewing potential. Also, murine plantar skin AFM measures of adult and aged dermis have shown an increase in stiffness in the aged condition[307]. This study identifies dermal vascular atrophy as a cause of the dermal stiffening, and focuses on the interaction between the aged vasculature

and epSCs differentiation status. Still, this work does not show any data on how the age-related mechanical changes affect epSC function.

Regardless of the differences in focus of the studies mentioned, they show that stiffness changes in the ECM and BM can influence epSC and epidermal cell functions. However, the specific consequences of the age-related increase in stiffness in the epSC niche, as well as the main players that orchestrate these changes, are still to be detailed. In our study, we have identified an increase in IFE niche stiffness during aging, which could be affecting keratinocyte gene output regulation and circadian transcription. Thus, we underscore an increase in BM stiffness as key in the development of epidermal aging traits, in a YAP/TAZ mechanotransduction pathway and core clock TF BMAL1 dependent manner.

Moreover, we have described changes in cell density during aging. We observe a lower number of epidermal cells per surface in the aged IFE. These results could suggest that there is a lower number of epidermal cells in the aged murine skin. There is controversy in the field regarding the preservation of the number of stem cells in the epidermis during aging[111,116]. With our results, we cannot contribute to any of these observations, as we have not quantified the number of epSCs in the total back skin per mouse. Hence, it is possible that the decreased epidermal cell density we describe could be accompanied by a decline in epSC number, but it could also be caused by other factors. These include an increase in total body size that we observe in aged mice, or changes in cell shape and cell-ECM adhesion, which are known to happen during aging[110]. Future studies should focus on understanding what these contradictions are dependent on, which could be the specific skin area of study, age, or the accumulation of insults though time.

2. YAP activity could sustain age-related inflammation

YAP/TAZ are required for epidermal homeostasis, as they regulate epidermal differentiation, clonal expansion, as well as cell and tissue growth[207]. Also, studies analyzing YAP genomic occupancy have shown that it controls the expression of genes involved in cell cycle progression, promoting an increase in total cell number[206].

The role of YAP in skin aging has been somewhat addressed in the past. More specifically, YAP/TAZ have been shown to decrease their expression levels during aging in stromal cells[223]. This data highlights a decline in YAP/TAZ functions in aged dermal fibroblasts, although the authors state that this does not occur in epithelial cells. Our work digs in deeper into the activity of YAP/TAZ in aged skin epithelial cells, showing that there is an increment in active YAP in these cells during aging. This underscores that YAP is tightly regulated in skin aging, as different layers seem to present opposing patterns. It is intriguing that YAP/TAZ activity attenuates in the aged dermis, even though the stiffness and mechanical inputs increase. Also, that in spite of this, there is a rise in its activity in aged epidermal cells. Consequently, future work should decipher the mechanisms leading to the differential regulation of YAP/TAZ during aging among the distinct skin layers.

We have observed that YAP activity increases in the aged epidermis, and that its genomic binding sites change towards inflammation-related genes. We hypothesize that YAP could be contributing to the pro-inflammatory scenario in the aged epidermis[156], by its age-associated binding to genes with inflammatory roles. This would mean that YAP could regulate part of the increase in the inflammatory environment in the skin, favoring aging trait acquisition. Interestingly, excessive YAP signaling has been described to be damaging in certain conditions. YAP overexpression is tightly linked to cancer development, such as in squamous cell carcinoma initiation[220,221]. Nonetheless, some studies show that YAP expression itself is not sufficient to trigger tumorigenesis.

YAP must synergize with other stimuli to initiate tumor formation. This is the case of chronic inflammation, as it can lead to tumor generation when coupled with YAP overexpression[206,220]. Moreover, in intestinal and liver cancer, coupling YAP expression with inflammatory stimuli has led to tumorigenesis[213,308].

Besides from requiring inflammation-related signals to favor tumor generation, YAP could also be contributing to the formation of a pro-inflammatory milieu to support tumor progression. Studies describe that YAP can upregulate cytokine production in the tumor microenvironment, aiding in the generation of inflammatory conditions[309,310]. Following this rationale, it is possible that the increased YAP levels we describe in aged epidermal cells have an equivalent effect to what is described for cancer progression. YAP could be helping to increase the inflammatory environment present during aging, as it does for cancer. If this were the case, it would reveal a YAP-dependent link between tumorigenesis and aging.

Still, cancer and aging are very divergent conditions with major differences that impede their comparison. Tumor initiation and progression are characterized by aberrant YAP expression, which causes damage in its surrounding cells and niche. Hence, cancer progression may be mirroring in a more exacerbated manner what we have described here for aging. Future work should compare both situations, and understand the differences in YAP expression levels between them. This would lead to comprehend if the activation of YAP during aging is as detrimental as in tumor progression. Also, new insights into how YAP activation status affects skin homeostasis would be unraveled, for conditions such as cancer and aging progression.

3. Circadian clock activity is affected by mechanical changes in the aged skin

On one hand, our lab and others have shown that the main skin epidermal functions are controlled by the circadian clock[182,183,185-187]. On the other hand, it is widely accepted that mechanical changes affect skin characteristics[31]. This gains relevance in an aging context, as there are alterations in both skin architecture, as the dermis becomes stiffer, and the circadian clock output, which reprograms in the epidermis[31,110,112].

Even though changes in the circadian clock and physical properties of the aged skin have been described in the past, not much is known about the connection between these two pathways. In spite of this, our work and others point towards thinking that changes in the mechanical features could be impacting the circadian clock during aging. For instance, one study has shown that the increased ECM stiffness present in the aged mammary gland can dampen the expression of core clock genes, as well as their ability to induce rhythmicity in output genes[226,230]. Our lab and others have shown otherwise in the past for epSCs, muscle SCs and liver. In these tissues, core clock genes still oscillate in a similar manner during aging, but it is the clock output what presents an age-associated change[112,190].

However, regardless of these observations, this study shows for the first time *in vivo* that circadian clock activity can be mechano-dependent. This leads us to hypothesize that the age-associated changes in rhythmicity we observe could be due to the ECM stiffness variations. Still, the precise factor sensing the age-associated mechanical changes in the skin, and communicating with the circadian clock machinery, has remained unrevealed until now with this work.

4. YAP and BMAL1 are key in the age-associated rewiring of circadian functions

In aged epidermal cells, there is a reprogramming of the circadian clock output with newly oscillating genes related to inflammation, ROS and DNA repair[112]. We find that BMAL1 binds directly to genes with inflammatory functions, and to some also coupled to ROS response. This happens with higher frequency in aged epidermal cells when compared to adults. As a result, we hypothesize that there are two branches of control of the age-related rewiring. On one hand, there is a subset dependent on BMAL1 direct binding, controlling the circadian activity of genes with roles relevant for inflammation, and to some extent to ROS metabolism. On the other hand, there is a group of genes important for DNA damage response that are circadian but that are not bound by BMAL1. This indicates that BMAL1 is critical for regulating the circadian activity of a subset of the reprogrammed clock output, and that there must be other elements in charge of the control of the rhythmic behavior of DNA damage-associated genes.

Moreover, we have discovered a functional relationship between YAP and the core clock TF BMAL1. We show that they bind to a highly overlapping set of genes, and shift towards binding to DNA regions close to inflammation-related genes during aging. Importantly, only some of those genes are circadian in aged epidermal cells. There is another set of inflammatory and homeostatic genes bound by both that are not oscillatory. This highlights that BMAL1 and YAP are still bound to homeostatic genes during aging, even if they are not expressed in a circadian manner. Also, that not all the pro-inflammatory genes bound by both TFs are transcriptionally oscillatory during aging.

All this indicates that YAP and BMAL1 binding alone is not sufficient to drive the circadian expression of genes. These differences in oscillatory behavior in YAP- and BMAL1-bound genes could be explained by the existence of other regulatory mechanisms. The transcriptional control of

genes by the circadian clock is critical to obtain rhythmic transcription, although there are other processes that regulate the oscillatory clock output. These include post-transcriptional, translational and post-translational mechanisms. As an example, post-transcriptional modifications include those involved in mRNA processing. The accumulation of mRNA through the day can lead to the circadian expression of genes[168]. This means that even though there is transcription of a specific gene at a determined time, it is not expressed in that moment, but after accumulating and reaching a threshold. This could suggest that even though we have coupled YAP and BMAL1 binding to the control of some circadian genes, there could be other relevant non-transcriptional factors. Therefore, future work should study the relevance of post-transcriptional mechanisms in this process.

In addition, there could be mediators of a different nature leading to the control of the rhythmicity of genes. They could be related to other mechano-sensing pathways, such as the Piezo channel family, particularly Piezo1. Piezo1 is expressed in epithelial cells, and converts mechanical information into elevated levels of calcium (Ca^{2+}) in the cytosol of cells, triggering various Ca^{2+}-dependent signaling pathways[311]. Also, Piezo1 has been described as relevant for epSC dysregulation during aging[307]. As a result, Piezo1 could be relevant in our setting, and it would be necessary to validate its role in following studies.

To sum up, it should be addressed if the additional gene regulation processes depend on non-transcriptional circadian regulatory elements, mechanotransduction pathways, or the interplay between both of them.

5. There is an age-related functional association between YAP and BMAL1

In this work, we aimed to understand the specifics of the relationship between BMAL1 and YAP in skin aging. Here, YAP could be the driver of this interaction. It could become activated during aging by mechanical

stimuli, driving BMAL1 to specific binding sites and circadian activation of genes. Another option is that YAP could be regulated by the circadian clock, and age-associated changes in BMAL1 could be leading to alterations in YAP activation status.

Our data in this regard is still preliminary, but points towards neither YAP or BMAL1 by themselves being responsible for driving the age-associated changes described. In the absence of BMAL1, YAP lost many binding sites in the genome of epidermal cells. These genes that lost YAP binding were related to homeostasis, development, and with functions crucial for its mechanotransduction activity. Thus, even if past studies have stated that YAP activity is not clock-dependent[230], our results suggest that it at least requires the core clock gene BMAL1 for its correct functionality. Still, YAP retained some of its binding in absence of BMAL1, highlighting that not all of its activity depends on it. It would be relevant to study to what extent YAP requires BMAL1 for its activity, and this unresolved question should be addressed in subsequent studies.

Also, BMAL1 activity is altered when YAP becomes hyperactivated. Our preliminary data shows that BMAL1 binds to a new pool of pro-inflammatory genes when constitutively active YAP is overexpressed, indicating that part of its functionality is related to YAP. This leads to hypothesize that the increase in pro-inflammatory circadian genes bound by BMAL1 during aging could be, at least partly, directed by YAP activation.

Besides, it is possible that changes in stiffness are enough to induce the circadian rewiring of genes, affecting both YAP and BMAL1 activity. Our ongoing work is focused on trying to unravel this hypothesis, and we are making use of a mouse model in which collagen XIV has been systemically KO (*Col14a1*[-/-]) for this. These mice present an insertion of a stop codon in exon 4 of the *Col14a1* gene, creating a nonsense mutation and producing a truncated non-functional collagen XIV protein[312]. Thus, this mouse model is especially relevant for tissues with

high mechanical stress like the skin, tendons, cornea, and articular cartilage usually expressing collagen XIV.

Collagen XIV absence causes a decrease in skin elasticity due to its role in fibrillogenesis, which is critical for collagen and ECM assembly[312]. Of note, one study has shown that in one-year-old aging collagen XIV KO mice, there is an increase in BM thickness and in stiffness in areas surrounding HFs in comparison to WT adults[113]. These physical alterations are reminiscent of what has been described for aged skin, and allows analyzing the impact of a decreased elasticity and increased stiffness in the skin without the presence of other age-related traits. We are determining if there is an increased YAP activation in the epidermal cells of the IFE in these mice at different ages. Once we identify the age at which YAP becomes active in the IFE of these mice, we will analyze their circadian transcriptome in aging epidermal cells. With this, we will detect if there is a rewiring towards pro-inflammatory functions, as well as identify changes in BMAL1 binding.

In addition, remaining questions include determining if the relationship between YAP and BMAL1 is also physical, as we are still studying if their binding to the same genomic locations is due to the formation of a direct complex between them. This would allow understanding how these age-associated traits in the skin crosstalk between one another.

To conclude, we have shown that YAP/TAZ mechotransduction pathway and the circadian clock activity, particularly of BMAL1, are functionally related. This gains relevance during aging, as there are age-related changes that impact their activity. These results give insights into how the skin aging process happens, and shows that aging does not result from single unrelated events, but from an accumulation of deteriorating and intertwined occurrences.

Conclusions

1. There is an increase in pro-inflammatory signals in the aged dermis, affecting immune and non-immune cell types

2. The levels of IL-17 are increased in the aged dermis, as there is a significantly elevated number of CD4+ Th, γδ T and ILCs cells expressing it.

3. The exacerbated levels of IL-17 appear in aged skin mainly, although this could be extrapolated in a milder manner to other aged barrier tissues such as the intestine, and across species in the aged human dermis

4. The increase in IL-17 in aged skin is not reminiscent of what has been described in psoriasis, because these are non-comparable contexts

5. The aberrant IL-17 levels in the aged skin are likely to be caused by an internal skew of lymphoid cell subsets

6. Systemic *in vivo* blocking of IL-17 function ameliorates the inflammatory scenario in the aged skin, affecting immune and non-immune dermal cells, and keratinocytes

7. IL-17 blockade slows down the appearance of age-related traits in the skin

8. IL-17 activity depends on downstream NFκB to carry out its functions in epidermal cells

9. The BM stiffens during aging in areas subjacent to the IFE, affecting the epSC niche. This is accompanied by a decrease in cell density in the aged IFE

10. YAP activity is increased in aged epidermal cells. It also changes its genomic location towards binding to genes with pro-inflammatory functions during aging

11. Aged epidermal cells rewire their circadian functions to adapt to stress, and this process is in part controlled by BMAL1 direct binding

12. YAP and BMAL1 bind to adjacent regions in the genome. During aging, these regions include mainly genes with inflammatory functions, some of which have a circadian expression

13. There is an age-related functional association between YAP and BMAL1. YAP needs BMAL1 to bind to essential genes to carry out its functions, and BMAL1 is bound to genes with inflammatory roles in a YAP-dependent manner

Materials and Methods

Disclaimers:

The materials and methods corresponding to chapter 1 have been adapted from our bioRxiv publication[313].

Methods were carried out in collaboration with Júlia Bonjoch and Dr. Guiomar Solanas. Other contributors are mentioned in each method section.

1. *In vivo* experiments

1.1. Mouse handling and husbandry

All procedures were approved by the Ethical Committee for Animal Experimentation (CEEA) from the Government of Catalunya. Mice were housed under 12-h/12-h light/dark cycles and in specific pathogen-free conditions, and were always sacrificed in the dark cycle for experiments in chapter 1, coinciding with their active phase. For chapter 2 experiments, mice were sacrificed at 6 time points to obtain an oscillatory transcriptome (ZT0, ZT4, ZT8, ZT12, ZT16 and ZT20 after turning on the lights), and at ZT4 for the rest of experiments.

Aged mice were between 80- to 90-weeks old, and adult mice were between 17- to 25-weeks old. Mice used were from the C57Bl/6J strain, and aged mice were either bred in-house at the Barcelona Science Park (PCB) or were retired C57Bl/6J breeder females purchased from Charles River and aged in-house at the PCB. Control adult mice were also either bred in-house or purchased from Charles River, and these were mostly females. This was due to the use of aged retired breeders, in order to use comparable cohorts between ages, and also because of existing differences in skin digesting efficiencies between sexes. Male skin digestion times are longer and this leads to a reduced cell survival, biasing the results towards the most resistant cell types. For experiments that did not require skin enzymatical digestion, males were also included in all conditions.

1.2. Epidermal and dermal cell isolation for genomics analysis

Mice were sacrificed, and whole torso skin was removed as fast as possible. Hypodermis was removed with scalpel and after 2 washes in PBS, skins were floated (dermis-side down) either in a Dispase II solution (5 mg/mL; D4693 Sigma-Aldrich) for scRNA-seq experiments, and in Trypsin 1:250 solution (0.8%, 27250-018 Gibco) for all other experiments, both diluted in PBS for 30- to 40 min at 37ºC. Epidermises were separated from dermises with a scalpel.

For dermal cell isolation: dermises were mechanically dissociated using a McIlwain Tissue Chopper (The Mickle Laboratory Engineering Co. LTD) and then further digested in Liberase TM (6.5 Wünsch units/reaction, Roche) diluted in DMEM (41965, Thermo Fisher Scientific) for 20 to 30 min at 37ºC with gentle agitation. Afterwards, DNase I (1 mg/ml DN25; Sigma-Aldrich) was added to the mix and incubated for 15 min at 37ºC without agitation. Digested dermises were strained first through a 100-μm strainer and then through a 40-μm strainer, to obtain single-cell suspensions.

For epidermal cell isolation: epidermises were mechanically dissociated using a McIlwain Tissue Chopper (The Mickle Laboratory Engineering Co. LTD). They were then strained through a 100-μm and then a 40-μm strainer to obtain single-cell suspensions.

1.3. RNA sequencing (RNA-seq)

For circadian bulk RNA-seq of **adult and aged** cells, cells were isolated at different times of the day (0, 4, 6, 8, 12, 16, 20, 24 hours after turning on the lights), and n=4 replicates per condition and timepoint. The bulk RNA-seq of adult and aged epidermal cells was extracted from the circadian transcriptome analysis, 12 hours after turning on the lights (ZT12). In the case of the **aged/control IgG treated and anti-IL-17A/F**, n= 4 per group were used.

Around 1 million epidermal cells were frozen in 1 ml of TRIzol (Invitrogen) for posterior RNA isolation. RNA was extracted from epidermal cell pellets frozen in TRIzol using the RNeasy Mini Kit (Qiagen) and further processed for mRNA-seq.

1.4. Chromatin immunoprecipitation and sequencing (ChIP-seq)

Around 30 million pelleted epidermal cells were used per reaction. The cells were crosslinked using Gold fixative (C01019027, Diagenode), following manufacturer's directions. After two PBS washes, a second fixation was done in methanol-free 1% formaldehyde (28908, ThermoFisher Scientific) in MEM calcium free medium with 10% Calcium-chelated FBS, for 10 minutes in rotation. Glycine was then added to a final concentration of 125mM to stop the crosslinking, and incubated for 5 minutes in rotation. Pellet was washed twice with cold PBS, and the cells were then resuspended in 7.5mL of swelling buffer (25mM Hepes pH 7.9, 1.5mM MgCl2, 10mM KCl, 0,1% NP-40 supplemented with 1X protease inhibitors without EDTA). This cell suspension was homogenized 50 times with a Dounce homogenizer and tight pestle (885302-0015, Kimble), and the extracts were centrifuged (3000 xg, 5 minutes). The pelleted nuclear extracts were resuspended (in 1/10 of the volume used for the swelling buffer) in ChIP buffer (10mM Tris-HCL pH 7.5, 150mM NaCl, 1% TX-100, 5mM EDTA, 0,5mM DTT, supplemented with 0.2% SDS and 1X protease inhibitors without EDTA). This suspension was incubated for 15 minutes, and transferred to sonication tubes (C01020031, Diagenode). The sonication was carried out in 30 cycles of 30" on/ 30" off at 4°C (Bioruptor Pico, Diagenode), and the sonicated supernatant was centrifuged (14000 xg, 10 minutes). The supernatant containing the chromatin was quantified for the following steps.

For the immunoprecipitation, 20μg- 30μg of chromatin was diluted with ChIP buffer without SDS to dilute the SDS concentration to 0.1% in all

samples. Then, the antibody was added and the samples were rotated O/N at 4°C. For **p65** ChIP-Seq (clone D14E12, CST #8242, 4μg/ml per reaction), there were 4 replicates per condition, with one mouse per replicate/condition. For **YAP** ChIP-seq in WT mice (clone D8H1X, CST #14074, 4-6 μg per reaction), 4 replicates were carried out per condition, with more than one mouse per replicate. For ChIP-seq in BMAL1ep cKO mice, 3 replicates were done per group, with one mouse per replicate. For **BMAL1** ChIP-seq in WT mice (ab93806, 4-6 μg per reaction), 4 replicates were carried out per condition, with more than one mouse per replicate. For ChIP-seq in iYAP mice, 2 replicates were carried out with one mouse per replicate. This is preliminary, as there is at least one more replicate being analyzed. Sepharose beads (17-5280-01, Merck) were used according manufacturers description, added to each sample, and incubated in rotation for 2 hours at 4°C. The samples were then centrifuged (1000 xg, 3 min) and washed with low (L) and high (H) salt buffers (L, H, L, H, L) centrifuging between washes. Low salt buffer is composed of 50mM HEPES pH 7.5, 140mM NaCl, 1% Triton, 1X protease inhibitors without EDTA, and high salt buffer contains 50mM HEPES pH 7.5, 500mM NaCl, 1% Triton, 1X protease inhibitors without EDTA. A final wash with TE buffer (10mM Tris-HCl pH=8.0, 1mM EDTA) was performed. Immunoprecipitated chromatin was eluted in elution buffer (1%SDS and 100mM NaHCO3, freshly prepared), by incubating samples in the buffer for 30 minutes at 65°C with agitation (1000 rpm). Samples were then centrifuged (3000 rpm, 3 min), and 5M NaCl was added to a final concentration of 200mM per sample, and incubated 5h to O/N at 65°C with agitation (1000 rpm). After this, Tris-HCl pH 6.8 was added to final concentration of 40mM, and EDTA to 10mM, Protease K to 50μg/ml and incubated 1h at 45°C. This product was purified with PCR columns.

1.5. Assay for Transposase-Accessible Chromatin using sequencing (ATAC-seq)

This experiment was conducted as previously described[266]. Epidermal cells were isolated following the epidermal isolation protocol mentioned. Then, 50,000 FACS sorted live epidermal cells in a single-cell suspension were lysed directly post-sorting. This was done by resuspending cells in 50μl of cold lysis buffer (10 mM Tris-HCl pH 7.4, 10 mM NaCl, 3 mM MgCl and 0.1% IGEPAL CA-630), and centrifuging immediately after for 10 min at 500 xg. Pellet including nuclei was further processed as stated in the library preparation section.

1.6. Flow cytometry and cell sorting

For CD45+, CD45–/EpCAM– and CD31+/MHCII. For 10× scRNA-seq, single-cell dermal suspensions (see Epidermal and dermal cell isolation for genomic analysis) were incubated with CD45–APC (clone 30-F11, 1:100, BD Biosciences) and EpCAM–PE (clone G8.8, 1:200, BD Biosciences) for 45 min on ice. After two washes in PBS, cells were resuspended in 2 μg/ml DAPI (32670, Sigma-Aldrich) to stain DNA and analysed using a BD FACSAria Fusion flow cytometer, in which CD45+/– cells were obtained and EpCAM+ cells excluded.

For MHCII analysis in CD31+ cells, single-cell dermal suspensions were incubated with CD31-PE (clone MEC13.3, 1:100, BD Bioscience) MHCII-BV650 (I-A/I-E, clone M5/114.15.2, 1:500, BioLegend), LYVE1-eFluor 660 (clone ALY7, 1:100, Invitrogen), and (as exclusion markers) CD45–FITC (clone 30-F11, 1:100, eBioscience), CD117-FITC (clone 2B8, 1:100, BDBiosciences), CD41-FITC (clone eBioMWReg30, 1:100, Invitrogen), or EpCAM–FITC (clone G8.8, 1:100, Biolegend). After two washes with PBS, cells were resuspended in 2 ug/ml DAPI (32670, Sigma-Aldrich) to stain DNA and analysed using a BD FACSAria Fusion flow cytometer.

1.7. *In vivo* α-IL-17A/F blocking antibody treatment

For the α-IL-17 blocking treatment, cohorts of 73-week-old aging mice were randomly distributed into two groups; treatment or control group. Mice from the treatment group were injected with a mixture of previously joined antibodies, formed by 105 μg α-IL-17A (clone 17F3, BioXCell) and 105μg α-IL-17F (clone MM17F8F5.1A9, BioXCell) antibodies. The control group mice were injected with 210 μg of control IgG1 antibody (clone MOPC-2, BioXCell). Injections in both groups consisted of 100 μl suspension of antibodies diluted in PBS. They were administered intraperitoneally (i.p.) 3 times per week during the dark phase. After 12 weeks of treatment, aged mice were either sacrificed for 10× scRNA-seq, bulk RNA-seq of the epidermis and histology, or they were used for skin integrity readouts.

1.8. Epilation

Females of adult (n=6; 18-20 weeks old), aged/IgG control treated and aged/α-IL-17A/F treated (n=6 per group; 85 weeks-old) groups were used. For anesthesia, i.p. injection of a mixture of ketamine (75 mg/kg body weight) and medetomidine (1 mg/kg) was used. For analgesia, subcutaneous (s.c.) injection of buprenorphine (0.05 mg/kg) was used. Then, epilation was carried out in the back skin of the mice, in an area of about 2- to 3-cm^2 using wax papers until there was no hair patches (2 or 3 rounds). Once the epilation was done, atipamezole (1 mg/kg) was injected to revert the anesthesia, and mice were left on a warm blanket until they awakened. Mice were housed individually to avoid scratching or fighting affecting the epilated areas, and their health status was daily monitored. Mice were sacrificed 8 days post-epilation, images of the back skins were taken, samples of the back skin were fixed in neutral buffered formalin (10%) for 3 h at room temperature, dehydrated, and included in paraffin blocks for posterior histological analysis.

1.9. Wound healing

For wound healing, adult (n=15; 18-20 weeks old), aged/IgG control (n=14; 85 weeks old) and aged/α-IL-17A/F treated (n=15; 85 weeks-old) male and female mice were used. IL-17A/F blocking and control injections were stopped one week prior to starting the assay to normalize IL-17 endogenous activity and separate the role of this cytokine in wound healing from its role during aging. This was decided due to recent literature describing the crucial role of IL-17 in the wound healing process[99].

Mice were anesthetized using 3-4% isoflurane, and buprenorphine (0.05mg/kg) was injected s.c. for analgesia. The body temperature was maintained by placing the animals on a heated pad throughout the process. The back skin region of the animals was shaved and this area was then sterilized with 10% povidone-iodine diluted in dH_20 solution. Two skin biopsies were carried out per animal, one per flank using a 5mm diameter sterile, disposable circular biopsy punch (Kai medical BP-50F). If needed, sharp scissors were used to dissect the skin biopsy and de-attach it from the mouse after using the punch. Mice were placed in heated pads until fully recovered from anesthesia, and they were housed individually throughout the entire experiment (10 days). Wound area was macroscopically assessed by daily measuring the length and width of the wounds using a digital caliper (Traceable® Digital Caliper). For wound area analysis, the measurements of the two wounds per animal were averaged. Mice were sacrificed at day 10 (5 females and 5 males for adult and aged/IL-17A/F treated, and 5 females and 4 males for the aged/IgG controls). All wounds were collected, fixed in neutral buffered formalin (10%) for 3 h at room temperature, dehydrated, and included in paraffin blocks for histological analysis. Qualitative analysis of granulation tissue and epidermal maturation were performed in a double-blind study by histopathologists.

1.10. Barrier recovery and trans epidermal water loss (TEWL)

Barrier integrity was assessed by measuring transepidermal water loss (TEWL), which measures water evaporation directly on the skin surface using a probe (Tewameter® TM Nano, Courage+Khazaka). The mice used included adult (n=6; 18-20 weeks old), aged/IgG control (n=7; 85 weeks old) and aged/IL-17A/F treated (n=5; 85 weeks old) female mice. Mice back skins were shaved 24 prior to the barrier disruption, and were anaesthetized using 3-4% isoflurane throughout the assay. The temperature of the animals was maintained constant at 37ºC at all times by keeping them placed on a tightly regulated thermal plate. The mice were left to acclimate after being anaesthetized and prior to starting the tape stripping and measurements for three minutes. All measurements were carried out in the same location and by the same person, and room temperature and humidity were recorded.

The epidermal barrier was disrupted by tape stripping (Corneofix® CF 20, Courage+Khazaka), and the number of tape strips was adjusted per age to obtain a TEWL of > 20g/m²/h[1231224](Uberoi et al. 2021)(Uberoi et al. 2021)[123]. A range of 6 to 10 strips was needed for adults, and of 12-16 for aged/IgG controls and for aged/IL-17 treated mice. For the TEWL measurements, the probe was used according to manufacturer's instructions. The probe was placed on each location of the skin surface being measured for 40 seconds before starting for stabilization, and each measurement lasted one minute. TEWL probe measurements were carried out immediately after tape stripping (t0), and 6, 10, 24 and 48 hours post tape stripping (t6, t10, t24, t48 respectively). There were two measurements done per animal, and we averaged their TEWL value to obtain one single value per animal and per timepoint. Also, the probe was placed at these same two locations for each consecutive measurement for consistency reasons. The locations used for measurements intendedly avoided areas where tape stripping had caused the

appearance of small wounds, in order to avoid altering the actual barrier recovery values.

1.11. YAP transgene induction in iYAP mice

To induce the expression of the *YAP* S127A-mutated transgene, we added doxycycline (2mg/ml doxycycline and 5% sucrose diluted in tap water) in the drinking water of control and iYAP mice. The induction was carried out for 36 hours, after which the mice were sacrificed following the epidermal and dermal isolation protocol described.

2. Sample processing and analysis

2.1. Hematoxylin and eosin staining

Carried out by the IRB histopathology facility. Formalin-fixed paraffin embedded (FFPE) blocks were cut in 2-4-μm sections. Hematoxylin and eosin (H&E) staining was performed according to the standard protocol.

2.2. Immunofluorescence (IF)

In all cases, FFPE blocks were cut in 2-4-μm sections.

IL-17A: after heat mediated antigen retrieval (20 min at 97ºC with citrate pH 6), sections were blocked with a 10% goat serum in PBS for 1 h at room temperature. Primary antibody incubation (anti-IL-17A, ab79056 abcam 1:200, in EnVision FLEX antibody diluent – Dako) was done overnight at 4ºC. After 3 washes in PBS, secondary antibody (anti-rabbit Alexa Fluor 488 – Molecular Probes, 1:400 in EnVision FLEX antibody diluent – Dako) incubation was done at room temperature for 1h. Nuclei were counterstained with 4',6-diamidino-2-phenylindole (DAPI; 5μg/ml for 10min at room temperature). Six adult and 5 aged mice per condition were analyzed.

CD4: antigen retrieval was performed using BOND Epitope Retrieval 2 – ER2 (AR9640, Leica). For primary antibody incubation, rat IgG2b kappa

anti-CD4 (clone 4SM95) (14-976-682, ThermoFisher) was used at 1:100 and incubated for 120 min, and performed using Leica BOND RX. Non-specific unions were blocked using 5% of goat normal serum mixed with 2.5% BSA diluted in wash buffer for 60 min at room temperature. For the secondary antibody incubation, goat anti-rat IgG (H+L) and Alexa Fluor 647 (A21247, ThermoFisher) were used at 1:500 for 60 min. Nuclei were stained with DAPI, and slides were mounted using fluorescence Mounting Medium (S3023, Dako – Agilent). Five adult and 5 aged mice per condition were analyzed.

Ccl19: antigen retrieval was performed for 20 min at 97ºC with citrate pH 6, and sections were blocked with 10% donkey serum in PBS 1 h at room temperature. Primary antibody incubation (anti-CCL19/MIP-3, BS-2454R Thermo Fisher) was done at 1:100 overnight at 4ºC. After 3 washes in PBS, secondary antibody (anti- rabbit Alexa Fluor 488 – Molecular Probes, 1:400 in EnVision FLEX antibody diluent – Dako) incubation was done at room temperature for 1h. Nuclei were counterstained with DAPI (5μg/ml for 10min at room temperature). Three adult and three aged mice were analyzed.

Active YAP: antigen retrieval was performed for 20 min at 97ºC with Tris-EDTA pH 9, and sections were blocked with 10% donkey serum in PBS 1 h at room temperature. Primary antibody incubation (clone EPR19812, ab205270, abcam) was done at 1:1000, diluted in in EnVision FLEX antibody diluent (Dako) overnight at 4ºC. After 3 washes in PBS, secondary antibody (anti- rabbit Alexa Fluor 488 – Molecular Probes, 1:400 in EnVision FLEX antibody diluent – Dako) incubation was done at room temperature for 1h. Nuclei were counterstained with DAPI (5μg/ml for 10min at room temperature). N= 10 adult, 12 aged mice.

Total YAP: antigen retrieval was performed for 20 min at 97ºC with Tris-EDTA pH 9, and sections were blocked with 10% donkey serum in PBS 1 h at room temperature. Primary antibody incubation (clone D8H1X, #14074, CST) was done at 1:400, diluted in in EnVision FLEX antibody

diluent (Dako) overnight at 4ºC. After 3 washes in PBS, secondary antibody (anti- rabbit Alexa Fluor 488 – Molecular Probes, 1:400 in EnVision FLEX antibody diluent – Dako) incubation was done at room temperature for 1h. Nuclei were counterstained with DAPI (5*μ*g/ml for 10min at room temperature). N=2 mice per condition (WT and iYAP mice).

Cell density: skin sections were stained with DAPI (5*μ*g/ml for 10min at room temperature). N=4 mice per group, with 10 IFE areas measured per animal.

2.3. Image acquisition

Carried out by the IRB histopathology facility. Full slide images were acquired with a NanoZoomer-2.0 HT C9600 digital scanner (Hamamatsu) with the 20X objective, in which 1 pixel corresponds to 0.46um, and coupled to a mercury lamp unit L11600-05 and using NDP.scan2.5 software U10074-03 (Hamamatsu, Photonics, France).

2.4. Histopathological analysis

Scaled images were analyzed with Qupath v0.3.2. For the **cornified layer thickness** measurements, we did 10 measures per mouse. These 10 values per mouse were averaged. Eight mice per condition and age were used. We always made sure that the analyzed area was in the resting hair follicle stage (telogen) to avoid interference of this parameter with the desired quantification. For **wound healing** assay, qualitative analysis of dermal granulation tissue and epidermal maturation were performed in a double-blind study by histopathologists. For **anagen stage** assessment, we assigned each HF to an anagen stage based on previous reports[16].

For **immunostainings**, multiple selections (region of interest – ROI) of the skin dermis, excluding the epidermis and hair follicles, were done manually in two sections of skin. The “Positive cell count” algorithm was

used to detect positive cells. Results are presented as percentage of positive cells. For CD4 immunofluorescence, the images displayed were captured with an SP5 confocal microscope (Leica). Images of the whole stack were projected on a single image and brightness and contrast were adjusted to enhance the signal of positive cells, using the same parameters for both conditions. For IL-17A, NDP view2 (v2.9.29 Hamamatsu, Japan) was used to generate snapshots from representative areas. Brightness and contrast were adjusted to help distinguish the positive cells from the background, using the same parameters for both conditions. Modified images were used exclusively for visualization, and never for quantification.

For ***IL17A* and *IL17F* FISH**, areas were selected manually. In case of tissue artefacts, those were excluded from the ROI (e.g. broken areas, folds). The “Positive cell count” algorithm was used to detect positive labeling in the TRITC channel. Results are presented as percentage of cells with *IL17A* or *IL17F* signal (either spots -single mRNA copy- or clusters -accumulation of several mRNA copies). For the skin samples, brightness and contrast were adjusted to help distinguish the positive cells from the background, using the same parameters for both conditions. Modified images were used exclusively for visualization, and never for quantification.

For ***Rspo3* FISH**, DP were selected manually in well-oriented telogen HFs. The “Cell detection” algorithm was used to detect nuclei inside the selected areas. The “Subcellular spot detection” algorithm was used to detect *Rspo3* positive labeling in the TRITC channel in those nuclei. Individual nuclei were not always distinguishable due to high packing of DP cells. Therefore, FISH signal (spots and clusters) was not calculated per cell, but per DP. Five mice per condition were used. Graphical representations were performed with GraphPad Prism 9. Brightness and contrast were adjusted to help distinguish the positive cells from the background, using the same parameters for both conditions. Modified

images were used exclusively for visualization, and never for quantification.

For **cell density analysis**, cells were counted per μm across IFE regions of adult and aged murine back skin. Values per animal are composed of an average of the total number of cells counted per μm in all 10 measurements done per section.

2.5. Bulk RNA-seq library construction and sequencing

For the **adult *vs* aged** comparison for chapter 1, and for circadian transcriptome samples in chapter 2, libraries were prepared using the TruSeq Stranded Total RNA Library Prep Kit with Ribo-Zero Human/Mouse/Rat Kit (cat. RS-122-2201/2202, Illumina) according to the manufacturer's protocol, using 150 to 300 ng of total RNA; ribosomal RNA depletion, RNA was then fragmented for 4.5 min at 94ºC. The remaining steps were followed according to the manufacturer's instructions. Final libraries were analyzed on an Agilent Technologies 2100 Bioanalyzer system using the Agilent DNA 1000 chip to estimate the quantity and validate the size distribution; libraries were then quantified by qPCR using the KAPA Library Quantification Kit KK4835 (cat. 07960204001, Roche) prior to amplification with Illumina's cBot. Finally, libraries were sequenced on the Illumina HiSeq 2500 sequencing system using paired-end 50-base pair (bp)-long reads.

For the **IL-17 neutralized *vs* control** samples, libraries were prepared using the TruSeq stranded mRNA Library Prep (cat. 20020595, Illumina) according to the manufacturer's protocol, to convert total RNA into a library of template molecules of known strand origin that is suitable for subsequent cluster generation and DNA sequencing. Briefly, 500–1000 ng total RNA was used for poly(A)-mRNA selection using poly-T oligonucleotides attached to magnetic beads with two rounds of purification. During the second elution of the poly-A RNA, RNA was fragmented under elevated temperature and primed with random

hexamers for cDNA synthesis. The cleaved RNA fragments were then copied into first-strand cDNA using reverse transcriptase (SuperScript II, ref. 18064-014, Invitrogen) and random primers. Note that addition of actinomycin D to the First Stand Synthesis Act D mix (FSA) improves strand specificity by preventing spurious DNA-dependent synthesis while allowing RNA-dependent synthesis. Second-strand cDNA was then synthesized by removing the RNA template and synthesizing a replacement strand, incorporating dUTP in place of dTTP to generate ds cDNA using DNA polymerase I and RNase H. These cDNA fragments then had a single A base added to the 3′-ends of the blunt fragments, to prevent them from ligating to one another during the adapter ligation. A corresponding single T-nucleotide on the 3′-end of the adapter provided a complementary overhang for ligating the adapter to the fragments, ensuring a low rate of chimera (concatenated template) formation. Subsequent ligation of the multiple indexing adapter to the ends of the double-strand cDNA was carried out. Finally, PCR selectively enriched DNA fragments with adapter molecules on both ends, and the amount of DNA in the library was amplified. PCR was performed with a PCR Primer Cocktail that anneals to the ends of the adapters. Final libraries were analyzed using Bioanalyzer DNA 1000 or Fragment Analyzer Standard Sensitivity (Agilent) to estimate the quantity and validate the size distribution; libraries were then quantified by qPCR using the KAPA Library Quantification Kit KK4835 (Roche) prior to amplification with Illumina's cBot. Finally, libraries were sequenced on the Illumina HiSeq 2500 sequencing system using single-end 50-bp-long reads.

2.6. ChIP-seq library amplification and sequencing

Libraries were prepared using the NEBNext Ultra DNA Library Prep for Illumina kit (ref. E7370) according to the manufacturer's protocol. Briefly, input and ChIP enriched DNA were subjected to end repair and addition of "A" bases to 3′ ends, ligation of the NEB adapter and USER excision.

All purification steps were performed using AgenCourt AMPure XP beads (ref. A63882, Beckman Coulter). Library amplification was performed by PCR using NEBNext Multiplex Oligos for Illumina (96 Unique Dual Index Primer Pairs, ref. E6440, E6442, E6444, E6446). Final libraries were analyzed using Agilent Bioanalyzer or Fragment analyzer High Sensitivity assay (ref. 5067-4626 or ref. DNF-474) to estimate the quantity and check size distribution, and were then quantified by qPCR using the KAPA Library Quantification Kit (ref. KK4835, KapaBiosystems). Libraries were sequenced 1 * 50+8+8 bp on Illumina's NextSeq2000. Between 35 and 40 million reads were obtained per sample.

2.7. ATAC-seq library amplification and sequencing

Isolated pelleted nuclei were placed on ice and resuspended in Tagment DNA Buffer and Tagment DNA Enzyme (Nextera, Illumina), and incubated for 30 min at 37ºC. The next step involved purification, using the MinElute PCR purification kit (Qiagen) and PCR-amplification for 10-12 cycles. The concentration and quality of libraries were confirmed by Qubit and Bioanalyzer. Paired-end sequencing and 50-cycle reads was done for sequencing.

2.8. 10× scRNA-seq

Stained dermal single-cell suspensions were prepared as previously explained. CD45+ and CD45–/EpCAM– cells were FACS sorted in a BD Fusion cell sorter separately to enrich for the less abundant CD45+ cells, following the sorting strategy depicted in Suppl. Fig. 1a. Cells were collected in PBS + 0.5% BSA at 4°C in LoBind tubes (Eppendorf) and processed immediately with the microfluidics Chromium platform (10× Genomics). For the adult and aged experiment, 3 technical replicates were performed for the CD45+ sorting per condition. Replicate 1 included skin dermal cells of 3 adult and 1 aged mouse, replicate 2 had 2 adult and 1 aged mouse, and replicate 3 was composed of 2 adult and 2 aged

mice. For CD45- EpCAM- cell sorting, 2 replicates were carried out, and each replicate was composed of 1 mouse per condition each. For the aged/IL-17 blocked and aged/IgG control 10X scRNA-seq of dermal skin cells, both CD45+ and CD45- EpCAM- conditions included 4 replicates in total. In both conditions, replicate 1 consisted of 2 aged/IL-17 blocked and 2 aged/IgG control mice. Replicates 2, 3 and 4 consisted in all cases of 1 aged/IL-17 blocked and 1 aged/IgG control.

2.9. Fluorescent *in situ* hybridization

Carried out by the IRB histopathology facility. For *IL17A* and *IL17F*, human adult (22-29 years old; n=4; 2 women and 2 men) and aged (60-72 years old; n=4; 2 women and 2 men) skin FFPE 5μm tissue sections were purchased from Genoskin. They were then stained with RNAscope Probes: Hs-IL17A - Interleukin 17A probe (310931, Bio-techne), Hs-IL17F - Interleukin 17F probe (313901, Bio-techne) using RNAscope Intro Pack 2.5 HD Reagent Kit Red (322350, Bio-techne). DAPI staining was used to stain all nuclei.

For *Rspo3*, FFPE 3μm tissue sections of mouse back skin from aged/anti-IL-17-treated or aged/IgG control were stained with RNAscope Probe Mm-Rspo3-O1 (429861, Bio-techne) using RNAscope Intro Pack 2.5 HD Reagent Kit Red (322350, Bio-techne). DAPI staining was used to stain all nuclei.

2.10. Atomic force microscopy (AFM)

Carried out by Dr. Yekaterina Miroshnikova in Dr. Sara Wickströms lab.
Atomic force microscopy (AFM) measurements of extracellular matrix stiffness were performed on freshly cut 16-micron thick cryosections using the JPK NanoWizard 2 (Bruker Nano) AFM mounted on an Olympus IX73 inverted fluorescent microscope (Olympus) and operated using the JPK SPM control software v.5. Briefly, cryosections were equilibrated in phosphate buffered saline (PBS) supplemented with 1X

protease inhibitors and measurements were performed within 20 min of thawing the samples. Silicon Nitride cantilevers (MLCT, Bruker) were used for the nanoindentation experiments. For all of the indentation experiments, forces of up to 3 nN were applied, and the velocities of cantilever approach and retraction were kept constant at 2 micron/second. Before fitting the Hertz model corrected by the tip geometry to obtain Young's Modulus (Poisson's ratio of 0.5), the offset was removed from the baseline, the contact point was identified, and cantilever bending was subtracted from all force curves. N=5 mice per condition, with 5 regions analyzed per mouse. For the analysis, the average of all regions was calculated per animal. These averages were used to compare the samples using the Mann-Whitney *U* non-parametric test, done with Prism v9.

3. Bioinformatic analysis

Disclaimers:

ChIP-seq analysis carried out by Dr. Guiomar Solanas

Bulk RNA-seq analysis carried out by Dr. Oscar Reina (Biostatistics Unit-IRB)

ATAC-Seq analysis was performed by Dr. Antoni Berenguer (Biostatistics Unit-IRB)

10X scRNA-seq, cell composition and age effect analysis carried out by Marta Casado-Peláez and Dr. Elisabetta Mereu (Institut d'Investigació contra la Leucèmia Josep Carreras)

3.1. Bulk RNA-seq analysis

FastQ files were aligned against the mm10 reference genome using STAR 2.5.2b[314] using default options. Unless otherwise specified, all downstream analyses were performed using R 3.5.1. Differentially expressed genes (DEGs) between conditions were determined using

DESeq2 1.22.1[315], using mm10 gene counts as generated with the featureCounts function from the RSubread package version 1.32.4[316] with options: *annot.inbuilt='mm10',allowMultiOverlap=TRUE,countMultiMappingReads=FALSE,minMQS=1,ignoreDup=FALSE).* Genes were selected as DEGs using the thresholds lfcShrink foldChangel>1.25 and Benjamini-Hochberg–determined $P < 0.1$, using experimental batch as covariate. Gene set enrichment analysis was performed using gene set collections at *Mus musculus* gene symbol level. The gene set collections used were: GOBP, GOMF, GOCC, and KEGG, obtained using the org.Mm.eg.db package, November 2014; GOSLIM, obtained from geneontology.org, November 2014; and Broad Hallmarks, obtained from the Broad Institute MSigDB website (https://www.gsea-msigdb.org/gsea/msigdb/) and mapped from human to mouse genes using homology information from Ensembl biomart archive July 2016. Analyses were performed using regularized log transformation (rlog) applied to the count data using the DESeq2 R package 1.22, with ROAST[317] and the MaxMean statistic (http://statweb.stanford.edu/~tibs/GSA/).

3.2. ATAC-seq analysis

N= 4 replicates. The alignment was performed with Bowtie[318], and the aligned read files were pooled for peak calling in multi-sample mode with no control samples using Genrich (https://github.com/jsh58/Genrich). Only peaks with a score >1000 were used, in adults= 25440, and aged=35238. Peaks were annotated to the closest gene, which were 11699 for adult and 13537 for aged.

3.3. ChIP-seq analysis

ChIP-seq of p65 consisted on a pool of 4 replicates per group. BMAL1 ChIP-seq of adult and aged included 4 replicates per condition, and YAP of adult and aged was formed of 3 replicates per condition. BMAL1 ChIP-

Seq of iYAP mice included 2 replicates per condition, and YAP in BMAL1ep cKO mice consisted of 3 replicates per group.

Reads were trimmed, adapters were removed and low-quality reads were dismissed using Trimmomatic[319] (version 0.36; *TRAILING:5 SLIDINGWINDOW:4:15 MINLEN:36*). The reads were then aligned to the mm10 genome with Burrows-Wheeler aligner[320] (version 0.7.12; *-n 2 -l 20 -k 1 -t 2*). Each sample was processed individually and then once the reads were aligned, the .bam files were merged and de-duplicated with SAMtools[321] (version 1.5) and down-sampled to 100 million reads in p65 ChIP-seq, and 60 million reads for the rest ChIP-seq, to obtain a pool of the all replicates per condition. Peaks were called in these pooled files with MACS2 with *-q 0.01 --nomodel --extsize 300 -B –SPMR* parameters. Peaks were then annotated to the closest gene with Homer[322] (version 4.11) and those peaks annotated to non-protein coding genes were not used for further analysis.

For BMAL1 ChIP in adult and aged cells, and p65 ChIPs-seq, peaks with a MACS2 score > 20 were used. For YAP ChIP-seq in adult and aged cells, peaks with a MACS2 score > 200 were used to remove less significant peaks. The following table summarizes the peak information from each ChIP-seq mentioned in this thesis (**Table 1**).

	Peak number	Type of peak used	Peaks annotated to protein-coding genes	Unique protein-coding genes
P65 aged/control IgG	4169	Qval 10^{-2}	3693	2773
P65 aged/anti-IL17A/F	6014	Qval 10^{-2}	5317	3718
P65 adult	8525	Qval 10^{-2}	7584	4910
BMAL1 adult	10070	Qval 10^{-2}	8427	4181
BMAL1 aged	11487	Qval 10^{-2}	9647	4901

YAP adult	5277	Qval 10^{-20}	4452	2803
YAP aged	19266	Qval 10^{-20}	16129	6653
BMAL1 iYAP	6604	Qval 10^{-2}	5886	4144
BMAL1 WT	9414	Qval 10^{-2}	8446	5708
YAP BMAL1ep cKO	4124	Qval 10^{-20}	3573	2557
YAP WT	12521	Qval 10^{-20}	10871	5701

For ChIP-seq and ATAC-seq peak overlap, only perfectly overlapping peaks were used. These were obtained with the bedtools multiIntersectBed function, where bed files of the pooled samples for ATAC-seq and ChIP-seq were used as inputs (**Table 2**).

3.4. Gene ontology (GO) analysis

GO analysis for **10X scRNA-seq** was performed on lists ranked by increasing BH-adjusted *P*-value with g:Profiler[323](https://biit.cs.ut.ee/gprofiler/gost), using the biological processes (BP) database and the option of ranked list. A GO category was considered significant if adj. *P*-value < 0.05. In the aged *vs*. adult comparison, genes with FC>0.35 (log2) were considered. In the aged/anti-IL-17A/F treated *vs*. aged/ IgG control treated, genes with FC>0.25 (log2) were considered.

Table 1. Summary of ChIP-seq pool data. Information of the peak number, threshold of the type of peaks used for further analysis, number of peaks annotated to protein-coding genes and of these, the number of protein-coding genes left after duplicate removal for each ChIP-seq conducted.

	Peak number	Type of peak used	Peaks annotated to protein-coding genes	Unique protein-coding genes
BMAL1- ATAC overlap adult	5322	Perfect overlap of bed files (peaks)	4495	2801
BMAL1-ATAC overlap aged	7692	Perfect overlap of bed files (peaks)	6516	3672

YAP-ATAC overlap adult	3019	Perfect overlap of bed files (peaks)	2559	1702
YAP-ATAC overlap aged	11520	Perfect overlap of bed files (peaks)	9706	4474

Table 2. Summary of ChIP-seq and ATAC-seq data overlap. Information of the peak number, threshold of the type of peaks used for further analysis, number of protein-coding genes to which a peak was annotated and of these genes, how many are left after duplicate removal for each overlap between ChIP-seq and ATAC-seq conducted.

GO analysis for epidermal **bulk RNA-seq** and for the p65 **ChIP-seq** was performed with enrichR[324] (https://maayanlab.cloud/Enrichr/). A category was considered significant if *P*-value < 0.01.

For **ChIP-seq** and **ATAC-seq** overlap of YAP and BMAL1-bound genes, and for the **bulk RNA-seq** of the circadian adult and aged genes, GO analysis was performed with enrichR[324] (https://maayanlab.cloud/Enrichr/) of genes with *P*-val <0.05. A category was considered significant if *P*-val <0.01.

3.5. Statistical analysis

Generally, graphs show individual values and median (depicted as a line) and *P*-values were obtained with the Mann-Whitney *U* test with Prism v9, unless otherwise stated in the figure legend.

3.6. 10X scRNA-seq data pre-processing

Sequences were demultiplexed and aligned according to Cell Ranger pipeline (version 6.0.0) with default parameters. Sequencing reads were mapped against the mouse GRCm38 reference genome to generate feature-barcode matrixes, separately for all CD45+ and CD45 – replicates.

3.7. 10X scRNA-seq quality control (QC) and technical bias corrections

Gene count matrixes were analyzed with Seurat package (version 4.0.4) in R (version 4.0.3)[325]. The replicates were merged, analyzed, and annotated separately for CD45+ and CD45– datasets before their integration. Cells were filtered with more than 10% of mitochondrial gene content and genes not found in at least 5 cells. As part of the quality control, cells situated between the minimum and 1st quartile (according to the distribution of number of genes per cell of each compartment dataset) were removed. To avoid contamination of epithelial cells in the immune compartment, EPCAM+ cells found in CD45+ sorted cells were filtered out.

Additionally, to remove the technical biases that arose after merging the different replicates, we computed the differentially expressed genes (DE) between replicates using the *FindAllMarkers* function. Then, we ensured that the top 500 DE genes between replicates are not present in the highly variable genes (HVGs). Thus, we removed the intersection between the computed DE genes and the HVG.

To evaluate the integration of the different replicates, we used the local inverse Simpson's Index (LISI)[232] (https://github.com/immunogenomics/LISI). This score defines the effective number of samples in the local neighborhood of a cell. Under ideal mixing, we would expect to obtain LISI scores equal to the number of different replicates in our datasets. This indicates that the neighborhoods are well represented by all samples and that the cell types/states that we have previously identified exhibit a good mixing across all replicates.

Additionally, we have assessed the performance of the replicate integration by qualitatively inspecting the UMAPs. We have checked that all cell types and states are well represented by each replicate and that

our dataset does not contain any technical cluster entirely driven by replicate effect.

3.8. 10X scRNA-seq clustering

Cell-to-cell variations were normalized by the expression values using a scale factor of 100,000 and a log transformation. The gene expression measurements were scaled and centered. The scaled Z-score values were then used as normalized gene measurement input for clustering and for visualizing differences in expression between cell clusters. HVGs were selected by assessing the relationship of log(variance) and log(mean) and choosing those with highest variance-to-mean ratio. Principal components analysis (PCA) was used to reduce the dimensionality of the dataset, and *ElbowGraph* was used to select the number of dimensions for the clustering for significant principal components. Cluster identification was performed using the functions *FindNeighbors* and *FindClusters*, which calculates the k-nearest neighbors and generates the shared nearest neighbor (SNN) graph to cluster the cells. The algorithm applied was the Louvain method, which allows the number of clusters to be tuned with a resolution parameter. To explore the clusters in more detail, the resolution parameter was increased in *FindClusters* function or *FindSubCluster* was used for specific clusters. The Uniform Manifold Approximation and Projection (UMAP) was used as a non-dimensional reduction method, to visualize the clustering.

3.9. Cell type annotation

To annotate the cell types and states, enriched genes were first identified in each of the clusters using *FindAllMarkers* function, using the Wilcoxon Rank Sum test to find cluster-specific markers. These cluster-specific genes were then explored to find previously reported cell population marker genes. Some examples of marker genes used to annotate the cell

populations are given here: Cd4+ T cells: *Cd28, Cd4;* Cd8+ T cells: *Cd8a, Cd8b1;* dermal cells (DC): *Cd207;* fibroblast_1: *Crabp1, Inhba, Notum;* fibroblast_2: *Col1a1, Col1a2, Cd34, Robo1, Col3a1*; fibroblast_3: *Efemp1, Il1r2, Ccl11*; fibroblast_4: *Col11a1, Aspn, Coch;* fibroblast_5: *Myoc, Dcn; ILC: Il13, Kit*; lymphatic endothelial cells (ECs): *Lyve1, Hes1;* macrophage_1: *Il1b*; macrophage_2: *Tnfsf9*; macrophage_3: *Ear2, Cd163;* monocyte_1: *Plac8, Cd14;* monocyte_2: *Ccl8, C1qa*; monocyte_3*: Retnla, C1qb, Ccr2;* NK cells: *Gzmc, Ccl5, Nkg7;* pericytes: *Acta2, Rgs5;* proliferating macrophages: *Mki67;* proliferating T cells: *Hmgb2proliferating T cell;* Schwann cells: *Cryab, Plekha4, Scn7a;* Schwann cells_1: *Kcna1;* Schwann cells_2: *Sox10*; T regulatory cells*: Foxp3;* VEC arterioles and capillary: *Ptprb, Flt1;* VEC venules: *Aqp1, Sele, Pecam1*; and γδ T cells: *Trdc, Tcrg-C1.*

3.10. Differential expression (DE) analysis for each cluster

To find differentially expressed genes between adult vs. aged, and aged/control IgG treated vs. aged/anti-IL-17A/F treated, in the different annotated cell type populations, DE analysis was performed between conditions for each cluster with *FindMarkers* function. To control for multiple comparisons, we used the FDR Benjamini and Hochberg (BH) method.

3.11. Cell composition analysis

To evaluate the significance of the differences in cell type abundance between conditions we applied *sccomp*[234], a tool designed for differential composition and variability analyses that relies on sum-constrained independent Beta-binomial distributions. This model uses mean-variability association, which allows to model the compositional properties of the data, while enabling the exclusion of outliers. We assessed significant differences (FDR<0.025) for composition and/or

group-specific variability in each cell type population, comparing adult vs. aged conditions and aged/control IgG treated vs. aged/anti-IL-17A/F treated.

3.12. Age-effect analysis

The effects of aging on dermis were evaluated based on how cell types differ transcriptionally between adult and aged mice. For this, the similarities of cell type-specific markers were evaluated by comparing the Jaccard Indexes between age groups across cell types. The Jaccard Index was computed using MatchScore2, which considers the top 100 DE markers as a signature of each population[326].

To further assess the age-related effects among the immune cells, a deep-learning approach was created that is based on auto-encoders. During training, this method can identify features that are relevant for the data structure and then use them to predict the different cell types in a test dataset. To generate the model, adult data was divided into two smaller subsets that could be used as training and test sets. The model displayed high probability scores ($P > 0.5$) in the prediction of cell types from the test set among the different immune cell types and a low rate of unpredicted cells (unclassified rate < 5%). If the rate of unclassified cell type was strictly biased for aged cells, this would reflect the effect of aging on the cell phenotype. Based on this assumption, an age deviance score was defined as 1-q, whereby q is the probability of the unpredicted cell being in the true corresponding cell type class in aged cells. The proportion of unclassified cells within each cell type in aged cells, and the proportion of age-affected cells, were then measured and normalized by the model's error rate (e.g., by subtracting the cell proportion in each adult cell type that could not be predicted by the model).

3.13. Jonckheere-Terpstra-Kendall (JTK) analysis

Analyses were conducted as described in publication[267]. N=4 biological replicates per timepoint and condition. JTK_Cycle is a non-parametric algorithm, and was used to detect the oscillatory behavior of genes when analyzing data from 6 different times of the day (0, 4, 8, 12, 16, 20) after turning on the lights. Genes considered circadian for further analysis had an adjusted *P*-val <0.05.

3.14. Overlapping regions analysis

Analysis of overlapping regions between YAP and BMAL1 was done using the RegioneR software as shown in its corresponding publication[268]. For BMAL1 ChIP-seq data peaks, Q-value of 1^{-3}, and for YAP ChIP-seq peaks, q value of 1^{-20} was used for the comparison. All peaks of both conditions were used for the analysis.

3.15. Distance between YAP and BMAL1 binding sites

The distribution of distances between YAP and BMAL1 binding in overlapping peaks was done comparing the TEAD3 motifs described in the HOMER software (http://homer.ucsd.edu/homer/), and Ahr::Arnt sites in the JASPAR software (https://jaspar.genereg.net). Only overlapping peaks between both ChIP-seq groups were used for the analysis.

3.16. Data availability

RNA-seq data of the is deposited at the NCBI GEO repository, accessions GSE190182

(https://www.ncbi.nlm.nih.gov/geo/query/acc.cgi?acc=GSE190182 token uheliwakztwhzat) and GSE190393

(https://www.ncbi.nlm.nih.gov/geo/query/acc.cgi?acc=GSE190393 token cvsfaicsvfufdcf) for the epidermal bulk RNA-seq and GSE193920

(https://www.ncbi.nlm.nih.gov/geo/query/acc.cgi?acc=GSE193920 token yzwpkkuqzhqlxwp) for the SC RNA-seq data.

ChIP-seq data is deposited at the NCBI GEO repository, accession GSE213732 (https://www.ncbi.nlm.nih.gov/geo/query/acc.cgi?acc=GSE213732 token ujctsmuodzkfruh).

Sc-RNA-seq analysis scripts are in https://github.com/mereulab/IL17-SkinAging.

References

1 Solanas, G. & Benitah, S. A. Regenerating the skin: a task for the heterogeneous stem cell pool and surrounding niche. *Nat Rev Mol Cell Biol* **14**, 737-748, doi:10.1038/nrm3675 (2013).

2 Schepeler, T., Page, M. E. & Jensen, K. B. Heterogeneity and plasticity of epidermal stem cells. *Development* **141**, 2559-2567, doi:10.1242/dev.104588 (2014).

3 Rognoni, E. & Watt, F. M. Skin Cell Heterogeneity in Development, Wound Healing, and Cancer. *Trends Cell Biol* **28**, 709-722, doi:10.1016/j.tcb.2018.05.002 (2018).

4 Watt, F. M. Mammalian skin cell biology: at the interface between laboratory and clinic. *Science* **346**, 937-940, doi:10.1126/science.1253734 (2014).

5 Woo, S. H., Stumpfova, M., Jensen, U. B., Lumpkin, E. A. & Owens, D. M. Identification of epidermal progenitors for the Merkel cell lineage. *Development* **137**, 3965-3971, doi:10.1242/dev.055970 (2010).

6 Nishimura, E. K. Melanocyte stem cells: a melanocyte reservoir in hair follicles for hair and skin pigmentation. *Pigment Cell Melanoma Res* **24**, 401-410, doi:10.1111/j.1755-148X.2011.00855.x (2011).

7 West, H. C. & Bennett, C. L. Redefining the Role of Langerhans Cells As Immune Regulators within the Skin. *Front Immunol* **8**, 1941, doi:10.3389/fimmu.2017.01941 (2017).

8 Sola, P. & Zinna, V. M. Isolation and Sorting of Epidermal Interfollicular Stem Cells for the Study of Circadian Rhythms. *Methods Mol Biol* **2482**, 243-253, doi:10.1007/978-1-0716-2249-0_16 (2022).

9 Blanpain, C., Horsley, V. & Fuchs, E. Epithelial stem cells: turning over new leaves. *Cell* **128**, 445-458, doi:10.1016/j.cell.2007.01.014 (2007).

10 Blanpain, C. & Fuchs, E. Epidermal homeostasis: a balancing act of stem cells in the skin. *Nat Rev Mol Cell Biol* **10**, 207-217, doi:10.1038/nrm2636 (2009).

11 Martino, P. A., Heitman, N. & Rendl, M. The dermal sheath: An emerging component of the hair follicle stem cell niche. *Exp Dermatol* **30**, 512-521, doi:10.1111/exd.14204 (2021).

12 Morris, R. J. *et al.* Capturing and profiling adult hair follicle stem cells. *Nat Biotechnol* **22**, 411-417, doi:10.1038/nbt950 (2004).

13 Blanpain, C., Lowry, W. E., Geoghegan, A., Polak, L. & Fuchs, E. Self-renewal, multipotency, and the existence of two cell populations within an epithelial stem cell niche. *Cell* **118**, 635-648, doi:10.1016/j.cell.2004.08.012 (2004).

14 Driskell, R. R., Clavel, C., Rendl, M. & Watt, F. M. Hair follicle dermal papilla cells at a glance. *J Cell Sci* **124**, 1179-1182, doi:10.1242/jcs.082446 (2011).

15 Rompolas, P. & Greco, V. Stem cell dynamics in the hair follicle niche. *Semin Cell Dev Biol* **25-26**, 34-42, doi:10.1016/j.semcdb.2013.12.005 (2014).

16 Muller-Rover, S. *et al.* A comprehensive guide for the accurate classification of murine hair follicles in distinct hair cycle stages. *J Invest Dermatol* **117**, 3-15, doi:10.1046/j.0022-202x.2001.01377.x (2001).

17 Plikus, M. V. *et al.* Cyclic dermal BMP signalling regulates stem cell activation during hair regeneration. *Nature* **451**, 340-344, doi:10.1038/nature06457 (2008).

18 Stenn, K. S. & Paus, R. Controls of hair follicle cycling. *Physiol Rev* **81**, 449-494, doi:10.1152/physrev.2001.81.1.449 (2001).

19 Greco, V. *et al.* A two-step mechanism for stem cell activation during hair regeneration. *Cell Stem Cell* **4**, 155-169, doi:10.1016/j.stem.2008.12.009 (2009).

20 Paus, R. & Cotsarelis, G. The biology of hair follicles. *N Engl J Med* **341**, 491-497, doi:10.1056/NEJM199908123410706 (1999).

21 Rompolas, P. *et al.* Live imaging of stem cell and progeny behaviour in physiological hair-follicle regeneration. *Nature* **487**, 496-499, doi:10.1038/nature11218 (2012).

22 Joost, S. *et al.* The Molecular Anatomy of Mouse Skin during Hair Growth and Rest. *Cell Stem Cell* **26**, 441-457 e447, doi:10.1016/j.stem.2020.01.012 (2020).

23 Fuchs, E. Scratching the surface of skin development. *Nature* **445**, 834-842, doi:10.1038/nature05659 (2007).

24 Schneider, M. R., Schmidt-Ullrich, R. & Paus, R. The hair follicle as a dynamic miniorgan. *Curr Biol* **19**, R132-142, doi:10.1016/j.cub.2008.12.005 (2009).

25 Ito, M. *et al.* Stem cells in the hair follicle bulge contribute to wound repair but not to homeostasis of the epidermis. *Nat Med* **11**, 1351-1354, doi:10.1038/nm1328 (2005).

26 Tumbar, T. *et al.* Defining the epithelial stem cell niche in skin. *Science* **303**, 359-363, doi:10.1126/science.1092436 (2004).

27 Lynch, M. D. & Watt, F. M. Fibroblast heterogeneity: implications for human disease. *J Clin Invest* **128**, 26-35, doi:10.1172/JCI93555 (2018).

28 Sorrell, J. M. & Caplan, A. I. Fibroblast heterogeneity: more than skin deep. *J Cell Sci* **117**, 667-675, doi:10.1242/jcs.01005 (2004).

29 Ganier, C., Rognoni, E., Goss, G., Lynch, M. & Watt, F. M. Fibroblast Heterogeneity in Healthy and Wounded Skin. *Cold Spring Harb Perspect Biol*, doi:10.1101/cshperspect.a041238 (2022).

30 Plikus, M. V. *et al.* Fibroblasts: Origins, definitions, and functions in health and disease. *Cell* **184**, 3852-3872, doi:10.1016/j.cell.2021.06.024 (2021).

31 Biggs, L. C., Kim, C. S., Miroshnikova, Y. A. & Wickstrom, S. A. Mechanical Forces in the Skin: Roles in Tissue Architecture, Stability, and Function. *J Invest Dermatol* **140**, 284-290, doi:10.1016/j.jid.2019.06.137 (2020).

32 Wickstrom, S. A., Radovanac, K. & Fassler, R. Genetic analyses of integrin signaling. *Cold Spring Harb Perspect Biol* **3**, doi:10.1101/cshperspect.a005116 (2011).

33 Pfisterer, K., Shaw, L. E., Symmank, D. & Weninger, W. The Extracellular Matrix in Skin Inflammation and Infection. *Front Cell Dev Biol* **9**, 682414, doi:10.3389/fcell.2021.682414 (2021).

34 Nystrom, A. & Bruckner-Tuderman, L. Matrix molecules and skin biology. *Semin Cell Dev Biol* **89**, 136-146, doi:10.1016/j.semcdb.2018.07.025 (2019).

35 Legate, K. R., Wickstrom, S. A. & Fassler, R. Genetic and cell biological analysis of integrin outside-in signaling. *Genes Dev* **23**, 397-418, doi:10.1101/gad.1758709 (2009).

36 Shaw, T. J. & Rognoni, E. Dissecting Fibroblast Heterogeneity in Health and Fibrotic Disease. *Curr Rheumatol Rep* **22**, 33, doi:10.1007/s11926-020-00903-w (2020).

37 Jiang, D. *et al.* Two succeeding fibroblastic lineages drive dermal development and the transition from regeneration to scarring. *Nat Cell Biol* **20**, 422-431, doi:10.1038/s41556-018-0073-8 (2018).

38 Phan, Q. M., Sinha, S., Biernaskie, J. & Driskell, R. R. Single-cell transcriptomic analysis of small and large wounds reveals the distinct spatial organization of regenerative fibroblasts. *Exp Dermatol* **30**, 92-101, doi:10.1111/exd.14244 (2021).

39 Abbasi, S. *et al.* Distinct Regulatory Programs Control the Latent Regenerative Potential of Dermal Fibroblasts during Wound Healing. *Cell Stem Cell* **28**, 581-583, doi:10.1016/j.stem.2021.02.004 (2021).

40 Talbott, H. E., Mascharak, S., Griffin, M., Wan, D. C. & Longaker, M. T. Wound healing, fibroblast heterogeneity, and fibrosis. *Cell Stem Cell* **29**, 1161-1180, doi:10.1016/j.stem.2022.07.006 (2022).

41 Driskell, R. R. *et al.* Distinct fibroblast lineages determine dermal architecture in skin development and repair. *Nature* **504**, 277-281, doi:10.1038/nature12783 (2013).

42 Driskell, R. R. & Watt, F. M. Understanding fibroblast heterogeneity in the skin. *Trends Cell Biol* **25**, 92-99, doi:10.1016/j.tcb.2014.10.001 (2015).

43 Rinkevich, Y. *et al.* Skin fibrosis. Identification and isolation of a dermal lineage with intrinsic fibrogenic potential. *Science* **348**, aaa2151, doi:10.1126/science.aaa2151 (2015).

44 Shook, B. A. *et al.* Dermal Adipocyte Lipolysis and Myofibroblast Conversion Are Required for Efficient Skin Repair. *Cell Stem Cell* **26**, 880-895 e886, doi:10.1016/j.stem.2020.03.013 (2020).

45 Nguyen, A. V. & Soulika, A. M. The Dynamics of the Skin's Immune System. *Int J Mol Sci* **20**, doi:10.3390/ijms20081811 (2019).

46 Naik, S. *et al.* Commensal-dendritic-cell interaction specifies a unique protective skin immune signature. *Nature* **520**, 104-108, doi:10.1038/nature14052 (2015).

47 Pasparakis, M., Haase, I. & Nestle, F. O. Mechanisms regulating skin immunity and inflammation. *Nat Rev Immunol* **14**, 289-301, doi:10.1038/nri3646 (2014).

48 Nahrendorf, M. & Swirski, F. K. Abandoning M1/M2 for a Network Model of Macrophage Function. *Circ Res* **119**, 414-417, doi:10.1161/CIRCRESAHA.116.309194 (2016).

49 Jakubzick, C. *et al.* Minimal differentiation of classical monocytes as they survey steady-state tissues and transport antigen to lymph nodes. *Immunity* **39**, 599-610, doi:10.1016/j.immuni.2013.08.007 (2013).

50 Guilliams, M., Mildner, A. & Yona, S. Developmental and Functional Heterogeneity of Monocytes. *Immunity* **49**, 595-613, doi:10.1016/j.immuni.2018.10.005 (2018).

51 Liu, C., Liu, Z., Li, Z. & Wu, Y. Molecular regulation of mast cell development and maturation. *Mol Biol Rep* **37**, 1993-2001, doi:10.1007/s11033-009-9650-z (2010).

52 Kabashima, K., Honda, T., Ginhoux, F. & Egawa, G. The immunological anatomy of the skin. *Nat Rev Immunol* **19**, 19-30, doi:10.1038/s41577-018-0084-5 (2019).

53 Niec, R. E., Rudensky, A. Y. & Fuchs, E. Inflammatory adaptation in barrier tissues. *Cell* **184**, 3361-3375, doi:10.1016/j.cell.2021.05.036 (2021).

54 Gebhardt, T. *et al.* Memory T cells in nonlymphoid tissue that provide enhanced local immunity during infection with herpes simplex virus. *Nat Immunol* **10**, 524-530, doi:10.1038/ni.1718 (2009).

55 Korn, T., Bettelli, E., Oukka, M. & Kuchroo, V. K. IL-17 and Th17 Cells. *Annu Rev Immunol* **27**, 485-517, doi:10.1146/annurev.immunol.021908.132710 (2009).

56 Bettelli, E., Korn, T. & Kuchroo, V. K. Th17: the third member of the effector T cell trilogy. *Curr Opin Immunol* **19**, 652-657, doi:10.1016/j.coi.2007.07.020 (2007).

57 Noack, M. & Miossec, P. Th17 and regulatory T cell balance in autoimmune and inflammatory diseases. *Autoimmun Rev* **13**, 668-677, doi:10.1016/j.autrev.2013.12.004 (2014).

58 Mathur, A. N. *et al.* Stat3 and Stat4 direct development of IL-17-secreting Th cells. *J Immunol* **178**, 4901-4907, doi:10.4049/jimmunol.178.8.4901 (2007).

59 Naik, S., Larsen, S. B., Cowley, C. J. & Fuchs, E. Two to Tango: Dialog between Immunity and Stem Cells in Health and Disease. *Cell* **175**, 908-920, doi:10.1016/j.cell.2018.08.071 (2018).

60 Arpaia, N. *et al.* A Distinct Function of Regulatory T Cells in Tissue Protection. *Cell* **162**, 1078-1089, doi:10.1016/j.cell.2015.08.021 (2015).

61 Ribot, J. C., Lopes, N. & Silva-Santos, B. gammadelta T cells in tissue physiology and surveillance. *Nat Rev Immunol* **21**, 221-232, doi:10.1038/s41577-020-00452-4 (2021).

62 Cai, Y. *et al.* Pivotal role of dermal IL-17-producing gammadelta T cells in skin inflammation. *Immunity* **35**, 596-610, doi:10.1016/j.immuni.2011.08.001 (2011).

63 McKenzie, D. R., Comerford, I., Silva-Santos, B. & McColl, S. R. The Emerging Complexity of gammadeltaT17 Cells. *Front Immunol* **9**, 796, doi:10.3389/fimmu.2018.00796 (2018).

64 Papotto, P. H., Ribot, J. C. & Silva-Santos, B. IL-17(+) gammadelta T cells as kick-starters of inflammation. *Nat Immunol* **18**, 604-611, doi:10.1038/ni.3726 (2017).

65 Kobayashi, T., Ricardo-Gonzalez, R. R. & Moro, K. Skin-Resident Innate Lymphoid Cells - Cutaneous Innate Guardians and Regulators. *Trends Immunol* **41**, 100-112, doi:10.1016/j.it.2019.12.004 (2020).

66 von Bubnoff, D. *et al.* Natural killer cells in atopic and autoimmune diseases of the skin. *J Allergy Clin Immunol* **125**, 60-68, doi:10.1016/j.jaci.2009.11.020 (2010).

67 McKee, S. J., Mattarollo, S. R. & Leggatt, G. R. Immunosuppressive roles of natural killer T (NKT) cells in the skin. *J Leukoc Biol* **96**, 49-54, doi:10.1189/jlb.4RU0114-001R (2014).

68 dela Paz, N. G. & D'Amore, P. A. Arterial versus venous endothelial cells. *Cell Tissue Res* **335**, 5-16, doi:10.1007/s00441-008-0706-5 (2009).

69 Pasut, A., Becker, L. M., Cuypers, A. & Carmeliet, P. Endothelial cell plasticity at the single-cell level. *Angiogenesis* **24**, 311-326, doi:10.1007/s10456-021-09797-3 (2021).

70 Huggenberger, R. & Detmar, M. The cutaneous vascular system in chronic skin inflammation. *J Investig Dermatol Symp Proc* **15**, 24-32, doi:10.1038/jidsymp.2011.5 (2011).

71 Li, K. N. *et al.* Skin vasculature and hair follicle cross-talking associated with stem cell activation and tissue homeostasis. *Elife* **8**, doi:10.7554/eLife.45977 (2019).

72 Gur-Cohen, S. *et al.* Stem cell-driven lymphatic remodeling coordinates tissue regeneration. *Science* **366**, 1218-1225, doi:10.1126/science.aay4509 (2019).

73 Al-Soudi, A., Kaaij, M. H. & Tas, S. W. Endothelial cells: From innocent bystanders to active participants in immune responses. *Autoimmun Rev* **16**, 951-962, doi:10.1016/j.autrev.2017.07.008 (2017).

74 Pober, J. S. & Sessa, W. C. Evolving functions of endothelial cells in inflammation. *Nat Rev Immunol* **7**, 803-815, doi:10.1038/nri2171 (2007).

75 Reynolds, G. *et al.* Developmental cell programs are co-opted in inflammatory skin disease. *Science* **371**, doi:10.1126/science.aba6500 (2021).

76 Abtin, A. *et al.* Perivascular macrophages mediate neutrophil recruitment during bacterial skin infection. *Nat Immunol* **15**, 45-53, doi:10.1038/ni.2769 (2014).

77 Natsuaki, Y. *et al.* Perivascular leukocyte clusters are essential for efficient activation of effector T cells in the skin. *Nat Immunol* **15**, 1064-1069, doi:10.1038/ni.2992 (2014).

78 Kogame, T. *et al.* Possible inducible skin-associated lymphoid tissue (iSALT)-like structures with CXCL13(+) fibroblast-like cells in secondary syphilis. *Br J Dermatol* **177**, 1737-1739, doi:10.1111/bjd.15349 (2017).

79 Honda, T., Egawa, G. & Kabashima, K. Antigen presentation and adaptive immune responses in skin. *Int Immunol* **31**, 423-429, doi:10.1093/intimm/dxz005 (2019).

80 Duraes, F. V. *et al.* Role of major histocompatibility complex class II expression by non-hematopoietic cells in autoimmune and inflammatory disorders: facts and fiction. *Tissue Antigens* **82**, 1-15, doi:10.1111/tan.12136 (2013).

81 Lim, W. C., Olding, M., Healy, E. & Millar, T. M. Human Endothelial Cells Modulate CD4(+) T Cell Populations and Enhance Regulatory T Cell Suppressive Capacity. *Front Immunol* **9**, 565, doi:10.3389/fimmu.2018.00565 (2018).

82 Abrahimi, P. *et al.* Blocking MHC class II on human endothelium mitigates acute rejection. *JCI Insight* **1**, doi:10.1172/jci.insight.85293 (2016).

83 Turesson, C. Endothelial expression of MHC class II molecules in autoimmune disease. *Curr Pharm Des* **10**, 129-143, doi:10.2174/1381612043453414 (2004).

84 Mai, J., Virtue, A., Shen, J., Wang, H. & Yang, X. F. An evolving new paradigm: endothelial cells--conditional innate immune cells. *J Hematol Oncol* **6**, 61, doi:10.1186/1756-8722-6-61 (2013).

85 Bray, E. R., Cheret, J., Yosipovitch, G. & Paus, R. Schwann cells as underestimated, major players in human skin physiology and pathology. *Exp Dermatol* **29**, 93-101, doi:10.1111/exd.14060 (2020).

86 Abdo, H. *et al.* Specialized cutaneous Schwann cells initiate pain sensation. *Science* **365**, 695-699, doi:10.1126/science.aax6452 (2019).

87 Parfejevs, V. *et al.* Injury-activated glial cells promote wound healing of the adult skin in mice. *Nat Commun* **9**, 236, doi:10.1038/s41467-017-01488-2 (2018).

88 Carr, M. J. & Johnston, A. P. Schwann cells as drivers of tissue repair and regeneration. *Curr Opin Neurobiol* **47**, 52-57, doi:10.1016/j.conb.2017.09.003 (2017).

89 Weddell, G., Cowan, M. A., Palmer, E. & Ramaswamy, S. Psoriatic Skin. *Arch Dermatol* **91**, 252-266, doi:10.1001/archderm.1965.01600090060012 (1965).

90 Watt, F. M. & Fujiwara, H. Cell-extracellular matrix interactions in normal and diseased skin. *Cold Spring Harb Perspect Biol* **3**, doi:10.1101/cshperspect.a005124 (2011).

91 Liu, T. *et al.* The IL-23/IL-17 Pathway in Inflammatory Skin Diseases: From Bench to Bedside. *Front Immunol* **11**, 594735, doi:10.3389/fimmu.2020.594735 (2020).

92 Amatya, N., Garg, A. V. & Gaffen, S. L. IL-17 Signaling: The Yin and the Yang. *Trends Immunol* **38**, 310-322, doi:10.1016/j.it.2017.01.006 (2017).

93 Su, Y. *et al.* Interleukin-17 receptor D constitutes an alternative receptor for interleukin-17A important in psoriasis-like skin inflammation. *Sci Immunol* **4**, doi:10.1126/sciimmunol.aau9657 (2019).

94 McGeachy, M. J., Cua, D. J. & Gaffen, S. L. The IL-17 Family of Cytokines in Health and Disease. *Immunity* **50**, 892-906, doi:10.1016/j.immuni.2019.03.021 (2019).

95 Schwandner, R., Yamaguchi, K. & Cao, Z. Requirement of tumor necrosis factor receptor-associated factor (TRAF)6 in interleukin 17 signal transduction. *J Exp Med* **191**, 1233-1240, doi:10.1084/jem.191.7.1233 (2000).

96 Giridharan, S. & Srinivasan, M. Mechanisms of NF-kappaB p65 and strategies for therapeutic manipulation. *J Inflamm Res* **11**, 407-419, doi:10.2147/JIR.S140188 (2018).

97 Kawasaki, T. & Kawai, T. Toll-like receptor signaling pathways. *Front Immunol* **5**, 461, doi:10.3389/fimmu.2014.00461 (2014).

98 Mills, K. H. G. IL-17 and IL-17-producing cells in protection versus pathology. *Nat Rev Immunol*, doi:10.1038/s41577-022-00746-9 (2022).

99 Konieczny, P. *et al.* Interleukin-17 governs hypoxic adaptation of injured epithelium. *Science* **377**, eabg9302, doi:10.1126/science.abg9302 (2022).

100 Veldhoen, M. Interleukin 17 is a chief orchestrator of immunity. *Nat Immunol* **18**, 612-621, doi:10.1038/ni.3742 (2017).

101 Veldhoen, M., Hocking, R. J., Flavell, R. A. & Stockinger, B. Signals mediated by transforming growth factor-beta initiate autoimmune encephalomyelitis, but chronic inflammation is needed to sustain disease. *Nat Immunol* **7**, 1151-1156, doi:10.1038/ni1391 (2006).

102 Brembilla, N. C., Senra, L. & Boehncke, W. H. The IL-17 Family of Cytokines in Psoriasis: IL-17A and Beyond. *Front Immunol* **9**, 1682, doi:10.3389/fimmu.2018.01682 (2018).

103 Warren, R. B. *et al.* Bimekizumab versus Adalimumab in Plaque Psoriasis. *N Engl J Med* **385**, 130-141, doi:10.1056/NEJMoa2102388 (2021).

104 Blauvelt, A. *et al.* Bimekizumab for patients with moderate to severe plaque psoriasis: 60-week results from BE ABLE 2, a randomized, double-blinded, placebo-controlled, phase 2b extension study. *J Am Acad Dermatol* **83**, 1367-1374, doi:10.1016/j.jaad.2020.05.105 (2020).

105 Flatt, T. A new definition of aging? *Front Genet* **3**, 148, doi:10.3389/fgene.2012.00148 (2012).

106 Lopez-Otin, C., Blasco, M. A., Partridge, L., Serrano, M. & Kroemer, G. The hallmarks of aging. *Cell* **153**, 1194-1217, doi:10.1016/j.cell.2013.05.039 (2013).

107 da Silva, P. F. L. & Schumacher, B. Principles of the Molecular and Cellular Mechanisms of Aging. *J Invest Dermatol* **141**, 951-960, doi:10.1016/j.jid.2020.11.018 (2021).

108 López-Otín, C., Blasco, M. A., Partridge, L., Serrano, M. & Kroemer, G. Hallmarks of aging: An expanding universe. *Cell*, doi:10.1016/j.cell.2022.11.001 (2023).

109 Farage, M. A., Miller, K. W., Elsner, P. & Maibach, H. I. Intrinsic and extrinsic factors in skin ageing: a review. *Int J Cosmet Sci* **30**, 87-95, doi:10.1111/j.1468-2494.2007.00415.x (2008).

110 Persa, O. D., Koester, J. & Niessen, C. M. Regulation of Cell Polarity and Tissue Architecture in Epidermal Aging and Cancer. *J Invest Dermatol* **141**, 1017-1023, doi:10.1016/j.jid.2020.12.012 (2021).

111 Liu, N. *et al.* Stem cell competition orchestrates skin homeostasis and ageing. *Nature* **568**, 344-350, doi:10.1038/s41586-019-1085-7 (2019).

112 Solanas, G. *et al.* Aged Stem Cells Reprogram Their Daily Rhythmic Functions to Adapt to Stress. *Cell* **170**, 678-692 e620, doi:10.1016/j.cell.2017.07.035 (2017).

113 Koester, J. *et al.* Niche stiffening compromises hair follicle stem cell potential during ageing by reducing bivalent promoter accessibility. *Nat Cell Biol* **23**, 771-781, doi:10.1038/s41556-021-00705-x (2021).

114 Doles, J., Storer, M., Cozzuto, L., Roma, G. & Keyes, W. M. Age-associated inflammation inhibits epidermal stem cell function. *Genes Dev* **26**, 2144-2153, doi:10.1101/gad.192294.112 (2012).

115 Walko, G., Castanon, M. J. & Wiche, G. Molecular architecture and function of the hemidesmosome. *Cell Tissue Res* **360**, 529-544, doi:10.1007/s00441-015-2216-6 (2015).

116 Giangreco, A., Qin, M., Pintar, J. E. & Watt, F. M. Epidermal stem cells are retained in vivo throughout skin aging. *Aging Cell* **7**, 250-259, doi:10.1111/j.1474-9726.2008.00372.x (2008).

117 Choi, E. H. Aging of the skin barrier. *Clin Dermatol* **37**, 336-345, doi:10.1016/j.clindermatol.2019.04.009 (2019).

118 Ghadially, R., Brown, B. E., Sequeira-Martin, S. M., Feingold, K. R. & Elias, P. M. The aged epidermal permeability barrier. Structural, functional, and lipid biochemical abnormalities in humans and a senescent murine model. *J Clin Invest* **95**, 2281-2290, doi:10.1172/JCI117919 (1995).

119 Ghadially, R. *et al.* Decreased epidermal lipid synthesis accounts for altered barrier function in aged mice. *J Invest Dermatol* **106**, 1064-1069, doi:10.1111/1523-1747.ep12338692 (1996).

120 Wang, Z., Man, M. Q., Li, T., Elias, P. M. & Mauro, T. M. Aging-associated alterations in epidermal function and their clinical

significance. *Aging (Albany NY)* **12**, 5551-5565, doi:10.18632/aging.102946 (2020).

121 Gregorio, J. *et al.* Plasmacytoid dendritic cells sense skin injury and promote wound healing through type I interferons. *J Exp Med* **207**, 2921-2930, doi:10.1084/jem.20101102 (2010).

122 Mathur, A. N. *et al.* Treg-Cell Control of a CXCL5-IL-17 Inflammatory Axis Promotes Hair-Follicle-Stem-Cell Differentiation During Skin-Barrier Repair. *Immunity* **50**, 655-667 e654, doi:10.1016/j.immuni.2019.02.013 (2019).

123 Uberoi, A. *et al.* Commensal microbiota regulates skin barrier function and repair via signaling through the aryl hydrocarbon receptor. *Cell Host Microbe* **29**, 1235-1248 e1238, doi:10.1016/j.chom.2021.05.011 (2021).

124 Eming, S. A., Martin, P. & Tomic-Canic, M. Wound repair and regeneration: mechanisms, signaling, and translation. *Sci Transl Med* **6**, 265sr266, doi:10.1126/scitranslmed.3009337 (2014).

125 Gurtner, G. C., Werner, S., Barrandon, Y. & Longaker, M. T. Wound repair and regeneration. *Nature* **453**, 314-321, doi:10.1038/nature07039 (2008).

126 Hsu, Y. C., Li, L. & Fuchs, E. Emerging interactions between skin stem cells and their niches. *Nat Med* **20**, 847-856, doi:10.1038/nm.3643 (2014).

127 Eming, S. A., Krieg, T. & Davidson, J. M. Inflammation in wound repair: molecular and cellular mechanisms. *J Invest Dermatol* **127**, 514-525, doi:10.1038/sj.jid.5700701 (2007).

128 Pastar, I. *et al.* Epithelialization in Wound Healing: A Comprehensive Review. *Adv Wound Care (New Rochelle)* **3**, 445-464, doi:10.1089/wound.2013.0473 (2014).

129 Gould, L. *et al.* Chronic wound repair and healing in older adults: current status and future research. *J Am Geriatr Soc* **63**, 427-438, doi:10.1111/jgs.13332 (2015).

130 Keyes, B. E. *et al.* Impaired Epidermal to Dendritic T Cell Signaling Slows Wound Repair in Aged Skin. *Cell* **167**, 1323-1338 e1314, doi:10.1016/j.cell.2016.10.052 (2016).

131 Mahmoudi, S. *et al.* Heterogeneity in old fibroblasts is linked to variability in reprogramming and wound healing. *Nature* **574**, 553-558, doi:10.1038/s41586-019-1658-5 (2019).

132 Ding, X., Kakanj, P., Leptin, M. & Eming, S. A. Regulation of the Wound Healing Response during Aging. *J Invest Dermatol* **141**, 1063-1070, doi:10.1016/j.jid.2020.11.014 (2021).

133 Stojadinovic, O. *et al.* Molecular pathogenesis of chronic wounds: the role of beta-catenin and c-myc in the inhibition of epithelialization and wound healing. *Am J Pathol* **167**, 59-69, doi:10.1016/s0002-9440(10)62953-7 (2005).

134 Matsumura, H. *et al.* Hair follicle aging is driven by transepidermal elimination of stem cells via COL17A1 proteolysis. *Science* **351**, aad4395, doi:10.1126/science.aad4395 (2016).

135 Matsumura, H. *et al.* Distinct types of stem cell divisions determine organ regeneration and aging in hair follicles. *Nature Aging* **1**, 190-204, doi:10.1038/s43587-021-00033-7 (2021).

136 Ge, Y. *et al.* The aging skin microenvironment dictates stem cell behavior. *Proc Natl Acad Sci U S A* **117**, 5339-5350, doi:10.1073/pnas.1901720117 (2020).

137 Zhang, C. *et al.* Escape of hair follicle stem cells causes stem cell exhaustion during aging. *Nature Aging* **1**, 889-903, doi:10.1038/s43587-021-00103-w (2021).

138 Chen, C. C. *et al.* Regenerative hair waves in aging mice and extra-follicular modulators follistatin, dkk1, and sfrp4. *J Invest Dermatol* **134**, 2086-2096, doi:10.1038/jid.2014.139 (2014).

139 Tigges, J. *et al.* The hallmarks of fibroblast ageing. *Mech Ageing Dev* **138**, 26-44, doi:10.1016/j.mad.2014.03.004 (2014).

140 Zou, Z. *et al.* A Single-Cell Transcriptomic Atlas of Human Skin Aging. *Dev Cell* **56**, 383-397 e388, doi:10.1016/j.devcel.2020.11.002 (2021).

141 Salzer, M. C. *et al.* Identity Noise and Adipogenic Traits Characterize Dermal Fibroblast Aging. *Cell* **175**, 1575-1590 e1522, doi:10.1016/j.cell.2018.10.012 (2018).

142 Sole-Boldo, L. *et al.* Single-cell transcriptomes of the human skin reveal age-related loss of fibroblast priming. *Commun Biol* **3**, 188, doi:10.1038/s42003-020-0922-4 (2020).

143 Campisi, J. & d'Adda di Fagagna, F. Cellular senescence: when bad things happen to good cells. *Nat Rev Mol Cell Biol* **8**, 729-740, doi:10.1038/nrm2233 (2007).

144 Parrinello, S., Coppe, J. P., Krtolica, A. & Campisi, J. Stromal-epithelial interactions in aging and cancer: senescent fibroblasts alter epithelial cell differentiation. *J Cell Sci* **118**, 485-496, doi:10.1242/jcs.01635 (2005).

145 Garcia-Prat, L. *et al.* Autophagy maintains stemness by preventing senescence. *Nature* **529**, 37-42, doi:10.1038/nature16187 (2016).

146 Sousa-Victor, P. *et al.* Geriatric muscle stem cells switch reversible quiescence into senescence. *Nature* **506**, 316-321, doi:10.1038/nature13013 (2014).

147 Maity, P. *et al.* Persistent JunB activation in fibroblasts disrupts stem cell niche interactions enforcing skin aging. *Cell Rep* **36**, 109634, doi:10.1016/j.celrep.2021.109634 (2021).

148 Wlaschek, M., Maity, P., Makrantonaki, E. & Scharffetter-Kochanek, K. Connective Tissue and Fibroblast Senescence in Skin Aging. *J Invest Dermatol* **141**, 985-992, doi:10.1016/j.jid.2020.11.010 (2021).

149 Waldera Lupa, D. M. *et al.* Characterization of Skin Aging-Associated Secreted Proteins (SAASP) Produced by Dermal Fibroblasts Isolated

from Intrinsically Aged Human Skin. *J Invest Dermatol* **135**, 1954-1968, doi:10.1038/jid.2015.120 (2015).

150 Yasui, T. *et al.* In vivo observation of age-related structural changes of dermal collagen in human facial skin using collagen-sensitive second harmonic generation microscope equipped with 1250-nm mode-locked Cr:Forsterite laser. *J Biomed Opt* **18**, 31108, doi:10.1117/1.JBO.18.3.031108 (2013).

151 Quan, T. & Fisher, G. J. Role of Age-Associated Alterations of the Dermal Extracellular Matrix Microenvironment in Human Skin Aging: A Mini-Review. *Gerontology* **61**, 427-434, doi:10.1159/000371708 (2015).

152 McCabe, M. C. *et al.* Alterations in extracellular matrix composition during aging and photoaging of the skin. *Matrix Biol Plus* **8**, 100041, doi:10.1016/j.mbplus.2020.100041 (2020).

153 Gruber, F., Kremslehner, C., Eckhart, L. & Tschachler, E. Cell aging and cellular senescence in skin aging - Recent advances in fibroblast and keratinocyte biology. *Exp Gerontol* **130**, 110780, doi:10.1016/j.exger.2019.110780 (2020).

154 Harn, H. I., Chen, C. C., Wang, S. P., Lei, M. & Chuong, C. M. Tissue Mechanics in Haired Murine Skin: Potential Implications for Skin Aging. *Front Cell Dev Biol* **9**, 635340, doi:10.3389/fcell.2021.635340 (2021).

155 Lynch, B. *et al.* How aging impacts skin biomechanics: a multiscale study in mice. *Sci Rep* **7**, 13750, doi:10.1038/s41598-017-13150-4 (2017).

156 Pilkington, S. M., Bulfone-Paus, S., Griffiths, C. E. M. & Watson, R. E. B. Inflammaging and the Skin. *J Invest Dermatol* **141**, 1087-1095, doi:10.1016/j.jid.2020.11.006 (2021).

157 Yousefzadeh, M. J. *et al.* An aged immune system drives senescence and ageing of solid organs. *Nature* **594**, 100-105, doi:10.1038/s41586-021-03547-7 (2021).

158 Florian, M. C. *et al.* Aging alters the epigenetic asymmetry of HSC division. *PLoS Biol* **16**, e2003389, doi:10.1371/journal.pbio.2003389 (2018).

159 Florian, M. C. *et al.* Cdc42 activity regulates hematopoietic stem cell aging and rejuvenation. *Cell Stem Cell* **10**, 520-530, doi:10.1016/j.stem.2012.04.007 (2012).

160 Krishnarajah, S. *et al.* Single-cell profiling of immune system alterations in lymphoid, barrier and solid tissues in aged mice. *Nature Aging* **2**, 74-89, doi:10.1038/s43587-021-00148-x (2021).

161 Mejia-Ramirez, E. & Florian, M. C. Understanding intrinsic hematopoietic stem cell aging. *Haematologica* **105**, 22-37, doi:10.3324/haematol.2018.211342 (2020).

162 Luo, O. J. *et al.* Multidimensional single-cell analysis of human peripheral blood reveals characteristic features of the immune system landscape in aging and frailty. *Nature Aging* **2**, 348-364, doi:10.1038/s43587-022-00198-9 (2022).

163 Linton, P. J. & Dorshkind, K. Age-related changes in lymphocyte development and function. *Nat Immunol* **5**, 133-139, doi:10.1038/ni1033 (2004).

164 Dulken, B. W. *et al.* Single-cell analysis reveals T cell infiltration in old neurogenic niches. *Nature* **571**, 205-210, doi:10.1038/s41586-019-1362-5 (2019).

165 Bharath, L. P. *et al.* Metformin Enhances Autophagy and Normalizes Mitochondrial Function to Alleviate Aging-Associated Inflammation. *Cell Metab* **32**, 44-55 e46, doi:10.1016/j.cmet.2020.04.015 (2020).

166 Chambers, E. S. *et al.* Recruitment of inflammatory monocytes by senescent fibroblasts inhibits antigen-specific tissue immunity during human aging. *Nature Aging* **1**, 101-113, doi:10.1038/s43587-020-00010-6 (2021).

167 Takahashi, J. S. Transcriptional architecture of the mammalian circadian clock. *Nat Rev Genet* **18**, 164-179, doi:10.1038/nrg.2016.150 (2017).

168 Yi, J. S., Diaz, N. M., D'Souza, S. & Buhr, E. D. The molecular clockwork of mammalian cells. *Semin Cell Dev Biol* **126**, 87-96, doi:10.1016/j.semcdb.2021.03.012 (2022).

169 Welz, P. S. & Benitah, S. A. Molecular Connections Between Circadian Clocks and Aging. *J Mol Biol* **432**, 3661-3679, doi:10.1016/j.jmb.2019.12.036 (2020).

170 Dibner, C., Schibler, U. & Albrecht, U. The mammalian circadian timing system: organization and coordination of central and peripheral clocks. *Annu Rev Physiol* **72**, 517-549, doi:10.1146/annurev-physiol-021909-135821 (2010).

171 Brown, S. A., Zumbrunn, G., Fleury-Olela, F., Preitner, N. & Schibler, U. Rhythms of mammalian body temperature can sustain peripheral circadian clocks. *Curr Biol* **12**, 1574-1583, doi:10.1016/s0960-9822(02)01145-4 (2002).

172 Welz, P. S. *et al.* BMAL1-Driven Tissue Clocks Respond Independently to Light to Maintain Homeostasis. *Cell* **178**, 1029, doi:10.1016/j.cell.2019.07.030 (2019).

173 Johnson, C. H., Elliott, J. A. & Foster, R. Entrainment of circadian programs. *Chronobiol Int* **20**, 741-774, doi:10.1081/cbi-120024211 (2003).

174 Vitaterna, M. H., Takahashi, J. S. & Turek, F. W. Overview of circadian rhythms. *Alcohol Res Health* **25**, 85-93 (2001).

175 Buhr, E. D. & Takahashi, J. S. Molecular components of the Mammalian circadian clock. *Handb Exp Pharmacol*, 3-27, doi:10.1007/978-3-642-25950-0_1 (2013).

176 Ko, C. H. & Takahashi, J. S. Molecular components of the mammalian circadian clock. *Hum Mol Genet* **15 Spec No 2**, R271-277, doi:10.1093/hmg/ddl207 (2006).

177 Trott, A. J. & Menet, J. S. Regulation of circadian clock transcriptional output by CLOCK:BMAL1. *PLoS Genet* **14**, e1007156, doi:10.1371/journal.pgen.1007156 (2018).

178 Lowrey, P. L. & Takahashi, J. S. Genetics of circadian rhythms in Mammalian model organisms. *Adv Genet* **74**, 175-230, doi:10.1016/B978-0-12-387690-4.00006-4 (2011).

179 Shearman, L. P. *et al.* Interacting molecular loops in the mammalian circadian clock. *Science* **288**, 1013-1019, doi:10.1126/science.288.5468.1013 (2000).

180 Brown, S. A., Kowalska, E. & Dallmann, R. (Re)inventing the circadian feedback loop. *Dev Cell* **22**, 477-487, doi:10.1016/j.devcel.2012.02.007 (2012).

181 Janich, P., Meng, Q. J. & Benitah, S. A. Circadian control of tissue homeostasis and adult stem cells. *Curr Opin Cell Biol* **31**, 8-15, doi:10.1016/j.ceb.2014.06.010 (2014).

182 Janich, P. *et al.* Human epidermal stem cell function is regulated by circadian oscillations. *Cell Stem Cell* **13**, 745-753, doi:10.1016/j.stem.2013.09.004 (2013).

183 Plikus, M. V. *et al.* The circadian clock in skin: implications for adult stem cells, tissue regeneration, cancer, aging, and immunity. *J Biol Rhythms* **30**, 163-182, doi:10.1177/0748730414563537 (2015).

184 Welz, P. S. Clock Regulation of Skin Regeneration in Stem Cell Aging. *J Invest Dermatol* **141**, 1024-1030, doi:10.1016/j.jid.2020.10.009 (2021).

185 Geyfman, M. *et al.* Brain and muscle Arnt-like protein-1 (BMAL1) controls circadian cell proliferation and susceptibility to UVB-induced DNA damage in the epidermis. *Proc Natl Acad Sci U S A* **109**, 11758-11763, doi:10.1073/pnas.1209592109 (2012).

186 Gaddameedhi, S., Selby, C. P., Kaufmann, W. K., Smart, R. C. & Sancar, A. Control of skin cancer by the circadian rhythm. *Proc Natl Acad Sci U S A* **108**, 18790-18795, doi:10.1073/pnas.1115249108 (2011).

187 Janich, P. *et al.* The circadian molecular clock creates epidermal stem cell heterogeneity. *Nature* **480**, 209-214, doi:10.1038/nature10649 (2011).

188 Lyons, A. B., Moy, L., Moy, R. & Tung, R. Circadian Rhythm and the Skin: A Review of the Literature. *J Clin Aesthet Dermatol* **12**, 42-45 (2019).

189 Gupta, M. A. & Gupta, A. K. Sleep-wake disorders and dermatology. *Clin Dermatol* **31**, 118-126, doi:10.1016/j.clindermatol.2011.11.016 (2013).

190 Sato, S. *et al.* Circadian Reprogramming in the Liver Identifies Metabolic Pathways of Aging. *Cell* **170**, 664-677 e611, doi:10.1016/j.cell.2017.07.042 (2017).

191 Dupont, S. & Wickstrom, S. A. Mechanical regulation of chromatin and transcription. *Nat Rev Genet*, doi:10.1038/s41576-022-00493-6 (2022).

192 Hayward, M. K., Muncie, J. M. & Weaver, V. M. Tissue mechanics in stem cell fate, development, and cancer. *Dev Cell* **56**, 1833-1847, doi:10.1016/j.devcel.2021.05.011 (2021).

193 Bertillot, F., Miroshnikova, Y. A. & Wickstrom, S. A. SnapShot: Mechanotransduction in the nucleus. *Cell* **185**, 3638-3638 e3631, doi:10.1016/j.cell.2022.08.017 (2022).

194 Wickstrom, S. A. & Niessen, C. M. Cell adhesion and mechanics as drivers of tissue organization and differentiation: local cues for large scale organization. *Curr Opin Cell Biol* **54**, 89-97, doi:10.1016/j.ceb.2018.05.003 (2018).

195 Miroshnikova, Y. A. & Wickstrom, S. A. Mechanical Forces in Nuclear Organization. *Cold Spring Harb Perspect Biol* **14**, doi:10.1101/cshperspect.a039685 (2022).

196 Miroshnikova, Y. A., Nava, M. M. & Wickstrom, S. A. Emerging roles of mechanical forces in chromatin regulation. *J Cell Sci* **130**, 2243-2250, doi:10.1242/jcs.202192 (2017).

197 Nava, M. M. *et al.* Heterochromatin-Driven Nuclear Softening Protects the Genome against Mechanical Stress-Induced Damage. *Cell* **181**, 800-817 e822, doi:10.1016/j.cell.2020.03.052 (2020).

198 Shutova, M. S. & Boehncke, W. H. Mechanotransduction in Skin Inflammation. *Cells* **11**, doi:10.3390/cells11132026 (2022).

199 Ning, W., Muroyama, A., Li, H. & Lechler, T. Differentiated Daughter Cells Regulate Stem Cell Proliferation and Fate through Intra-tissue Tension. *Cell Stem Cell* **28**, 436-452 e435, doi:10.1016/j.stem.2020.11.002 (2021).

200 Miroshnikova, Y. A. *et al.* Adhesion forces and cortical tension couple cell proliferation and differentiation to drive epidermal stratification. *Nat Cell Biol* **20**, 69-80, doi:10.1038/s41556-017-0005-z (2018).

201 Salbreux, G., Charras, G. & Paluch, E. Actin cortex mechanics and cellular morphogenesis. *Trends Cell Biol* **22**, 536-545, doi:10.1016/j.tcb.2012.07.001 (2012).

202 Aragona, M. *et al.* Mechanisms of stretch-mediated skin expansion at single-cell resolution. *Nature* **584**, 268-273, doi:10.1038/s41586-020-2555-7 (2020).

203 Samuel, M. S. *et al.* Actomyosin-mediated cellular tension drives increased tissue stiffness and beta-catenin activation to induce epidermal hyperplasia and tumor growth. *Cancer Cell* **19**, 776-791, doi:10.1016/j.ccr.2011.05.008 (2011).

204 Rognoni, E. & Walko, G. The Roles of YAP/TAZ and the Hippo Pathway in Healthy and Diseased Skin. *Cells* **8**, doi:10.3390/cells8050411 (2019).

205 Hansen, C. G., Moroishi, T. & Guan, K. L. YAP and TAZ: a nexus for Hippo signaling and beyond. *Trends Cell Biol* **25**, 499-513, doi:10.1016/j.tcb.2015.05.002 (2015).

206 Moya, I. M. & Halder, G. Hippo-YAP/TAZ signalling in organ regeneration and regenerative medicine. *Nat Rev Mol Cell Biol* **20**, 211-226, doi:10.1038/s41580-018-0086-y (2019).

207 Totaro, A., Panciera, T. & Piccolo, S. YAP/TAZ upstream signals and downstream responses. *Nat Cell Biol* **20**, 888-899, doi:10.1038/s41556-018-0142-z (2018).

208 Panciera, T., Azzolin, L., Cordenonsi, M. & Piccolo, S. Mechanobiology of YAP and TAZ in physiology and disease. *Nat Rev Mol Cell Biol* **18**, 758-770, doi:10.1038/nrm.2017.87 (2017).

209 Aragona, M. *et al.* A mechanical checkpoint controls multicellular growth through YAP/TAZ regulation by actin-processing factors. *Cell* **154**, 1047-1059, doi:10.1016/j.cell.2013.07.042 (2013).

210 Camargo, F. D. *et al.* YAP1 increases organ size and expands undifferentiated progenitor cells. *Curr Biol* **17**, 2054-2060, doi:10.1016/j.cub.2007.10.039 (2007).

211 Halder, G., Dupont, S. & Piccolo, S. Transduction of mechanical and cytoskeletal cues by YAP and TAZ. *Nat Rev Mol Cell Biol* **13**, 591-600, doi:10.1038/nrm3416 (2012).

212 Dupont, S. *et al.* Role of YAP/TAZ in mechanotransduction. *Nature* **474**, 179-183, doi:10.1038/nature10137 (2011).

213 Zanconato, F., Cordenonsi, M. & Piccolo, S. YAP/TAZ at the Roots of Cancer. *Cancer Cell* **29**, 783-803, doi:10.1016/j.ccell.2016.05.005 (2016).

214 Wada, K., Itoga, K., Okano, T., Yonemura, S. & Sasaki, H. Hippo pathway regulation by cell morphology and stress fibers. *Development* **138**, 3907-3914, doi:10.1242/dev.070987 (2011).

215 Elosegui-Artola, A. *et al.* Force Triggers YAP Nuclear Entry by Regulating Transport across Nuclear Pores. *Cell* **171**, 1397-1410 e1314, doi:10.1016/j.cell.2017.10.008 (2017).

216 Elbediwy, A. *et al.* Integrin signalling regulates YAP and TAZ to control skin homeostasis. *Development* **143**, 1674-1687, doi:10.1242/dev.133728 (2016).

217 Totaro, A. *et al.* YAP/TAZ link cell mechanics to Notch signalling to control epidermal stem cell fate. *Nat Commun* **8**, 15206, doi:10.1038/ncomms15206 (2017).

218 Zhang, H., Pasolli, H. A. & Fuchs, E. Yes-associated protein (YAP) transcriptional coactivator functions in balancing growth and differentiation in skin. *Proc Natl Acad Sci U S A* **108**, 2270-2275, doi:10.1073/pnas.1019603108 (2011).

219 Walko, G. *et al.* A genome-wide screen identifies YAP/WBP2 interplay conferring growth advantage on human epidermal stem cells. *Nat Commun* **8**, 14744, doi:10.1038/ncomms14744 (2017).

220 Schlegelmilch, K. *et al.* Yap1 acts downstream of alpha-catenin to control epidermal proliferation. *Cell* **144**, 782-795, doi:10.1016/j.cell.2011.02.031 (2011).

221 Debaugnies, M. *et al.* YAP and TAZ are essential for basal and squamous cell carcinoma initiation. *EMBO Rep* **19**, doi:10.15252/embr.201845809 (2018).

222 Kazanci, A., Kurus, M. & Atasever, A. Analyses of changes on skin by aging. *Skin Res Technol* **23**, 48-60, doi:10.1111/srt.12300 (2017).

223 Sladitschek-Martens, H. L. *et al.* YAP/TAZ activity in stromal cells prevents ageing by controlling cGAS-STING. *Nature* **607**, 790-798, doi:10.1038/s41586-022-04924-6 (2022).

224 Pelissier, F. A. *et al.* Age-related dysfunction in mechanotransduction impairs differentiation of human mammary epithelial progenitors. *Cell Rep* **7**, 1926-1939, doi:10.1016/j.celrep.2014.05.021 (2014).

225 Sherratt, M. J. *et al.* Circadian rhythms in skin and other elastic tissues. *Matrix Biol* **84**, 97-110, doi:10.1016/j.matbio.2019.08.004 (2019).

226 Yang, N. *et al.* Cellular mechano-environment regulates the mammary circadian clock. *Nat Commun* **8**, 14287, doi:10.1038/ncomms14287 (2017).

227 Balsalobre, A., Damiola, F. & Schibler, U. A serum shock induces circadian gene expression in mammalian tissue culture cells. *Cell* **93**, 929-937, doi:10.1016/s0092-8674(00)81199-x (1998).

228 Williams, J. *et al.* Epithelial and stromal circadian clocks are inversely regulated by their mechano-matrix environment. *J Cell Sci* **131**, doi:10.1242/jcs.208223 (2018).

229 Stokes, K. *et al.* The Circadian Clock Gene, Bmal1, Regulates Intestinal Stem Cell Signaling and Represses Tumor Initiation. *Cell Mol Gastroenterol Hepatol* **12**, 1847-1872 e1840, doi:10.1016/j.jcmgh.2021.08.001 (2021).

230 Streuli, C. H. & Meng, Q. J. Influence of the extracellular matrix on cell-intrinsic circadian clocks. *J Cell Sci* **132**, doi:10.1242/jcs.207498 (2019).

231 Shin, J. W. *et al.* Molecular Mechanisms of Dermal Aging and Antiaging Approaches. *Int J Mol Sci* **20**, doi:10.3390/ijms20092126 (2019).

232 Korsunsky, I. *et al.* Fast, sensitive and accurate integration of single-cell data with Harmony. *Nat Methods* **16**, 1289-1296, doi:10.1038/s41592-019-0619-0 (2019).

233 Stuart, T. *et al.* Comprehensive Integration of Single-Cell Data. *Cell* **177**, 1888-1902 e1821, doi:10.1016/j.cell.2019.05.031 (2019).

234 Mangiola, S. *et al.* Robust differential composition and variability analysis for multisample cell omics. *BioRxiv*, doi:10.1101/2022.03.04.482758 (2022).

235 Balakrishnan, A. *et al.* Insights Into the Role and Potential of Schwann Cells for Peripheral Nerve Repair From Studies of Development and Injury. *Front Mol Neurosci* **13**, 608442, doi:10.3389/fnmol.2020.608442 (2020).

236 Kastriti, M. E. *et al.* Schwann cell precursors represent a neural crest-like state with biased multipotency. *EMBO J* **41**, e108780, doi:10.15252/embj.2021108780 (2022).

237 Fletcher, J. S., Pundavela, J. & Ratner, N. After Nf1 loss in Schwann cells, inflammation drives neurofibroma formation. *Neurooncol Adv* **2**, i23-i32, doi:10.1093/noajnl/vdz045 (2020).

238 Ulvmar, M. H. & Makinen, T. Heterogeneity in the lymphatic vascular system and its origin. *Cardiovasc Res* **111**, 310-321, doi:10.1093/cvr/cvw175 (2016).

239 Pober, J. S., Merola, J., Liu, R. & Manes, T. D. Antigen Presentation by Vascular Cells. *Front Immunol* **8**, 1907, doi:10.3389/fimmu.2017.01907 (2017).

240 Shaikh, H. *et al.* Endothelial Cells Activate Alloreactive CD4+ T Cells to Initiate Acute Graft-Versus-Host Disease. *Blood* **140**, 1157-1158, doi:10.1182/blood-2022-167245 (2022).

241 Muhl, L. *et al.* Single-cell analysis uncovers fibroblast heterogeneity and criteria for fibroblast and mural cell identification and discrimination. *Nat Commun* **11**, 3953, doi:10.1038/s41467-020-17740-1 (2020).

242 Rendl, M., Polak, L. & Fuchs, E. BMP signaling in dermal papilla cells is required for their hair follicle-inductive properties. *Genes Dev* **22**, 543-557, doi:10.1101/gad.1614408 (2008).

243 Korsunsky, I. *et al.* Cross-tissue, single-cell stromal atlas identifies shared pathological fibroblast phenotypes in four chronic inflammatory diseases. *Med (N Y)* **3**, 481-518 e414, doi:10.1016/j.medj.2022.05.002 (2022).

244 Campisi, J. Aging, cellular senescence, and cancer. *Annu Rev Physiol* **75**, 685-705, doi:10.1146/annurev-physiol-030212-183653 (2013).

245 Gorgoulis, V. *et al.* Cellular Senescence: Defining a Path Forward. *Cell* **179**, 813-827, doi:10.1016/j.cell.2019.10.005 (2019).

246 Blauvelt, A. & Chiricozzi, A. The Immunologic Role of IL-17 in Psoriasis and Psoriatic Arthritis Pathogenesis. *Clin Rev Allergy Immunol* **55**, 379-390, doi:10.1007/s12016-018-8702-3 (2018).

247 Stubbington, M. J. *et al.* An atlas of mouse CD4(+) T cell transcriptomes. *Biol Direct* **10**, 14, doi:10.1186/s13062-015-0045-x (2015).

248 Ciofani, M. *et al.* A validated regulatory network for Th17 cell specification. *Cell* **151**, 289-303, doi:10.1016/j.cell.2012.09.016 (2012).

249 Carr, T. M., Wheaton, J. D., Houtz, G. M. & Ciofani, M. JunB promotes Th17 cell identity and restrains alternative CD4(+) T-cell programs during inflammation. *Nat Commun* **8**, 301, doi:10.1038/s41467-017-00380-3 (2017).

250 Liu, Y. *et al.* Upregulation of toll-like receptor 2 gene expression in macrophage response to peptidoglycan and high concentration of lipopolysaccharide is involved in NF-kappa b activation. *Infect Immun* **69**, 2788-2796, doi:10.1128/IAI.69.5.2788-2796.2001 (2001).

251 An, H. *et al.* Involvement of ERK, p38 and NF-kappaB signal transduction in regulation of TLR2, TLR4 and TLR9 gene expression induced by lipopolysaccharide in mouse dendritic cells. *Immunology* **106**, 38-45, doi:10.1046/j.1365-2567.2002.01401.x (2002).

252 Nielsen, M. M., Witherden, D. A. & Havran, W. L. gammadelta T cells in homeostasis and host defence of epithelial barrier tissues. *Nat Rev Immunol* **17**, 733-745, doi:10.1038/nri.2017.101 (2017).

253 Bowcutt, R. *et al.* Heterogeneity across the murine small and large intestine. *World J Gastroenterol* **20**, 15216-15232, doi:10.3748/wjg.v20.i41.15216 (2014).

254 McGinley, A. M. *et al.* Interleukin-17A Serves a Priming Role in Autoimmunity by Recruiting IL-1beta-Producing Myeloid Cells that Promote Pathogenic T Cells. *Immunity* **52**, 342-356 e346, doi:10.1016/j.immuni.2020.01.002 (2020).

255 Ito, M. *et al.* Wnt-dependent de novo hair follicle regeneration in adult mouse skin after wounding. *Nature* **447**, 316-320, doi:10.1038/nature05766 (2007).

256 Harshuk-Shabso, S., Dressler, H., Niehrs, C., Aamar, E. & Enshell-Seijffers, D. Fgf and Wnt signaling interaction in the mesenchymal niche regulates the murine hair cycle clock. *Nat Commun* **11**, 5114, doi:10.1038/s41467-020-18643-x (2020).

257 Hagner, A. *et al.* Transcriptional Profiling of the Adult Hair Follicle Mesenchyme Reveals R-spondin as a Novel Regulator of Dermal Progenitor Function. *iScience* **23**, 101019, doi:10.1016/j.isci.2020.101019 (2020).

258 Markovic, I. & Savvides, S. N. Modulation of Signaling Mediated by TSLP and IL-7 in Inflammation, Autoimmune Diseases, and Cancer. *Front Immunol* **11**, 1557, doi:10.3389/fimmu.2020.01557 (2020).

259 Singh, T. P. *et al.* Involvement of IL-9 in Th17-associated inflammation and angiogenesis of psoriasis. *PLoS One* **8**, e51752, doi:10.1371/journal.pone.0051752 (2013).

260 Wang, Y. *et al.* NF-kappaB signaling in skin aging. *Mech Ageing Dev* **184**, 111160, doi:10.1016/j.mad.2019.111160 (2019).

261 Wullaert, A., Bonnet, M. C. & Pasparakis, M. NF-kappaB in the regulation of epithelial homeostasis and inflammation. *Cell Res* **21**, 146-158, doi:10.1038/cr.2010.175 (2011).

262 Sevilla, L. M. *et al.* Mice deficient in involucrin, envoplakin, and periplakin have a defective epidermal barrier. *J Cell Biol* **179**, 1599-1612, doi:10.1083/jcb.200706187 (2007).

263 Coulombe, P. A., Kopan, R. & Fuchs, E. Expression of keratin K14 in the epidermis and hair follicle: insights into complex programs of differentiation. *J Cell Biol* **109**, 2295-2312, doi:10.1083/jcb.109.5.2295 (1989).

264 Estrach, S., Cordes, R., Hozumi, K., Gossler, A. & Watt, F. M. Role of the Notch ligand Delta1 in embryonic and adult mouse epidermis. *J Invest Dermatol* **128**, 825-832, doi:10.1038/sj.jid.5701113 (2008).

265 MacQuarrie, K. L., Fong, A. P., Morse, R. H. & Tapscott, S. J. Genome-wide transcription factor binding: beyond direct target regulation. *Trends Genet* **27**, 141-148, doi:10.1016/j.tig.2011.01.001 (2011).

266 Buenrostro, J. D., Wu, B., Chang, H. Y. & Greenleaf, W. J. ATAC-seq: A Method for Assaying Chromatin Accessibility Genome-Wide. *Curr Protoc Mol Biol* **109**, 21 29 21-21 29 29, doi:10.1002/0471142727.mb2129s109 (2015).

267 Hughes, M. E., Hogenesch, J. B. & Kornacker, K. JTK_CYCLE: an efficient nonparametric algorithm for detecting rhythmic components in genome-scale data sets. *J Biol Rhythms* **25**, 372-380, doi:10.1177/0748730410379711 (2010).

268 Gel, B. *et al.* regioneR: an R/Bioconductor package for the association analysis of genomic regions based on permutation tests. *Bioinformatics* **32**, 289-291, doi:10.1093/bioinformatics/btv562 (2016).

269 Jansson, L. & Larsson, J. Normal hematopoietic stem cell function in mice with enforced expression of the Hippo signaling effector YAP1. *PLoS One* **7**, e32013, doi:10.1371/journal.pone.0032013 (2012).

270 Franceschi, C. & Campisi, J. Chronic inflammation (inflammaging) and its potential contribution to age-associated diseases. *J Gerontol A Biol Sci Med Sci* **69 Suppl 1**, S4-9, doi:10.1093/gerona/glu057 (2014).

271 Li, J., Casanova, J. L. & Puel, A. Mucocutaneous IL-17 immunity in mice and humans: host defense vs. excessive inflammation. *Mucosal Immunol* **11**, 581-589, doi:10.1038/mi.2017.97 (2018).

272 von Stebut, E. *et al.* IL-17A in Psoriasis and Beyond: Cardiovascular and Metabolic Implications. *Front Immunol* **10**, 3096, doi:10.3389/fimmu.2019.03096 (2019).

273 Zhang, H., Bernuzzi, F., Lleo, A., Ma, X. & Invernizzi, P. Therapeutic Potential of IL-17-Mediated Signaling Pathway in Autoimmune Liver Diseases. *Mediators Inflamm* **2015**, 436450, doi:10.1155/2015/436450 (2015).

274 Zhou, L. *et al.* Centenarians Alleviate Inflammaging by Changing the Ratio and Secretory Phenotypes of T Helper 17 and Regulatory T Cells. *Front Pharmacol* **13**, 877709, doi:10.3389/fphar.2022.877709 (2022).

275 Emson, C. L. *et al.* A pilot study demonstrating a non-invasive method for the measurement of protein turnover in skin disorders: application to psoriasis. *Clin Transl Med* **2**, 12, doi:10.1186/2001-1326-2-12 (2013).

276 Mosca, M. *et al.* The Role of IL-17 Cytokines in Psoriasis. *Immunotargets Ther* **10**, 409-418, doi:10.2147/ITT.S240891 (2021).

277 Naik, S. *et al.* Inflammatory memory sensitizes skin epithelial stem cells to tissue damage. *Nature* **550**, 475-480, doi:10.1038/nature24271 (2017).

278 Morhenn, V. B., Nelson, T. E. & Gruol, D. L. The rate of wound healing is increased in psoriasis. *J Dermatol Sci* **72**, 87-92, doi:10.1016/j.jdermsci.2013.06.001 (2013).

279 Amberg, N., Holcmann, M., Stulnig, G. & Sibilia, M. Effects of Imiquimod on Hair Follicle Stem Cells and Hair Cycle Progression. *J Invest Dermatol* **136**, 2140-2149, doi:10.1016/j.jid.2016.06.613 (2016).

280 Sawan, S. & Descamps, V. Scalp psoriasis: a paradigm of "switch-on" mechanism to anagen hair growth? *Arch Dermatol* **144**, 1064-1066, doi:10.1001/archdermatol.2008.2 (2008).

281 Runne, U. & Kroneisen-Wiersma, P. Psoriatic alopecia: acute and chronic hair loss in 47 patients with scalp psoriasis. *Dermatology* **185**, 82-87, doi:10.1159/000247418 (1992).

282 George, S. M., Taylor, M. R. & Farrant, P. B. Psoriatic alopecia. *Clin Exp Dermatol* **40**, 717-721, doi:10.1111/ced.12715 (2015).

283 Huang, M. C., Liao, J. J., Bonasera, S., Longo, D. L. & Goetzl, E. J. Nuclear factor-kappaB-dependent reversal of aging-induced alterations in T cell cytokines. *FASEB J* **22**, 2142-2150, doi:10.1096/fj.07-103721 (2008).

284 Lim, M. A. *et al.* Increased Th17 differentiation in aged mice is significantly associated with high IL-1beta level and low IL-2 expression. *Exp Gerontol* **49**, 55-62, doi:10.1016/j.exger.2013.10.006 (2014).

285 Chen, H. C. *et al.* IL-7-dependent compositional changes within the gammadelta T cell pool in lymph nodes during ageing lead to an unbalanced anti-tumour response. *EMBO Rep* **20**, e47379, doi:10.15252/embr.201847379 (2019).

286 Chung, Y. *et al.* Critical regulation of early Th17 cell differentiation by interleukin-1 signaling. *Immunity* **30**, 576-587, doi:10.1016/j.immuni.2009.02.007 (2009).

287 Gelinas, D. S. & McLaurin, J. PPAR-alpha expression inversely correlates with inflammatory cytokines IL-1beta and TNF-alpha in aging rats. *Neurochem Res* **30**, 1369-1375, doi:10.1007/s11064-005-8341-y (2005).

288 Sha, Y. & Markovic-Plese, S. A role of IL-1R1 signaling in the differentiation of Th17 cells and the development of autoimmune diseases. *Self Nonself* **2**, 35-42, doi:10.4161/self.2.1.15639 (2011).

289 Yang, X. O. *et al.* Regulation of inflammatory responses by IL-17F. *J Exp Med* **205**, 1063-1075, doi:10.1084/jem.20071978 (2008).

290 Gordon, K. B. *et al.* Bimekizumab efficacy and safety in moderate to severe plaque psoriasis (BE READY): a multicentre, double-blind, placebo-controlled, randomised withdrawal phase 3 trial. *Lancet* **397**, 475-486, doi:10.1016/S0140-6736(21)00126-4 (2021).

291 Reich, K. *et al.* Bimekizumab versus ustekinumab for the treatment of moderate to severe plaque psoriasis (BE VIVID): efficacy and safety from a 52-week, multicentre, double-blind, active comparator and placebo controlled phase 3 trial. *Lancet* **397**, 487-498, doi:10.1016/S0140-6736(21)00125-2 (2021).

292 Kashetsky, N. *et al.* Treatment Outcomes of IL-17 Inhibitors in Hidradenitis Suppurativa: A Systematic Review. *J Cutan Med Surg* **26**, 79-86, doi:10.1177/12034754211035667 (2022).

293 Fletcher, J. M., Moran, B., Petrasca, A. & Smith, C. M. IL-17 in inflammatory skin diseases psoriasis and hidradenitis suppurativa. *Clin Exp Immunol* **201**, 121-134, doi:10.1111/cei.13449 (2020).

294 Glatt, S. *et al.* Efficacy and Safety of Bimekizumab in Moderate to Severe Hidradenitis Suppurativa: A Phase 2, Double-blind, Placebo-Controlled Randomized Clinical Trial. *JAMA Dermatol* **157**, 1279-1288, doi:10.1001/jamadermatol.2021.2905 (2021).

295 Ramot, Y., Marzani, B., Pinto, D., Sorbellini, E. & Rinaldi, F. IL-17 inhibition: is it the long-awaited savior for alopecia areata? *Arch Dermatol Res* **310**, 383-390, doi:10.1007/s00403-018-1823-y (2018).

296 Loh, S. H., Moon, H. N., Lew, B. L. & Sim, W. Y. Role of T helper 17 cells and T regulatory cells in alopecia areata: comparison of lesion and serum cytokine between controls and patients. *J Eur Acad Dermatol Venereol* **32**, 1028-1033, doi:10.1111/jdv.14775 (2018).

297 Yajima, M., Akeda, T., Kondo, M., Habe, K. & Yamanaka, K. Alopecia Diffusa while Using Interleukin-17 Inhibitors against Psoriasis Vulgaris. *Case Rep Dermatol* **11**, 82-85, doi:10.1159/000499030 (2019).

298 Tan, T. L., Taglia, L. & Yazdan, P. Drug-induced psoriasiform alopecia associated with interleukin-17 inhibitor therapy. *J Cutan Pathol* **48**, 771-774, doi:10.1111/cup.13952 (2021).

299 Chakievska, L. *et al.* IL-17A is functionally relevant and a potential therapeutic target in bullous pemphigoid. *J Autoimmun* **96**, 104-112, doi:10.1016/j.jaut.2018.09.003 (2019).

300 Yun, J. S., Scardamaglia, L., Tan, C. G. & McCormack, C. J. Successful secukinumab treatment of active bullous pemphigoid and chronic severe psoriasis: a case report. *Australas J Dermatol* **63**, e155-e158, doi:10.1111/ajd.13803 (2022).

301 Gautam, P. *et al.* Emerging role of IkappaBzeta in inflammation: Emphasis on psoriasis. *Clin Transl Med* **12**, e1032, doi:10.1002/ctm2.1032 (2022).

302 Bertelsen, T., Iversen, L. & Johansen, C. The human IL-17A/F heterodimer regulates psoriasis-associated genes through IkappaBzeta. *Exp Dermatol* **27**, 1048-1052, doi:10.1111/exd.13722 (2018).

303 Johansen, C. *et al.* IkappaBzeta is a key driver in the development of psoriasis. *Proc Natl Acad Sci U S A* **112**, E5825-5833, doi:10.1073/pnas.1509971112 (2015).

304 Wang, Y., Wang, G., Luo, X., Qiu, J. & Tang, C. Substrate stiffness regulates the proliferation, migration, and differentiation of epidermal cells. *Burns* **38**, 414-420, doi:10.1016/j.burns.2011.09.002 (2012).

305 Wickert, L. E., Pomerenke, S., Mitchell, I., Masters, K. S. & Kreeger, P. K. Hierarchy of cellular decisions in collective behavior: Implications for wound healing. *Sci Rep* **6**, 20139, doi:10.1038/srep20139 (2016).

306 Kenny, F. N. *et al.* Tissue stiffening promotes keratinocyte proliferation through activation of epidermal growth factor signaling. *J Cell Sci* **131**, doi:10.1242/jcs.215780 (2018).

307 Ichijo, R. *et al.* Vasculature atrophy causes a stiffened microenvironment that augments epidermal stem cell differentiation in aged skin. *Nature Aging* **2**, 592-600, doi:10.1038/s43587-022-00244-6 (2022).

308 Piccolo, S., Panciera, T., Contessotto, P. & Cordenonsi, M. YAP/TAZ as master regulators in cancer: modulation, function and therapeutic approaches. *Nat Cancer*, doi:10.1038/s43018-022-00473-z (2022).

309 Wang, G. *et al.* Targeting YAP-Dependent MDSC Infiltration Impairs Tumor Progression. *Cancer Discov* **6**, 80-95, doi:10.1158/2159-8290.CD-15-0224 (2016).

310 Matthaios, D., Tolia, M., Mauri, D., Kamposioras, K. & Karamouzis, M. YAP/Hippo Pathway and Cancer Immunity: It Takes Two to Tango. *Biomedicines* **9**, doi:10.3390/biomedicines9121949 (2021).

311 Jiang, Y., Yang, X., Jiang, J. & Xiao, B. Structural Designs and Mechanogating Mechanisms of the Mechanosensitive Piezo Channels. *Trends Biochem Sci* **46**, 472-488, doi:10.1016/j.tibs.2021.01.008 (2021).

312 Ansorge, H. L. *et al.* Type XIV Collagen Regulates Fibrillogenesis: PREMATURE COLLAGEN FIBRIL GROWTH AND TISSUE DYSFUNCTION IN NULL MICE. *J Biol Chem* **284**, 8427-8438, doi:10.1074/jbc.M805582200 (2009).

313 Solá, P. *et al.*, doi:10.1101/2022.01.31.478459 (2022).

314 Dobin, A. *et al.* STAR: ultrafast universal RNA-seq aligner. *Bioinformatics* **29**, 15-21, doi:10.1093/bioinformatics/bts635 (2013).

315 Love, M. I., Huber, W. & Anders, S. Moderated estimation of fold change and dispersion for RNA-seq data with DESeq2. *Genome Biol* **15**, 550, doi:10.1186/s13059-014-0550-8 (2014).

316 Liao, Y., Smyth, G. K. & Shi, W. The R package Rsubread is easier, faster, cheaper and better for alignment and quantification of RNA sequencing reads. *Nucleic Acids Res* **47**, e47, doi:10.1093/nar/gkz114 (2019).

317 Wu, D. *et al.* ROAST: rotation gene set tests for complex microarray experiments. *Bioinformatics* **26**, 2176-2182, doi:10.1093/bioinformatics/btq401 (2010).

318 Langmead, B., Trapnell, C., Pop, M. & Salzberg, S. L. Ultrafast and memory-efficient alignment of short DNA sequences to the human genome. *Genome Biol* **10**, R25, doi:10.1186/gb-2009-10-3-r25 (2009).

319 Bolger, A. M., Lohse, M. & Usadel, B. Trimmomatic: a flexible trimmer for Illumina sequence data. *Bioinformatics* **30**, 2114-2120, doi:10.1093/bioinformatics/btu170 (2014).

320 Li, H. & Durbin, R. Fast and accurate short read alignment with Burrows-Wheeler transform. *Bioinformatics* **25**, 1754-1760, doi:10.1093/bioinformatics/btp324 (2009).

321 Danecek, P. *et al.* Twelve years of SAMtools and BCFtools. *Gigascience* **10**, doi:10.1093/gigascience/giab008 (2021).

322 Heinz, S. *et al.* Simple combinations of lineage-determining transcription factors prime cis-regulatory elements required for macrophage and B cell identities. *Mol Cell* **38**, 576-589, doi:10.1016/j.molcel.2010.05.004 (2010).

323 Raudvere, U. *et al.* g:Profiler: a web server for functional enrichment analysis and conversions of gene lists (2019 update). *Nucleic Acids Res* **47**, W191-W198, doi:10.1093/nar/gkz369 (2019).

324 Xie, Z. *et al.* Gene Set Knowledge Discovery with Enrichr. *Curr Protoc* **1**, e90, doi:10.1002/cpz1.90 (2021).

325 Hao, Y. *et al.* Integrated analysis of multimodal single-cell data. *Cell* **184**, 3573-3587 e3529, doi:10.1016/j.cell.2021.04.048 (2021).

326 Mereu, E. *et al.* Benchmarking single-cell RNA-sequencing protocols for cell atlas projects. *Nat Biotechnol* **38**, 747-755, doi:10.1038/s41587-020-0469-4 (2020).